Discovery of small molecule modulators of protein-protein interactions by FRET-based high-throughput screening and structure-based drug design

A DISSERTATION

SUBMITTED TO THE FACULTY OF

UNIVERSITY OF MINNESOTA

BY

Chih Hung Lo

IN PARTIAL FULFILLMENT OF THE REQUIREMENTS

FOR THE DEGREE OF

DOCTOR OF PHILOSOPHY

Dr. Jonathan N. Sachs (Advisor)

Dr. David D. Thomas (Co-Advisor)

August 2019

ACKNOWLEDGEMENT

My journey as a graduate student at the University of Minnesota is an extremely unique experience where, for the first time, I learned the limit of myself and the reality of life. From arriving at Minneapolis alone five year ago to having many supportive friends now, this experience has been shaped by a great number of people who I deeply appreciate. First and foremost, I am eternally grateful to my advisors, mentors and friends, Dr. Jonathan Sachs and Dr. David Thomas, for creating this valuable and exciting co-advising opportunity for me and supporting my passion in research as well as my interests in technology commercialization. I would not be where I am today without their coaching and guidance. Jonathan always gives me the freedom to explore my own interests and capability while every now and then challenging me intellectually and keeping me in check on my priority and work progress. Jonathan also seizes every opportunity to expand my trainings in new fields and important skills as well as encourage me to be involved in various exciting collaborations with multiple laboratories to allow me to gain exposure and experiences. Dave sets a strong foundation in my research career in training me to work systematically with the powwow meetings in my early years here as a graduate student. In addition, Dave welcomes me into his lab as a formal DDT lab member and provides me with access to many important expertise and resources, which greatly facilitates my research progress. I believe Jonathan and Dave are the best advisors that a graduate student could ever dream to have.

I also want to thank the Sachs Lab members, both current and former, that personally helped me along the way. Specifically, I want express my gratitude to Nagamani Vunnam and Andrew Lewis who guided me since my first day in the lab and provided me with trainings in the fundamental research skills and various experimental

techniques. I would also like to thank Anthony Braun for sharing his broad knowledge related to IDPs and his latest ideas to allow me to gain extensive exposure to this exciting field as well as his guidance in harnessing my grant writing skills. I am also thankful to Ting-Lan Chiu, Benjamin Brummel and Tiffany Senkow for their patience in teaching me skills in molecular docking and computational work. Malaney Young, Oscar Bastidas and Sophia Szymonski's enthusiasm and passion for science raised my spirits on numerous occasions and made graduate school enjoyable. Finally and importantly, I would not have been able to advance my thesis research this far without the tremendous help and assistance provided by all the brilliant undergraduate and graduate students who have worked closely with me. Special thanks to Breeanne Brand, Colin Lim, Edward Ding and Evan Huber for their time and effort contributing to my research work, bearing with my demanding trainings and instructions, and the times that we had fun sharing about life together. I wish them the best in their future endeavors!

I would also like to express my deepest gratitude to the all members of the Thomas Lab for accommodating me in the lab. Specifically, I want to thank Tory Schaaf, Samantha Yuen, Robyn Rebbeck and Prachi Bawaskar, who also provided me with much of the trainings in instrument techniques and assay preparations since my first day in the lab as well as your encouragements, positivity and chocolates along the way. I also want to thank Razvan Cornea, Mike Autry, Andrew Thompson, Dan Stroik, Ji Li, Evan Kleinboehl and Ang Li for all the discussion and advice that they have given me.

I am also especially grateful to Dr. Courtney Aldrich and all the members of the Aldrich Lab for willing to accommodate me (a novice in chemistry) in the chemistry lab and their constant support, discussion and important feedback and advice during lab meetings. Specifically, I want to thank Dr. Courtney Aldrich, William Fiers and Evan Alexander for being so patient in teaching me the necessary chemistry skills from

compound synthesis to characterization as well as bearing with my naïve questions. I also want to thank Marzena Baran, Kaja Rožman, Ruiqin Wang (Steve) and Peter Larson (Ferguson Lab) for all the technical discussion and assistance in chemistry. Lastly, I also want to express my gratitude to Dr. David Ferguson for willing to host me in his lab space as well as provide me with advice along the way.

I am also extremely thankful to all my committee members and collaborators. I want to thank Dr. David Odde for being the chair of my committee and providing feedback and advice on my thesis research since my preliminary examination and in multiple project meetings. I also want to thank Dr. Daniel Mooradian for being my committee member and reading my thesis as well as his inspiration in commercializing science and technology. Special thanks to Dr. Elizabeth Rhoades (University of Pennsylvania) and Dr. Ralf Langen (University of Southern California) for providing much of the tau and huntingtin DNA plasmids and proteins as well as the extremely helpful comments to my papers. I also want to thank Dr. Karen Ashe for her inspiration in me pursuing the research direction related to neuroscience as well as her insightful comments to my paper. Lastly, I want to thank Dr. Jon Hawkinson and Dr. Michael Walters from ITDD for allowing me to use the equipment in their laboratories.

Finally, I want to thank my parents, Wen Tai Lo and Ming Hua Lin, for their endless support and understanding in me traveling nearly ten thousand miles away from home to pursue my dreams. Lastly, I want to thank the love of my life and my wife-to-be, Jialiu Zeng, for never giving up on me, supporting me throughout this journey and always standing by my side as we continue to pursue our dreams together.

DEDICATIONS

To my parents Wen Tai Lo and Ming Hua Lin, and my love Jialiu Zeng.

ABSTRACT

Protein–protein interactions (PPIs) are of pivotal importance in the regulation of biological systems and are consequently implicated in the development of disease states. Here, we investigated two classes of protein, including a transmembrane protein (tumor necrosis factor receptor 1 (TNFR1)) and intrinsically disordered proteins (tau and huntingtin (HTT)), which are implicated in autoimmune diseases and neurodegenerative diseases respectively. Receptor-specific inhibition of TNFR1 signaling is a highly sought after strategy for treatment of inflammatory diseases such as rheumatoid arthritis. In this study, we investigated the structure-function relationship of TNFR1 by engineering a TNFR1 fluorescence resonance energy transfer (FRET) biosensor to monitor the structural and conformational changes of the receptor. We have also shown using small-molecule tool compounds, that the disruption of receptor-receptor interactions (competitive inhibition) and perturbation of the receptor conformational dynamics (allosteric inhibition) are both feasible approaches to inhibit TNFR1 signaling. We have also made a major discovery showing that long-range structural couplings, between TNFR1 membrane distal and proximal domains, mediated through the ligand-binding loop, determine the conformational states of the receptor that act as a molecular switch in receptor function. In addition to deepening the understanding of a novel mechanism in TNF receptor activation, we have optimized a lead compound through medicinal chemistry by improving its potency by more than sixty-fold to the nanomolar range, thereby advancing therapeutic developments in these clinically important targets. The heterogeneity of tau and HTT pathology is one of the major challenges that plagues current clinical trials, hence impeding the discovery of a cure for Alzheimer's disease (AD) and Huntington's disease (HD). We have engineered novel FRET biosensors of these proteins to target the ensemble of heterogeneous protein oligomers or aggregates

in cells. The biosensors are not only capable of monitoring oligomer conformations, but can also be used as a high-throughput screening platform. Using these technologies, we have discovered small-molecule inhibitors of tau oligomerization or HTT aggregation that rescue cell cytotoxicity with nanomolar potency.

ADVISOR:

Dr. Jonathan N. Sachs, Ph.D.

Professor of Biomedical Engineering, University of Minnesota, Twin Cities

CO-ADVISOR:

Dr. David D. Thomas, Ph.D.

Professor of Biochemistry, Molecular Biology, and Biophysics, University of Minnesota, Twin Cities

COMMITTEE MEMBERS:

Dr. David J. Odde, Ph.D.

Professor of Biomedical Engineering, University of Minnesota, Twin Cities

Dr. Courtney C. Aldrich, Ph.D.

Professor of Medicinal Chemistry, University of Minnesota, Twin Cities

Dr. Daniel L. Mooradian, Ph.D.

Professor of Technological Leadership Institute, University of Minnesota, Twin Cities

Table of contents

LIST OF TABLES

LIST OF FIGURES

LIST OF SCHEMES

PREFACE

The work presented in this thesis is divided into two broad sections: 1) the study of the structure-function relationship of tumor necrosis factor receptor 1 (TNFR1) and the development of new receptor-specific targeting strategies; and 2) the investigation of conformational heterogeneity in intrinsically disordered proteins (IDP) including tau and huntingtin (HTT), and the development of novel strategy in targeting the ensemble of IDP oligomers or aggregates. Chapter 1 describes the implication of TNFR1 and IDPs (tau and HTT) in autoimmune diseases and neurodegenerative diseases respectively. This chapter also provides a detailed literature review on the current therapeutics and their limitations and a description of our proposed targeting strategy.

From Chapter 2 to 6, the structure-function relationship of TNFR1 is investigated using a small-molecule drug discovery approach. In Chapter 2, we developed a TNFR1 fluorescence resonance energy transfer (FRET) biosensor to monitor the structural and conformational change of the receptor. In Chapter 3, we used the FRET biosensor in high-throughput screening (HTS) of NIH clinical collection (NCC) library. We identified a new small molecule that disrupts TNFR1 receptor-receptor interaction without ablating ligand binding and inhibits the receptor function. In Chapter 4, we expanded the scale of the HTS and screened a large 50,000-compounds DIVERSet library using the TNFR1 FRET biosensor. In this study, we discovered a novel small molecule that inhibits TNFR1 signaling through an allosteric mechanism by altering the receptor conformational states. We also provided the first definitive experimental proof of long-range allosteric coupling in the extracellular domain of TNFR1 that can be exploited to inhibit receptor activation. Building upon the above study, in Chapter 5, we found both small molecule activator and inhibitor of TNFR1 from screening of the LOPAC library.

We explored both the activation and inhibition mechanism of these small molecules and discovered that receptor conformational states can act as a molecular switch in determining receptor function. Driven by the motivation to discover potential therapeutics, in Chapter 6, we performed medicinal chemistry to establish a structure-activity relationship (SAR) of a lead compound and improved its potency by more than sixty-fold to the nanomolar range, making it a potential drug candidate.

In the second half of this thesis, we expanded the use of FRET approach in HTS to the investigation of heterogeneity in IDPs, including tau (Chapter 7) and HTT (Chapter 8). We developed novel tau and HTT FRET biosensors that are capable of monitoring oligomer or aggregate conformations as well as being a high-throughput screening platform. Using these technologies, we discovered small molecules that perturb the ensemble of heterogeneous tau oligomers or HTT aggregates and inhibit the self-association of these proteins, resulting in the rescue of cell cytotoxicity. In our future work, we will make use of these technologies as well as develop new technologies to further understand the fundamental of these structured proteins and IDPs for more effective targeting. In addition, we will advance the small molecules discovered from this work to animal studies as well as potential clinical applications.

CHAPTER 1: INTRODUCTION

1.1 Background on protein-protein interactions

Protein–protein interactions (PPIs) are highly specific physical contacts established between different protein molecules because of biochemical events steered by electrostatic forces such as the hydrophobic effect. PPIs are **i**mportant for protein functions, such as protein signaling transduction, and their regulation, in most of the structured proteins. Aberrant PPIs, in particular from intrinsically disordered proteins (IDPs), are the basis of multiple aggregation-related diseases, such as Alzheimer's disease (AD) and Huntington's disease (HD). PPIs have been studied from different perspectives including biochemistry, molecular dynamics, and signal transduction in particular. All the garnered information enables the creation of protein interaction networks that can elucidate the pathology of diseases, as well as the discovery of protein targets of therapeutic interest (*1*).

1.1.1. Structured proteins vs. intrinsically disordered proteins

Structured proteins have a stable tertiary protein structure. They consist of various structural domains, such as binding motifs/domain. For example, members of the tumor necrosis factor receptor (TNFR) family contain an extracellular domain responsible for ligand binding, transmembrane domain that anchors the receptor in the cell membrane and an intracellular domain that mediates activation of signaling pathway (*2*). On the other hand, proteins without stable tertiary structure and have a greater portion of small and hydrophilic amino acids and proline residues, are known as intrinsically disordered proteins. IDPs possess functions that complement functions of structured proteins, and are commonly related to recognition, as well as control and regulation of various signaling pathways (*3*). IDPs are usually tightly controlled via ways

such as alternative splicing, controlled expression and degradation, and post-translational modifications. However, distortions in the regulation and control of IDPs, together with aberrant interactivity are commonly associated with various human diseases (*3*). For both types of proteins, they have dynamic behaviors, with ability to adopt different conformational states. The transitions between these states typically occur on nanoscales, and have been linked to functionally relevant phenomena such as allosteric signaling and enzyme catalysis (*3*). Therefore, studying the protein structural dynamics and associated conformational changes are essential for understanding protein function, and development of targeting strategies.

1.2 TNFR receptor

1.2.1. Background on TNFR1 induced autoimmune diseases

Tumor necrosis factor receptor 1 (TNFR1) is a characteristic member of the TNF receptor superfamily, a family of 27 type I transmembrane receptors (*4*). TNFR1 binds either of its two cognate ligands, tumor necrosis factor (TNF or TNF-α) or lymphotoxin-alpha (LT-α or TNF-β), via its extracellular domain (*5*), which leads to the activation of two distinct, well-understood signaling pathways. While one pathway results in programmed cell death (apoptosis) and programmed necrosis (necroptosis) (*6, 7*), the other leads to an inflammation response (*8*) and cell survival (*9*), mainly through the activation of the transcription factor NF-κB (*10*). TNFR1 is most commonly associated with its inflammatory pathway (*11*) (**Figure 1.1**)**.** Upregulation of both TNF and LT-α ligand level,has been associated with several autoimmune diseases, such as rheumatoid arthritis (RA), juvenile RA, multiple sclerosis, psoriatic arthritis, Crohn's disease, and inflammatory bowel disease (*12-16*). These diseases have impinged on 23.5 million people in the United States, affecting up to 8% of the population (*17*) and

incurred over 50 billion dollars in societal costs (*18*). Therefore, modulation of TNFR is important for therapeutics development for disease.

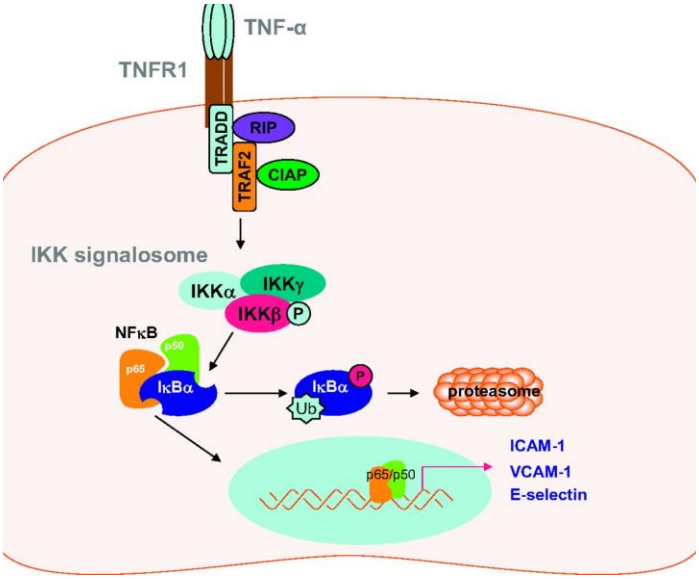

Figure 1. 1. TNFR1 signaling pathways.

The binding of ligand (TNF-α) with TNFR1 causes the recruitment of TNFR-associated via death domain protein (TRADD), receptor-interacting serine or threonine-protein kinase 1 (RIP), and TNFR-associated factor 2 (TRAF2). These molecules form the TNFR1 signalosome. TRAF2 catalyzes the ubiquitination (Ub) of RIP and recruits the IκB kinase (IKK) complex, leading to the phosphorylation (P) of IκBα by IKKβ and the ensuing ubiquitination and degradation of IκBα in proteasome. The release of NF-κB p65 and p50 into nucleus results in the transcriptional activation of the proinflammatory target genes such as ICAM-1, VCAM-1, and E-selectin (*19*).

1.2.2 Current therapeutics and limitations

Anti-TNF therapeutics

Over the past decades, significant work has been done to study the inhibition of the TNFR1-induced NF-κB pathway to reduce the symptoms of the diseases. Currently, the most commonly used treatments are anti-TNF therapeutics such as Etanercept (Enbrel®), Infliximab (Remicade®), Adalimumab (Humira®), Certolizumab Pegol (Cimzia®) and Golimumab (Simponi®) that work based on sequestration of free ligands (*14, 16, 20-22*) (**Figure 1.2A**)**.** However, these treatments are expensive and induce dangerous side-effects, including reactivation of tuberculosis, development of

autoimmune disease and increased susceptibility to infection and lymphoma, mainly due to the removal of membrane TNF (memTNF) by the drugs which disrupt the TNFR2 and memTNF interaction (*23-26*). To resolve these problems and reduce the side effects arising from non-specific inhibition, new therapeutics that inhibit the undesirable signaling cascade resulting from TNFR1 and ligands interactions, while preserving the constitutive signaling from the TNFR2 and memTNF interaction need to be developed. Two novel approaches for specific targeting of the inflammatory effects from TNFR1 and ligands interaction have been developed that include the exclusive inhibition of soluble TNF and the direct blocking of TNFR1 signaling by anti-TNFR1 monoclonal antibodies (*14, 27, 28*)**.** For exclusive inhibition of soluble TNF, researchers have developed signaling-incompetent dominant-negative TNF derivatives (*29*) such as XPro1595 (*30*) that specifically inhibit soluble TNF, hence preserving signaling via memTNF. In addition, a small-molecule inhibitor that promotes subunit disassembly of trimeric TNF has been identified (*31*).

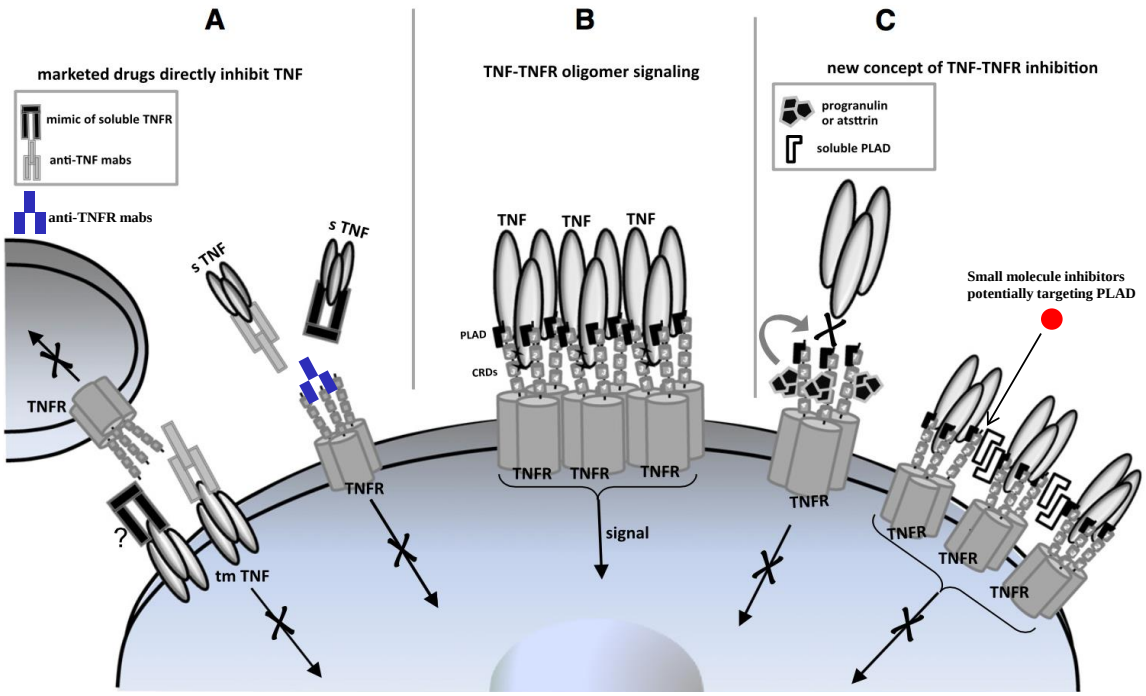

Figure 1. 2. Current therapeutics and the proposed PLAD targeting strategy.

(A) Inhibition by anti-TNF and anti-TNFR monoclonal antibodies, and mimic of soluble TNFR. (B) TNF-TNFR oligomer signaling held together by PLAD. (C) New concept of TNF-TNFR inhibition by potentially targeting the pre-ligand assembly domain (PLAD) by soluble PLAD and small molecules (*32*).

Blocking of ligand binding

For direct blocking and inhibition of TNFR1 signaling, antagonists specific to TNFR1 can be used to neutralize the pro-inflammatory activity of TNF. Examples of TNFR1-specific antagonists and antibodies include R1antTNF (*33*), DMS5540 (*34*), and ATROSAB (*35*). Small molecules that competitively block receptor-ligand interaction between TNFR1 and TNF have also been identified (*36, 37*). The ligand binding affinity of TNFα to TNFR1 is very high (*38*), so small molecules that work by competitively eliminating ligand binding may not be effective. Additionally, it has been suggested that

TNFR1 antagonists that block ligand binding reduce the TNFα neutralizing capacity of soluble TNFR1, as the circulating forms of the receptor may function as decoys for the ligand, and their concentrations may reflect long-term exposure to this proinflammatory cytokine (*39-41*). At low concentrations, soluble TNFR1 enhances the actions of TNFα, but at higher concentrations the effects of TNFα are abrogated (*42*). Furthermore, cell-autonomous interaction between TNFα and TNFR1 is critical for cell survival, maintenance and function as well as neuroprotective (*43, 44*). As such, approaches that do not involve eliminating ligand binding are highly attractive, though have proved elusive.

1.2.3. Potential or novel targeting strategy

PLAD targeting strategy

Despite the advancement of these approaches, there is still tremendous interest in disrupting the protein-protein interaction (*45, 46*), particularly at the interface between the pre-ligand associated receptors known as the pre-ligand assembly domain (PLAD) to directly inhibit TNFR1 activation (*47*), and reduce off-target side-effects. An inhibition model has been proposed where targeting the TNFR1 pre-ligand assembly domain (PLAD) disrupts the pre-ligand associated receptors (*47, 48*). The PLAD is a portion of the extracellular region of TNFR1 that contains the noncovalent interactions responsible for the TNFR1 pre-ligand associated dimer, which has been shown via crystallography (*49, 50*). This association may further results in an oligomeric network structure formed by the receptor and ligand upon activation (**Figure 1.2B**). It is crucial in mediating receptor-chain association essential for signaling and hence an important therapeutic target (*47, 48*). A provisional model has been proposed where soluble PLAD binds to TNFR1, causing a disruption of pre-ligand associated receptors and blocking the

biochemical effect of ligand in *vitro* (*51*), which potently inhibits arthritis in animal models (*52-54*). This motivates the discovery of small-molecule inhibitors that could potentially target TNFR1 PLAD to modulate receptor-receptor and/or receptor-ligand interactions, thereby inhibiting downstream signaling and reducing inflammatory responses (**Figure 1.2C**). Competitively eliminating the PLAD-PLAD interaction is an attractive alternative to blocking ligand binding because the monomer-monomer interaction (low micromolar) is weaker than the ligand-receptor affinity (*55, 56*).

Allosteric modulation by targeting receptor conformational dynamics

Ligand binding induces TNFR1 trimerization, leading to trimerization of cytosolic death domains and concomitant recruitment of downstream signaling machinery (*21, 57*). This model is primarily based off the original crystal structure of a ligand-bound, trimeric receptor complex, in which there are no direct receptor-receptor interactions (*57*). However, it has been found that TNFR1 is actually pre-assembled as high-affinity receptor dimers in the plasma membrane (*55, 58, 59*), where there is no overlap between its ligand-binding and self-assembly domains. Crystal structure and subsequent mutagenesis studies (*55, 58-60*) show that pre-ligand dimerization is driven by well-defined monomer-monomer interactions across the pre-ligand assembly domains (PLAD), located within the N-terminal cysteine-rich domain (CRD1) and far from the ligand binding loop. Critically, there is no evidence to suggest that these dimer structures dissociate on ligand binding, despite the lack of receptor-receptor interactions in the trimeric structure. Instead, it would form an extended hexagonal network in which the vertices are formed by ligand/receptor complexes and edges are formed by receptor dimers (*59*). This model was advocated for TNFR1 (*61-63*). Crosslinking experiments confirmed the formation of high-molecular weight oligomeric complexes of TNFR1 upon ligand binding (*58*), and confocal microscopy have visualized clustering for TNFR1 (*64,*

65). Hence the trimerization model is incomplete as it lacks the explanation on the importance of receptor self-interaction or ligand/receptor network formation. It is possible that the pre-assembled dimer remains intact upon ligand binding, and undergo a conformational change that propagates from the extracellular domain (ECD) to the cytosol without dimer dissociation, and this receptor conformational dynamics can serve as a potential target for inhibitory small molecules.

1.3. Intrinsically disordered proteins

1.3.1 Heterogeneity in intrinsically disordered proteins

Intrinsically disordered proteins such as tau or huntingtin (HTT) are characterized by the exceptional spatiotemporal heterogeneity, where different parts of a protein are ordered or disordered to a different degree, and this distribution is constantly changing over time (*66*). IDPs have a very complex structural organization that includes foldons (independently foldable units of a protein), inducible foldons (disordered regions that can fold at least in part due to their interaction with binding partners), non-foldons (non-foldable protein regions), semi-foldons (regions that are always in a semi-folded form), and unfoldons (ordered regions that have to undergo an order-to-disorder transition to become functional) (*67*). Since these differently disordered structural elements might have well-defined and specific functions, an IDP can be multifunctional, being involved in interaction with or regulation of, and can be controlled by a multitude of structurally unrelated partners. Consequently, the nature of IDP's heterogeneity also limits the identification of specific targets that can modulate its behaviors.

1.3.2 Tau protein

Tau is an intrinsically disordered protein that plays an important role in the regulation of microtubule stability and axonal transport (*68*). Tau has been implicated in

a group of neurodegenerative disorders, or tauopathies, such as AD, where it is characterized by the presence of tau inclusions in affected brain regions (*69*). Under pathological conditions, tau exhibits aberrant behavior where it becomes hyperphosphorylated and detaches from microtubules, thereby accumulating in the cytosol (*70*). This has been correlated with upstream mitochondrial dysfunctions such as in the electron transport system or Krebs cycle, oxidative stress (*71, 72*), as well as neuron morphology and axonal transport defects (*73*). Unbound tau has a tendency to misfold and undergo conformational changes starting with the formation of tau oligomers that subsequently nucleate into paired helical filaments (PHFs), and eventually into intracellular NFTs (*74*) (**Figure. 1.3**). NFTs have been the regarded as the primary causative of tauopathies, where their presence in the brain show significant correlation with the degree of cognitive impairment (*75*). However, recent studies suggest that soluble oligomeric tau promote cytotoxicity *in vitro*, and are linked to cognitive phenotypes *in vivo* (*76-82*), thereby contributing a major role to the induction of neurodegeneration (*78, 83*). As a result, the focus in therapeutic development has begun to shift from targeting large NFTs to inhibiting or disrupting the formation of toxic soluble tau oligomers (*83-86*). Tau oligomers exist as an ensemble of distinct assemblies including both toxic and non-toxic, on- and off-pathway species along the fibrillogenesis cascade (*87-93*). However, no specific toxic tau oligomer species has been isolated or identified to date (*86, 94, 95*). Despite decades of rigorous and focused research, there are currently no significant disease modifying therapies for tauopathies (*96*). Furthermore, there is a dearth of compounds that target tau, with only five out of the 105 small molecules currently in clinical trials being tau-focused (*97, 98*). Hence, there is desperate need for technologies that enable the identification of tau-focused disease-modifying therapies (*98-100*).

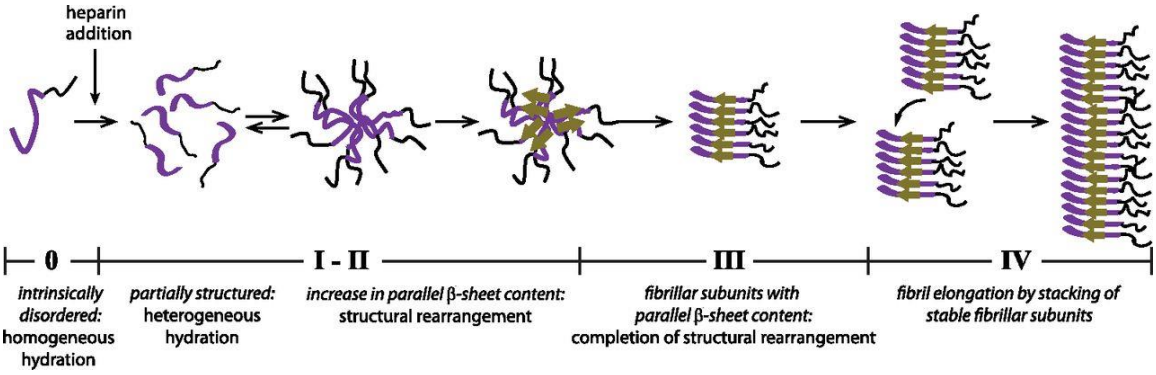

Figure 1. 3. Tau fibrillogenesis cascade.

The intrinsically disordered tau monomer is capable of misfolding into spontaneously formed oligomers, producing toxic assemblies implicated in AD (I-II). While oligomers are metastable and difficult to monitor with high precision and accuracy, the large assemblies (paired helical filaments (PHFs) and neurofibrillary tangles (NFTs) form irreversibly with β-sheet structures (III-IV) (*101*). The fibrillar species can be excreted via exosomes leading to a prion-like cell-to-cell propagation of pathology and may induce seeded oligomerization. NFTs may be neuroprotective by sequestering toxic oligomers and disruption of NFTs may induce toxicity from elevated concentrations of toxic oligomers.

1.3.3 Huntingtin protein

Huntington's disease (HD) is an inherited neurodegenerative disorder caused by expansion of a CAG repeat in the exon 1 of huntingtin (HTT) gene, which translates into an abnormal polyglutamine (polyQ) in HTT protein (*102, 103*). It has the highest prevalence in United States and European countries, with a prevalence of 100 cases per million (*104*). HTT is an IDPs that regulates fast axonal trafficking, vesicle transport (including transport of brain-derived neurotrophic factor (BDNF)) and synaptic transmission (*105*). It also plays an important role in neurons in the brain and is essential for normal fetal development (*106*). HD is caused by an abnormal expansion of CAG

repeats at the exon 1 of the IT15 gene of HTT protein, encoding a polyQ stretch in various proteins (*107*) (**Figure 1.4A**). The wild type protein contains 35 glutamine repeats or less (≤Q35, no pathology) while in the mutant forms the expanded glutamines are more than 35 repeats (Q36-39, late onset; ≥Q40, observed pathology) (*108*) (**Figure 1.4B**). Importantly, the length of the polyQ stretch and the age of disease onset are inversely correlated, with longer stretches resulting in earlier onset and increased severity of the disease(*108-110*). In addition, it has been shown that N-terminal HTT with polyQ tracts in the pathological range (>Q35), but not with polyQ tracts in the normal range (≤Q35), form high molecular weight protein aggregates with a β-sheet fibril morphology (**Figure 1.4C-D**) (*111*).

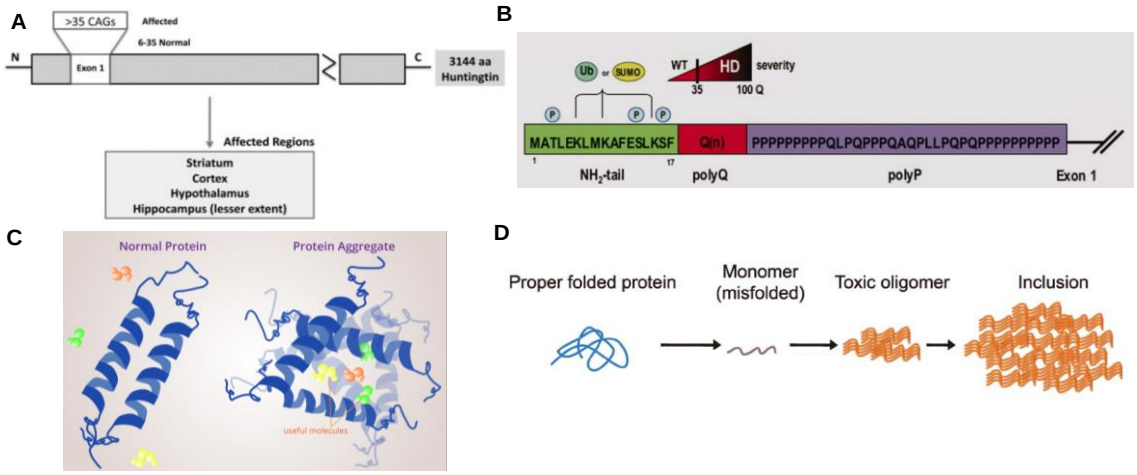

Figure 1. 4. HTT pathophysiology.

(A and B) HD is caused by an abnormal expansion of CAG repeats at the exon 1 of the IT15 gene of HTT protein (*112, 113*). (C) Aggregated proteins forms β-sheet fibrils (*114*). (D) Aggregation cascade of HTT, from misfolding of monomer to toxic oligomer to inclusion bodies (*115*).

Mutant HTT protein disrupts multiple physiological processes leading to homeostasis of apoptotic molecules imbalance, transcriptional dysregulation, autophagy deficits, mitochondrial abnormalities, axonal transport impairment, reduced cellular BDNF support, and glutamate excitotoxicity (*116*) (**Figure 1.5**).

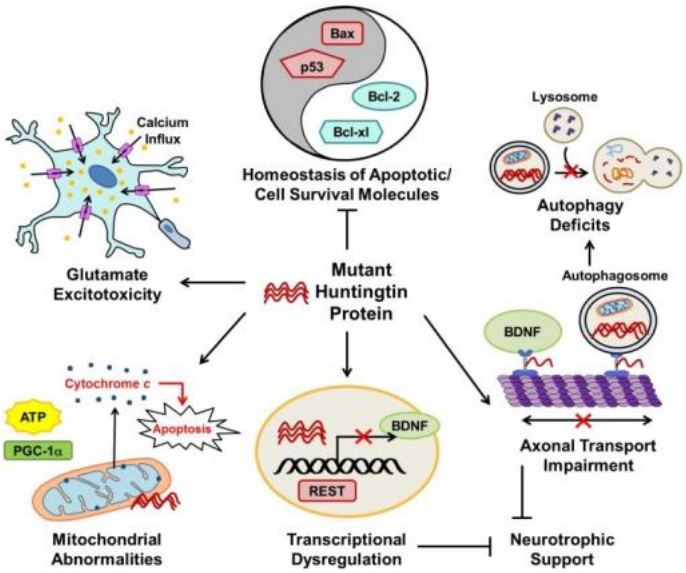

Figure 1. 5. Mutant HTT affects a plethora of cell functions

Consequences of non-specific interaction between HTT and other proteins include cell survival, mitochondrial abnormalities and axonal transport impairments (*117*).

While aggregate formation is regarded as the hallmark of HD (*111, 118*), its effect on toxicity remains debatable. It has been shown that the prominent inclusion bodies (IBs) have been shown to decrease mutant HTT levels elsewhere in the neuron, prolonging cell survival (*119*), suggesting that large contained aggregates may have a neuro-protective response. Instead, there has been strong evidence for the toxicity of monomeric and small oligomeric species of mutant HTT with specific conformational states (*120-130*), but the true toxic species remains unknown (*121, 131-133*). To date, there are still no cures or significant disease modifying therapies available for HD (*103*). While there has been clinical trials of potential compounds acting through indirect mechanism (not directly targeting HTT), there is no ongoing clinical trial of small molecules acting through direct disruption of HTT aggregation, which remains an important area for targeting (*134-136*).

1.3.4. Current therapeutics and limitations

There are numerous recent efforts to discover small molecules that target toxic tau oligomers, with some yielding efficacious compounds (*137-143*). These include curcumin (K_d=3.3 μM; fibrillization IC_{50}=10.6 μM) (*140*), heparin-like oligosaccharides (K_d=140-350 nM; cell cytotoxicity rescued at 10 μM) (*141*), phenothiazines such as methylene blue (MB) and its derivatives Azure A, Azure B and Azure C (K_d=100 nM-3.4 μM; fibrillization IC_{50}=1-10 μM; Azure C rescues cell cytotoxicity at 5 μM) (*137, 138, 142*), and polyphenols such as epigallocatechin gallate (EGCG) (cell cytotoxicity and fibrillization inhibited at 12.5 μM)(*139*). However, only MB has reached phase III clinical trials, although there was no significant improvement in patient cognition reported (*144*). However, all the compounds were were protective only in the low micromolar range (*137-143*). A possible limitation with these studies could be due to poor recapitulation of the cellular environment, where only purified proteins were used, instead of also including numerous chaperone proteins that may be required to produce the ensemble of tau oligomers that populate the fibrillogenesis cascade. Moreover, purified protein assays are only capable of identifying hits that directly perturb tau and unable to elucidate any indirect mechanisms of action.

For HTT, three major classes of screening campaigns - targeted phenotype of aggregation, enhanced clearance and inhibition of cell death have been reported (*145*), including recent efforts in indirect HTT targeting mechanisms (*146*) using antibodies fragments (*147*), antisense oligonucleotides (*148*), and small molecules (*149*). Screens that discovers small molecules directly targeting HTT aggregation identified MB (inhibition of protein aggregation by targeting monomer, oligomer and aggregates tested at 1-100 μM; inhibition of cell cytotoxicity tested at 100 nM) (*150*), C2-8 (inhibition of

protein aggregation IC_{50}=25 μM; inhibition of cell cytotoxicity tested with IC_{50}=50 nM) (*151*), epigallocatechin gallate (EGCG) inhibition of protein aggregation (perturb oligomer conformation with IC_{50}=~1 μM; inhibition of toxicity tested in yeast model of HD (at 500 μM) and HD transgenic flies (at 0.1–100 μM)) (*152, 153*), leflunomide and teriflunomide (inhibition of HTT-Q72-Luc protein aggregation reporter assay with IC_{50}=1–3 μM; inhibition of HTT protein aggregation tested at 100 μM) (*154*), PGL-135 and PGL-137 (inhibition of HTT aggregation with IC_{50}=40 μM (PGL-135) and IC_{50}=100 μM (PGL-137); reduction of inclusion bodies in cells tested at 25 μM (PGL-135) and 50 μM (PGL-137)) (*155*), congo red (inhibition of HTT aggregation with IC_{50}=0.3 μM) (*129, 156*), thioflavin-S (inhibition of HTT aggregation with IC_{50}=20 μM) (*156*), and xyloketal derivatives (inhibition of HTT aggregation tested in *Caenorhabditis elegans* model of HD at 100 μM) (*157*). However, none of these compounds has successfully advanced to become an effective therapeutic, and the small molecules MB and EGCG have also been reported in tau screens and are hence promiscuous compounds. All the molecules were initially identified through direct measurements of HTT aggregation and disaggregation, and lack the monitoring of and information on the HTT conformational changes or dynamics. The targeting of HTT conformations has only recently been proposed, and efforts have focused on repurposing some of the previously identified small molecules such as MB (*150*), EGCG (*152*) and congo red (*129*). Similar to the tau screens, most of the studies were also performed using *in vitro* purified protein assays, which do not reliably represent the cellular environment, and faces similar limitations of identifying hits that only directly perturb HTT protein, but not able to distinguish indirect mechanisms of action, affecting other pathologically relevant cellular processes. Hence,

a cellular approach that monitors HTT aggregation holds promise as a novel HTS platform to discover more effective therapeutics.

1.4. Proposed targeting strategy

1.4.1 Small molecule drug discovery through high-throughput screening (HTS)

HTS of small-molecule compounds to identify modulators of molecular targets is a mainstay of pharmaceutical development. Increasingly, HTS is being used to identify chemical probes of signaling pathways and cell functions, with the ultimate goal of establishing the relationship between chemical structures and biological activities. The majority of the conventional assays capable of quantifying intermediate signal transduction events are limited to biochemical assays, immunoassays, and complex image-based assays (*158*). However, these technologies generally suffer from the lack of biological relevance, excessive hands-on time, and lack of adequate signal-to-noise and reproducibility required for HTS applications (*158*). Therefore, there is a need for new methods of HTS to produce rich data sets that can be immediately mined for reliable biological activities, thereby providing a platform for chemical genomics and accelerating the identification of leads for drug discovery (*159*). Examples of TNFR1-related HTS include the development of two homogenous TNF-α assays based on homogenous time resolved fluorescence and AlphaLISA (*160*). In addition, a high-throughput NF-κB b-lactamase reporter gene assay has been used to identify nineteen drugs that inhibit NF-κB activation possibly through inhibition of TNFR1-activated pathway (*161*). Bioluminescence resonance energy transfer (BRET) is also a method associated with HTS. To study the interaction between two proteins by BRET, the first protein is genetically fused to energy donor, and the second protein is fused to an energy acceptor. The two proteins are then co-expressed in cells, and the BRET signal

is measured as a readout of molecular proximity. While BRET can detect PPIs in all cellular compartments, it does not experimentally distinguish between dimeric or multimeric interactions and cannot provide information on subcellular sites of interaction (*162*). Time-resolved fluorescence resonance energy transfer (TR-FRET) has also been proposed to study PPIs, and offers advantages such as high resolution conformational sensitivity and high-throughput recording (*163*). Hence, TR-FRET may be a good tool for the detection of TNFR1 receptor-receptor interactions and conformational dynamics as well as IDP self-association.

1.4.2 Structure based drug design through medicinal chemistry

From high-throughput screening of a library containing of thousands of small molecules, hundreds of hits are potentially expected (*164*). The hits have to undergo an inherently multi-objective optimization process to develop a drug that satisfies the key objectives of safety and efficacy. Their structures are listed, analyzed and clustered to obtain a molecular scaffold, which is a fixed part of a molecule where functional groups are substituted or exchanged. There are many proposed ways to generate a SAR library, such as using NMR spectroscopy, computer-aided drug design (CADD) or medicinal chemistry structure-based drug design (SBDD). NMR spectroscopy is limited by constraints on the molecular size of the protein and the requirement for multiple isotopic labeling and uncertainty in the identity or location of protein or ligand atoms. Crystallization (for X-ray structure determination) may change the structure of the ligand-protein interaction (*165*). CADD techniques uses prototypical ligand based approaches (LBDD) including quantitative structure−activity relationships models or pharmacophore based models and use physicochemical properties and conformational preferences to explain the variation in SARs. However, ligand-based approaches can only be used

when sufficient activity data are available, and their utility for pose prediction depends on the availability of the bioactive conformations of one or more active compounds. For example, a receptor may have more than a single active site and may adapt to different ligands, and multiple pharmacophores may be possible for a single site. Furthermore, selecting a model that reflects the biochemical reality is a difficult issue, as selection criteria that use statistical significance alone might lead to erroneous model prioritization from a pool of possible models. Overall, CADD is limited in the case of scoring functions, such as incorporating molecular flexibility and solvent effects, targeting receptors with little to no structural information, increasing computational efficiency and limited accuracy in virtual screening (*166*).

Determination of the molecular scaffold is more cost-effective if done earlier in the drug discovery process because it drastically affects the SAR. However, the main challenge is to understand how to choose a suitable scaffold, because there is no direct or obvious set of criteria for scaffold identification. Nonetheless, there are still general frameworks that can be adopted to better identify the scaffold, such as Maximum Common Substructure clustering method (*167*), Murcko Framework (*168*), and Scaffold Tree (*169*), which are robust and effective (*170*). Once the scaffold is determined, the functional groups around the scaffold can be substituted or exchanged by ways of hit evolution, bio-isosteric replacements and hit fragmentation (*171*) to determine the SAR. Examples of TNFR1-related SAR studies include a series of *N*-alkyl 5-arylidene-2-thioxo-1,3-thiazolidin-4-ones which are antagonists of TNF-α binding to TNFR1 (*36*) and a series of coumarin-based TNF-α inhibitors (*172*). Therefore, medicinal chemistry based SAR is essential for structure-based drug design.

CHAPTER 2: FLUORESCENCE BASED TNFR1 BIOSENSOR FOR MONITORING OF RECEPTOR STRUCTURAL AND CONFORMATIONAL DYNAMICS AND DISCOVERY OF SMALL MOLECULE MODULATORS

Chih Hung Lo[1], Tory M. Schaaf[2], David D. Thomas[2,3] and Jonathan N. Sachs[1*]

Manuscript to be submitted to *Methods in Molecular Biology*

[1]Department of Biomedical Engineering, [2]Department of Biochemistry, Molecular Biology and Biophysics, University of Minnesota, Minneapolis, Minnesota 55455

[3]Photonic Pharma LLC, Minneapolis, MN 55410

Author contributions: C.H.L. wrote the manuscript. T.M.S, D.D.T and J.N.S. provided comments and edits to the manuscript.

2.1 Summary

Inhibition of tumor necrosis factor receptor 1 (TNFR1) is a billion dollar industry for treatment of autoimmune and inflammatory diseases. As current therapeutics of anti-TNF leads to dangerous side effects due to global inhibition of the ligand, receptor-specific inhibition of TNFR1 signaling is a highly sought after strategy. To directly monitor the receptor structural and conformational changes, we engineered a fluorescence resonance energy transfer (FRET) biosensor by fusing green and red fluorescent proteins to TNFR1. Expression of the FRET biosensor in living cells allows for detection of receptor-receptor interactions and receptor conformational dynamics. Using the TNFR1 FRET biosensor, in conjunction with a high-precision and high-throughput fluorescent lifetime detection technology, we developed a time-resolved FRET-based high-throughput screening platform to discover small molecules that

directly target and modulate TNFR1 functions. Using this method in screening multiple pharmaceutical libraries, we have discovered a competitive inhibitor that disrupts receptor-receptor interactions and allosteric inhibitors that alter the conformational states of the receptor. This enables scientists to conduct high-throughput screening through a biophysical approach with relevance to compound perturbation of receptor structure and conformations, for the discovery of novel lead compounds with high specificity for inhibition of TNFR1 signaling.

2.2 Introduction

Tumor necrosis factor receptor 1 (TNFR1) is a membrane receptor in which its activation is most commonly associated with the signal transduction to induce inflammation (*5*). Upon ligand stimulation by tumor necrosis factor-alpha (TNFα) or lymphotoxin-alpha (LTα), the downstream signaling complex inclusive of receptor interacting protein-1 (RIP1), TNF receptor-associated death domain (TRADD) and TRAF2 is recruited and further led to the degradation of the inhibitor of nuclear factor Bα (IκBα) and the activation of nuclear factor κB (NF-κB) (*11*). Over-activation of TNFR1 results in excessive NF-κB activation which has been associated with several autoimmune diseases such as rheumatoid arthritis (*173*). Therapeutic targeting of TNFR1 signaling is a billion-dollar industry (*17*). Current therapeutics include anti-TNF which are antibodies that sequester free ligand (*15, 21*). However, global inhibition of ligand can cause severe side effects such as reactivation of tuberculosis, increased risk of inflammation or lymphoma (*15, 25, 174*). This is primarily due to the off-target inhibition of TNFR2, which mediates immune modulatory functions (*175*). Hence, there is a need for TNFR1-selective inhibitors that specifically block TNFR1 signaling without interfering other receptors (*39*).

To achieve this, novel therapeutics that bind and target TNFR1 directly are needed in order to exert the receptor-specific effects. Previous reports include small molecules that bind the receptor and prevent ligand binding (*35-37, 176*). In addition, the isolated soluble pre-ligand assembly domain (PLAD) of TNFR1 was shown to inhibit TNF-α induced inflammatory signaling *in vitro* and to ameliorate arthritis in a mouse model and the proposed mechanism is that the PLAD protein disrupted receptor-receptor interactions (*52*). However, this study showed the soluble GST-tagged PLAD protein ablated ligand binding, making it unclear whether the small protein was targeting the PLAD and disrupting the pre-ligand receptor dimer (*52*). Furthermore, it has been suggested that a non-competitive targeting strategy may be more effective in inhibiting protein or receptor function (*177-179*). To make progress in these therapeutic windows, it requires the field to exploit the understanding of the structure and dynamics of the receptor for therapeutic developments (*62, 180-184*). A small molecule (F002), which was discovered by computational design, binds to a cavity distal to the ligand binding loop and perturbs the ligand binding residue of tryptophan 107 (W107), leading to allosteric inhibition of TNFR1 signaling (*38*). Even though the F002 does not directly prevent ligand binding to the receptor, the movement of the ligand binding residue induced by the small molecule results in weakened ligand affinity for the receptor and reduced effective ligand stimulated signaling. Moreover, the functional efficacy of F002 is sixty-fold weaker than its binding affinity, suggesting that this small molecule perhaps competes with ligand binding and may not be truly allosteric. Hence, there is still potential to discover more effective allosteric small molecules that inhibit TNFR1 signaling by neither ablating ligand binding nor disrupting receptor-receptor interactions.

While the crystal structures of TNFR1 have been available for the past two decades (*57, 59*), there is a lack of effort towards targeting the receptor, based on

information for its structure and dynamics. Here, we engineered a TNFR1 FRET biosensor that detects compounds that directly alter the structure or the conformational status of the receptor by measuring the distance between the receptor monomers (**Figure 2.1A**). Here we present a FRET-based high-throughput screening (HTS) assay, using the TNFR1 FRET biosensor in conjunction with a fluorescence lifetime detection technology, the probability of finding novel chemical structures that directly perturb the receptor for lead development rather than any indirect effect on the inhibition of NF-κB activation is drastically increased.

The FRET-based HTS assay to discover receptor-specific small molecules targeting TNFR1 is enabled by high density well plates (384 or 1536 wells) containing the TNFR1 FRET biosensor in conjunction with fluorescence lifetime readout using a direct waveform recording method incorporated in a fluorescence lifetime plate-reader (FLT-PR) (*185*). This nanosecond time-resolved fluorescence spectrometer acquires fluorescence decay waveforms from each well of a 384-well microplate in 3 minutes with signal-to-noise exceeding 400 (*186*). In addition, lifetime measurements are 5- to 30-fold more precise than the simultaneously acquired intensity measurements (*163, 186*). Furthermore, waveforms acquired in 0.1 seconds, by 1000 laser pulses with the FLT-PR instrument were of sufficient precision to analyze two samples having different lifetimes, resolving minor components with high accuracy with respect to both lifetime (nanosecond decay rate of the fluorescent molecule) and mole fraction (existence of multiple species with different lifetime that depict multiple structural states of the TNFR1 biosensor) (*187*). Concurrent to the lifetime measurements, we also record a complete high-quality fluorescence emission spectrum on a well-by-well basis using a spectral unmixing plate reader (SUPR). While SUPR can give an accurate quantitation of FRET of an intramolecular FRET system (fluorophores attached to the same protein), its

application on an intermolecular system (fluorophores attached to the separate protein) requires further testing (*188, 189*). Hence, we have primarily used the new SUPR technology to filter fluorescence compounds in the screening libraries for this intermolecular FRET biosensor.

In this FRET assay, changes in FRET (either increase or decrease) correspond to structural or conformational changes of TNFR1, induced by the compounds. However, it does not give a functional readout of the effect of the compounds on receptor signaling. Hence, the FRET assay has to be coupled with other functional assays such as NF-κB activation luciferase assay, as well as other biochemical and biophysical assays to validate the functional and mechanistic effects of the hit compounds. Using this approach, we have screened multiple chemical libraries including the NIH clinical collection (NCC), library of pharmaceutically active compounds (LOPAC) and ChemBridge DIVERSet. We have discovered compounds that inhibit TNFR1 signaling by disrupting receptor-receptor interactions (zafirlukast) (*190*) or altering the conformational states of the receptor (e.g. DS42) (*191*). Interestingly, we have also found a small molecule activator that perturbs the receptor conformational dynamics (unpublished results). Putting these findings together, we have suggested that the conformational states of TNFR1 can act as a molecular switch in determining receptor function and the TNFR1 FRET biosensor is a useful and important technology to study the structure and conformations of the receptor.

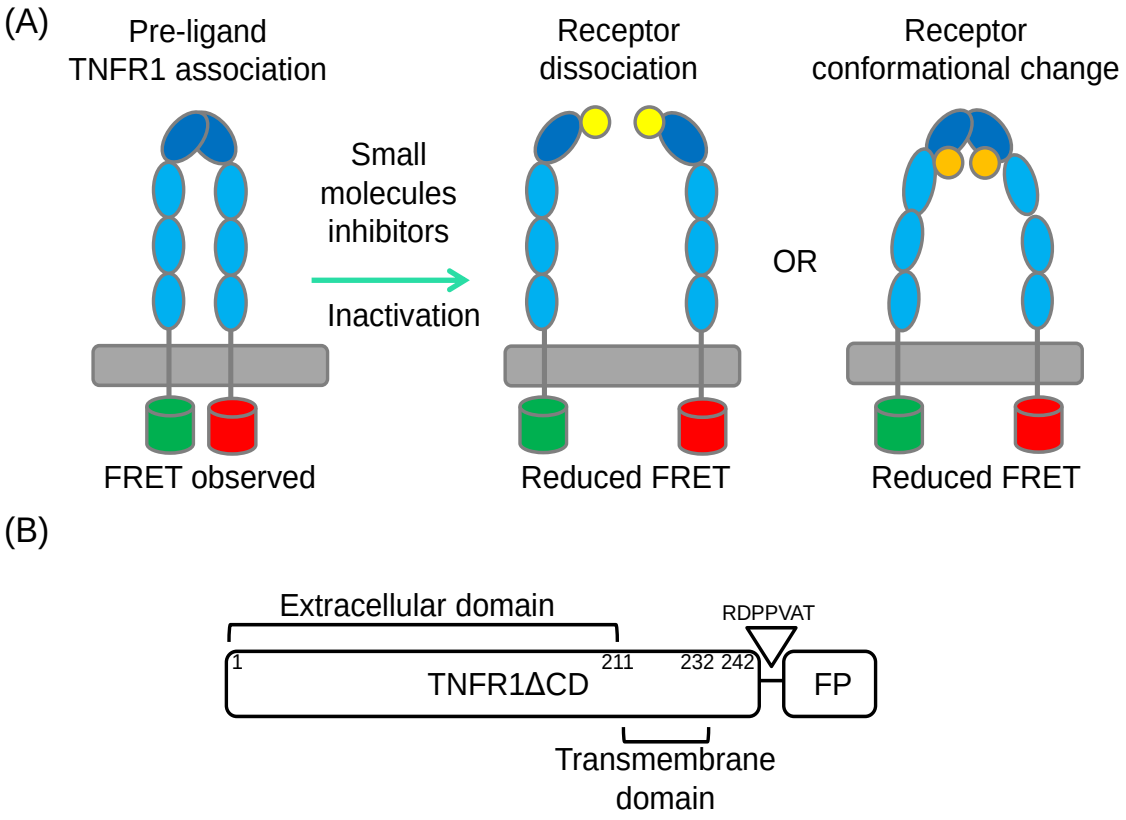

Figure 2. 1. Schematic representation of the TNFR1 FRET biosensor.

(A) FRET is observed when the receptor dimerizes or adopts a close conformation and the fluorophores are in close proximity to each other. Treatment with small molecule inhibitors lead to either disruption of receptor-receptor interactions (yellow compound) or perturbation of the receptor conformational states (orange compound) and both result in reduced FRET as the receptor monomers are further apart. (B) Plasmids encoding the TNFR1 gene of interest fused to the fluorescent proteins (FP) used for transfection of the TNFR1 FRET biosensor into mammalian cells.

2.3. Materials

2.3.1. Scientific Equipment

1. Fluorescence lifetime plate-reader (Fluorescence Innovations, Minneapolis, MN, USA).
2. Spectral unmixing plate-reader (Fluorescence Innovations, Minneapolis, MN, USA).
3. EVOS-FL cell imaging system (Thermo Fisher Scientific, Waltham, MA, USA).
4. FACSAria II flow cytometry equipment (BD Biosciences, San Jose, CA, USA).
5. Olympus IX2 inverted confocal fluorescence microscope equipped with a FluoView FV1000 laser scanning confocal head and 60× (1.42NA) oil immersion objective lenses (Olympus, Waltham, MA, USA).
6. Mosquito HV liquid handler (TTP Labtech Ltd., Hertfordshire, UK).
7. Multidrop Combi reagent dispenser (Thermo Fisher Scientific, Waltham, MA, USA).
8. Echo Acoustic Liquid Dispenser (Labcyte, San Jose, CA, USA)

2.3.2. Plasmid DNA, Cell Culture, Transfection, and Small-Molecule Treatments

1. Plasmid DNA: The TNFR1ΔCD-GFP plasmid was cloned in a custom expression vector (pRH132 vector) with EF-1 alpha promoter and puromycin mammalian selection marker and the TNFR1ΔCD-RFP was cloned in pRFP vector with CMV promoter and neomycin mammalian selection marker (**Figure 2.1B**) (see Note 1).
2. Plasmids preparation: Following the manufacturer's protocol from plasmid maxiprep kit. Resuspend plasmid DNA in autoclaved and 0.2 μm filterd water at a concentration of 0.5 μg/μL. Determine DNA concentration using Cytation 3 imaging reader.

3. HEK293.2sus cells (ATCC): Maintain and culture in an incubator at 37 °C in 5% CO_2, and routinely passage with sterile technique in a cell culture biosafety hood (*see* Note 2).
4. Complete Dulbecco's Modified Eagle Medium (DMEM) cell culture media: phenol red-free DMEM supplemented with heat-inactivated 10% fetal bovine serum (FBS), 2 mM L-glutamine, 100 U/ml penicillin and 100 μg/ml streptomycin. (*see* Note 3).
5. Mammalian cell antibiotic selection: Aliquoted stocks of puromycin (10 mg/mL) and geneticin (50 mg/mL) can be store up to a year at −20 °C. Puromycin (0.5 μg/mL for selection and 0.25 μg/mL for maintenance) and geneticin (500 μg/mL for selection and 250 μg/mL for maintenance) are freshly diluted in complete DMEM media prior to use.
6. Lipofectamine 3000™.
7. Serum-free Opti-MEM™ media.
8. TrypLE™ Express.
9. Cell culture centrifuge.
10. Sterile phosphate buffered saline (PBS).
11. Trypan blue solution (0.2 μm filtered).
12. Sterile cell strainer with 70 μm nylon mesh.
13. Cell counter with function to check cell viability (e.g. automated cell counter (Countess, Invitrogen).
14. Sterile dimethyl sulfoxide (DMSO).
15. Drug plates containing libraries of chemical compounds such as from NIH clinical collection (NCC), library of pharmaceutically active compounds (LOPAC) or

ChemBridge DIVERSet 50,000 compounds. (*see* Note 4). These drug plates are frozen at -20 °C prior to screening.

2.4. Methods

2.4.1. Generation of stable cell lines expressing TNFR1-GFP only or TNFR1-GFP/RFP (TNFR1 FRET biosensor)

This section describes a method for generating a stably expressing TNFR1 FRET biosensor that can be expanded and directly used for FRET measurements by acquiring the fluorescence lifetime. We describe the use of adapted HEK293.2sus cells and transfection with the Lipofectamine 3000™ reagent, but other cell lines and analogous approaches for introducing plasmids into mammalian cells should work equally well. Co-transfection of the FRET biosensor plasmids with orthogonal antibiotic selection allows for high stringency in selecting high TNFR1-GFP and TNFR1-RFP co-expressing cells.

1. Start with a healthy and low passage adapted HEK293.2sus cell culture. Split one million cells per well in a 6-well or 35 mm plate.
2. After 24 h, confirm that HEK293.2sus cells have attached and are evenly distributed in the 6-well plate under bright field of a light microscope. Transfect these cells with Lipofectamine 3000™, following manufacturer's protocol (*see* Note 5).

   For the transfection, we prepare two 1.5 mL tubes prefill with serum-free Opti-MEM™ media. To one tube, we mix the TNFR1-GFP only or TNFR1-GFP/RFP (1:6 ratio) (total DNA is 2.5 μg) and 5 μL of P reagent (2 μL/μg of DNA used) from the transfection kit to the Opti-MEM™ media. To the other tube of Opti-MEM™ media, we add 7.5 μL of the Lipofectamine 3000™ (3 μL/μg of DNA used). We then mix

both tubes, vortex gently and incubate at room temperature for 15 min. After the incubation, add this mixture dropwise to the HEK293.2sus cells in the 6-well plate.

3. After 6 h, gently remove media on cells and replace with fresh growth media.
4. Allow cells to express the TNFR1-GFP only control or the TNFR1 FRET biosensor from the transfected plasmids for 48 h. Confirm this expression and a >90% transfection efficiency with fluorescent microscopy using EVOS-FL cell imaging system. Successful transfection should show fluorescent signal in both the green and red channel as well as the merged channel (**Figure 2.2A**). Very gently transport the plate to and from the incubator, as the cells are liable to detach very easily at this stage. (*see* Note 6)
5. Trypsinize and count HEK293.2sus cells from a healthy transfected culture. Mix 1×10^3 cells with 20 mL of fresh growth media supplemented with puromycin and geneticin. Plate these cells into a 96-well plate with 5-10 cells per well in 200 μL volume with 0.5 μg/mL puromycin and 500 μg/mL genecitin for selection. Multiple 96-well plates can be used. As a control, an untransfected 6-well plate of cells is also split into growth media containing puromycin and geneticin. The cells in this control should not survive the puromycin selection because they are not transfected, and in contrast the transfected cells should fluoresce green and proliferate under the same puromycin selection conditions. (*see* Note 7).
6. Check cells undergoing puromycin selection daily. If there are many unhealthy or unattached cells in the culture, gently wash away the debris from attached growing cells by removing the media and replacing with fresh growth media containing puromycin and geneticin.

7. Cell lines should be expanded and grown under puromycin and geneticin selection for a minimum of 1–2 weeks. The resulting stable cell lines should also be evaluated by flow cytometry to confirm a high population of cells expressing the TNFR1 FRET biosensor (**Figure 2.2B**) as well as their proper folding and trafficking to the cell membrane (**Figure 2.2C**) (*see* Note 8). At this point, cells can be frozen in 10% DMSO in FBS as freezer stocks for storage at −80 °C overnight and in liquid nitrogen for long term (*see* Note 9).

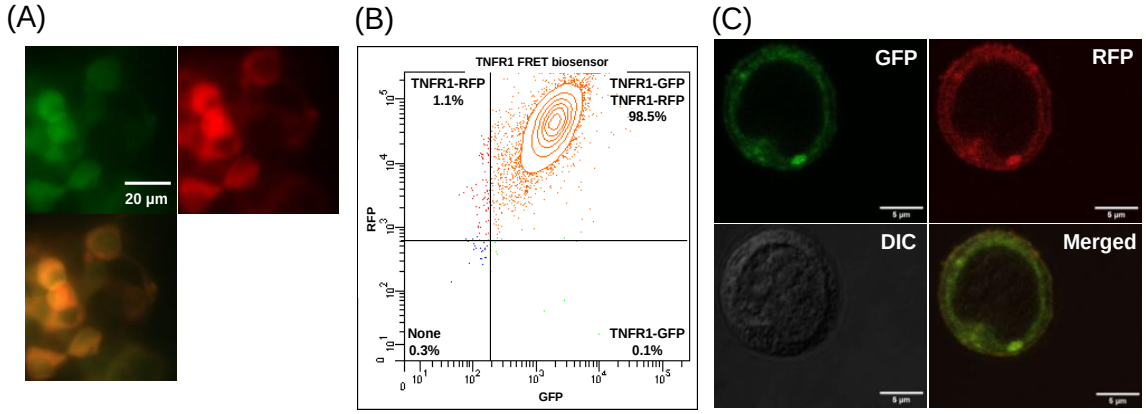

Figure 2. 2. Characterization of the TNFR1 FRET biosensor.

(A) Fluorescence microscopy images of HEK293.2sus cells stably expressing the TNFR1 FRET biosensor with co-localization of both TNFR1-GFP and TNFR1-RFP. (B) Flow cytometry analysis of the stable cells expressing the TNFR1 FRET biosensor shows that nearly all cells contain both TNFR1-GFP and TNFR1-RFP. (C) Confocal microscopy images showing the GFP, RFP, DIC and merged channel of the stable cells expressing TNFR1 FRET biosensor indicates the co-localization of TNFR1-GFP and TNFR1-RFP at the cell membrane.

2.4.2. Preparation of the FRET biosensor for HTS

1. Four days prior to each screening, vials containing the frozen stock of the stable TNFR1ΔCD-GFP (donor-only control) or TNFR1-GFP/RFP (TNFR1 FRET

biosensor) cells are thawed and plated in two 225 cm^2 flasks to ensure the same passage of cells are used in screening (*see* Note 10).

2. After 24 h, the cells are expanded into six 225 cm^2 flasks to obtain sufficient number of cells for screening.
3. The cells are lifted from the 225 cm^2 flasks by incubating with 6 mL of TrypLE™ Express for 5-10 min followed by neutralization with 6 mL of complete DMEM media and harvested in 50 mL conical.
4. The cells are then washed three times in PBS by centrifugation at 300 g and resuspending in 20 mL of PBS
5. Each tube of cells in PBS is filtered using 70 µm cell strainers into a glass flask.
6. Cell viability was assessed using trypan blue assay with viability above 95%.
7. A small aliquot of the cells goes through flow cytometry measurement to confirm that the expression of TNFR1ΔCD-GFP and TNFR1-GFP/RFP (TNFR1ΔCD-FRET pair) in stable cells is above 95%.
8. The cells are counted and diluted to one million cells/mL using an automated cell counter.
9. After resuspension and dilution in PBS, the stable cells were constantly and gently stirred using a magnetic stir bar at room temperature, keeping the cells in suspension and evenly distributed to avoid clumping.

2.4.3. High-throughput screening in 384-well or 1536-well plates

1. The fluorescence lifetime plate-reader utilizes a 473 nm microchip laser for excitation of the GFP fluorescence and a 488 nm long pass filter, as well as a 517/20 nm band pass to filter the emission. The 473-nm passively Q-switched microchip laser (Concepts Research Corporation, Italy) delivers highly reproducible and high-energy

pulses (~1 µJ) at a 5-kHz repetition rate. A full fluorescence decay waveform was detected in response to each laser pulse over a 128-ns time window, using a photomultiplier module from Hamamatsu (Bridgewater, NJ; cat. H10720-210) and a proprietary transient digitizer from Fluorescence Innovations (Minneapolis, MN). A 488-nm long-pass filter from Semrock (Rochester, NY) and 517/20 bandpass emission filter were used, ensuring that only emission from the GFP donor was detected. A 488-nm dichroic mirror directed fluorescence signal toward the PMT (lifetime mode) or spectrograph (spectral mode) using a fiber-optic cable (*see* Notes 11 and 12).

2. The instrument response function (IRF), acquired by recording scatter from 0.31-µm latex microsphere suspensions (Thermo Fisher Scientific).(*see* Note 13)
3. The spectral unmixing plate-reader provides direct high-throughput detection of the complete fluorescence emission spectrum (emission vs. wavelength), with excitation provided by a 473-nm continuous wave laser. Spectra are recorded using a grating-based fiber-optic input spectrograph equipped with linear-array CCD detector (Sony ILX511B; Sony, Tokyo, Japan). The recorded wavelength range in these experiments spanned the entire visible spectrum, but only the 500- to 700-nm range was used in the data analysis.
4. On the day of screening, the compound plates were equilibrated for 30 minutes at room temperature (25 °C).
5. The fluorescence measurement of a 384 well plate containing only the TNFR1 FRET biosensor without any compounds is conducted before any drug treatment. This is to ensure that the signal intensity (**Figure 2.3A**), coefficient of variation (**Figure 2.3B**) and the lifetime of the biosensor giving the basal FRET level (**Figure 2.3C**) is excellent for HTS.

6. Cells (50 µl/well at one million cells per mL concentration) were dispensed by a Multidrop Combi Reagent Dispenser into the 384-well assay plates containing the compounds.
7. Once the drug plates are equilibrated to room temperature (25 °C), cells are dispensed over the drug plates for incubation.
8. The cells and compounds are incubated at room temperature for 2 hours before readings were taken by the fluorescence lifetime and spectral unmixing plate-reader (*see* Note 14).

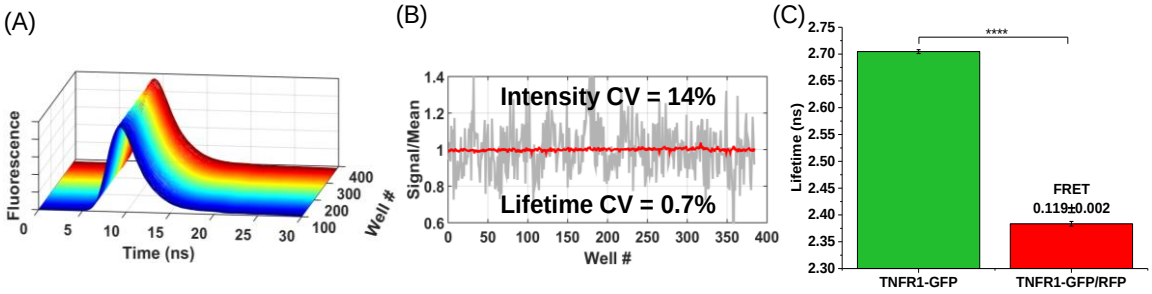

Figure 2. 3. FRET measurements of TNFR1 biosensor using fluorescence lifetime technology.

(A) The fluorescence decay waveforms from a 384-well plate containing the stable cells expressing TNFR1 FRET biosensor. Very little variations between the fluorescence decay waveforms are observed. (B) A comparison between the coefficient of variation (CV) between the intensity vs. the lifetime based FRET measurements. The CV of the lifetime measurement is 20 times less than the intensity measurements, making it an excellent approach for high-throughput screening assay and allowing better selection of hits. (C) Fluorescence lifetime measurement for the stable cells expressing TNFR1 FRET biosensor and the calculated FRET obtained from the measurement.

2.4.4. Data analysis and selection of hits

1. Time-resolved fluorescence waveforms for each well are fitted to single-exponential

decays using least-squares minimization global analysis software (Fluorescence Innovations, Inc.) to give donor lifetime (τ_D) and donor-acceptor lifetime (τ_{DA}).

2. FRET efficiency (*E*) was then calculated based on Equation 1.

$$E = 1 - \left(\frac{\tau_{DA}}{\tau_D}\right) \qquad Eq.1$$

3. Fluorescent compounds are flagged as potential false positives due to interference from compound fluorescence by the spectral recording method based on the assessment of the similarity index of each well from the screening plates obtained from the spectral unmixing waveforms (*188*).
4. Once the data are fitted using a custom MATLAB analysis software or Fluorescence Innovation Data analysis software. This software trasnforms the lifetime and spectral data into a easy to use excel spreadsheet which is generated with columns including index, row and column number, compound ID, lifetime, FRET, spectral ratio and similarity index.
5. After removal of fluorescent compounds, a histogram of the average FRET distribution from all compounds in the screens was processed and fitted to a Gaussian curve to obtain a mean and standard deviation (SD).
6. A hit was defined as a compound that changed the average FRET efficiency by more than three times the standard deviation (3SD) relative to the mean (*see* Note 15).
7. Assay quality was determined with hit compounds as positive controls and DMSO as negative controls and calculated based on Equation 2 (*192*).

$$Z' = 1 - \frac{3(\sigma_p + \sigma_n)}{|\mu_p - \mu_n|} \qquad Eq.2$$

where σ_p and σ_n are the standard deviations (SD) of the observed τ_{DA} values, and μ_p and μ_n are the mean τ_{DA} values of the positive and negative controls. To make this

metric less sensitive to strong outliers, we utilized the normalized median absolute deviation (1.4826*MAD) and median in place of the standard deviation and mean, respectively (*193*). (*see* Note 16).

Table 2. 1. Reference compounds and their FRET EC_{50} values, Z' and functional NF-κB activation IC_{50} values obtained from NCC and DIVERSet HTS using the TNFR1 FRET biosensor in the 384-well format.

Compound	FRET EC_{50} (μM)	Z' (200 μM)	NF-κB activation absolute IC_{50} (μM)	References
Zafirlukast	18.2	0.76±0.02	48.0	(*190*)
DS42	101.7	0.63±0.03	49.8	(*191*)

2.5. Notes

1. We describe the fusion of TNFR1 with truncated cytosolic domain (TNFR1ΔCD) to GFP and RFP but other fluorophores such as the red-shifted orange and maroon fluorescent proteins (OFP and MFP) FRET pair can be used too with adjustment to the respective lasers and filters required to measure the fluorescence waveforms of these proteins (*185*). Alternatively, chemical dyes (Alexa Fluor 488 or 562) can also be used to label the receptor at region of interactions (e.g. PLAD) for fluorescence lifetime measurements.
2. We describe the use of HEK293.2sus cells which are suspension cells. In our study, we titrated FBS to the cells to allow them to become adapted cells that adhere to the surface of the cell culture plates or flasks for ease of transfection (*194*). Other suspension or adherent cell lines may be used with some optimization required to obtain a good FRET signal.
3. Phenol-red free media is used for cell culture as it avoids the risk of fluorescence interference of the lifetime measurements. Unwashed media will not interfere with the fluorescence reading. Phenol red media can still be used but the user has to

make sure that the cells are washed thoroughly with PBS and there is no interference in the reading by any leftover media.

4. The chemical libraries (NCC, LOPAC, ChemBridge DIVERSet, etc.) was purchased and formatted into 96-well mother plates using a FX liquid dispenser, and subsequently formatted across 384 well plates at 50 nl or 1536 well plates at 5 nl (10 μM final concentration per well) using an Echo liquid dispenser. DMSO (matching %v/v) was loaded as in-plate no-compound controls as well as in column 1, 2, 23 and 24 of the 384 well plates or column 1, 2, 23, 24, 25, 26, 47 and 48 of the 1536 well plates (negative controls). The flat, black-bottom polypropylene plates (384w: PN 781209, Greiner Bio-One) were selected as the assay plates for their low auto-fluorescence, and low inter-well cross-talk. The plates were sealed and stored at −20 °C until use.
5. We describe transfection with the Lipofectamine 3000™ reagent, but analogous approaches such as using calcium phosphate, electroporation or lentivirus for introducing plasmids into mammalian cells work equally well. These protocols should be optimized by the FRET efficiency observed when different method of transfection is adopted.
6. The lifetime measurements of the TNFR1-GFP donor-only cell line is required to act as a control in determining the lifetime of the GFP fluorophore when it is not in close proximity to an acceptor fluorophore (e.g. RFP) or when there is no energy transfer. The lifetime of both the donor-only and the donor-acceptor samples are needed in the calculation of FRET using Equation 1.
7. We describe creation of stable cell line using the dilution method but other methods of creating stable cell line such as using lentivirus can also be used. Characterization

of the stable cell line has to be performed to ensure the quality of the TNFR1 FRET biosensor.

8. Western blotting can also be performed to ensure the gene of interest and the fluorophores are expressed. Western blot should indicate the correct molecular weight of the receptor and that there is no protein degradation due to attachment of the fluorescent proteins.
9. Our frozen stock of the FRET biosensor has been made more than 4 years ago. We thaw the frozen stock to check on the expression of the FRET biosensor at least once a year and ensure that they are still functional. We suggest users to do the same routine check at least once a year. When a drift in the expression of the FRET biosensor is observed, exposure of the cells to respective antibiotic may restore the expression. Alternatively, fluorescence-activated cell sorting (FACS) on the cell line can be performed to select the cells with co-expression of TNFR1-GFP and TNFR1-RFP for further growth and expansion.
10. During large scale screening, more than six T225 cm^2 flasks of cells may be required (typically 30-35 flasks of cells are required), fresh frozen stock of the cell lines have to be thawed a week in advance. After 24 h of thawing, split the cells into six T225 cm^2 flasks for 3 days and further split each of the six flasks into six more flasks, making a total of 36 flasks for screening. On the other hand, much less cells are required for screening in 1536 well plates with 5 μL of cells per well at one million cells per mL (*185*).
11. Fluorescence lifetime plate-reader enables high-throughput fluorescence lifetime detection at high precision by utilizing a unique direct waveform recording technology.(*195*) The performance of this fluorescence lifetime plate-reader has been previously demonstrated with FRET-based HTS that targets both structured

proteins (e.g. SERCA and ryanodine receptor) (*163, 188, 196-198*) and intrinsically disordered proteins (e.g. tau) (*199*).

12. We have developed fluorescence resonance energy transfer (FRET) biosensors with red-shifted fluorescent proteins, yielding improved characteristics for time-resolved (lifetime) fluorescence measurements. In comparison to biosensors with green and red FRET pairs (GFP/RFP), FPs that emit at longer wavelengths (orange and maroon, OFP/MFP) increased the FRET efficiency, dynamic range, and signal-to-background of high-throughput screening (HTS) (*185*). There is also a big reduction in compounds that exhibit fluorescent interference.
13. The instrument response function (IRF) needs to be acquired to remove background contributions from the FLT-PR laser and detection equipment. It is convolved with an exponential to measure the lifetime of the samples. The decay found from the instrument itself is removed by convolution of the samples. This convolution is performed in an iterative process using MATLAB or Fluorescence Innovations data analysis software.
14. Different incubation timings such as 20 min, 1 h or anytime up to 4 h can be monitored for kinetics measurements. The FRET signal has been determined to be stable for up to 4 h (unpublished results).
15. In determining the hits, a minimum of 3SD should be used for statistical significance. User can increase the stringency of the hit selection by adopting a higher SD cut off (e.g. 4SD, 5SD, etc.) with the purpose to limit the hit rate to 0.5-1% for ease of subsequent testing of the hits. Each FRET biosensor will behave differently, so threshold should be defined on a screen by screen basis.
16. For control inhibitor compounds during HTS, the user can choose from several well-characterized small molecules that disrupt receptor-receptor interaction or

perturb receptor conformational dynamics leading to inhibition of TNFR1-induced NF-κB activation (see Table 2.1).

CHAPTER 3: AN INNOVATIVE HIGH-THROUGHPUT SCREENING APPROACH FOR DISCOVERY OF SMALL MOLECULES THAT INHIBIT TNF RECEPTORS

Adapted with permission from:

Chih Hung Lo[1], Nagamani Vunnam[1], Andrew K. Lewis[1], Ting-Lan Chiu[1], Benjamin E. Brummel[1], Tory M. Schaaf[2], Benjamin D. Grant[3], Prachi Bawaskar[2], David D. Thomas[2,4] and Jonathan N. Sachs[1*]. An Innovative High-Throughput Screening Approach for Discovery of Small Molecules That Inhibit TNF Receptors. *SLAS DISCOVERY: Advancing Life Sciences R&D*, 2017, 22(8): 950-961

[1]Department of Biomedical Engineering, [2]Department of Biochemistry, Molecular Biology and Biophysics, University of Minnesota, Minneapolis, Minnesota 55455

[3]Fluorescence Innovations Inc., Minneapolis, MN 55455

[4]Photonic Pharma LLC, Minneapolis, MN 55410

Author contributions: C.H.L. designed and conducted all experiments. N.V. and A.K.L. contributed to some molecular biology and biochemical assays. T.L.C. and B.E.B. performed computational docking and analysis. T.M.S., B.D.G. and D.D.T. provided expertise in HTS and assisted in the data analysis of HTS. P.B. assisted in cell culture. C.H.L and J.N.S. wrote the manuscript.

3.1 Summary

Tumor necrosis factor receptor 1 (TNFR1) is a transmembrane receptor that binds tumor necrosis factor or lymphotoxin-alpha and plays a critical role in regulating

the inflammatory response. Upregulation of these ligands is associated with inflammatory and autoimmune diseases. Current treatments reduce symptoms by sequestering free ligands, but this can cause adverse side effects by unintentionally inhibiting ligand binding to off-target receptors. Hence, there is a need for new small molecules that specifically target the receptors, rather than the ligands. Here, we developed a TNFR1 FRET biosensor expressed in living cells to screen compounds from the NIH Clinical Collection. We used an innovative high-throughput fluorescence lifetime screening platform that has exquisite spatial and temporal resolution to identify two small-molecule compounds, zafirlukast and triclabendazole,that inhibit the TNFR1-induced IκBα degradation and NF-κB activation. Biochemical and computational docking methods were used to show that zafirlukast disrupts the interactions between TNFR1 pre-ligand assembly domain (PLAD), whereas triclabendazole acts allosterically. Importantly, neither compound inhibits ligand binding, proving for the first time that it is possible to inhibit receptor activation by targeting TNF receptor-receptor interactions. This strategy should be generally applicable to other members of the TNFR superfamily, as well as to oligomeric receptors in general.

3.2 Introduction

Tumor necrosis factor receptor 1 (TNFR1) is a transmembrane receptor that regulates the inflammatory pathways (*5*). Binding of tumor necrosis factor (TNF-α) or lymphotoxin-alpha (LT-α) to the extracellular domain of TNFR1 leads to IκBα degradation and NF-κB activation (*11*). Upregulation of these ligands has been associated with several inflammatory and autoimmune diseases, including rheumatoid arthritis (RA), juvenile RA, multiple sclerosis, Crohn's disease, and inflammatory bowel disease (*200*). Therapeutic targeting of TNFR1 signaling is a billion-dollar industry. Current treatments involve

monoclonal antibodies (e.g. infliximab, golimumab and adalimumab) that function by sequestering and blocking ligand binding (*15*). Unfortunately, these anti-TNF drugs also inhibit ligand binding to related TNF receptors that are not involved in the disease condition. As such, current treatments can induce dangerous side-effects such as lupus-like disease and increased incidence of lymphoma (*25, 174*). In order to overcome these limitations, there is a desperate need to develop new receptor-specific treatments that take advantage of recent breakthroughs regarding the structure and dynamics of the receptor itself (*62, 201*).

TNFR1 exists as ligand-independent, homophilic dimers that are stabilized by the extracellular pre-ligand assembly domain (PLAD) (*49, 202*). The PLAD is structurally distinct from the ligand-binding domain, and mutational analysis of the PLAD has shown the importance of receptor pre-assembly in signaling (*202, 203*). As a consequence, competitively blocking pre-ligand receptor dimerization via the PLAD has been considered a potential therapeutic target. Suggestively, the isolated, soluble PLAD of TNFR1 was shown to inhibit TNF-α induced inflammatory signaling *in vitro* and to ameliorate arthritis in a mouse model (*52*). In that study, the PLAD molecule (which was GST-tagged) ablated ligand binding, making it impossible to determine whether the small protein was targeting its intended site and, in fact, disrupting the dimer. Therefore, there remains no direct or unambiguous evidence in the literature that inhibition of receptor-receptor interactions is a viable targeting strategy for TNFR inhibition.

In the current study, our goal was to establish a small-molecule approach that ablates receptor-receptor interactions, or alters receptor conformational dynamics, without interrupting ligand binding (**Figure 3.1**). We used an innovative time-resolved FRET (TR-FRET) based strategy, which combines fluorescent biosensor engineering and fluorescence lifetime measurements in a high-throughput screening (HTS) platform

to identify small-molecule inhibitors of TNFR1 signaling. The screen was enabled by the first truly high-throughput fluorescence lifetime plate-reader, which increases the speed of lifetime detection by a factor of 10^5 and the precision of FRET-based screening by a factor of thirty (*163*). This extra precision, enabling reliable detection of protein structural changes of 1Å, is particularly powerful for the detection of allosteric regulation of receptors by small molecules. By using this strategy, we found two small-molecule compounds that inhibit TNFR1-induced IκBα degradation and NF-κB activation. As such, the results of our study should not only impact TNFR research, but should also have a very broad impact on drug discovery efforts wherever protein-protein interactions are targeted.

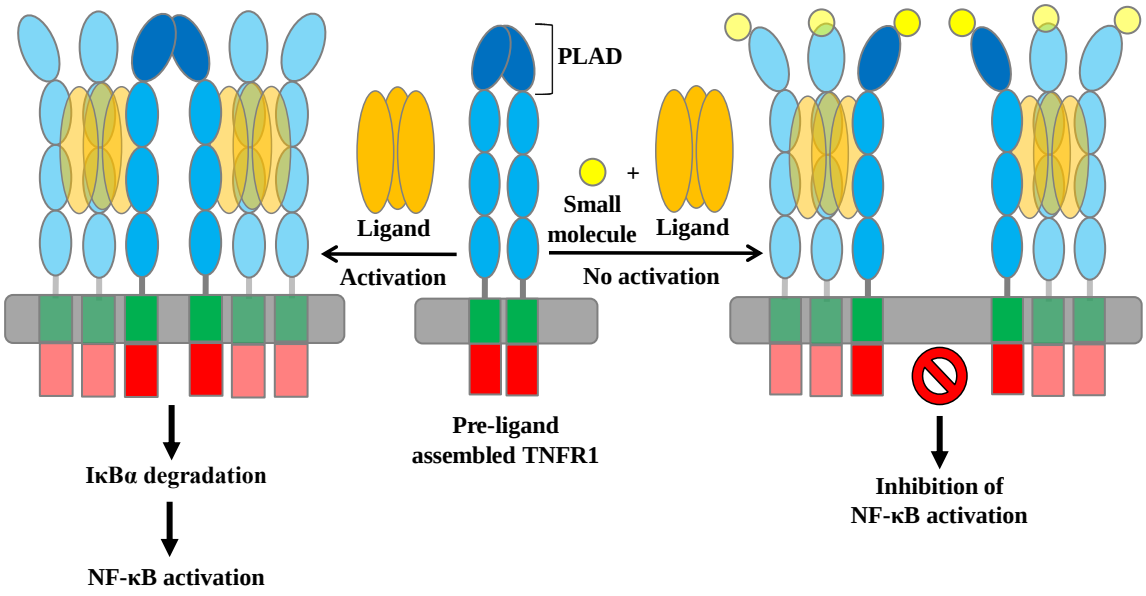

Figure 3. 1. Inhibition of TNFR1 signaling by small molecules targeting receptor-receptor interactions.

Small molecules could inhibit ligand-induced NF-κB activation by targeting TNFR1 pre-ligand assembly domain (PLAD) and disrupting the receptor-receptor interactions without affecting ligand binding.

3.3. Materials and Methods

3.3.1. Molecular biology

To generate TNFR1ΔCD-GFP and TNFR1ΔCD-RFP, cDNAs encoding truncated TNFR1ΔCD (amino acids 1-242) were fused to the N-terminus of the EGFP and TagRFP vectors using standard cloning techniques. For photobleaching FRET assays, TNFR1ΔCD was inserted at the N-terminus of the pEYFP-N1 and pECFP-N1 vectors. All mutations were introduced by Quikchange mutagenesis and sequenced for confirmation. All vectors contain the monomeric mutation A206K to the fluorescent proteins preventing constitutive fluorophore clustering (*204*). EGFP, TagRFP, pEYFP-N1, pECFP-N1 and GFP-linker-RFP vectors were a kind gift from David D Thomas.

3.3.2. Cell culture and generation of stable cell lines

Human embryonic kidney cells 293 (HEK293) were cultured in phenol red-free DMEM (Gibco) supplemented with 2 mM L-Glutamine (Invitrogen), heat-inactivated 10% fetal bovine serum (FBS HI, Gibco), 100 U/mL penicillin and 100 μg/mL streptomycin (HyClone). Cell cultures were maintained in an incubator with 5% CO_2 (Forma Series II Water Jacket CO_2 Incubator, Thermo Scientific) at 37 ºC. To generate TNFR1ΔCD-FRET pair stable cell line, HEK293 cells were transiently transfected using Lipofectamine 3000 (Invitrogen) with TNFR1ΔCD-GFP only or with both TNFR1ΔCD-GFP and TNFR1ΔCD-RFP (1:6 ratio). Transiently transfected cells were treated with two antibiotics, G418 (Enzo Life Sciences) and puromycin (Gibco) to eliminate non-expressing cells. Stable cell lines expressing TNFR1-GFP or TNFR1-GFP/RFP (TNFR1ΔCD-FRET pair or TNFR1 biosensor) with the largest population of expressing

cells were selected by flow cytometry and fluorescence microscopy. Aliquots of the stable cell lines have been monitored continuously for over a year with expression maintaining above 95% characterized by flow cytometry.

3.3.3. Flow cytometry

Homogeneous expression of the TNFR1ΔCD-FRET pair stable cells was determined by flow cytometry performed with FACSAria II (BD Biosciences) with GFP laser (488 nm) at 250V and RFP laser (561 nm) at 500V. HEK293 cells stably expressing TNFR1ΔCD-FRET pair were harvested from a 6-well plate by detaching cells with TrypLE (Invitrogen) and washing three times with phosphate buffer solution (PBS, Thermo Scientific). Next, cells were passed through a polystyrene round-bottom tube with cell-strainer cap (BD Falcon). Data were analyzed by using FlowJo (Company Name) software.

3.3.4. Fluorescence microscopy

Localization of the TNFR1ΔCD-FRET pair on plasma membrane of stable cells was determined by confocal fluorescence microscopy (ATCC, Manassas, VA). Images were taken in a glass-bottom chambered coverslips (Matek Corporation, Ashland, MA) using an Olympus IX2 inverted confocal fluorescence microscope equipped with a FluoView FV1000 laser scanning confocal head and 60X (1.42NA) oil immersion objective lenses. Excitation was accomplished with laser illumination at 488 nm for GFP and 561 nm for RFP.

3.3.5. Preparation of cells for FRET measurements and specificity of TNFR1 biosensor

TNFR1ΔCD-FRET pair stable cells were cultured in 225 cm^2 flask (Corning). On the day of measurement, cells were harvested by incubating with TrypLE (Invitrogen) for 5 min, washed three times with PBS by centrifugation at 300 g, filtered using 70 µm cell

strainers (BD Falcon) and resuspended in PBS at a concentration of one million cells/ml using an automated cell counter (Countess, Invitrogen). For lifetime measurements, cells were dispensed (50 µl/well) into a 384 well-plate (PN 781209, Greiner Bio-One) by a Multidrop Combi Reagent Dispenser (Thermo Scientific). Binding specificity of the TNFR1ΔCD-FRET pair was tested by transiently transfecting (Invitrogen Lipofectamine 3000) stable cells with full length unlabeled Death Receptor 5 (DR5) (440 amino acids) and full length unlabeled TNFR1 (455 amino acids). Two days after transfection, cells were harvested and prepared as above for fluorescence lifetime measurements. For comparison between the control and the treated samples, an unpaired t-test was used to validate statistical differences.

3.3.6. Fluorescence data acquisition

Fluorescence lifetime measurements were carried out by a prototype fluorescence lifetime plate-reader (Fluorescence Innovations, Inc., Minneapolis, MN) (*163, 188, 196, 197*). GFP fluorescence was excited with a 473 nm microchip laser from Concepts Research Corporation (Belgium, WI) and emission was filtered with 488 nm long pass and 517/20 nm band pass filters (Semrock, Rochester, NY) (*163, 186*). This instrument enables high-throughput fluorescence lifetime detection at high precision by utilizing a unique direct waveform recording technology (*195*). The performance of this fluorescence lifetime plate-reader has been previously demonstrated with FRET-based HTS that targets SERCA and ryanodine receptor (*163, 188, 196, 197*).

3.3.7. Pilot screening with NIH Clinical Collection library

The NIH Clinical Collection (NCC) library containing 446 compounds was purchased from Evotec, formatted into 96-well mother plates using a FX liquid dispenser, and subsequently formatted across two 384 well plates at 50 nl (10 µM final concentration per well) using an Echo liquid dispenser. DMSO (matching %v/v) was

loaded as in-plate no-compound controls as well as in column 1, 2, 23 and 24 (negative controls). The 384 well flat, black-bottom polypropylene plates (PN 781209, Greiner Bio-One) were selected as the assay plates for their low auto-fluorescence, and low inter-well cross-talk. The plates were sealed and stored at −20 °C until use.

Three days prior to screening, stable TNFR1ΔCD-GFP (donor only control) or TNFR1-GFP/RFP (TNFR1ΔCD-FRET pair) cells were expanded in five 225 cm^2 flasks (Corning). On each day of screening, the compound plates were equilibrated to room temperature (25 °C). The cells were harvested from the 225 cm^2 flasks by incubating with TrypLE (Invitrogen) for 5 min, washed three times in PBS by centrifugation at 300 g and filtered using 70 µm cell strainers (BD Falcon). Cell viability was assessed using trypan blue assay with viability above 95% and diluted to 1 million cells/ml using an automated cell counter (Countess, Invitrogen). Expression of TNFR1ΔCD-GFP and TNFR1-GFP/RFP (TNFR1ΔCD-FRET pair) in stable cells was confirmed by flow cytometry to be above 95% prior to each screen. After resuspension and dilution in PBS, the stable cells were constantly and gently stirred using a magnetic stir bar at room temperature, keeping the cells in suspension and evenly distributed to avoid clumping. During screening, cells (50 µl/well) were dispensed by a Multidrop Combi Reagent Dispenser (Thermo Scientific) into the 384-well assay plates containing the compounds and allowed to incubate at room temperature for 20 min before readings were taken by the fluorescence lifetime plate-reader (Fluorescence Innovations, Inc.).

3.3.8. HTS data analysis

Time-resolved fluorescence waveforms for each well were fitted to single-exponential decays using least-squares minimization global analysis software (Fluorescence Innovations, Inc.) to give donor lifetime (τ_D) and donor-acceptor lifetime (τ_{DA}). FRET efficiency (*E*) was then calculated based on Equation 1.

$$E = 1 - \left(\frac{\tau_{DA}}{\tau_D}\right) \qquad Eq.1$$

Assay quality was determined with NCC hits as positive controls and DMSO as negative controls and calculated based on Equation 2.(*192*)

$$Z' = 1 - \frac{3(\sigma_p + \sigma_n)}{(\mu_p - \mu_n)} \qquad Eq.2$$

where σ_p and σ_n are the standard deviations and μ_p and μ_n are the means of the positive and negative controls, respectively.

FRET data from four independent NCC screens were collected and averaged. Fluorescent compounds were flagged as potential false positives due to interference from compound fluorescence by the spectral recording method based on the assessment of the similarity index of each well from the pilot NCC screens (*188*). T-test was performed on the data and the left and right 5% tails were classified as outliers and removed. After removal of fluorescent compounds, histogram of the average FRET distribution from all compounds in the screens was plotted and fitted to a Gaussian curve to obtain a mean and standard deviation (SD). A hit was defined as a compound that changed the average FRET efficiency by more than four times the standard deviation (4SD) relative to the mean.

3.3.9. FRET dose-response assay

The hit compounds, triclabendazole (PubChem CID: 50248) and zafirlukast (PubChem CID: 5717), were purchased from (AK Scientific, Inc.). These drug compounds were dissolved in DMSO to make10 mM stock solution anddiluted into 50X concentrations which were then subsequently serially diluted in 96 well mother plates. Hits were screened at nine different concentrations (0.1 to 200 μM). Compounds (1 μL) were transferred from the mother plates into assay plates using a Mosquito HV liquid

handler (TTP Labtech Ltd, UK). The same procedure of cell culture and dispensing as the pilot screening was applied in the FRET dose response assays.

3.3.10. IκBα degradation assay

HEK293 cells were cultured in a 150 cm^2 flask (Corning) for three days and dispensed into two 6 well plates at 1.5 million cells/well and incubated overnight before treating with drugs. Next day, cells were treated with DMSO (negative control) and respective doses of drug compounds (0.1 to 200 μM) for 2 hours followed by 30 min of LT-α (100 ng/ml) or TNF-α (1 ng/ml) (210-TA-005, R&D Systems) treatment at 37 °C. Cells were lysed for 30 min on ice with RIPA lysis buffer (Pierce RIPA buffer, Thermo Scientific) containing 1% of protease inhibitor (Clontech) and centrifuged at 15,000 g at 4 °C for 30 minutes. Total protein concentration of lysates was determined by BCA assay (Pierce) and equal amounts of total protein (60 µg) were mixed with 4X Bio-Rad sample buffer and boiled for 3-5 minutes, and loaded on 4-15% Tris-glycine SDS-PAGE gels (Bio-Rad). Proteins were transferred to nitrocellulose membrane and probed using antibodies against IκBα (44D4, Cell Signaling Technology) and β-actin (ab8227, Abcam). Blots were quantified on the Odyssey scanner and densitometric analysis was carried by the Image Studio (LI-COR Biosciences).

3.3.11. NF-κB luciferase reporter gene assay

HEK293 cells were transfected with the NF-κB-luciferase reporter gene in a 100 mm plate with Lipofectamine 3000. On the following day, cells were lifted with TrypLE and resuspended in phenol red-free DMEM (Gibco). These cells were dispensed in 96-well (30000 cells/well) white solid bottom plates (Greiner Bio-One North America) and incubated with drugs (0.1 to 200 μM) or DMSO (negative control) in the presence (100 ng/ml) and absence of LT-α for 18 hours at 37 °C. After incubation, 50 μl of Dual-Glo

Luciferase Reagent (Promega) was added, incubated at room temperature for 15 min, and measured firefly luminescence using a Cytation 3 Cell Imaging Multi-Mode Reader luminometer (BioTek). Next, 50 μl of Dual-Glo Stop & Glo Reagent (Promega) was added, incubated at room temperature for 15 min, and measured *Renilla* luminescence using luminometer.

3.3.12. Overexpression and Purification of Recombinant Proteins

The N-terminal FLAG-tagged LT-α and FLAG-tagged TNFR1 PLAD (residues 30-82) were overexpressed using the pT7-FLAG-1 inducible expression system in Escherichia coli (E. coli) and purified by anti-FLAG affinity column (M2 anti-FLAG affinity agarose resin, Sigma-Aldrich). Purity of the proteins was assessed by 4-15% SDS-PAGE gels (Bio-Rad) under reducing conditions followed by Coomassie staining. Protein concentrations were measured using BCA assay (Thermo Fisher Scientific).

3.3.13. Co-immunoprecipitation

Anti-FLAG magnetic beads were mixed with soluble FLAG-tagged LT-α and incubated for 2-4 hours at 4 °C. The unbound FLAG-tagged LT-α were then removed by washing the beads with wash buffer (150 mM NaCl, 50 mM Tris, 10% Glycerol, pH 7.5). HEK293 and transiently transfected cells were washed three times with ice-cold PBS before lysis with immunoprecipitation (IP) buffer (20 mM Tris-HCl, 1 mM EDTA, 100 mM NaCl, pH 7.5 and 0.5% NP-40) containing complete protease inhibitors cocktail (Roche). Subsequently, cells were sonicated for 30 seconds, incubated for 15 minutes on ice, and centrifuged at 16,000 g for 30 min at 4 °C. Next, the supernatant was transferred to a tube containing magnetic beads coated with anti-FLAG antibody bound to FLAG-tagged LT-α. The tube was rotated for 4 hours at 4 °C, followed by three washes with IP buffer. Immunoprecipitate samples and whole-cell lysates were resolved using 4-15% SDS-

PAGE gels and subjected to Western blotting using FLAG (2044S, Cell Signaling Technology) and TNFR1 (Ab19139, Abcam) antibodies.

3.3.14. Analytical SEC and native characterization of proteins

Analytical size exclusion chromatography (SEC) was used to detect the oligomeric states of soluble PLAD. SEC experiments were performed using BioLogic DuoFlow Chromatography System (Bio-Rad) with a Superose-12 10/300 GL column (GE LifeSciences) with detection at 280 nm and 0.5 mL/min flow rate. SEC column was calibrated with protein standard mix (69385, Sigma-Aldrich). Purified soluble PLAD and LT-α was accessed by Native-PAGE gels (Bio-Rad) in the absence and presence of DMSO and hit compounds (200 μM) under non-reducing conditions followed by Coomassie staining.

3.3.15. Photobleaching FRET assay

HEK293 cells were transiently transfected using the calcium phosphate method with 0.5 μg pECFP-TNFR1ΔCD and 1.5 μg pEYFP-TNFR1ΔCD in a 12-well plate. The following day, cells were lifted with TrypLE, resuspended in phenol red-free DMEM, and plated on poly-D-Lysine coated plates. Cells were allowed to settle at room temperature for 1 hour before imaging. Live-cell FRET imaging was performed on a Nikon Eclipse TE200 inverted microscope and a 20x objective configured as in our previous study with minor modifications detailed here.(*181*) Cells were imaged in the EYFP and ECFP channels every 15 s for 5 min. Between image captures, acceptor was bleached by continuous exposure through the EYFP excitation channel. Image analysis was carried out in ImageJ. FRET efficiency was calculated as the intercept of the linear fit of normalized EYFP fluorescence plotted against normalized ECFP enhancement with typical R^2 values of around 0.90. The FRET efficiencies measured from individual cells were plotted against EYFP intensity for qualitative analysis.

3.3.16. Molecular dynamics and computational docking

For analysis of the TNFR1 dimer interface residues, Visual Molecular Dynamics (VMD) was used. For computational docking, the structure preparation of TNFR1 monomers, dimers and NCC compounds was done in MOE 2015.1001 (Chemical Computing Group, Inc.). *TNFR1 monomer:* The protein structure of TNFR1 was downloaded from the Protein Data Bank (PDB: 1NCF) (*49*). The water molecules and chain B were removed before the chain A was prepared using Structure Preparation application of MOE. *TNFR1 dimer:* The same procedure was followed to prepare the dimer except that only the water molecules were removed. *NCC compounds:* The 446 compounds from the NCC were downloaded (Evotec), and the compounds were prepared by Database Wash program in MOE. Subsequently, the compounds were subjected to energy minimization using Energy Minimize application of MOE with MMFF94s force field until the gradient of 0.05 rms kcal/(mol.Å^2) was met.

The molecular docking simulation was done using Dock application of MOE. *Docking on chain A:* The PLAD residues (i.e. residues 12-53 in 1NCF) were specified as the docking site. NCC compounds were docked individually into the PLAD region of 1NCF chain A using the rigid receptor protocol of MOE Dock (*205, 206*). Initially, 10,000 poses were generated by the Triangle Matcher method and scored by London dG. The top 1,000 docked poses from the initial scoring moved on to the next refinement stage where poses were scored and ranked using GBVI/WSA (*205*), a forcefield-based scoring function which estimates the free energy of binding of the ligand from a given pose. It should be noted that lower/more negative scores indicate more favorable poses. Only the top 100 poses were considered in the subsequent statistical analysis. *Docking on dimer:* The same docking procedure was followed except: (i) The prepared TNFR1 dimer was used; (ii) The PLAD residues on both chains were specified as the docking site.

For statistical analysis, a Matlab (MathWorks, Inc.) script was written to calculate the Boltzmann-weighted scores by multiplying the probability of contacting a given residue by the mean Boltzmann-weighted predicted free energy for each pose contacting that residue: $P\left\langle e^{\frac{-\Delta G}{k_B T}}\right\rangle$, where P is the probability of contacting either a specific residue, or the interface, ΔG is the predicted free energy of binding from the docking simulation, and T is the temperature (300 K), and the brackets represent the average weighted value for all scores where either a specific residue, or the interface is contacted. Structural analysis of the hit compounds was carried by MarvinSketch (ChemAxon Ltd.).

3.4. Results

3.4.1. TNFR1ΔCD FRET biosensor and fluorescence lifetime technology as HTS platform

To develop a HTS platform that can detect small-molecule modulation of TNFR1 receptor-receptor interactions, we engineered a TNFR1ΔCD FRET biosensor expressed in living cells. We used HEK293 cells stably expressing TNFR1ΔCD fused to green (GFP) or red (RFP) fluorescent proteins (TNFR1ΔCD-FRET pair) (**Figure 3.2A**) to identify small molecules that inhibit the endogenous TNFR1-TNFR1 interaction. Homogeneity of the TNFR1ΔCD-FRET pair on the plasma membrane was determined by flow cytometry and confocal microscopy. Flow cytometry analysis showed extremely low background with a 97% induction of TNFR1ΔCD-FRET pair, which suggested that most of the stable cells were capable for high-throughput screening to identify compounds that modulate TNFR1 interactions (**Figure 3.2B**). Confocal images showed that the receptors were evenly distributed on the cell membrane (**Figure 3.2C**). We then tested the functionality of TNFR1ΔCD-FRET pair by measuring FRET efficiency. Lifetime measurements showed a substantial decrease in the donor fluorescence lifetime in the

presence of the acceptor compared with the donor only, which indicated efficient FRET (**Figure 3.2D**), and recapitulates the known ligand-independent association of TNFR1 receptors (*49*). As there is no known positive control that targets TNFR1 receptor-receptor interactions, we transfected the stable cells with either unlabeled-TNFR1 or DR5 (negative control) to confirm that the measured FRET was specific to TNFR1-TNFR1 interactions and could be modulated. DR5 caused no significant FRET change, but TNFR1 showed a significant decrease in FRET, indicating that TNFR1 interactions were specific and not affected by other superfamily members (**Figure 3.2E**). This established the lifetime-based FRET detection with TNFR1ΔCD-FRET pair stable cells as a powerful platform for the identification of compounds that modulate TNFR1 receptor-receptor interactions.

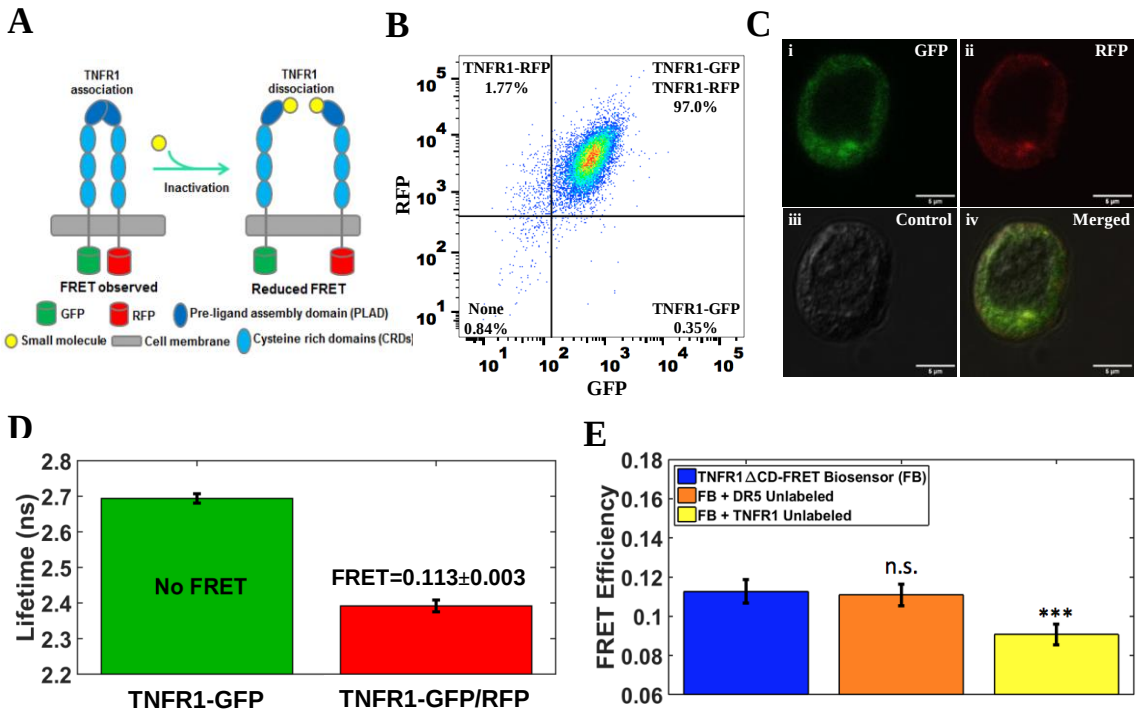

Figure 3. 2. TNFR1ΔCD FRET biosensor and fluorescence lifetime technology as high-throughput screening (HTS) platform.

(A) Schematics and principles of TNFR1ΔCD-FRET pair biosensor in identifying small-molecule compounds that modulate receptor-receptor interactions and inhibit receptor signaling. Pre-ligand assembled TNFR1 dimers exhibit FRET which will be reduced upon disruption of receptor-receptor interaction by small-molecule inhibitors. (B) Flow cytometry analysis of the TNFR1ΔCD-FRET pair stable cells show that nearly all of the stably dual transfected cells contain both TNFR1ΔCD-GFP and TNFR1ΔCD-RFP. (C) Confocal microscopy images i) GFP channel, ii) RFP channel, iii) differential interference contrast (DIC) and iv) merged channel of the dual GFP and RFP-tagged stable cells indicate the presence of both TNFR1ΔCD-GFP and TNFR1ΔCD-RFP co-localized at the cell membrane. (D) Fluorescence lifetime measurements with TNFR1ΔCD-FRET pair stable cells show FRET, indicating ligand-independent association of TNFR1 receptors. Values are mean ± S.D. (n=384). (E) Specificity of TNFR1ΔCD-FRET pair was confirmed by transfecting the stable cells with unlabeled-TNFR1 or DR5 (another TNF superfamily receptor as control). Cells transfected with DR5 show no significant FRET change and with unlabeled-TNFR1 show a significant decrease in FRET. Values are mean ± SD ***P<0.0001 (n=32) for treated vs control group.

3.4.2. High-throughput screening of NCC library to identify compounds that modulate TNFR1 receptor-receptor interactions

Using the TNFR1ΔCD-FRET pair stable cells, we performed high-throughput screening of NIH Clinical Collection (NCC: 446 bioactive compounds) to identify compounds that disrupt endogenous TNFR1 receptor-receptor interactions. The NCC library is a collection of small molecules that have been previously tested in clinical trials, and therefore have known safety profiles. These compounds can provide excellent starting points for medicinal chemistry optimization and may even be appropriate for direct human use in new disease areas. After an initial quality control check of the stable cell lines expressing the TNFR1 biosensor on each day of screening (signal level and

coefficient of variance), the cells were dispensed into the drug plates and incubated with the compounds or DMSO control wells. A single-exponential fit was used to obtain the lifetime from cell line expressing TNFR1ΔCD-FRET pair (τ_{DA}) and from the TNFR1ΔCD-GFP donor-only control cell line (τ_D) to determine FRET efficiency (Eq. 1). The fluorescence lifetime measurement is prone to interference from fluorescent compounds, so a stringent fluorescent compound filter was used to flag 26 compounds as potential false-positives due to interference from compound fluorescence (*188*). This filter did not change significantly the mean or standard deviation of the histogram (**Figures 3.3A** and **3.3B**). FRET efficiency from all compounds that passed the fluorescent compound filter were averaged from four independent NCC screens. Histogram of the average FRET distribution from these compounds was plotted and fitted to a Gaussian curve to obtain a mean and standard deviation (SD) (**Figures 3.3A** and **3.3B**). Two hits from the library, zafirlukast (PubChem CID: 5717) and triclabendazole (PubChem CID: 50248), were identified to decrease the average FRET by more than 4SD greater than the mean of control cells (**Figure 3.3A**). In addition, each NCC screen was analyzed independently with two to eight hits being identified. zafirlukast and triclabendazole were discovered to be reproducible hits in three or more screens (**Figure 3.3C**). Both compounds decreased FRET efficiency in a dose-dependent manner (**Figure 3.3D**), with half-maximal effects at relative EC_{50}values of 15 μM (triclabendazole) and 18 μM (zafirlukast). To calculate Z' (Eq. 2) for this assay, these two hits with maximum changes of FRET of 0.038 (triclabendazole) and 0.055 (zafirlukast) were used as positive controls and DMSO as negative controls. Using the latter value from zafirlukast in the Z' calculation (Eq. 2), we obtain a value of $Z' = 0.521 \pm 0.014$, which indicates excellent assay quality. This value of Z' is likely to increase, indicating even better assay quality, once a larger library is screened, since better positive controls are likely to be discovered, increasing the signal

window, (μ_p - μ_n) in Eq. 2 (*192*). Remarkably, both of these compounds—which were blindly identified in our screen—have been shown to play a role in NF-κB inhibition through the TNFR1-induced pathway (*161*), but no molecular mechanisms to explain their impacts have been explored. Zafirlukast is a FDA-approved inflammatory mediator that has been used for the treatment of asthma in adults (*207*), In addition, zafirlukast is effective as an anti-inflammatory agent in the treatment of adults with cystic fibrosis (*208*)—a disease in which TNF-α has been implicated (*209*)—as well as in patients with autoimmune chronic urticarial (*210*). On the other hand, triclabendazole is a member of the benzimidazole family of anthelmintics which displays high efficacy against helminthiasis in both immature and adult live flukes especially related to hermaphroditic trematondes known as *clonorchis sinensis* (*211*). *Clonorchis sinensis* can cause an inflammatory response that induces the likelihood of forming cholangiocarcinoma (*212*).

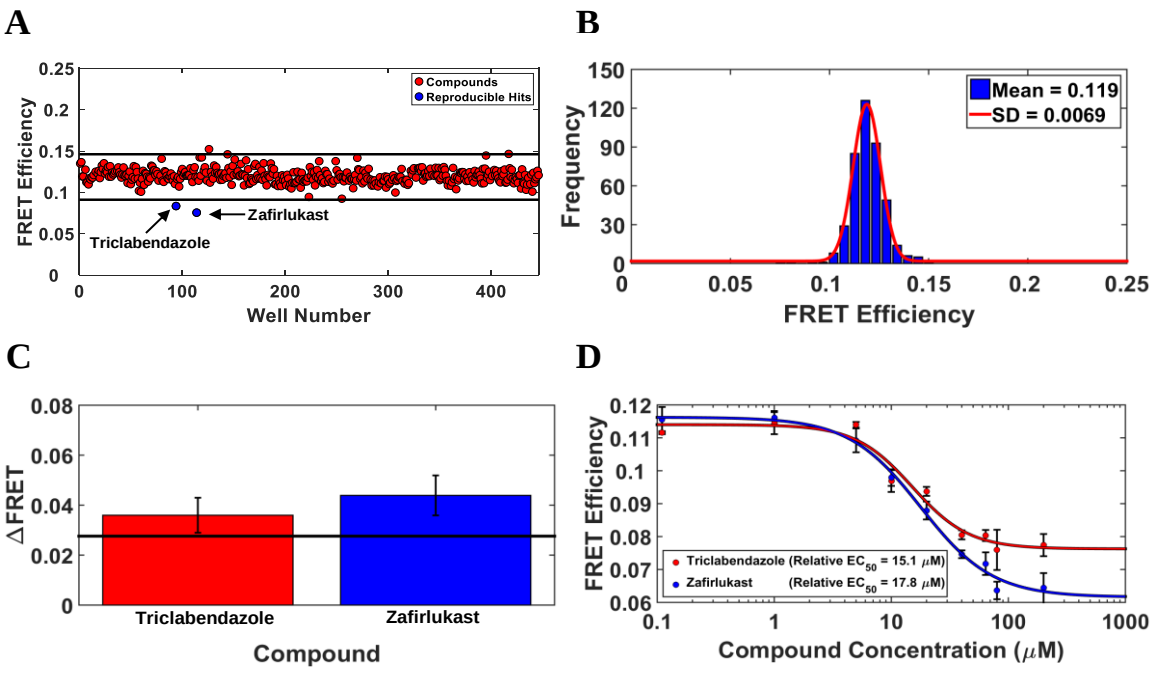

Figure 3. 3. Time-resolved FRET-based high-throughput screening of NCC library for compounds that inhibit TNFR1 receptor-receptor interactions.

(A) Pilot screening with NCC library containing 446 compounds. Applied threshold at a change in FRET efficiency of 0.028 (4SD) is shown by the black lines. Two hits with reproducible FRET change were identified from the pilot screens (blue). (B) Histogram plots of all compounds from NCC screen after removal of fluorescent compounds show an average FRET efficiency of 0.119 ± 0.0069. (C) Reproducibility of the two hits across four independent screens with 0.028 threshold of FRET change (4SD) shown in black line. (D) The two reproducible FRET hits identified were dispensed into 384 well-plates at nine different concentrations from 0.1 to 200 μM and both produce a dose-dependent FRET change.

3.4.3. Cell-based assays to determine the biological activity and efficacy of hit compounds

The effect of triclabendazole and zafirlukast on ligand-induced IκBα degradation and NF-κB activation was determined by immunoblotting and cell-based assays.

Potency measurements showed an absolute inhibitory concentration (absolute IC_{50}) of 67 μM (triclabendazole) and 114 μM (zafirlukast) for inhibiting LT-α mediated IκBα degradation in HEK293 cells (**Figures 3.4A** and **3.4B**). Similarly, both compounds inhibited LT-α mediated NF-κB activation in a dose-dependent manner, with absolute IC_{50} of 55 μM (triclabendazole) and 50 μM (zafirlukast) (**Figure 3.4C**). The partial inhibition by zafirlukast could be due to NF-κB activation being further downstream in the signaling pathway, as well as influence from biological crosstalk (*213*). Similar results were observed from IκBα degradation assay with TNF-α treated cells (**Figure 3.4D**), indicating that triclabendazole and zafirlukast are inhibiting TNFR1 function. For the functional assays, we calculated *Z´* (Eq. 2) by using the maximum inhibition of the two hits as positive controls and DMSO as a negative control in each assay. The *Z´* values obtained were more than 0.5 for both hits in each assay.

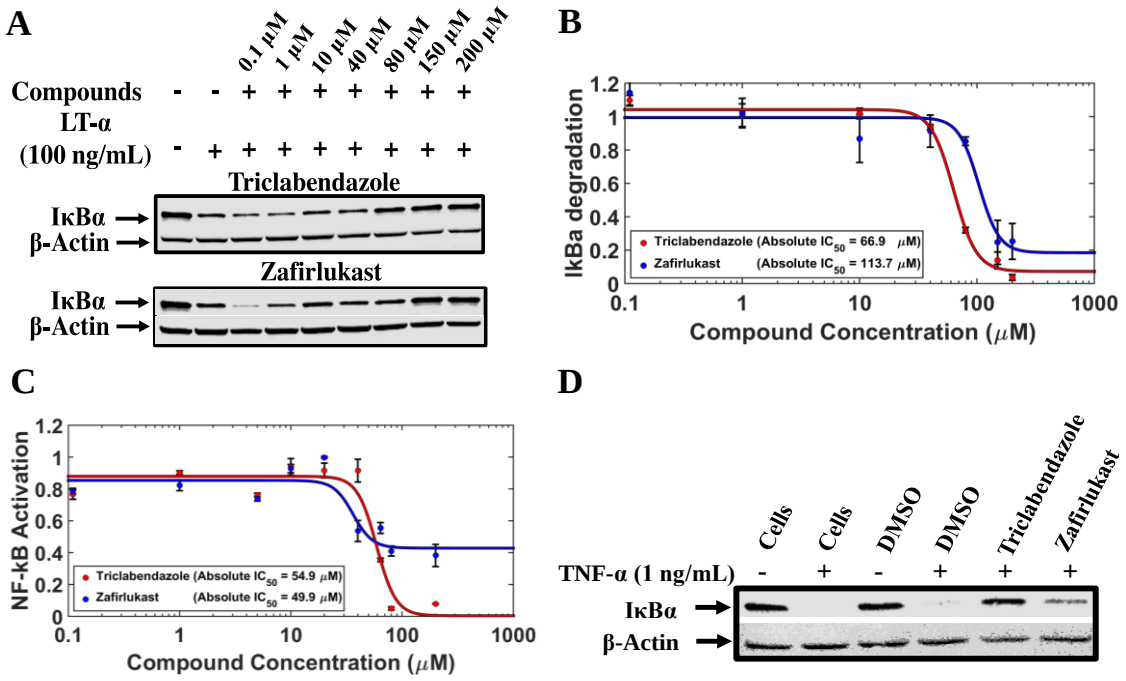

Figure 3. 4. Hit compounds inhibit ligand-induced IκBα degradation and NF-κB activation in HEK293 cells.

(A) Effect of triclabendazole and zafirlukast on LT-α induced IκBα degradation was analyzed by Western blot. HEK293 cells with endogenous TNFR1 receptors were treated with DMSO and the two hit compounds in a dose dependent manner from 0.1 to 200 μM for 2 hours followed by the addition of LT-α (100 ng/ml) for 30 min and Western blotting analysis. Qualitative dose dependent inhibition of IκBα degradation was observed from the increase in the intensity of the IκBα protein bands. (B) Densitometric analysis of Western blots (n=3) to quantify the effects of hit compounds on IκBα degradation. (C) NF-κB activation luciferase assay with HEK293 cells treated with triclabendazole and zafirlukast followed by the addition of LT-α (100 ng/ml) (n=3). Both compounds inhibited IκBα degradation and NF-κB activation in a dose dependent manner. (D) Effect of hit compounds on TNF-α induced IκBα degradation. HEK293 cells were treated with the two hit compounds (200 μM) followed by the addition of TNF-α (1 ng/ml). Cell lysates were analyzed by 4-15% Tris-glycine SDS-PAGE gel, followed by Western blotting with antibody against IκBα.

3.4.4. Mode of inhibition of TNFR1 signaling by zafirlukast and triclabendazole

Fundamental to our stated goal, we then determined whether the inhibitory effects of these drugs are due to perturbations in ligand-receptor and/or receptor-receptor interactions. We monitored ligand-receptor binding in the presence and absence of drugs using co-immunoprecipitation. Western blot results illustrated that neither drug inhibited ligand-receptor binding (**Figure 3.5A**). In addition, we confirmed that the drugs had no effect on ligand-ligand interactions (**Figure S3.1A**). We then tested the effect of drugs on fluorophores with cells expressing GFP-linker-RFP (linker contains 32 amino acids). FRET measurements showed no change in the FRET efficiency in the presence and absence of drug compounds (**Figure S3.1B**), which confirmed that the small molecules were not acting through disrupting interactions between the cytosolic fluorophores. Thus, by elimination, the two compounds were causing a change in FRET through interactions with either the extracellular or transmembrane (TM) domain.

In order to investigate the hypothesis that these compounds are acting directly on PLAD-PLAD assembly, or through another indirect/allosteric mechanism, we tested their effects on soluble FLAG-tagged PLAD. Size exclusion chromatography showed that soluble PLAD existed as a dimer in the native condition (**Figure 3.5B**). Next, we tested the effect of zafirlukast and triclabendazole on the dimerization of PLAD. We treated soluble PLAD with zafirlukast or triclabendazole and compared with the untreated protein on a native gel. These results clearly showed that zafirlukast disrupted the dimerization of PLAD (**Figure 3.5C**). However, triclabendazole did not disrupt the isolated PLAD-PLAD dimer, which implied that it might be binding to the conformationally active regions of the receptor that are important for its function.

3.4.5. Virtual screening by computational docking of the NCC library to both monomeric and dimeric TNFR1 PLAD

To further explore the relative potency of zafirlukast in disrupting PLAD-PLAD interactions, we carried out a virtual screen by computational docking of the NCC library to both monomeric and dimeric PLAD (Protein Data Bank (PDB): 1NCF) (*49*), zafirlukast ranked sixth among 446 compounds (**Figures S3.2A** and **S3.2B**). Importantly, zafirlukast scored substantially better than triclabendazole. This was especially so when considering interactions with key residues at the dimer interface (**Figures 3.5D, S3.2C** and **S3.2D**), including those previously identified (e.g. K19, K32, and Q48, amongst others) (*202*). We then experimentally tested the impact of mutating a subset of interfacial residues (Q17, K19, H34 and Q48) that potentially stabilize the receptor chains. Photobleaching FRET assay showed that K19, H34 and Q48 were crucial for stabilizing the affinity of receptor monomers (**Figures S3.3A** and **S3.3B**), but individually do not eliminate ligand binding (**Figure S3.3C**). Thus, the most likely mode of binding for zafirlukast is at the PLAD interface, although it remains possible that the binding is elsewhere within the PLAD and that the impact on dimerization is non-competitive/allosteric. Triclabendazole, which is a more potent compound than zafirlukast (**Figure 3.4**), does not biochemically disrupt the isolated PLAD-PLAD dimer. Structural analysis of the two compounds has shown that zafirlukast is a more polar molecule than triclabendazole. Under physiology conditions, zafirlukast has a charge of -1, with 2 hydrogen bond donors and 6 hydrogen bond acceptors, suggesting that it should interact with charged and polar amino acid residues at the dimer interface (**Figure 3.5D**). On the other hand, triclabendazole is less polar with no charge and has only 1 hydrogen bond donor and 3 hydrogen bond acceptors, suggesting that triclabendazole should not binding to the polar dimer interface but rather to a less polar

region. In addition, we have recently shown that the other regions of TNFR1, including the cysteine rich domain that connects to the TM domain (CRD4), and the TM domain itself, are conformationally active (*62*). Triclabendazole's relative potency, which bears future investigation, is therefore consistent with the notion that non-competitive inhibitors that alter conformationally active regions of proteins should be more potent (*214*).

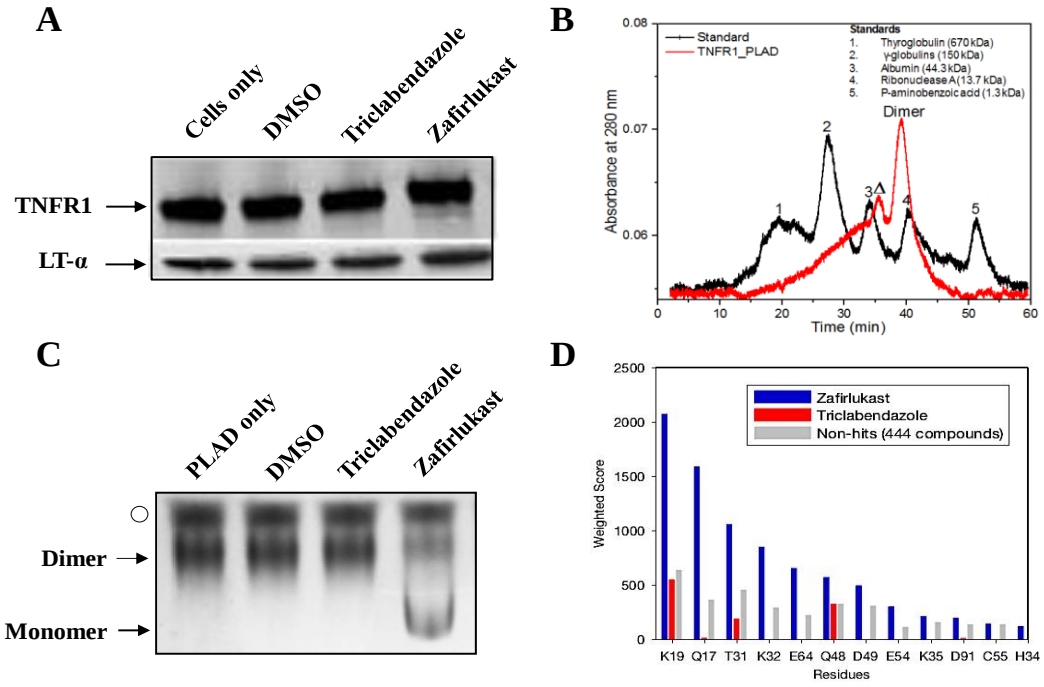

Figure 3. 5. Mode of inhibition of TNFR1 signaling by zafirlukast and triclabendazole.

(A) Effect of zafirlukast and triclabendazole (200 μM) on TNFR1-LTα interaction was determined by co-immunoprecipitation with anti-FLAG–conjugated agarose beads. (B) Oligomeric states of PLAD were determined by analytical size-exclusion chromatography. Dimer peak is indicated. Open triangle indicates non-specific protein. (C) Effect of zafirlukast and triclabendazole on PLAD-PLAD interactions was determined by Native-PAGE. Open circle indicates nonspecific band. (D) Docking scores for zafirlukast and triclabendazole on TNFR1 chain B (PDB: 1NCF) interfacial residues. Boltzmann-weighted scores were calculated by multiplying the probability of

contacting a given residue by the mean Boltzmann-weighted predicted free energy for each pose contacting that residue.

3.5. Discussion

New receptor-specific approaches are needed to treat diseases associated with over-activation of TNFR1 as conventional therapeutics of anti-TNF cause dangerous side effects due to off-target inhibition of related TNF receptors (*25, 174*). Here, we sought to inhibit TNFR1 signaling by altering the oligomeric assembly of the receptors without disrupting ligand binding. Our results suggest two distinct modes of action in targeting receptor assembly. The first mode, which we anticipated in our experimental design (**Figure 3.1**), was to competitively target PLAD-PLAD interactions and in so-doing disrupt oligomerization of endogenous TNFR1. We proved the viability of this approach in targeting TNFR1 with zafirlukast. The second mode, which emerged as something of a surprise, is to target the receptor with small molecules that act non-competitively: triclabendazole does not compete with ligand or with PLAD-PLAD assembly.

One obvious limitation of these two small molecules isolated from the relatively small NCC library is the micromolar concentrations needed for inhibition. Moving forward in optimizing the small molecule approach, it is provocative that triclabendazole is a slightly more potent compound than zafirlukast (**Figure 3.4**). In general, small-molecule inhibitors that do not directly compete with protein-protein interactions may be the most effective for the simple fact that they are unencumbered by competition (*214-216*). In the specific case of triclabendazole, we can safely assume that the binding of the small molecule is to either the ECD or TM domain of TNFR1, because the intracellular domains in our FRET constructs are replaced with fluorescent tags, which were shown to have no interaction with the small-molecule compounds (**Figure S3.1B**). Therefore,

triclabendazole may act allosterically to disrupt receptor oligomerization; or, based on more recent discussions of small-molecule strategies for targeting receptor-receptor interactions (*214, 216*). it may bind to conformationally active sites of the receptor and disrupt the propagation of the downstream signaling. In this vein, recent work has fundamentally altered the view of TNFR activation. Older models involved ligand-induced receptor oligomerization absent any backbone conformational changes in the participating monomers. However, it is now believed that pre-assembled oligomers serve as conformational switching stations that are activated when ligand binds (*62, 180, 181, 217, 218*). In the context of this new dynamic model of activation, then, it is intriguing to think that small molecules that perturb TNFR dynamics, rather than preventing oligomerization, could be the most effective.

Regardless of the specific mechanism, our novel therapeutic strategy using small molecules that target receptor-receptor interactions holds great promise for ongoing efforts to develop more effective anti-TNFR drugs. The TNFR1ΔCD-FRET pair (TNFR1 biosensor) can be improved by increasing the FRET efficiency through optimization of donor and acceptor ratio and using other fluorescent proteins that have increased brightness, photostability, and ability to detect larger distances of separation between their fluorophores. In addition, the stable cells expressing TNFR1 biosensor will be further used in large-scale screening to identify potent compounds that reduce FRET to a greater extent. Increasing the dynamic range of the biosensor as well as identifying compounds that are more potent will result in a higher Z' value and enhance the assay quality. This strategy, using our TR-FRET based high-throughput screening approach, should be generally applicable to other drug discovery efforts targeting receptor-receptor interactions.

3.6. Supplemental figures

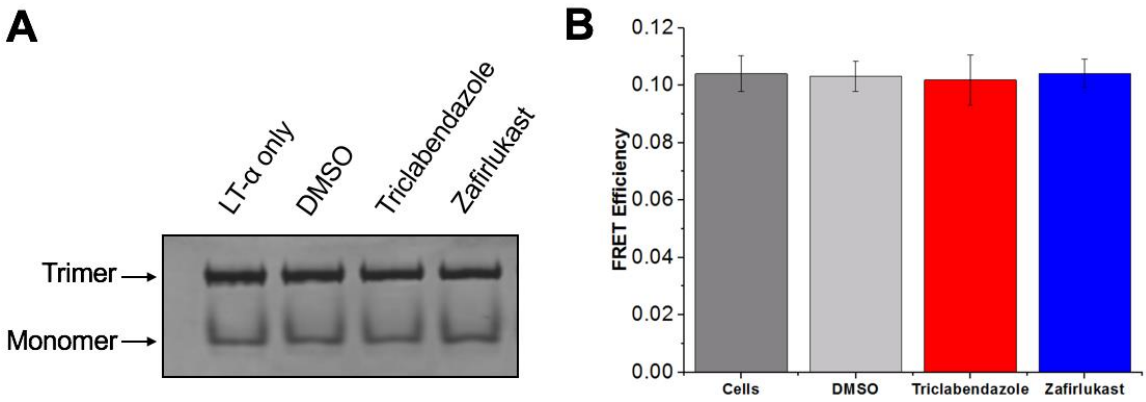

Supplemental Figure 3. 1. Effect of Triclabendazole and Zafirlukast on the oligomeric assembly of ligand and the cytosolic fluorophores.

(A) Coomassie-stained Native-PAGE gel of LT-α with two hit compounds. (B) Effect of both drugs on fluorophores by FRET measurements.

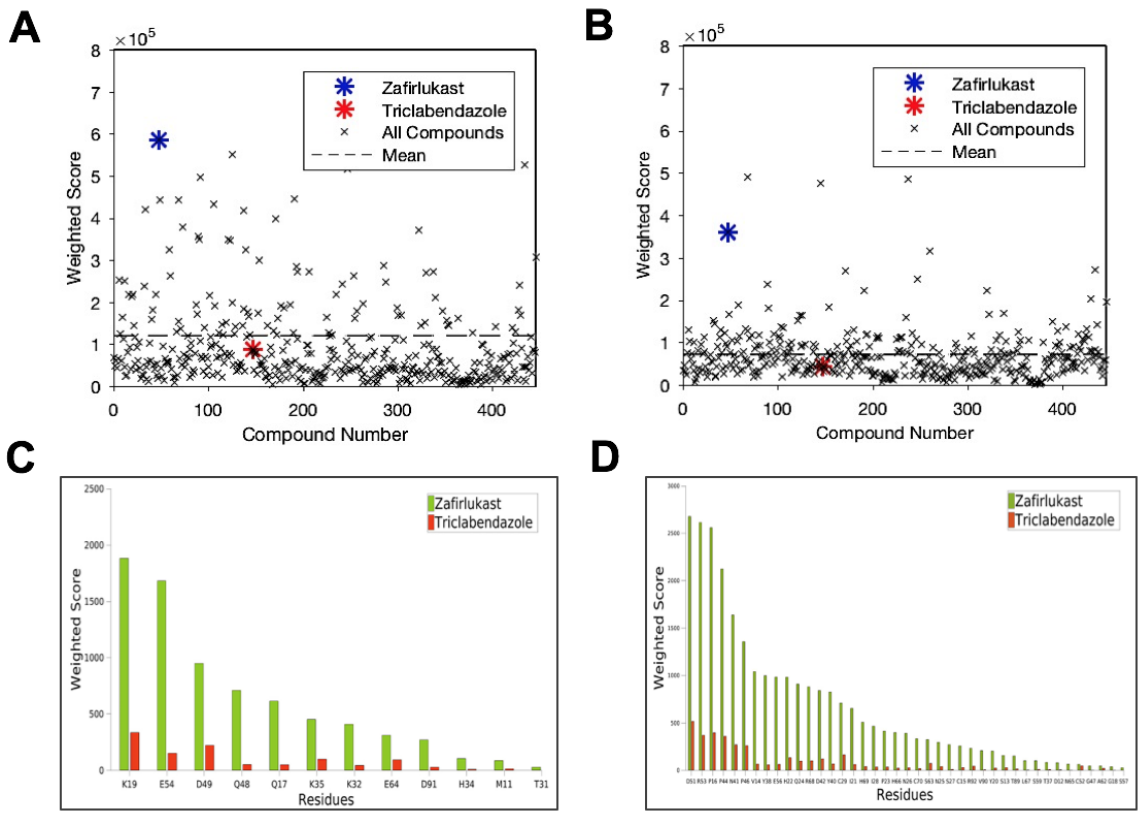

Supplemental Figure 3. 2. Analysis of molecular docking of NCC library and hit compounds.

(A) Weighted docking scores for each compound contacting interfacial residues. (B) Weighted docking scores for each compound when not in contact with interfacial residues. (C) Weighted scores for Zafirlukast and Triclabendazole docking to the TNFR1 dimer interface residues. (D) Weighted scores for Zafirlukast and Triclabendazole docking to the dimer non-interface residues.

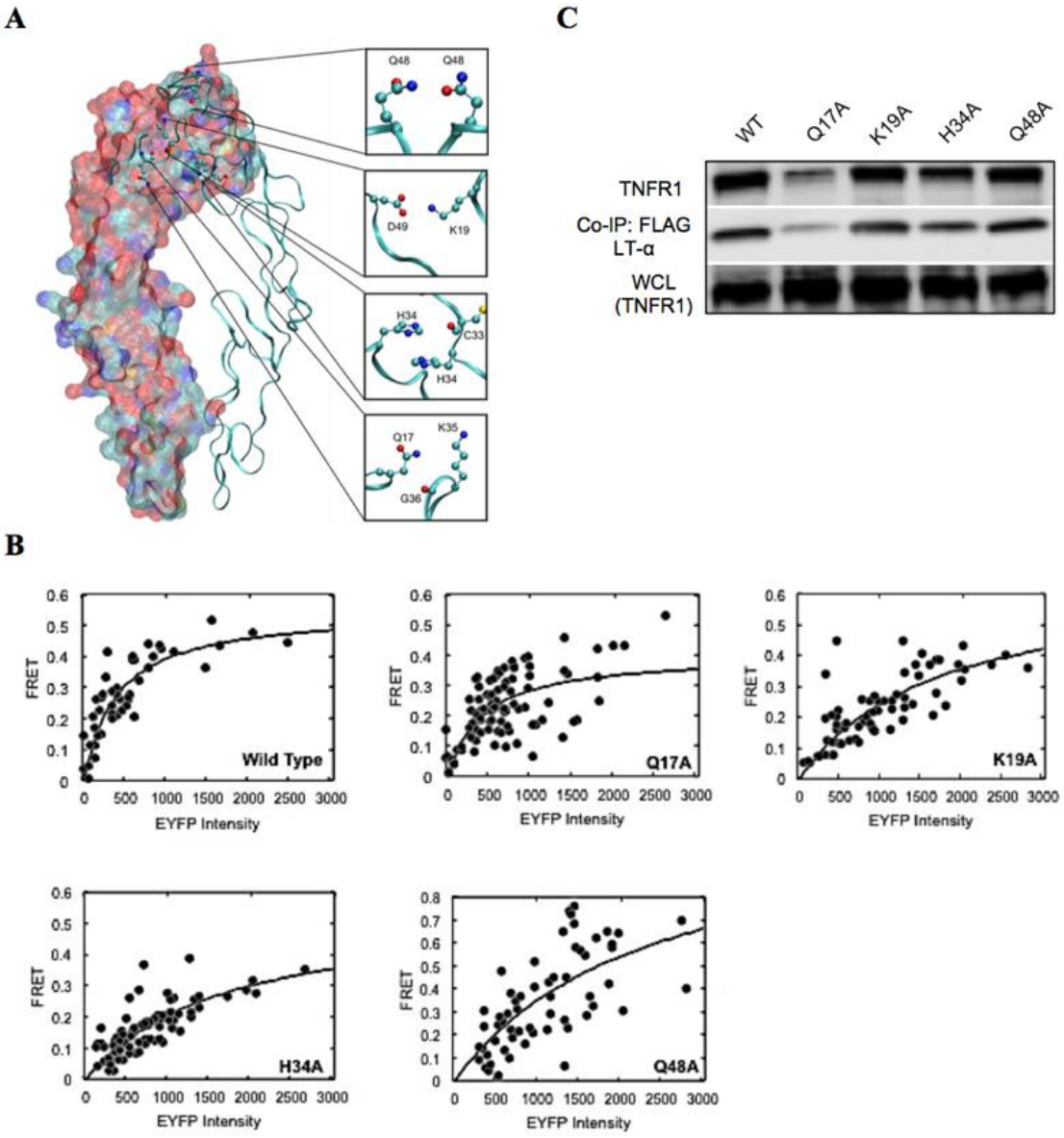

Supplemental Figure 3. 3. Mutational analysis of the TNFR1 dimer interface residues.

(A) Rationally selected residues (Q17, K19, H34 and Q48) for mutation and their interaction partners in the TNFR1 PLAD (PDB: 1NCF). (B) Qualitative FRET analysis shows a higher concentration of acceptor required to reach saturation for K19A, H34A and Q48A compared to wild type, which indicates that these residues play significant roles in pre-ligand association of TNFR1. (C) Co-immunoprecipitation of TNFR1 mutants with FLAG-tagged LT-α indicates that the mutations do not eliminate ligand binding. **CHAPTER 4: NONCOMPETITIVE INHIBITORS OF TNFR1 PROBE CONFORMATIONAL ACTIVATION STATES**

Adapted with permission from:

Chih Hung Lo[1], Tory M. Schaaf[2], Benjamin D. Grant[3], Colin Kin-Wye Lim[1], Prachi Bawaskar[2], Courtney C. Aldrich[4], David D. Thomas[2,5], and Jonathan N. Sachs[1,*].

Noncompetitive inhibitors of TNFR1 probe conformational activation states. *Science Signaling*, 2019, 12(592): eaav5637.

[1]Department of Biomedical Engineering, University of Minnesota, Minneapolis, MN 55455, USA.

[2]Department of Biochemistry, Molecular Biology, and Biophysics, University of Minnesota, Minneapolis, MN 55455, USA.

[3]Fluorescence Innovations, Inc., Minneapolis, MN 55414, USA.

[4]Department of Medicinal Chemistry, University of Minnesota, Minneapolis, MN 55455, USA.

[5]Photonic Pharma LLC, Minneapolis, MN 55410, USA.

Author contributions: C.H.L. designed and conducted all the experiments. T.M.S., B.D.G. and D.D.T. provided technical support and data analysis for the TR-FRET experiments and high-throughput screening. C.K.W.L. contributed to some cell-based assays and biochemical experiments. P.B. provided technical assistance in cell culture. C.C.A. provided expertise and input for the structure-activity relationship analysis. J.N.S. provided input for research design and interpretation. C.H.L and J.N.S. wrote the manuscript.

4.1. Summary

Tumor necrosis factor receptor 1 (TNFR1) is a central mediator of the inflammatory pathway and is associated with several autoimmune diseases such as rheumatoid arthritis. A revision to the canonical model of TNFR1 activation suggests that activation involves conformational rearrangements of pre-assembled receptor dimers. Herein, we identified small molecule allosteric inhibitors of TNFR1 activation and probed receptor dimerization and function. Specifically, we used a fluorescence lifetime-based high-throughput screening and biochemical, biophysical and cellular assays to identify small molecules that non-competitively inhibit the receptor without reducing ligand affinity or disrupting receptor dimerization. We also found that residues in the ligand binding loop critical to the dynamic coupling between the extracellular and the transmembrane domains, played a key gatekeeper role in the conformational dynamics associated with signal propagation. Finally, using a simple structure-activity relationship analysis we demonstrated that these newly discovered molecules were further optimizable for improved potency and specificity. Together these data solidify and deepen the new model for TNFR1 activation.

4.2. Introduction

Tumor necrosis factor receptor 1 (TNFR1) plays a key role in the transduction of inflammatory signals (*5*). Binding of its native ligands, tumor necrosis factor-alpha (TNFα) and lymphotoxin-alpha (LTα), to TNFR1 stimulates IκBα degradation and NF-κB activation, which has been associated with several autoimmune diseases such as rheumatoid arthritis (*5, 11, 173*). Therapeutic targeting of TNFR1 signaling is a billion-dollar industry (*17*). Unfortunately, and despite the availability of crystal structures for over two decades (*57, 59*), currently available anti-TNF therapeutics do not directly or specifically target the receptors, and as a consequence induce dangerous side-effects (*21, 23-25*). Thus, there is an urgent need to develop a new approach to inhibition of TNFRs. The most promising approach will be to take advantage of the available structures to deepen our understanding of the structure-function relationship of TNFR1, with the goal of rationally maximizing the efficiency of inhibitors.

Ligand binding induces TNFR1 trimerization, which promotes trimerization of cytosolic death domains and concomitant recruitment of downstream signaling machinery (*21, 57*). This model is primarily based on the original crystal structure of a ligand-bound, trimeric receptor complex, in which there are no direct receptor-receptor interactions (*57*). However, this model is confounded by the fact that TNFR1 is pre-assembled as high-affinity receptor dimers in the plasma membrane (*55, 58, 59*). Based on the crystal structure, and on subsequent mutagenesis studies (*55, 58-60*), pre-ligand dimerization is driven by well-defined monomer-monomer interactions across the pre-ligand assembly domains (PLAD), located within the N-terminal cysteine-rich domain (CRD1) and far from the ligand binding loop. Critically, there is no evidence to suggest that these dimer structures dissociate on ligand binding, despite the lack of receptor-

receptor interactions in the trimeric structure. Thus, reconciling this apparent inconsistency in the dimer and trimer structures is a long-standing goal within the field (*182*).

Using TNFR1 and Death Receptor 5 (DR5), another member of the TNFR superfamily, we have provided evidence for a revision to the accepted model of TNFR activation that reconciles both structural states (*60, 62, 180, 181, 219, 220*). We and others speculate that TNF receptor dimers may form the nexus for larger scale networks of ligand-bound TNFR trimers (*181, 221-223*), and we show this to be the case in one of two alternatively spliced isoforms of DR5 (*181*). Based on the crystal structures of TNFR1 (*57, 59*), we build a structural model of this oligomeric network, which in its minimal, active state consists of a dimer of ligand-bound trimers (**Figure 4.1A**) (*62*). This minimal size has been supported by super-resolution techniques (*183*). In this model, the pre-assembled dimer remains intact upon ligand binding, and is predicted to undergo a conformational change that propagates from the extracellular domain (ECD) to the cytosol without dimer dissociation. Our focus here is the further exploration of conformational dynamics as central to TNFR1 inhibition, and as a potential target for inhibitory small molecules. While we have focused on the idea that dimer itself is the functional signaling unit, the receptor trimer complex (non-interacting receptor monomers stabilized by ligand binding) may still be functional (though perhaps less so). Regardless of this open controversy, the idea that activation is accompanied by conformational changes, be they in the dimer or trimer, now has solid support (*62, 224*). In particular, fluorescence resonance energy transfer (FRET) data suggest, without delineating a clear mechanism, that ligand binding causes a conformational change in the pre-assembled TNFR1 complex (*61, 224*). In addition, we use FRET to show that a constitutively active, disease-related mutant (R92Q) is, like wild-type, pre-assembled as

a dimer (*62*). Importantly, the FRET measurements show that this active R92Q dimer is conformationally distinct from wild-type, the first direct evidence of a correlation between the backbone structure of the pre-assembled TNFR1 dimer and receptor activity. As further support, our computational normal mode analysis of an elastic network model of the TNFR1 crystal structures suggests a long-range, anti-correlated motion near the ligand binding loop that propagates a conformational change through the backbone of the ECD (*62*).

Collectively, these findings strongly suggest that TNFR1 activation is accompanied by backbone conformational changes. However, whether the backbone conformational state of TNFR1 is critical to its activation and whether altering the native conformation of the pre-assembled dimer is a viable strategy for inhibition, remain open and provocative questions. To address this, we used small molecule discovery driven by time-resolved FRET (TR-FRET) measurements of inter-monomeric spacing as a means to probe previously undetected conformational states of the pre-assembled TNFR1 dimer. We discovered a class of small molecules that perturb the conformation of TNFR1 and, critically, that do so without altering either ligand binding affinity or receptor pre-assembly. In so doing, we provided experimental proof of long-range allosteric coupling in the extracellular domain of TNFR1, which could be exploited to inhibit activation. In addition to providing further evidence for a new model of TNFR1 activation, we showed that these new molecules could be optimized for binding affinity, potency and receptor specificity, for development as potential therapeutics to directly target TNFR1.

4.3 Materials and methods

4.3.1. Molecular biology

The DNAs (TNFR1ΔCD-GFP and TNFR1ΔCD-RFP) used in the engineering of the TNFR1 FRET biosensor was generated in our previous work (*190*). Briefly, cDNAs encoding truncated TNFR1ΔCD (amino acids 1-242) were fused to the N-terminus of the EGFP and TagRFP vectors using standard cloning techniques. The mutations of the key ligand binding residues (Q107A, S108A, QS107/108AA and M80A) and the control mutant (V90A) in the TNFR1ΔCD-GFP and TNFR1ΔCD-RFP plasmids were introduced by Quikchange mutagenesis (Agilent Technologies) and sequenced for confirmation. To prevent constitutive fluorophore clustering, all vectors contain the monomeric mutation A206K to the fluorescent proteins (*204*).

4.3.2. Cell culture and generation of stable cell lines

Human embryonic kidney cells 293 (HEK293, ATCC) were cultured in phenol red-free Dulbecco's Modified Eagle Medium (DMEM, Gibco) supplemented with 2 mM L-Glutamine (Invitrogen), heat-inactivated 10% fetal bovine serum (FBS HI, Gibco), 100 U/ml penicillin and 100 μg/ml streptomycin (Gibco). HAP1 wild-type and TNFR1 knockout cells (Horizon) were cultured in Iscove's Modified Dulbecco's Medium (IMDM, Gibco) supplemented with 10% FBS (Gibco), 100 U/ml penicillin and 100 μg/ml streptomycin (Gibco). Cell cultures were maintained in an incubator with 5% CO_2 (Forma Series II Water Jacket CO_2 Incubator, Thermo Scientific) at 37 ºC. The HAP1 TNFR1 knockout cell line was edited by CRISPR/Cas to contain a 70 base pair (bp) insertion in a coding exon of TNFRSF1A. Sanger sequencing was performed as a quality control to confirm the knockout. The TNFR1ΔCD-FRET pair stable cell line was generated as described in our previous work and have been monitored continuously for over three

years with expression maintaining above 95% characterized by flow cytometry (*190*). The high expression of the TNFR1ΔCD-FRET pair in the stable cell line indicates that they are functional and applicable in high-throughput screening. The mutant forms of the TNFR1 FRET biosensor (Q107A, S108A, QS107/108AA, M80A and V90A) were generated by transiently transfecting HEK293 cells using Lipofectamine 3000 (Invitrogen) with TNFR1ΔCD-GFP and TNFR1ΔCD-RFP DNAs containing the respective mutations.

4.3.3. Large-scale high-throughput screening with ChemBridge DIVERSet library

The DIVERSet library containing 50,000 compounds was purchased from ChemBridge Corp., formatted into 96-well mother plates using a FX liquid dispenser, and subsequently formatted across 157 plates of the 384-well plate at 50 nl (10 µM final concentration per well) using an Echo liquid dispenser. Dimethyl sulfoxide (DMSO) was loaded in matching %v/v as in-plate no-compound controls as well as in column 1, 2, 23 and 24 (negative controls). The 384-well flat, black-bottom polypropylene plates (PN 781209, Greiner Bio-One) were chosen as the assay plates for their low auto-fluorescence and low inter-well cross-talk. The plates were sealed and stored at −20 °C until use. The screening was carried out across five days with ~10,000 compounds (~32 compound plates) screened each day. A week prior to screening, a fresh vial of TNFR1ΔCD-GFP/RFP (TNFR1ΔCD-FRET pair) cells were thawed, plated in a 225 cm^2 flask (Corning) and checked for expression. The cells were then expanded into six 225 cm^2 flasks for three days and further expanded into 36 flasks for another three days. Prior to each day of screening, the stable cells expressing the TNFR1 FRET biosensor were harvested to check for expression and response variation in fluorescent intensity. Stable cells were then dispensed into the drug plates (50,000 cells/well) and incubated with the compounds or DMSO as a negative control followed by fluorescence lifetime

measurements. The fluorescence waveforms were acquired by a prototype fluorescence lifetime plate-reader (Fluorescence Innovations, Inc.) as described (*190*).

4.3.4. HTS data analysis

Time-resolved fluorescence waveforms obtained for each well were fitted to single-exponential decays using least-squares minimization global analysis software (Fluorescence Innovations, Inc.) to give donor-acceptor lifetime (τ_{DA}) from the TNFR1ΔCD-GFP/RFP (FRET pair) cell line and donor lifetime (τ_D) from a TNFR1ΔCD-GFP donor-only control cell line. FRET efficiency (*E*) was then calculated based on Equation 1.

$$E = 1 - \left(\frac{\tau_{DA}}{\tau_D}\right) \qquad Eq.1$$

The Z-factor, a HTS assay quality indicator, was determined with zafirlukast as a positive control and DMSO as a negative control and calculated based on Equation 2 (*192*).

$$Z' = 1 - \frac{3(\sigma_p + \sigma_n)}{|\mu_p - \mu_n|} \qquad Eq.2$$

where σ_p and σ_n are the standard deviations of the observed τ_{DA} values, and μ_p and μ_n are the mean τ_{DA} values of the positive and negative controls, respectively. To make this metric less sensitive to strong outliers, we utilized the normalized median absolute deviation (1.4826*MAD) and median in place of the standard deviation and mean, respectively (*225*). The Z-factor obtained was 0.76±0.02, indicating excellent assay quality.

Fluorescent compounds were flagged as potential false positives due to interference from compound fluorescence by a set of stringent fluorescent compound filters based on analysis of the spectral waveforms of each well from the DIVERSet screen (*226*). After removal of fluorescent compounds, histogram of the FRET

distribution from all compounds in the screen was plotted and fitted to a Gaussian curve to obtain a mean and standard deviation (SD). A hit was defined as a compound that decreased the FRET efficiency by more than three times the standard deviation (3SD) relative to the mean.

4.3.5. FRET dose-response assay

The hit compounds, DS41 (ID 19298144), DS42 (ID 43812755), DS43 (ID 23420063), DS44 (ID 95020298), DS45 (ID 45055796), DS50 (ID 33619467) and DS51 (ID 74188632) were purchased from ChemBridge Corp. A negative control compound (ID 65311687) was also purchased. These drug compounds were dissolved in DMSO to make 10 mM stock solution which were then subsequently serially diluted in 96-well mother plates to obtain eight doses at 50X concentrations. Hits were screened at eight different concentrations (0.1 to 200 μM). Compounds (1 μl) were transferred from the mother plates into assay plates using a Mosquito HV liquid handler (TTP Labtech Ltd.). The cell preparation of the wild-type TNFR1 FRET biosensor in the FRET dose-response assays were carried out through the same way as the high-throughput screening.

4.3.6. Functional assays (IκBα degradation assay and NF-κB activation assay)

IκBα degradation assay and NF-κB activation assay with HEK293 cells were carried out as described (*190*). Densitometry of the Western blots was performed using Image Studio (LI-COR Biosciences) and data are normalized to the β-actin loading control and the amount of IκBα in the control cells in the absence of ligand. For TRADD-induced NF-κB activation in HEK293 cells, cells (1×10^6) in a 6-well plate were transfected with 1 μg of NF-κB firefly luciferase reporter genes, 0.1 μg of *Renilla* luciferase reporter genes, 1 μg of TRADD plasmid and 0.4 μg of control plasmid to give

2.5 μg of total DNA. In the control cells, the TRADD plasmid was replaced with control plasmid. After 3 hours of transfection, cells were harvested and plated (30,000 cells/well, total volume 50 μl) into 96-well white solid bottom assay plates (Greiner Bio-One North America). Drug treatments (0.1 to 200 μM) or DMSO (negative control) was performed 5 hours after cell plating. Luciferase activities were determined 24 hours after treatments. Briefly, 50 μl of Dual-Glo Luciferase Reagent (Promega) was added, incubated at room temperature for 15 min, and measured firefly luminescence using a Cytation 3 Cell Imaging Multi-Mode Reader luminometer (BioTek). Next, 50 μl of Dual-Glo Stop & Glo Reagent (Promega) was added, incubated at room temperature for 15 min, and measured *Renilla* luminescence using luminometer. The luciferase activities were normalized on the basis of *Renilla* expression levels.

For NF-κB activation luciferase assay with HAP1 wild-type and TNFR1 knockout cells, the cells were transfected with the NF-κB-luciferase reporter genes (10 μg of firefly luciferase genes and 1 μg of *Renilla* luciferase genes) in a 100 mm plate with Lipofectamine 3000 (Invitrogen). On the following day, cells were lifted with TrypLE and resuspended in phenol red-free DMEM (Gibco). These cells were dispensed into 96-well assay plates (30000 cells/well, total volume 50 μl) and incubated with drugs (0.1 to 200 μM) or DMSO (negative control) in the presence (0.1 μg/ml) and absence of LTα for 18 hours at 37 °C. Readings for luciferase activities were acquired as described above. All data from NF-κB activation assays were normalized to luciferase activity of cells in the presence of ligand or TRADD overexpression.

4.3.7. Mechanistic assays (co-immunoprecipitation and native gel characterization)

Co-immunoprecipitation between endogenous TNFR1 and ligand LTα in the presence and absence of hit compounds was performed as described previously (*190*). The overexpression and purification of the N-terminal FLAG-tagged LTα and FLAG-tagged TNFR1 PLAD (residues 30-82) were carried out as described previously and the soluble PLAD protein was shown to exist as dimers under native conditions (*190*). The recombinant human TNFR1 extracellular domain (ECD) was purchased from Abcam. The purity of the proteins was assessed by 4%–15% SDS-PAGE gels (Bio-Rad) under reducing conditions, followed by Coomassie staining. Protein concentrations were measured using the BCA assay (Thermo Fisher Scientific). To test the disruption of receptor-receptor or ligand-ligand interactions, purified soluble TNFR1 PLAD or ECD and LTα (5 μg) were assessed by Native-PAGE gels (Bio-Rad) in the absence and presence of hit compounds (200 μM) under non-reducing conditions followed by Coomassie staining. Native-PAGE gel of soluble PLAD was also characterized by Western blot with TNFR1-specific antibody (H-5) (sc-8436, Santa Cruz Biotechnology) that targets the extracellular domain of the receptor. Competition assay between the hit compounds and zafirlukast was performed by the co-treatment of both the hit compounds (200 or 1000 μM) and zafirlukast (200 μM) at the same time to soluble PLAD and observed the extent of disruption of PLAD-PLAD interactions.

4.3.8. Surface plasmon resonance (SPR) binding assay

Binding affinity between TNFR1 ECD and compounds or ligand was determined by SPR analysis using BIAcore S200. Recombinant human TNFR1 ECD (Abcam) was immobilized on the CM5 sensor chip (Biacore, GE Healthcare) by amine coupling.

Briefly, the dextran surface was activated with a 1:1 mixture of 0.4 M 1-ethyl-3-(3-dimethylaminopropyl)carbodiimide hydrochloride and 0.1 M N-hydroxysuccinimide. TNFR1 ECD (20 µg/ml) in 10 mM sodium acetate at pH 5 was flowed past a working surface before blocking the remaining activated carboxymethyl groups with 1 M ethanolamine at pH 8.5 to achieve a level of 2500 RU suitable for binding analysis. The reference surface was activated and reacted with only ethanolamine.

For direct binding assays between the receptor and the small molecules, the hit compounds and the analogues at eight different concentrations (0.1-200 µM) as well as DMSO-only controls were prepared in HEPES-EP containing a total of 2% DMSO. For competition assays between ligand and small molecules, ligand at eight different concentrations (LTα = 0.1-200 nM) was prepared in HEPES-EP in the presence of saturated dose of compounds (200 µM) or DMSO containing a total of 2% DMSO. For other competition assays, samples containing small molecules and/or antibody were prepared in HEPES-EP buffer. The samples were injected over both the reference and ECD immobilized surfaces at 10 µl/min for 90 seconds and dissociated in glycine-HCl pH 2.5. All of the samples, along with blanks from buffer and DMSO-only controls were measured on a 96-well microplate (Biacore, GE Healthcare) at 25 °C. Reflectivity response data points were extracted from response curves at 5 seconds prior to the end of the injection to determine steady-state binding. All the data were double referenced with blanks using standard procedures with Biacore S200 Evaluation Software v1.0.

4.3.9. Computational analysis of crystal structure

For analysis of the TNFR1 crystal structure, visual molecular dynamics (VMD) was used. The crystal structure of the pre-ligand dimer of TNFR1 ECD was downloaded from the Protein Data Bank (PDB: 1NCF) (*59*) and the structure preparation was done in CHARMM-GUI. The distance measurement of the TNFR1 ECD was performed in VMD.

The hydrogen bonds between the residues in the ligand binding loop were determined by VMD with distance cutoff of <3.2Å and angle cutoff of <60^{o}.

4.3.10. Structure-activity relationship (SAR) analysis

The analogues of the lead compound (DS41) were identified through a search of the company's database (ChemBridge) that share more than 90% similarity (based on the chemical functionality and scaffolding as determined by the company's similarity search engine) to the lead compound. A total of 19 analogues of DS41 (compound IDs in table S1) were purchased from ChemBridge Corp. The analogues were dissolved in DMSO to make 10 mM stock solution which were then subsequently serially diluted in 96 well mother plates at eight different doses (0.1 to 200 μM) at 50X concentration. FRET measurements were performed using the wild-type TNFR1 FRET biosensor at a compound concentration of 50 μM. The inhibition of IκBα degradation of the analogue was tested at a compound concentration of 200 μM and the inhibition of NF-κB activation was determined in a dose-dependent manner to obtain the IC_{50} values and percent inhibition listed in table S1. SPR binding assays, specificity tests and mechanistic assays were conducted with methods and materials as described above.

4.3.11. Statistical analysis

Data are presented as mean ± standard deviation unless stated otherwise. To determine statistical significance for all experiments, data analysis was performed by a two-tailed unpaired *t* test (Student's *t* test) with *P* values determined by using GraphPad Software. Values of $P < 0.05$ were considered statistically significant. GraphPad style in using asterisks to denote *P* values in figures was used (*$P < 0.05$, **$P < 0.01$, ***$P < 0.001$ and ****$P < 0.0001$).

4.4. Results

4.4.1. Discovery of small molecules that modulate conformational states of pre-assembled dimeric TNFR1

We performed high-throughput screening of the 50,000 compound ChemBridge DIVERSet library to identify small molecules that modulate TNFR1 conformational states. To detect changes in the cytosolic spacing between receptor monomers, we used our previously engineered stable cell lines expressing a TNFR1ΔCD-FRET pair construct, in which either a green or red fluorescent protein (GFP or RFP) is fused to the C-terminus of TNFR1 with a truncated cytosolic domain (ΔCD) (TNFR1ΔCD-GFP as donor and TNFR1ΔCD-RFP as acceptor) (**Figure 4.1B**)**.** We show that these truncated receptor constructs are properly trafficked to the plasma membrane where they maintain their pre-assembled dimeric assembly (*62*), and are validated for high-throughput screening on a smaller library in the absence of ligand (*190*). As will be clarified below, changes in FRET could represent either: 1) dissociation of the TNFR1 dimer; or 2) as is our focus in this study, a change in the backbone conformation of the receptor that results in small changes in inter-monomeric spacing without inhibiting dimerization. The screen was enabled by a high-throughput fluorescence lifetime plate-reader technology that has an increased precision of TR-FRET based screening by a factor of thirty (*163*), which allows for reliable detection of subtle protein structural changes and is capable of monitoring allosteric regulation of receptors by small molecules.

The FRET efficiency for all of the compounds, after removing the potential false negatives, was plotted (**Figure 4.1C**) and the distribution of efficiencies was fitted to a Gaussian distribution to obtain a mean and standard deviation (SD). The top forty compounds, each of which decreased the average FRET by more than 3SD greater than

the mean of control cells, were selected and purchased from ChemBridge Corp. For simplicity we have limited our search to compounds that reduce FRET, though others that increase FRET may also be of interest in future studies. The compounds were then tested for dose-dependent FRET change to confirm their specific interactions with the biosensor as well as to measure the potency and the extent of receptor perturbation by the compounds. Seven of the forty hit compounds had a dose-dependent decrease in FRET efficiency (**Figure 4.1D**) with half-maximal effects (relative EC_{50}) ranging between 20-110 μM, with DS43 having the lowest EC_{50}. No FRET change was observed with a negative control compound (fig. S3.1A). We note that from our previous study the EC_{50} of the dimer-breaking compound zafirlukast was at the lower end of this spectrum (18 μM) (**Figure 4.1D**). The structures of these seven novel compounds identified from the screen are given (fig. S4.1B).

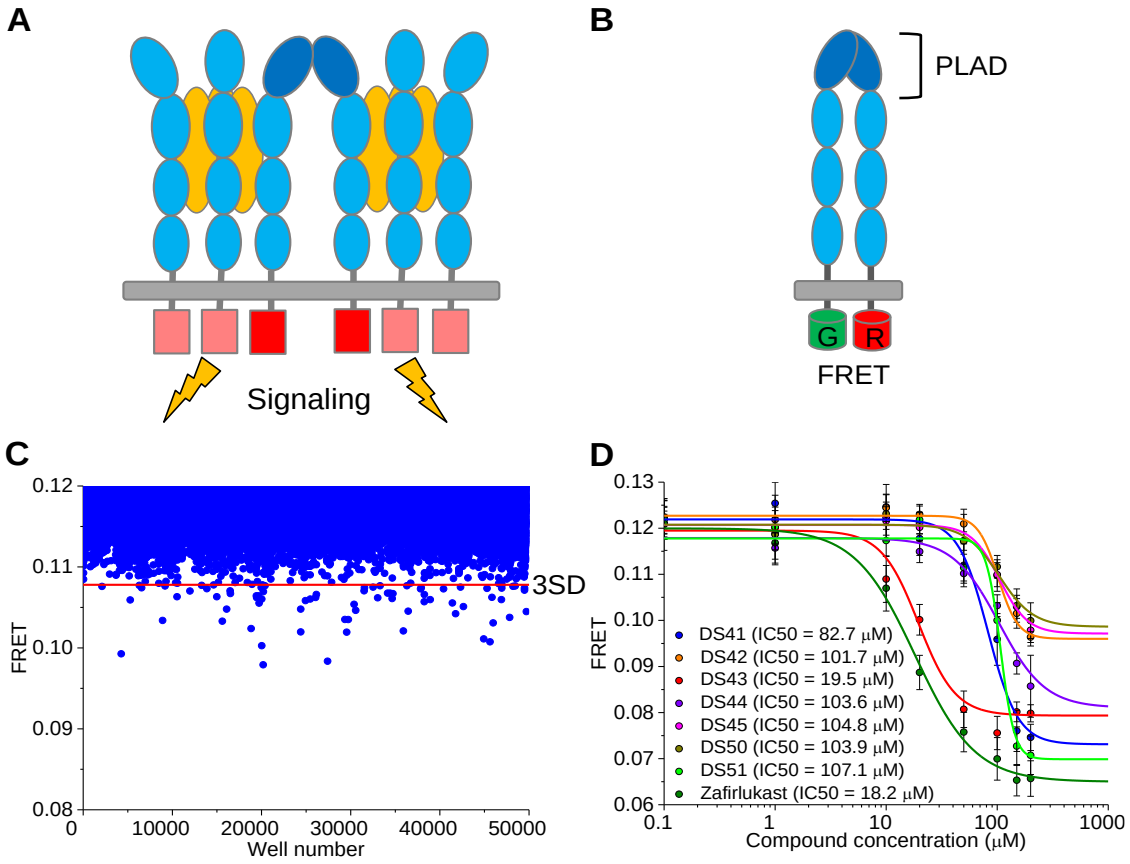

Figure 4. 1. Discovery of small molecules that perturb conformational states of pre-assembled TNFR1 dimer.

(A) Schematic of ligand-induced oligomerization of TNFR1 trimers held together by the pre-ligand assembly domain (PLAD). (B) Schematic of the TNFR1ΔCD-FRET biosensor engineered by fusing the green or red fluorescent proteins (GFP or RFP) to the C-terminus of TNFR1 with truncated cytosolic domain. Ligand-independent association of the fluorophore-tagged receptors through PLAD-PLAD interactions results in fluorescence resonance energy transfer (FRET). The FRET biosensor is capable of detecting changes in the cytosolic spacing between receptor monomers. (**C**) High-throughput screening of ChemBridge DIVERSet 50,000 compound library using the TNFR1 FRET biosensor expressed in HEK293 cells. Compounds that reduced the FRET efficiency below the applied threshold (red line) were selected for further characterization. Data are representative of one experiment. (**D**) Secondary FRET analysis of the dose response

of the seven hit compounds and zafirlukast (known TNFR1 inhibitor). Data are means ± SD from three independent experiments.

4.4.2. Cell-based assays to determine the biological activity and efficacy of hit compounds

The dose-dependent effect of hit compounds on ligand-induced IκBα degradation was determined by immunoblotting (**Figure 4.2A**). After LTα treatment, IκBα was degraded to 20% of the basal levels in HEK293 cells (**Figure 4.2B**). IκBα degradation was inhibited in a dose-dependent manner with treatment of each of the seven hit compounds, and potency measurements showed relative inhibitory concentrations (relative IC_{50}) between 30 μM and 111 μM (**Figure 4.2C**). To test inhibition of NF-κB activation, a luciferase assay was performed in the presence of LTα (**Figure 4.2D**). Hit compounds again inhibited ligand-induced NF-κB activation in a dose-dependent manner, with relative IC_{50} of the compounds between 14 μM and 90 μM (**Figure 4.2E**). We note that both functional assays produced IC_{50} values that roughly correspond to the FRET results, although important differences do exist that reflect differences in the specificity of the individual compounds for the receptor. This important nuance will be addressed below with studies using TNFR1 knockout cell line. Additionally, we note from the luciferase assay that a basal NF-κB activation (20% relative luciferase activity) was observed in HEK293 cells in the absence of exogenous ligands. This has been suggested to be due to constitutive signaling of cytokine receptors in the ligand-free state including TNFR1 (*227, 228*). Specific inhibition of TNFR1 such as through upregulation of silencer of death domain (SODD) has been shown to be able to reduce this constitutive signaling (*228*).

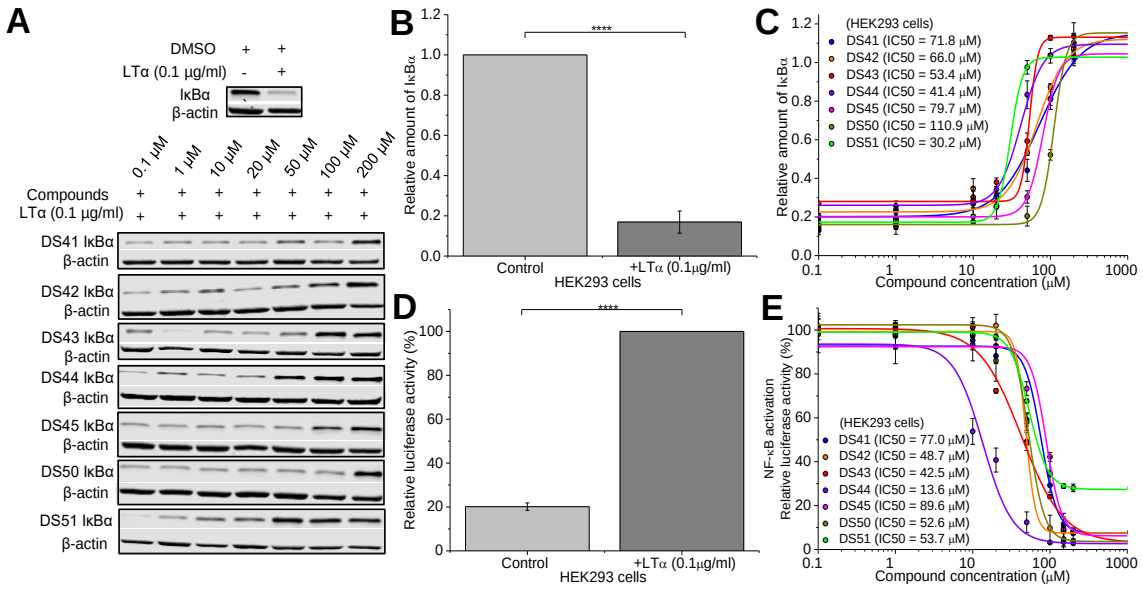

Figure 4. 2. Hit compounds inhibit TNFR1-stimulated NF-κB activation.

(A to C) Western blot analysis of IκBα abundance in lysates of HEK293 cells treated with LTα and the hit compounds at the indicated doses. Western blots (A) are representative of three independent experiments. Quantified band intensity values (B and C) are means ± SD from all experiments. ****P < 0.0001 versus control by two-tailed unpaired t test. (D and E) Luciferase assay of NF-κB activation in HEK293 cells transfected with reporter plasmids and treated with LTα and DMSO control (D) or LTα and increasing concentrations of hit compounds (E). Data are means ± SD of three independent experiments. ****P < 0.0001 versus control by two-tailed unpaired t test.

4.4.3. A subset of hit compounds are receptor-specific in blocking TNFR1-induced NF-κB activation

To determine which, if any, of the seven hit compounds are acting directly on TNFR1, we first performed measurements with surface plasmon resonance (SPR). Purified TNFR1 extracellular domain (ECD) was immobilized onto the SPR chip, which was followed by flowing the compounds through the chip to allow for binding. All hit

compounds showed dose-dependent binding to the TNFR1 ECD with binding affinities (K_d) between 31 and 81 μM, as compared to 86 μM for zafirlukast (**Figure 4.3A** and fig. S4.2, A to H).

Next, we aimed to establish whether the functional effects of the hit compounds (**Figure 4.2E**) are specifically due to binding the receptor and alteration of the receptor conformation, rather than through the inhibition of proteins in alternate signaling pathways. To do so, we first used a TNFR1 knockout (KO) HAP1 cell line established by CRISPR. We treated both parental wild-type (WT) and TNFR1 KO HAP1 cells with increasing doses of LTα. As expected, WT HAP1 cells showed a dose-dependent increase in luciferase activity which was not observed in the TNFR1 KO cells, confirming that the TNFR1 KO cells were not functionally sensitive to TNFR1 stimulation (**Figure 4.3B**). A ligand concentration of 0.1 μg/ml was chosen for treatment of both WT and TNFR1 KO HAP1 cells as maximum NF-κB activation measured by luciferase activity was obtained at this concentration in the WT cells while the TNFR1 KO cells remained non-functional (**Figure 4.3C**).

As in the case of the HEK293 cells (**Figure 4.2D**), the KO cells showed basal activation of the NF-κB pathway (approximately 20% relative luciferase activity). Importantly, this basal activity was unchanged in the presence of ligand. This feature makes these cell lines useful as a first control to ensure that the functional effects we observed in the HEK293 cells were due to direct interactions with TNFR1 and not due to the compounds indirectly acting on other proteins on alternate NF-κB pathways. As expected, all compounds reduced ligand-induced NF-κB activation in the WT HAP1 cells to very a similar extent as was observed in the HEK293 cells (**Figure 4.3D** and fig. S4.3A). Then, the TNFR1 specificity of the compounds was determined by monitoring

whether and to what extent they altered the basal level of NF-κB activation in the TNFR1 KO cells. Our expectation was that the truly specific compounds should have no impact on this basal activity. To show the effectiveness of this approach, DS44 and DS50 reduced the basal level of NF-κB activation in the TNFR1 KO cells at similar IC_{50} to the WT cells (fig. S4.3B), clearly demonstrating a non-specific interaction with other proteins in the cells and ruling these two compounds out as specific inhibitors of TNFR1. We noted that DS44 was the compound with the highest binding affinity for TNFR1, as measured by SPR, highlighting the importance of this specificity test. DS41, DS43, DS45 and DS51 are all specific at the range near their IC_{50}, but each of these compounds do show some non-specificity at higher concentrations (**Figure 4.3E** and fig. S4.3B). DS42, on the other hand, together with zafirlukast, emerged as the most specific of the newly discovered inhibitors, showing almost no effect on basal levels in the TNFR1 KO cells even at high concentrations (**Figure 4.3E**).

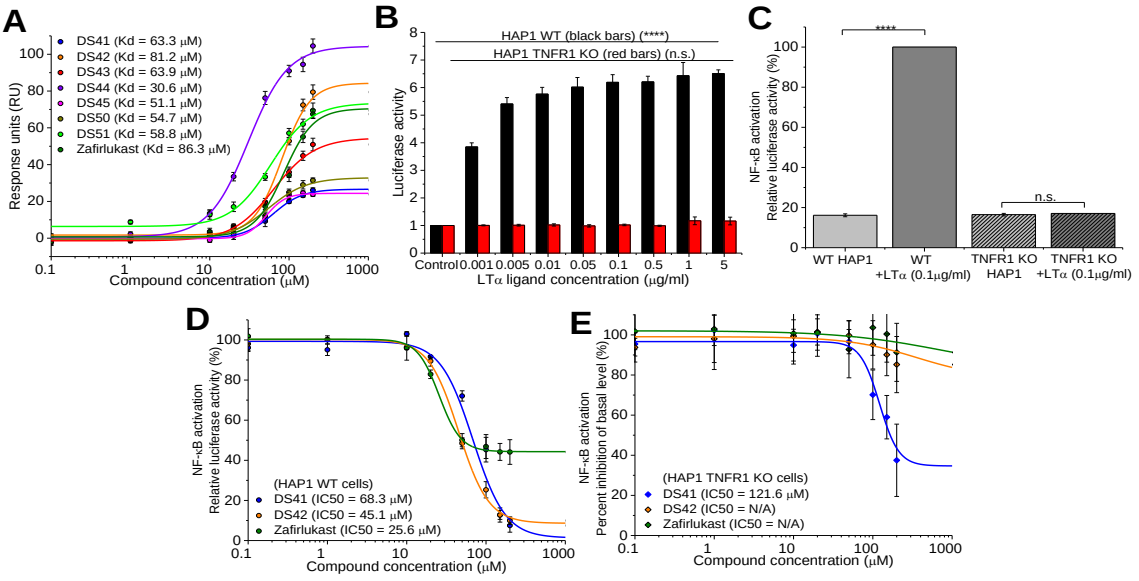

Figure 4. 3. Hit compounds bind TNFR1 and require the receptor for their effects.

(A) Direct binding of the hit compounds to the TNFR1 extracellular domain (ECD) was characterized by surface plasmon resonance (SPR). Data are means ± SD from three

independent experiments. (B) Dose-dependent ligand-induced NF-κB activation in both wild-type (WT) and TNFR1 knockout (KO) HAP1 cells. Data are means ± SD of three independent experiments. ****P < 0.0001 versus control by two-tailed unpaired t test and n.s. indicates not significant. (C) NF-κB activation in WT and TNFR1 KO HAP1 cells with the optimized LTα concentration of 0.1 μg/ml. Data are means ± SD of three independent experiments. ****P < 0.0001 versus control by two-tailed unpaired t test and n.s. indicates not significant. (D and E) NF-κB activation in WT HAP1 cells (D) and TNFR1 KO HAP1 cells (E) treated with LTα and increasing concentration of compounds (DS41, DS42 and zafirlukast) to test the specificity of the compounds to TNFR1. Data are means ± SD of three independent experiments.

As a second control to further determine the specificity of the compounds, we tested their effect on TNFR1-associated death domain (TRADD)-induced NF-κB activation, independent of ligand activation of TNFR1. Because TRADD is the first cytosolic protein in the TNFR1 cascade, testing the effect of the compounds after stimulating TRADD—without involving TFNR1—represents the most complete control for specificity. Overexpression of TRADD significantly increased the NF-κB activation in HEK293 cells (fig. S4.4A), which was shown previously (*229*). Both DS42 (fig. S4.4B) and zafirlukast (fig. S4.4C) had little effect on TRADD-induced NF-κB activation, even at relatively high concentrations; DS42 did show partial inhibition at 200 μM, though this is well above its IC_{50}. In contrast, DS41, which showed some non-specificity in inhibiting basal NF-κB activity in the TNFR1 KO HAP1 cells, also inhibited TRADD-induced NF-κB activation at a similar IC_{50} to its inhibition of the TNFR1-induced NF-κB activation (fig. S4.4D). These results further confirmed the high specificity of DS42 and zafirlukast in targeting TNFR1.

4.4.4. Small-molecule inhibitors do not change binding affinity of ligand to TNFR1

After determining the specificity of each of the compounds, we then aimed to parse whether the mechanisms of action of these compounds is to perturb ligand-receptor interactions, receptor-receptor interactions such as dimerization, or a new mechanism: alteration of conformational states of the receptor. We note that DS42 had only a small, though significant, effect on FRET. If we were able to show that the compound does not prevent ligand binding or dimerization, this would highlight the possibility that subtle changes in conformation of the pre-assembled dimer may be enough to inhibit the receptor in the ligand-bound, fully assembled state.

First, to test whether the compounds act by blocking ligand binding, we monitored ligand-receptor binding in the absence and presence of the compounds using co-immunoprecipitation (co-IP) and SPR. Co-IP experiments qualitatively confirmed that none of the hit compounds eliminate ligand-receptor interactions (**Figure 4.4A**). To quantitatively confirm the non-competitive nature of the compounds, we performed SPR measurements in the presence of both the ligand and the compounds. Both LTα (50 nM) and the compounds (DS42 and zafirlukast at 200 μM) were passed through the TNFR1 ECD immobilized surface for SPR measurements with individual treatment of ligand-only or compound-only as controls. For both DS42 and zafirlukast, the response from co-treatment of ligand and compounds was equal to the sum of the individual response from ligand-only or compound-only binding, indicating simultaneous binding of the ligand and the small-molecule inhibitors to the receptor (**Figure 4.4B**). We then investigated the dose-dependence of ligand binding to TNFR1 in the presence of the compounds to determine if either had any effect on ligand binding affinity (K_d). We found that in the absence of compounds, the K_d of LTα is 37 nM (**Figure 4.4C** and fig. S4.5A)**,** as expected (*230*). In the presence of saturating concentrations of the compounds, DS42

(200 μM) or zafirlukast (200 μM), LTα binding affinity was essentially unchanged (within error of the measurements) (**Figure 4.4,** D to F and fig. S4.5, B and C).

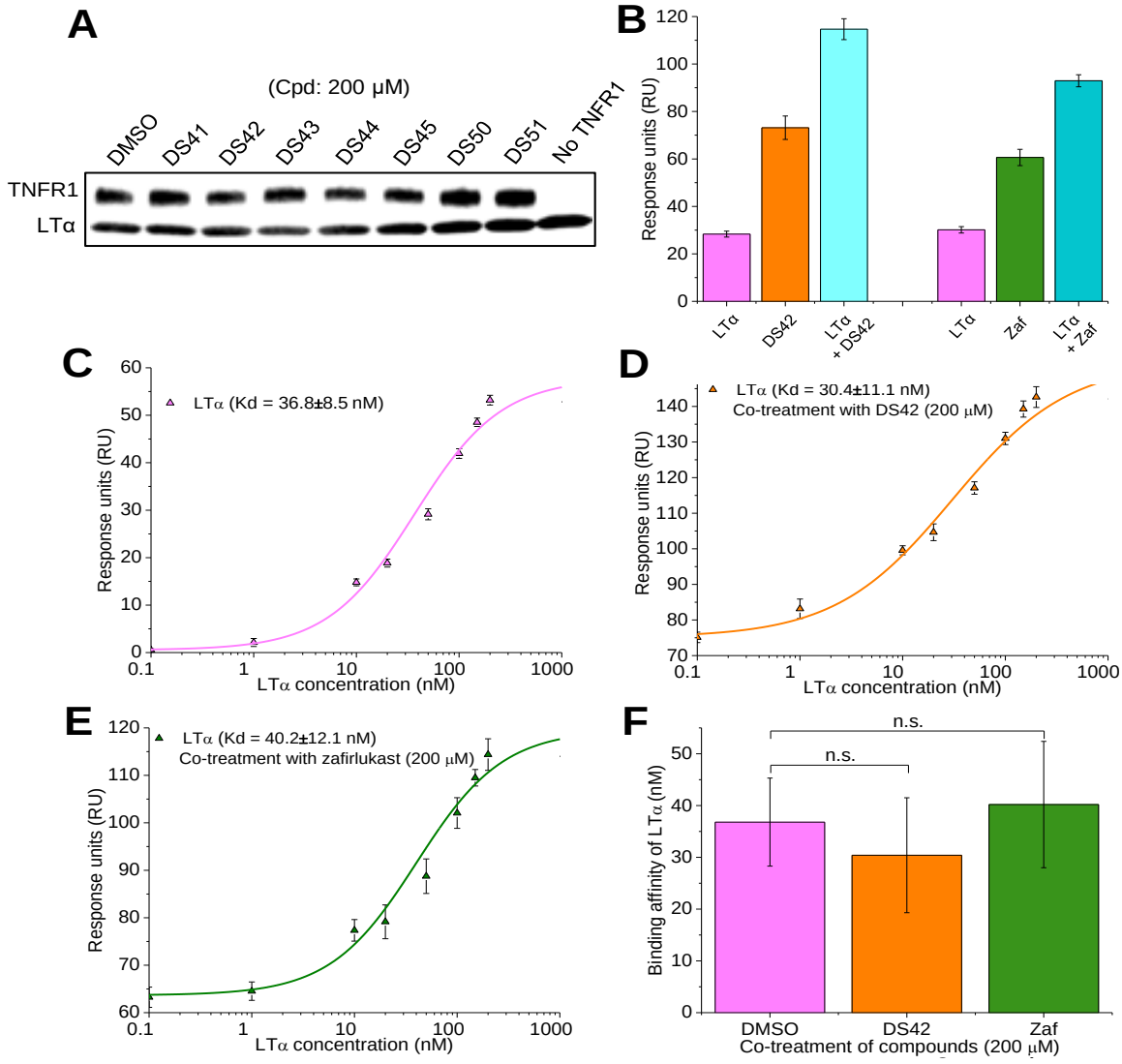

Figure 4. 4. Small-molecule inhibitors do not block ligand-receptor interactions.

(A) Co-immunoprecipitation between TNFR1 and ligand LTα with treatment of hit compounds at saturation dose of 200 μM. Equal amount of LTα is shown as pull-down controls. Western blots are representative of three independent experiments. (**B**) Non-competitive binding assay of LTα (50 nM) and compounds (DS42 or zafirlukast at 200 μM) to TNFR1 ECD was performed by SPR.

Data are means ± SD of three independent experiments. (**C**) Dose-dependent binding of LTα to TNFR1 ECD with increasing concentration of ligand. Data are means ± SD of three independent experiments. (**D** and **E**) Dose-dependent binding of LTα in the presence of compounds, DS42 (D) or zafirlukast (E), at saturated compound concentration of 200 μM. Data are means ± SD of three independent experiments. (**F**) Comparison of the binding affinity of LTα to TNFR1 in the absence and presence of compounds (DS42 or zafirlukast). Data are means ± SD of three independent experiments and n.s. indicates not significant by two-tailed unpaired *t* test.

4.4.5. Small-molecule inhibitors also do not change dimerization of the TNFR1 PLAD or ECD

Having shown that the new compounds do not act by disrupting ligand binding, we next investigated whether, like zafirlukast, they act by disrupting the dimerization of TNFR1 extracellular domains through the PLAD. We illustrate that purified soluble TNFR1 PLAD exists as dimers under native conditions which can be disrupted to form a monomer band by small molecules that disrupt receptor-receptor interaction such as zafirlukast (*190*). Following this biochemical approach (*190*), we first tested each of the compounds' ability to disrupt soluble PLAD dimers under native conditions. The results show that none of the new hit compounds, except zafirlukast, disrupted the PLAD dimer (**Figure 4.5A**). We used antibody staining to show that the higher molecular weight bands in the native gel of soluble PLAD are aggregates of PLAD protein, and that these were not altered by the compounds (fig. S3.6A). To test if the compounds could be binding elsewhere on the ECD of the receptor and causing PLAD dissociation by inducing long-range allosteric coupling, we tested their ability to disrupt dimers of purified, full-length TNFR1 ECD proteins under native conditions. The results again showed that none of the compounds other than zafirlukast disrupted the TNFR1 ECD

dimer (**Figure 4.5B**). In addition, we confirmed that none of the hit compounds had any effect on ligand-ligand interactions (fig. S4.6B).

Collectively, these findings clearly distinguish the new compounds discovered here from zafirlukast and from previous small molecules targeting TNFR1 by blocking the ligand binding (*36-38*). It is important to pause in clarifying the nature of zafirlukast as a competitive inhibitor, as it is not competitive in the most traditional sense of preventing ligand binding. Instead, zafirlukast competes with monomer-monomer binding, without disrupting ligand binding, and diminishes function by reducing dimerization (**Figure 4.5C**). We have here shown that the new compounds, on the other hand, act non-competitively, blocking neither ligand binding or TNFR1 monomer-monomer interactions. Instead, the TNFR1 specific compounds are exerting their inhibitory effect by altering the conformational state of the pre-assembled dimer (as observed from the FRET changes), and somehow do so in a way that does not prevent ligand binding or dimerization (**Figure 4.5D**). From the perspective of understanding the mechanism of TNFR1 activation, this demonstrates that TNFR1 can be inactive, even if ligand is bound and the receptor dimer is intact.

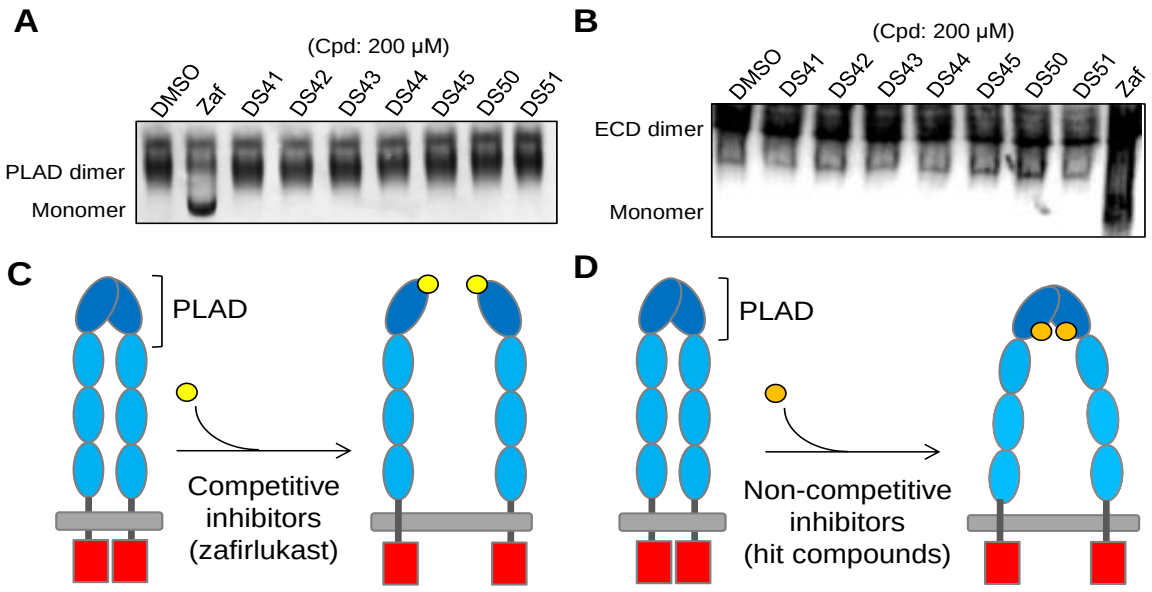

Figure 4. 5. Small-molecule inhibitors do not disrupt receptor-receptor interactions.

(A) Native gel characterization of soluble pre-ligand assembly domain (PLAD) of TNFR1 with treatment of DMSO control, zafirlukast and hit compounds (200 μM). Gels are representative of three independent experiments. (B) Native gel characterization of soluble extracellular domain (ECD) of TNFR1 with treatment of DMSO control, zafirlukast and hit compounds (200 μM). Gels are representative of three independent experiments. (C) Schematics illustrating the mechanism of competitive inhibition by zafirlukast in disrupting receptor-receptor interactions. (D) Schematics illustrating the mechanism of non-competitive inhibition by the new hit compounds in stabilizing the non-functional conformational states of TNFR1 without disrupting receptor-receptor interactions.

4.4.6. New non-competitive inhibitors are more efficient than zafirlukast, a competitive inhibitor

We next compared the efficiency of inhibition of DS42, a non-competitive inhibitor, and zafirlukast, a competitive inhibitor. In theory, given equal affinity for its binding site on the receptor, a non-competitive compound should be more efficient than a competitive one. Indeed, using inhibition of NF-κB activation as a metric for this, we

observed that DS42 achieves a far better percent inhibition (93%) as compared to zafirlukast (55%) (**Figure 4.6A**). By comparing the binding and inhibitory profiles of DS42 and zafirlukast, we found that both compounds have very similar binding affinity (K_d) and absolute IC_{50} (**Figure 4.6B**). This indicates that the increase in inhibition by DS42 is due to more efficient allosteric inhibition unencumbered by competition and not due to increased binding. The inability to obtain maximum inhibition by zafirlukast could be attributed to its competition with native receptor monomers, which are in dynamic equilibrium with the dimeric form, making it difficult for zafirlukast to achieve maximum inhibition with the low binding affinity.

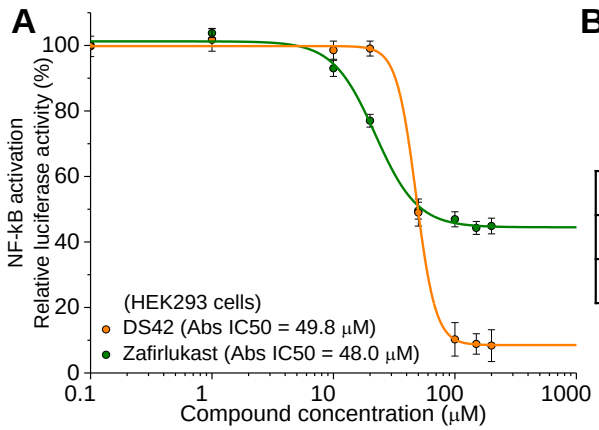

B

	Zafirlukast	DS42
K_d (μM)	86.3±5.5	81.2±7.0 (n.s.)
Abs IC_{50} (μM)	48.0±5.2	49.8±3.8 (n.s.)
% inhibition	55.1±2.4	92.6±2.5 (****)

Figure 4. 6. Non-competitive inhibitors are more efficient than competitive inhibitor.

(A) NF-κB activation in HEK293 cells treated with LTα and increasing concentration of compounds (DS42 and zafirlukast) to compare the inhibition efficiency between non-competitive and competitive inhibitors. Data are means ± SD of three independent experiments. (B) Comparison of the binding affinity, the absolute IC_{50} and the percent inhibition of NF-κB activation between DS42 and zafirlukast. Data are means ± SD of three independent experiments. ****P < 0.0001 for DS42 versus zafirlukast by two-tailed unpaired *t* test and n.s. indicates not significant.

4.4.7. Long-range perturbation of TNFR1 conformational dynamics by non-competitive inhibitors is mediated by residues in the ligand binding loop

Next, we asked whether we could use the small molecules to elucidate any details regarding the changes in conformational states in the pre-assembled dimer. We show that the constitutively active, dimeric R92Q mutant adopts an altered, active conformation compared to wild-type (*62*). We also use computational normal mode analysis of the available TNFR1 crystal structures and predict the implicit capacity of the receptor (in both the pre-ligand and ligand-bound states) to undergo an anti-correlated motion that couples conformational changes across the ECD (*62*). In particular, even in the absence of ligand we highlight conformational coupling between residues in the ligand binding loop (residues: 77-81 and 107−113) and the membrane proximal domain. We then predict a hinge that connects the domains and hence serves a critical role in propagating activating conformational changes. Here, by further examining the residues in the ligand binding loop in the crystal structure of the pre-ligand dimer (PDB: 1NCF), we found that the key ligand binding residues W107, S108 and M80 form four hydrogen pairs, W107-Q113, W107-L111, S108-L111 and M80-C114 in this hinge region (**Figure 4.7**, A and B). This led us to ask whether these critical residues and this same coupling might also be important in propagating the long-range conformational changes induced by our new small molecules, despite the fact that the inhibited conformation state is by definition distinct from the active state.

To test this hypothesis experimentally, we made single and double mutants of these three critical residues (W107A, S108A, WS107/108AA and M80A) in the FRET biosensor as well as a control mutant (V90A) located far from the ligand binding loop. To be clear, while these residues are essential in ligand binding (*62, 231, 232*), here we are interrogating the conformations in the absence of ligand to further elucidate the details of

our FRET results and understand the mechanism of inhibition by the small molecules. If these residues form a critical region in the conformational network within the ECD, then by breaking these hydrogen bonds we hypothesized that we would de-couple the domains and reduce the ability of the small molecules to cause the inhibitory conformational change. To start, the mutations did not have an effect on the basal FRET observed from pre-ligand receptor dimers (fig. S3.7A). While the compounds did still reduce FRET in the mutants (fig S3.7B), the magnitude of the effect was significantly diminished with each of the compounds (except DS50), thus supporting the hypothesis of a loss in conformational coupling between the loop and the remainder of the ECD (**Figure 4.7C**). We note that the biggest effect of the mutations was on DS41 which is, quite interestingly, a compound that showed one of the largest FRET changes in the wild-type receptor (**Figure 4.1E**). As a negative control, the extent of FRET change induced by all compounds in the control mutant (V90A) is similar to that of the WT FRET biosensor (**Figure 4.7C**).

We also asked whether we could use zafirlukast to probe, at low resolution, the potential binding regions for the small molecules. In particular, as the hit compounds bind TNFR1 ECD with higher affinity than zafirlukast (**Figure 4.3A**) but do not disrupt the PLAD-PLAD interaction (**Figure 4.5A**), we hypothesized that compounds that compete with zafirlukast and prevent its disruption of PLAD-PLAD interaction might be binding in the PLAD. Co-treatment of soluble dimeric PLAD with the hit compounds and zafirlukast revealed that some compounds, in particular DS41, DS42 and DS43, were competitive to zafirlukast in binding to PLAD and prevented disruption of PLAD dimerization (**Figure 4.7D** and fig. S4.8, A and B**)**. Compounds that have little or no effect in competing with zafirlukast may be binding to the part of CRD2 that is not responsible for ligand binding which is close to the PLAD or CRD4 nearer to the region of perturbation. In addition, we

quantitatively showed that co-treatment of DS42 and zafirlukast reduced the binding affinity of DS42 (K_d from 73 μM to 112 μM) to TNFR1 ECD (fig. S4.8C) and decreased its potency in inhibiting TNFR1-induced NF-κB activation (IC_{50} from 52 μM to 142 μM) (fig. S4.8D) as compared to DS42-only treatment. However, whether these compounds are directly competing with zafirlukast or allosterically changing the conformation of receptor such that it cannot bind zafirlukast remains to be investigated. It is also important to note that there are both the dimer binding interface and non-binding interface in the PLAD and our results do not distinguish between these two surfaces; however, this result can suggest that some compounds interact directly with the PLAD.

To further probe the specific mechanisms of DS42 and zafirlukast, we tested the effects of these small molecules in the presence of H398 human TNFR1-specific antibody. The binding epitope of the H398 antibody has been shown to be in regions of the CRD1 and CRD2 of TNFR1, and inhibits receptor function by blocking ligand binding (*35*). We hypothesized that DS42 and zafirlukast, which did not ablate ligand binding, would not be competitive to H398 binding and function. SPR binding indicated that indeed DS42 and zafirlukast (200 μM) do not compete with H398 (at its K_d of 1.0 nM (*35*)) for binding TNFR1 (fig. 4.S9A). Furthermore, H398 antibody inhibited TNFR1-induced NF-κB activation with an IC_{50} of 1.2 nM (fig. S4.9B), similar to a previous report (*35*). Consistent with our hypothesis, the IC_{50} values for DS42 and zafirlukast inhibition of NF-κB are unchanged by the presence of H398, illustrating that neither compound competes with H398 in inhibiting receptor function (fig. S4.9, C and D).

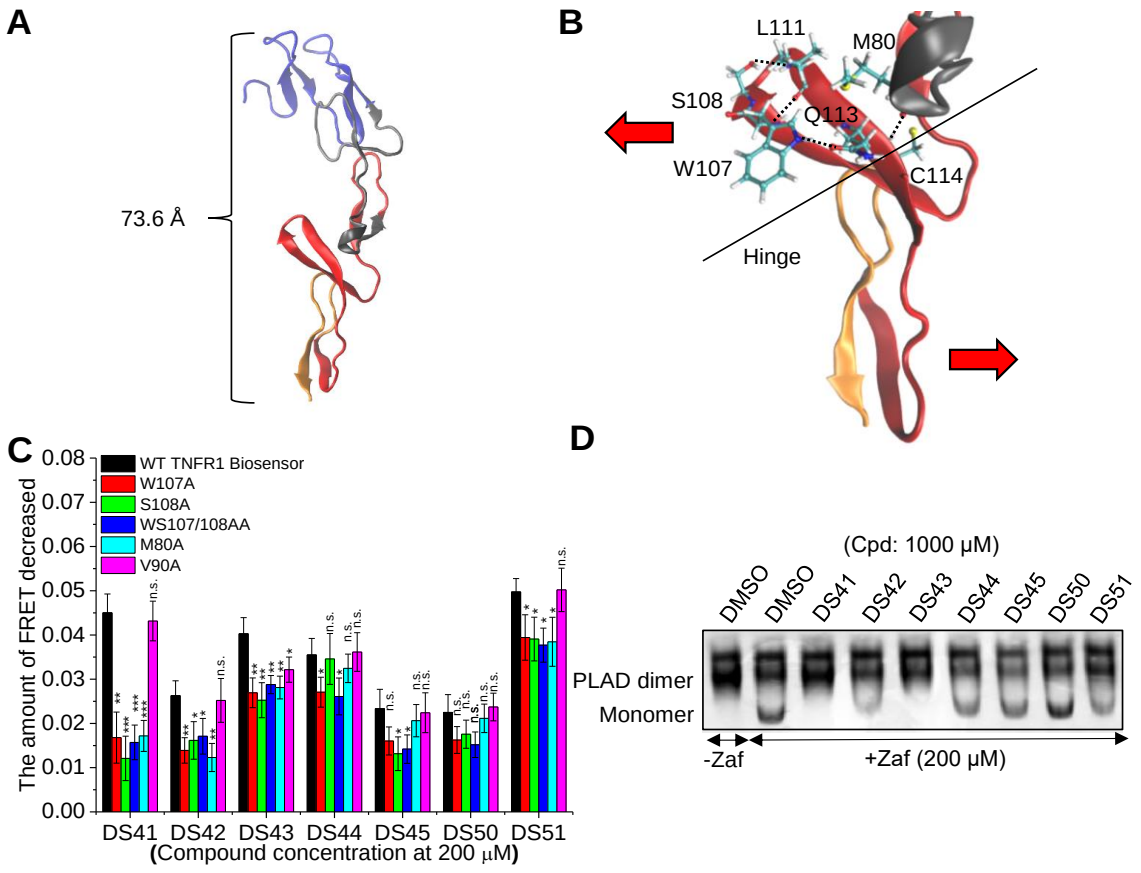

Figure 4. 7. Long-range perturbation of TNFR1 conformational dynamics by non-competitive inhibitors is mediated by residues in the ligand binding loop.

(A) Crystal structure of TNFR1 ECD indicates the distance between the membrane distal domain, including PLAD, and the membrane proximal domain is estimated to be 73.6 Å, which suggests a potential long-range signal propagation between non-competitive inhibitors binding at the PLAD or the ECD and the perturbation of the membrane proximal domain as shown by FRET change. Four different cysteine rich domains (CRD 1 to 4) are colored in blue, gray, red and orange respectively. (B) Surface representation showing the coupling motions between residues in the ligand binding loop and the membrane proximal domain. The key ligand binding residues, W107, S108 and M80 form four hydrogen bonds with L111, Q113 and C114 which stabilize the conformation of the region to behave like a hinge in aiding the opening of the receptor. Abolishing the hydrogen bonds may de-couple the domains and prevent conformational change acting

through the hinge. (C) Comparison of the amount of FRET decreased between HEK293 cells expressing WT and mutant TNFR1 FRET biosensors (W107A, S108A, WS107/108AA, M80A and V90A) treated with non-competitive inhibitors (200 μM) in the absence of ligand. Data are means ± SD of three independent experiments. *P < 0.05, **P < 0.01, ***P < 0.001 for WT versus mutant biosensors by two-tailed unpaired t test and n.s. indicates not significant. (D) Native gel characterization of soluble PLAD with co-treatment of DMSO control or hit compounds (1000 μM) and zafirlukast (200 μM) to test the competition between the hit compounds and zafirlukast in interacting with PLAD. Gels are representative of three independent experiments.

4.4.8. Preliminary SAR of a representative hit compound

The best compounds identified from screening the 50,000 compound DIVERSet library have absolute IC_{50} values (inhibition of NF-κB activation) around 50 μM, similar to the value we obtain for zafirlukast (50 μM) (*190*). In order to test whether we could improve on this, we performed a preliminary structure-activity relationship (SAR) analysis of the hit compounds to optimize the small molecules for improved potency and specificity. We chose DS41 as our main focus for SAR analysis for several reasons. First, DS41 showed the biggest effect in the mutant study (**Figure 4.7C**), suggesting that chemical aspects of this compound, if harnessed, may be most efficient in targeting the novel allosteric mechanism of action described in this study. Second, however, DS41 has non-specific effects as shown in two assays (**Figure 4.3E** and fig. S4.4D). Thus, we wanted to know if we could optimize the compound by both eliminating this non-specificity and by increasing binding affinity, thereby improving the potency such that the compound is specific at its effective concentration (IC_{50}). We obtained 19 analogues from ChemBridge (table S4.1) to probe the SAR. One analogue, DSA114, showed a strong increase in binding affinity to the TNFR1 ECD (**Figure 4.8A** and fig. S4.10A), strong inhibition of IκBα degradation (fig. S4.10, B and C)**,** and a 3-fold increase in the

potency of inhibiting NF-κB activation as compared to the lead compound, DS41 (**Figure 4.8B** and fig. S4.10D). Most importantly, DSA114 is substantially more specific than DS41 (**Figure 4.8C**) especially at its IC_{50} (fig. S4.10, D and E), and maintained its core mechanistic features (does not block ligand-receptor interactions (**Figure 4.8D** and fig. S4.10, F to H), does not disrupt PLAD-PLAD interactions (**Figure 4.8E**), and prevents zafirlukast from disrupting the PLAD-PLAD interactions (fig. S4.10I)). Additionally, DSA114 decreased FRET in the WT TNFR1 biosensor more significantly than DS41 at the same compound concentration (**Figure 4.8F**).

In terms of the chemical structure, DS41 contains a 4-piperidinyl-1*H*-pyrazol-5-yl core with 2-methyl-3-phenyl-2-propen-1-yl (R^1) attached to the nitrogen of the piperidine and cyclopentanecarboxamide (R^2) to the pyrazole (table S4.1, Cpd **1**). Our preliminary SAR analysis of DS41 has illustrated that both its R^1 and R^2 groups play important roles in determining compound binding affinity and potency. In particular, the R^1 group is preferred in order to maintain potent activity (IC_{50} and percent inhibition) inhibition as deviation from the current 2-methyl-3-phenyl-2-propen-1-yl group resulted in a substantial decreased percent inhibition (table S4.1, Cpd **2** to **14**). However, modification of R^1 did modulate the potency in terms of IC_{50} and hydrophobic groups were better tolerated than substituents containing polar moieties. Interestingly, simplification of the 2-methyl-3-phenyl-2-propen-1-yl substituent by reduction of the olefin and removal of the phenyl ring substantially enhanced potency at the expense of percent inhibition (table S4.1, Cpd **8**). Our data suggest that the 2-methyl and 3-phenyl groups on the 2-propene of the R^1 of DS41 may be important for increasing the percent inhibition and a flexible carbon chain (changing propene to propane) may favor binding and increase potency (table S4.1, Cpd **2** vs **5**). On the other hand, the R^2 group was much more tolerant to modification and five of the six derivatives containing benzyl, substituted phenyl and 3-

phenylpropyl groups maintained or exceeded the percent inhibition of the initial hit while varying in potency from 26 to 115 μM (table S4.1, Cpd **15** to **20**). One cannot extrapolate too much from this limited series, but it is clear this position offers more opportunity to modulate potency and drug disposition properties while maintaining high percent inhibition. A comparison between the structures of DS41 and DSA114, and other hit compounds such as DS42 indicates moderate structural similarity as all contain a substituted piperidine core (fig. S4.1B). This preliminary SAR, together with the comparison with other hit compounds, suggests that some of these structurally similar compounds may be acting through the same inhibitory mechanism.

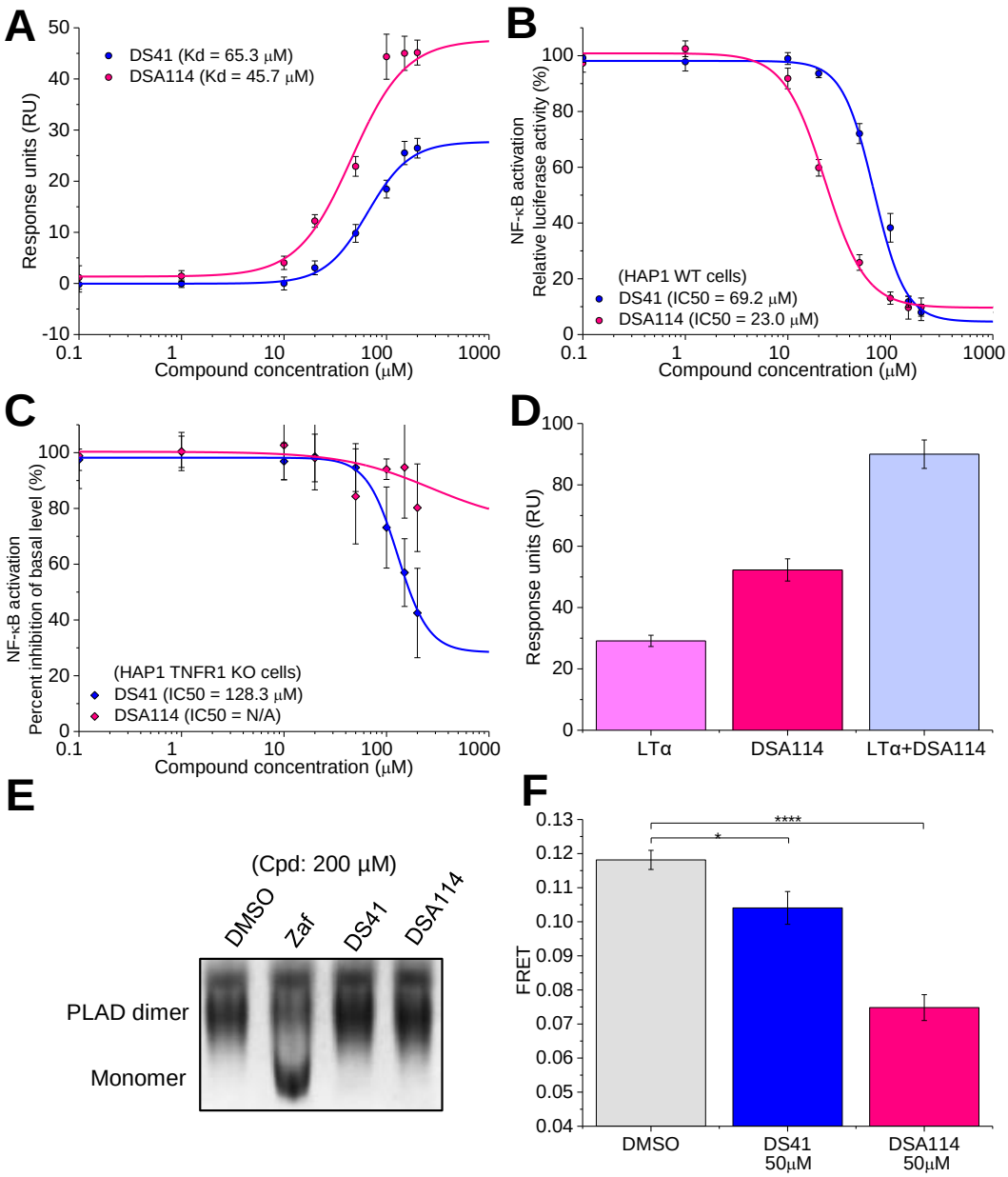

Figure 4. 8. Lead compounds are optimizable for binding affinity, potency and specificity.

(A) SPR characterization of binding affinity of hit compound (DS41) or its analogue (DSA114) to TNFR1 ECD. Data are means ± SD of three independent experiments. (B and C) NF-κB activation in WT HAP1 cells (B) and TNFR1 KO HAP1 cells (C) treated with LTα and increasing concentration of hit compound (DS41) or its analogue (DSA114) to test the improvements in the potency and specificity of the analogue. Data are means ± SD of three independent experiments.

(D) Non-competitive binding test of LTα (50 nM) and DSA114 (200 μM) to TNFR1 ECD was performed by SPR. Data are means ± SD of three independent experiments. (E) Native gel characterization of soluble PLAD with treatment of DMSO control, zafirlukast, DS41 or DS114 (200 μM) to test the disruption of PLAD dimerization by the compounds. Gels are representative of three independent experiments. (F) FRET measurements using HEK293 cells expressing WT TNFR1 FRET biosensor treated with DMSO control, DS41 (50 μM) and DSA114 (50 μM) in the absence of ligand to compare the extent of receptor perturbation by the hit compound and its analogue. Data are means ± SD of three independent experiments. *$P < 0.05$ and ****$P < 0.0001$ versus control by two-tailed unpaired *t* test.

4.5. Discussion

There are currently five FDA-approved biologic agents including monoclonal antibodies (infliximab, adalimumab, certolizumab pegol, golimumab) and soluble TNF receptor (etanercept) that target TNFα for treatment of TNFR1-related inflammatory diseases (*21, 233-235*). Despite high potency, these therapeutics result in global TNFα blockade, which has several negative consequences: low rates of disease remission; the development of fatal side effects such as lupus-like symptoms and lymphomas; and the generation of antibodies against biologic TNFα inhibitors (*235, 236*). In addition, compared to small molecules, antibodies are expensive and often fail to cross the blood-brain barrier, and can also lead to injection site reactions or infusion reactions (*21, 237, 238*).

To overcome these limitations, the therapeutic paradigm in this field has shifted from targeting TNFα to developing inhibitors that directly target TNFR1. Largely TNFR1 receptor-specific inhibitors are antibodies (*33, 35, 176, 239*) or small molecules that competitively block ligand-receptor interactions (*36, 37*). One notes that the ligand binding affinity of TNFα to TNFR1 is very high (K_d=0.38 nM) (*38*), and so small

molecules that work by competitively eliminating ligand binding have a very steep hill to climb. Additionally, it has been suggested that TNFR1 antagonists that block ligand binding reduce the TNFα neutralizing capacity of soluble TNFR1 as the circulating forms of the receptor may function as decoys for the ligand and their concentrations may reflect long-term exposure to this proinflammatory cytokine (*39-41*). At low concentrations, soluble TNFR1 enhances the actions of TNFα, but at higher concentrations the effects of TNFα are abrogated (*42*). Furthermore, cell-autonomous interaction between TNFα and TNFR1 is critical for cell survival, maintenance and function as well as neuroprotective (*43, 44*).

As such, approaches that do not involve eliminating ligand binding are highly attractive, though have proved elusive. One approach has been to block the pre-assembly of TNFR1 dimers by targeting the pre-ligand assembly domain (PLAD). Competitively eliminating the PLAD-PLAD interaction is an attractive alternative to blocking ligand binding because the monomer-monomer interaction (low micromolar) is weaker than the ligand-receptor affinity (*55, 56*). In a seminal study, it was suggested that soluble TNFR1 PLAD was able to disrupt TNFR1 receptor-receptor interaction and inhibit TNFα-induced inflammatory signaling in vitro as well as to ameliorate arthritis in a mouse model (*52*). However, in that study, the glutathione S transferase (GST)-tagged PLAD protein ablated ligand binding, making it unclear whether the effect of inhibition was, in fact, due to disruption of the receptor dimer (*52*). In our previous high-throughput screening study, we showed for the first time that a small molecule (zafirlukast) is capable of disrupting the dimeric PLAD-PLAD interaction without blocking ligand binding, inhibiting ligand-induced NF-κB activation with a potency of 50 μM (absolute IC_{50}) (*190*). To our knowledge, this was the only small-molecule inhibitor that had been demonstrated to inhibit TNFR1 without blocking ligand binding, before the current study.

However, zafirlukast has relatively low affinity and only partially inhibits activation. Besides the need to compete with the PLAD-PLAD interaction that has a much higher homotypic affinity than the zafirlukast-PLAD affinity, we speculate that the inability of zafirlukast to completely inhibit TNFR1 could be due to preservation of a functionally inefficient ligand-bound trimeric structure, despite elimination of the dimer (*223*).

Nonetheless, the relatively low affinity and inhibition efficiency of zafirlukast and related compounds suggested a pressing need for a non-competitive targeting strategy for more effective inhibition of TNF receptors. To make progress in this way has required that the field exploit developments in understanding the structure and dynamics of the receptors (*62, 180-184*). We are aware of one important study that utilized computational design to discover a small molecule (called F002) that binds to a cavity distal to the ligand binding loop and inhibits TNFR1 allosterically (*38*). Even though the binding cavity of the small molecule is located away from the ligand interaction site and the binding of the small molecule may not directly prevent ligand binding to the receptor, there was no evidence given to rule out the possibility of reduced or eliminated ligand-binding. Importantly, the functional efficacy of F002 was determined to be sixty-fold weaker than its binding affinity, strongly suggesting that this small molecule was competing with some other process, perhaps ligand-binding.

In theory, small molecules that act at allosteric sites but cause conformational changes that reduce ligand binding suffer the same competitive disadvantage of orthosteric modulators that directly eliminate ligand binding (*240*). Allosteric small-molecule inhibitors that do not influence ligand binding or require outcompeting receptor-receptor interactions may be more efficient for the simple fact that they are unencumbered by competition (either ligand-receptor or receptor-receptor) (*177-179*). But by what mechanism could such a small molecule operate? Here, we have

demonstrated one approach to receptor inhibition by small molecules acting non-competitively on the receptor: stabilization of non-functional conformational states of the receptor that is independent of ligand binding or receptor dimerization. Not only are these molecules more efficient in inhibiting TNFR1 signaling, small modifications to the chemical structures allow us to easily increase the potency of the lead compounds. These scaffolds may be further optimized by medicinal chemistry for potential therapeutic developments.

4.6. Supplemental figures

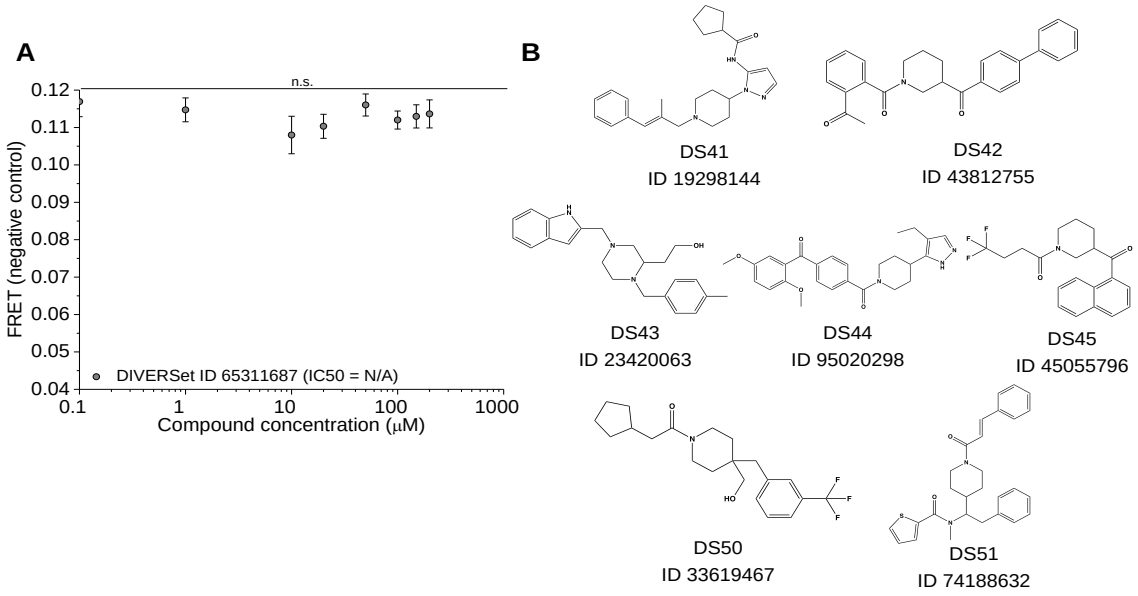

Supplemental Figure 4. 1. Negative control compound does not cause a FRET change and chemical structures of novel small molecules that perturb the conformational states of the pre-assembled TNFR1 dimer.

(A) No FRET change was observed with a negative control compound. Data are means ± SD of three independent experiments and n.s. indicates not significant by two-tailed unpaired t test. (B) The chemical structures and the ChemBridge IDs of the seven previously unidentified small molecules, discovered from high-throughput screening of the ChemBridge DIVERSet 50,000 compound library, that perturb the conformational states of the pre-assembled TNFR1 dimer.

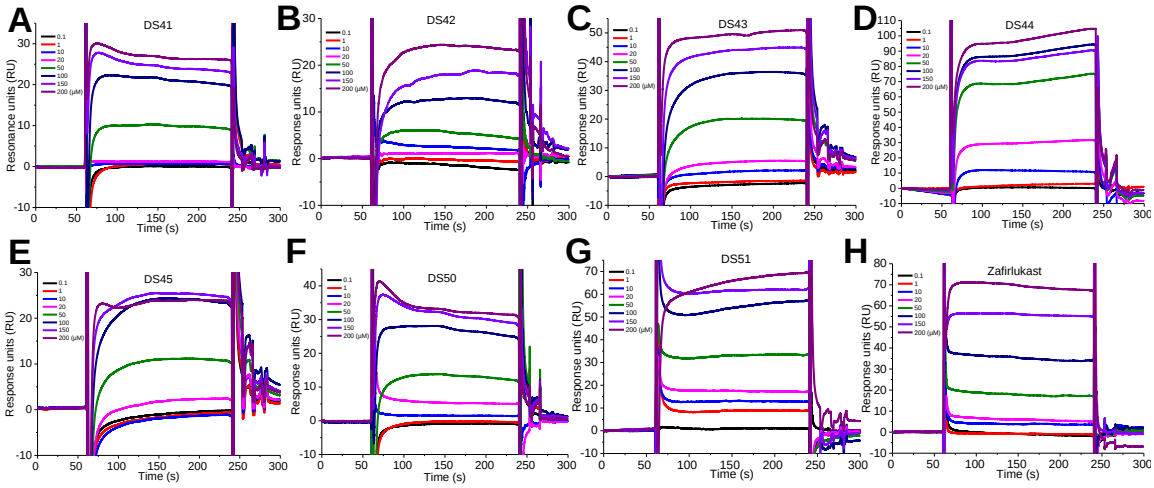

Supplemental Figure 4. 2. The seven hit compounds and zafirlukast bind TNFR1 ECD as characterized by SPR measurements.

SPR raw binding curves for (A) DS41, (B) DS42, (C) DS43, (D) DS44, (E) DS45, (F) DS50, (G) DS51, and (H) zafirlukast. Bind curves are representative of three independent experiments.

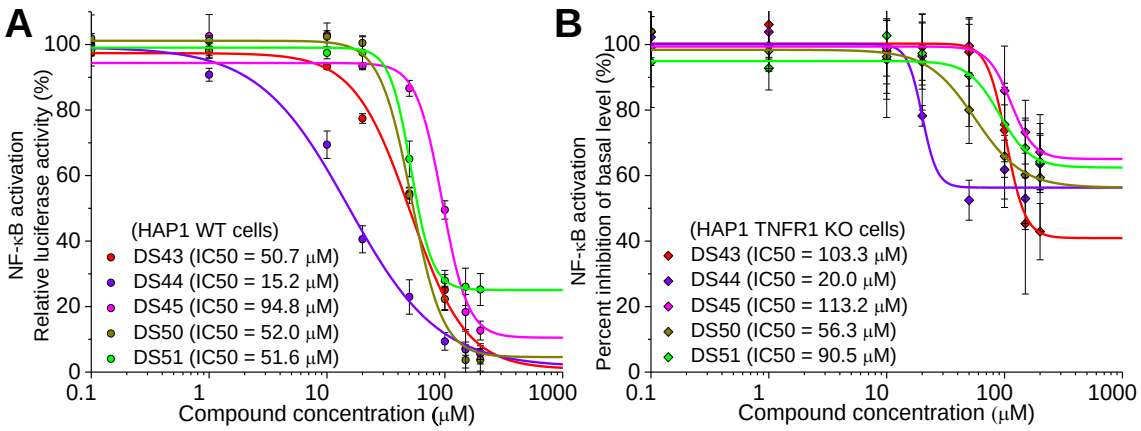

Supplemental Figure 4. 3. Some hit compounds illustrate non-specificity to TNFR1 in the inhibition of NF-κB activation.

(A and B) NF-κB activation in WT HAP1 cells (A) and TNFR1 KO HAP1 cells (B) treated with LTα and increasing concentration of hit compounds (DS43, DS44, DS45, DS50 and DS51) to test the compound specificity to TNFR1. Data are means ± SD of three independent experiments.

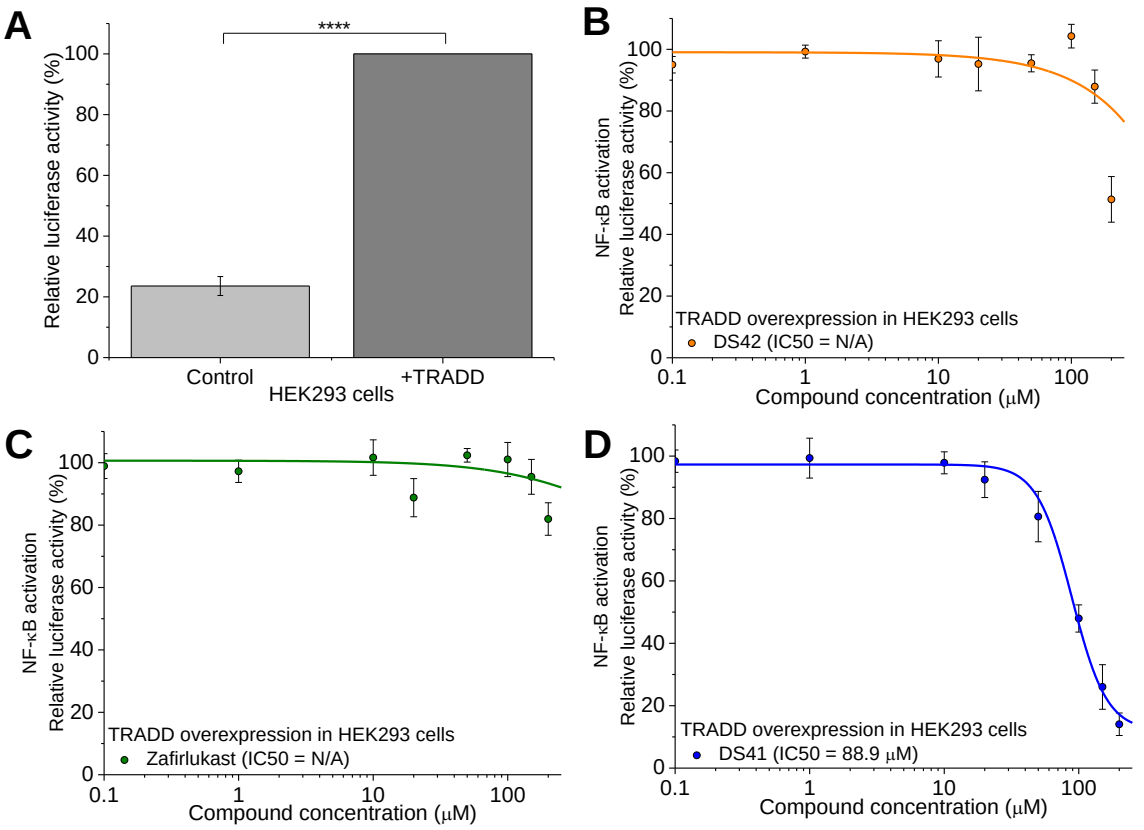

Supplemental Figure 4. 4. DS42 and zafirlukast do not inhibit TRADD-induced NF-κB activation in HEK293 cells but DS41 does.

(A) NF-κB activation in HEK293 cells expressed with reporter plasmids as well as overexpression of control plasmids (no TRADD) or TRADD plasmids, and treated with DMSO control. Data are means ± SD of three independent experiments and ****P < 0.0001 versus control by two-tailed unpaired t test. (B to D) TRADD-induced NF-κB activation from (A) with HEK293 cells treated with increasing concentration of compounds (DS42 (B), zafirlukast (C) and DS41 (D)). Data are means ± SD of three independent experiments.

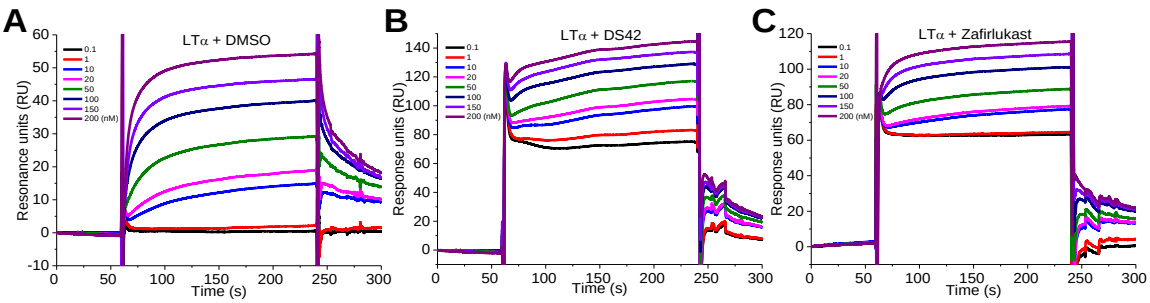

Supplemental Figure 4. 5. Small-molecule inhibitors do not disrupt ligand-receptor interactions as characterized by SPR measurements.

SPR raw binding curves for (A) LTα and DMSO, (B) LTα and DS42, and (C) LTα and zafirlukast. Binding curves are representative of three independent experiments.

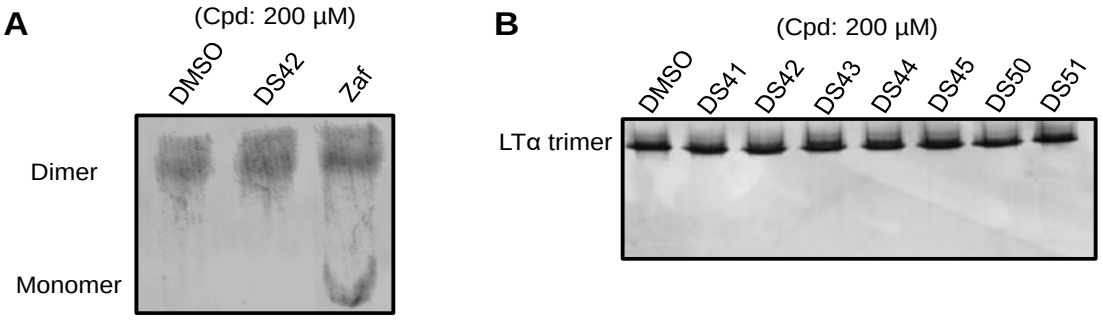

Supplemental Figure 4. 6. Hit compounds do not disrupt both TNFR1 PLAD dimer and LTα trimer.

(A) Western blot analysis of soluble TNFR1 PLAD with treatment of DMSO control, DS42 and zafirlukast. Western blots are representative of three independent experiments. (B) Native gel characterization of LTα with treatments of DMSO control and hit compounds. Gels are representative of three independent experiments.

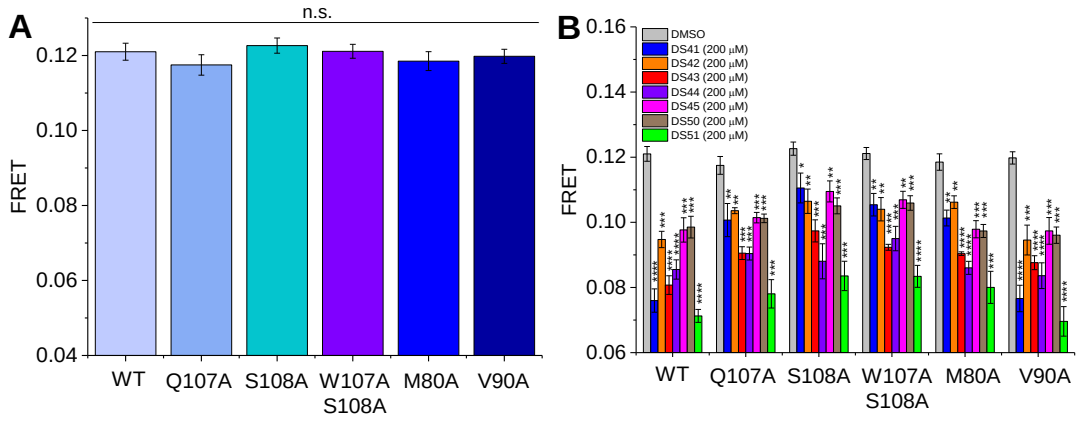

Supplemental Figure 4. 7. Hit compounds reduce FRET in the TNFR1 mutant biosensors.

(A) TNFR1 mutant FRET biosensors were created with mutations at the ligand binding loop and the conformationally active region of the receptor (W107A, S108A, WS107/108AA and M80A). A control mutant (V90A) which is located far from the ligand binding loop was also created. FRET was measured by the fluorescence lifetime plate-reader and the basal FRET calculated for all the biosensors are shown. Data are means ± SD of three independent experiments and n.s. indicates not significant by two-tailed unpaired t test. (B) All of the hit compounds (200 μM) reduced FRET significantly in the TNFR1 mutant biosensors. Data are means ± SD of three independent experiments and *P < 0.05, **P < 0.01, ***P < 0.001, ****P < 0.0001 by two-tailed unpaired t test.

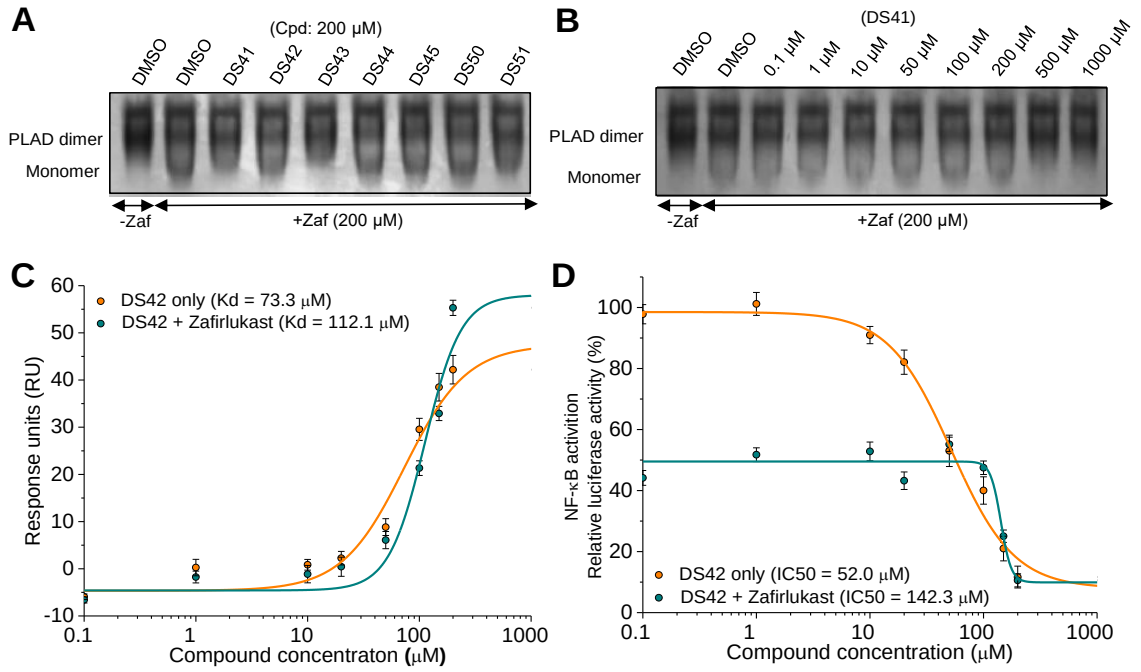

Supplemental Figure 4. 8. Hit compounds are competitive to zafirlukast in binding to the TNFR1 pre-ligand assembly domain (PLAD) and in NF-κB activation functional assay.

(A) Native gel characterization of soluble TNFR1 PLAD with co-treatment of the hit compounds (200 μM) and zafirlukast (200 μM). Gels are representative of three independent experiments. (B) Native gel characterizations of soluble TNFR1 PLAD with co-treatment of increasing concentration of DS41 (0.1 to 1000 μM) and a single dose of zafirlukast (200 μM). Gels are representative of three independent experiments. (C) SPR competition assay between increasing concentration of DS42 and a single dose of zafirlukast (100 μM). Data are means ± SD of three independent experiments. (D) NF-κB activation in HEK293 cells treated with LTα, increasing concentration of DS42 and a single dose of zafirlukast (100 μM) to test the competition of DS42 to zafirlukast in functional assay. Data are means ± SD of three independent experiments.

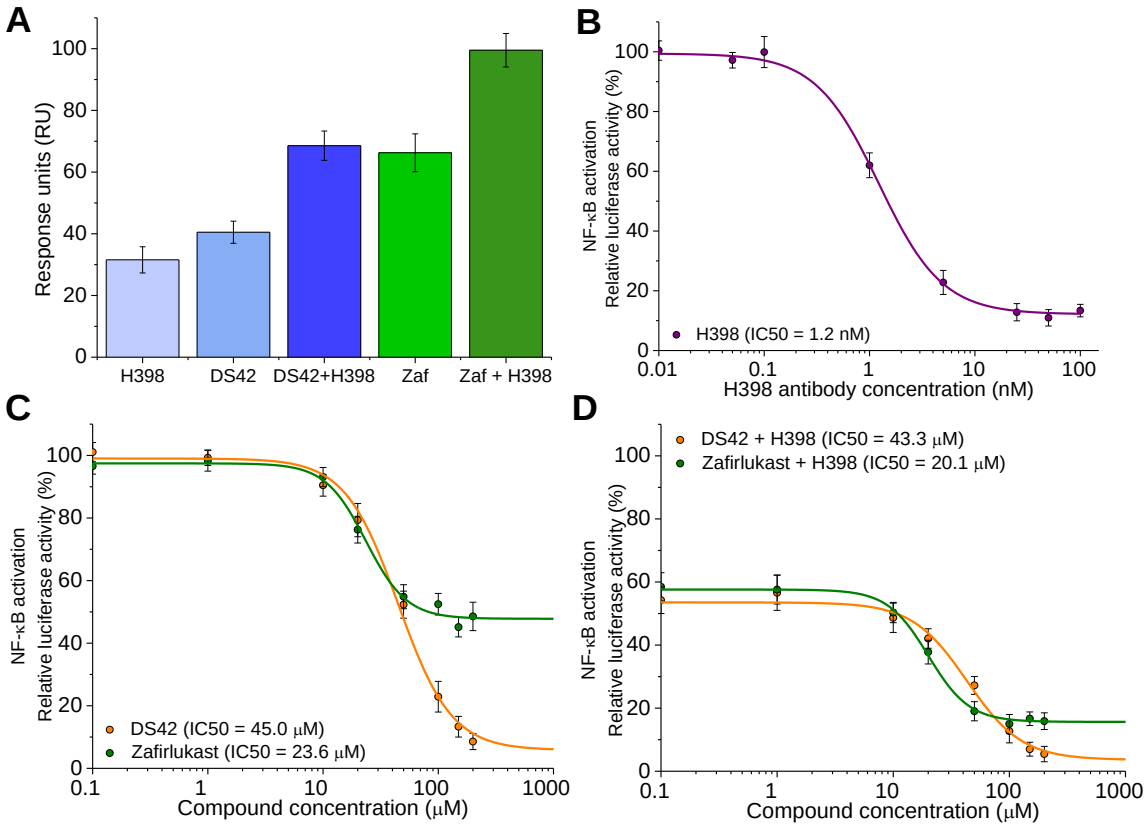

Supplemental Figure 4. 9. Hit compounds are not competitive to H398 antibody modulation of TNFR1 signaling.

(A) Non-competitive binding assay of H398 antibody (1 nM) and compounds (DS42 or zafirlukast at 200 μM) to TNFR1 ECD was performed by SPR. Data are means ± SD of three independent experiments. (B) NF-κB activation in HEK293 cells treated with LTα and increasing concentration of H398 antibody to test the functional inhibition effects of the antibody. Data are means ± SD of three independent experiments. (C and D) NF-κB activation in HEK293 cells treated with LTα and increasing concentration of compounds (DS42 and zafirlukast) in the absent (C) and present of H398 antibody (1 nM) (D) to test the competition in functional effects between the compounds and the antibody. Data are means ± SD of three independent experiments.

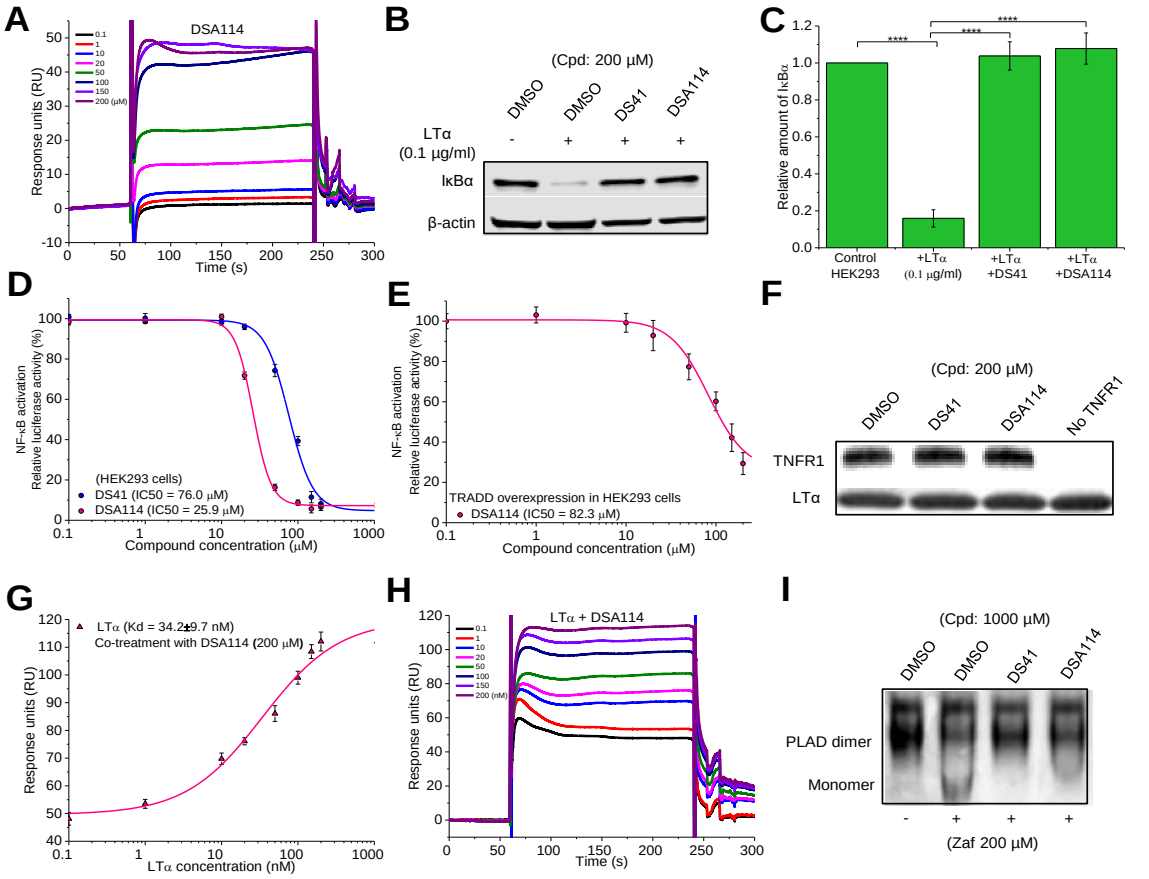

Supplemental Figure 4. 10. DSA114, an analogue of DS41, illustrates improved potency and specificity by acting through the same non-competitive inhibition mechanism.

(A) Surface plasmon resonance (SPR) raw curves for the binding of DSA114 to TNFR1 ECD. Binding curves are representative of three independent experiments. (B and C) Western blot analysis of IκBα abundance in lysates of HEK293 cells treated with LTα and the hit compound (DS41) and its analogue (DSA114) at 200 μM. Western blots (B) are representative of three independent experiments. Quantified band intensity values (C) are means ± SD from all experiments. ****P < 0.0001 versus control by two-tailed unpaired t test. (D) NF-κB activation in HEK293 cells treated with LTα and increasing concentration of hit compound (DS41) or its analogue (DSA114) to test the improvements in the potency of the analogue. Data are means ± SD of three independent experiments. (E) TRADD-induced NF-κB activation in HEK293 cells treated with increasing concentration of DSA114. Data are means ± SD of three independent experiments. (F) Co-immunoprecipitation between TNFR1 and ligand LTα with treatment of DMSO control, hit compound (DS41) and its analogue (DSA114) at saturation dose of 200 μM. Equal amount of LTα is shown as pull-down controls. Western blots are representative of three independent experiments. (G) Dose-dependent binding of LTα in the presence of DSA114 at saturated compound concentration of 200 μM. Data are means ± SD of three independent experiments. (H) SPR raw curves of the dose-dependent binding of LTα to TNFR1 ECD in the presence of DSA114 (200 μM). Binding curves are representative of three independent experiments. (I) Native gel characterization of soluble TNFR1 PLAD with co-treatment of DS41 or DSA114 (1000 μM) and zafirlukast (200 μM). Gels are representative of three independent experiments.

Supplemental Table 4. 1. Functional characterization of DS41 and its analogues.

NF-κB activation in HEK293 cells treated with LTα and lead compound (DS41) or its analogues in a dose-dependent manner to characterize their functional potency.

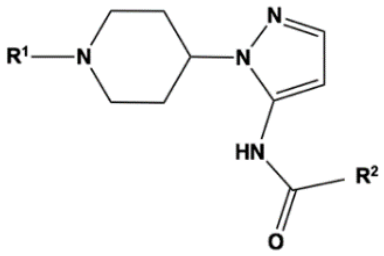

Cpd	R^1	R^2	NF-κB IC_{50} (μM)	NF-κB % inhibition	DIVERSet Cpd ID
1 (lead)	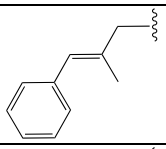	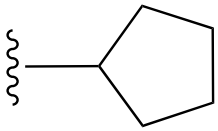	76.0	91.8%	19298144 (DS41)
2	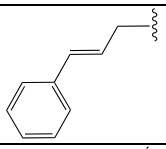	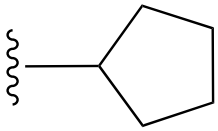	112.0	47.9%	55283788 (DSA103)
3	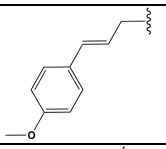	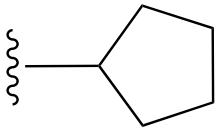	18.8	50.5%	75039431 (DSA104)
4	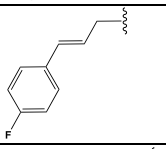	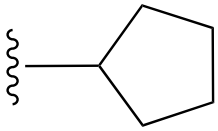	9.23	50.6%	50757273 (DSA105)
5	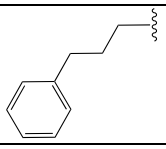	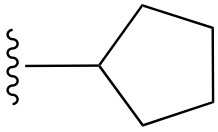	45.2	51.3%	74382948 (DSA106)
6	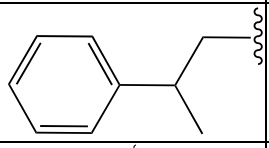	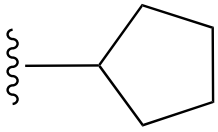	>200	0%	48067447 (DSA109)
7	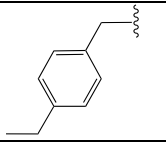	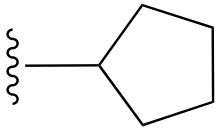	77.7	59.2%	38690331 (DSA108)
8	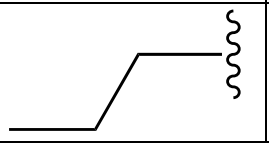	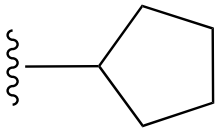	10.1	35.6%	84403474 (DSA102)

9	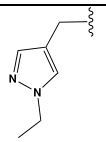	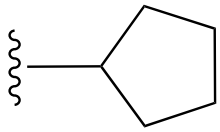	156.3	20.5%	33398307 (DSA110)
10	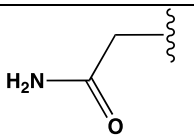	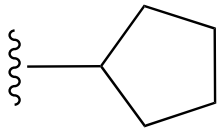	35.5	18.9%	95764424 (DSA117)
11	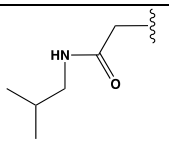	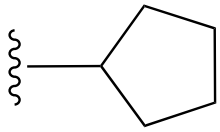	>200	0%	95807637 (DSA118)
12	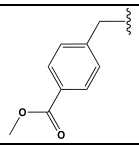	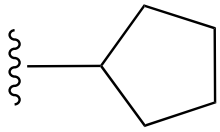	153.0	56.7%	92297604 (DSA119)
13	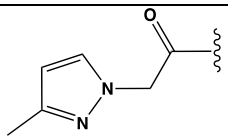	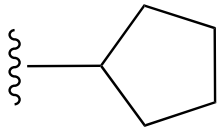	>200	0%	17903419 (DSA120)
14	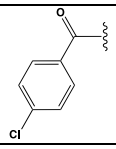	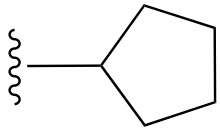	>200	0%	25121369 (DSA121)
15	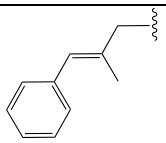	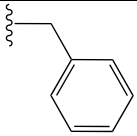	77.3	95.5%	52016291 (DSA111)
16	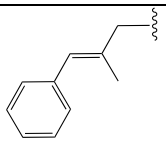	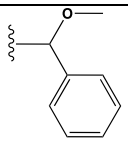	115.0	85.7%	74438793 (DSA112)
17	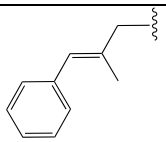	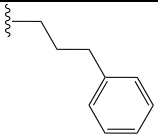	51.3	90.8%	41340052 (DSA113)
18	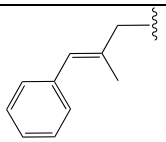	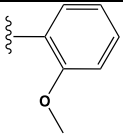	25.9	93.5%	16888972 (DSA114)
19	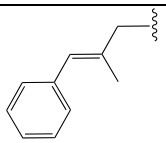	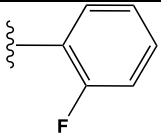	29.7	94.3%	59182823 (DSA115)

20	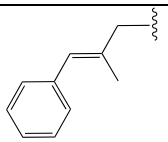	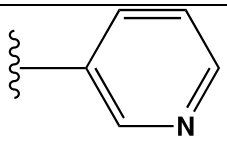	>200	0%	72564798 (DSA116)

CHAPTER 5: CONFORMATIONAL STATES OF TNFR1 AS A MOLECULAR SWITCH IN RECEPTOR FUNCTION

Chih Hung Lo[1], Evan C. Huber[1] and Jonathan N. Sachs[1,*]

Manuscript to be submitted to *Protein Science*

[1]Department of Biomedical Engineering, University of Minnesota, Minneapolis, MN 55455, USA.

Author contributions: C.H.L. designed and conducted all the experiments. E.C.H. provided technical support for functional and mechanistic assays. C.H.L and J.N.S. wrote the manuscript.

5.1. Summary

Tumor necrosis factor receptor 1 (TNFR1) is a transmembrane receptor which plays a key role in the regulation of the inflammatory pathway. While inhibition of TNFR1 has been the focus of many studies for treatment of autoimmune diseases such as rheumatoid arthritis, intervened activation of the receptor is important for treatment of immunodeficiency diseases such as HIV or neurodegenerative diseases such as Alzheimer's disease that required a boost in the proliferation or immune signaling. In addition, activation of other TNF receptors such as death receptor 5 or FAS receptor is important for cancer therapy. Here, we used TNFR1 as a model to investigate the conformational rearrangement of the pre-ligand assembled receptor dimers that corresponds to the active states of the receptor. Specifically, we used a previously established TNFR1 FRET biosensor together with a fluorescence lifetime technology as a high-throughput screening platform to identify a novel small molecule that activates the TNFR1 by altering the receptor conformational dynamics independent of ligand stimulation. By probing the interaction between the receptor and its downstream

signaling molecule, we suggest that the conformational states of TNFR1 could act as a molecular switch in determining receptor functions.

5.2. Introduction

The receptors and ligands in the tumor necrosis factor (TNF) superfamily have unique structural attributes that couple them directly to signaling pathways that are responsible for a wide-range of cellular activities such as cell proliferation, differentiation or death (*4, 241*). Within this superfamily, tumor necrosis factor receptor 1 (TNFR1) is a characteristic member and a central mediator in the signal transduction of the inflammatory pathway (*5*). Stimulation by the native ligands of TNFR1, tumor necrosis factor-alpha (TNFα) and lymphotoxin-alpha (LTα), leads to the recruitment of TNFR1 associated death domain (TRADD) followed by IκBα degradation and NF-κB activation (*11*). While over-activation of TNFR1 results in excessive NF-κB activation which has been associated with several autoimmune diseases such as rheumatoid arthritis (*5, 11, 173*), lack of NF-κB activation has been implicated in diseases related to immune deficiency and cell death such as HIV, neurodegeneration and tissue degeneration (*242-245*). Hence, there is a need for increased activation of TNFR1 beyond its native activation to promote NF-κB activation for treatment of these diseases (*246-251*). In addition, activation of other TNF receptors such as death receptor 5 or FAS receptor is important for cancer therapy (*252-255*).

Current methods of TNFR1 activation include ligand mimics such as staphylococcus aureus protein A which has been shown to act as a ligand and mimic TNFα in order to activate TNFR1 (*256*). Burkholderia cenocepacia BC7 also has been shown to bind to and activate TNFR1 (*257*). Another way to increase the activation of

TNFR1 is by increasing the expression of TNFR1 in cells (*258*), though the presence of native ligand is still required for the receptor activation. The limitation for proteins that mimic the ligand is that they compete with native ligand binding, diminishing the potential elevated effects in activating TNFR1. Hence, the most effective way in activating of TNFR1 would be a receptor-specific approach that activates the receptor regardless of ligand stimulation or amplifies the effect of ligand stimulation by making use of the receptor structures and conformations.

Recent evidences have provided a revision to the accepted model of TNFR activation that the pre-assembled dimer remains intact upon ligand binding, potentially forming the nexus for larger scale networks of ligand-bound TNFR trimers (*181, 221-223*). This reconciles the controversy between the two crystal structures of TNFR1 trimerization induced by ligand binding without direct receptor-receptor interactions (*57*) and that TNFR1 forms pre-ligand assembled dimers held together by the pre-ligand assembly domain (PLAD) (*55, 58, 59*). Several works have been done on directly targeting the receptor dimer to alter its function based on this revised model. In our previous work, we have shown that disruption of receptor-receptor interactions by zafirlukast, a small molecule, without ablating ligand binding inhibits TNFR1 signaling, supporting the oligomeric network model (*190*). In addition, we have also shown that small molecule allosteric inhibitors (e.g. DS42) exert their inhibitory effect by altering the conformational state of the pre-assembled dimer without blocking ligand binding or dimerization, demonstrating that TNFR1 can be inactive, even if ligand is bound and the receptor dimer is intact (*191*). This suggests that the possibility to further activate the receptor from its native signaling complex potentially through perturbation of receptor conformational dynamics. This possibility is supported by a study showing that ligand

binding causes a conformational change in the pre-assembled TNFR1 complex as measured by fluorescence resonance energy transfer (FRET) but the exact activation mechanism was not delineated (*61, 224*). In addition, we used FRET to show that a disease-related mutant (R92Q), which is constitutively active, also forms a pre-ligand assembled dimer (*62*). Importantly, the FRET measurements show that this active R92Q dimer is conformationally distinct from wild-type, suggesting the correlation between the TNFR1 conformational states and receptor activity. Furthermore, our recent computational and experimental results suggest that long-range perturbation of TNFR1 conformational dynamics mediated by the ligand binding loop with signal propagation through the backbone of the ECD is feasible approach to control receptor function (*62, 191*).

To investigate whether multiple conformational states corresponding to receptor activation or inhibition exist in TNFR1, we used the previously established TNFR1 FRET biosensor to perform high-throughput screening (HTS) on the library of pharmacologically active compounds (LOPAC) to discover small molecules that perturb the pre-ligand assembled TNFR1 dimer. We considered compounds that altered FRET in the biosensor in search for activators. We discovered a small molecule, SB-200646 hydrochloride (SBH), which binds TNFR1, reduces FRET of the biosensor and importantly, increases NF-κB activation by the same fold change both in the presence and absence of the ligand. In addition, the activating effect of SBH was diminished in the TNFR1 knockout cells, indicating its specificity to TNFR1. Furthermore, we showed that this small molecule is exerting the activating signal propagation through the conformationally active region of the ligand binding loop of the receptor. Probing the interaction between the receptor and its downstream signaling molecule, we suggest

that the ensemble of TNFR1 conformational states can be stabilized by small molecules for its activation, hence acting like a molecular switch.

5.3. Materials and methods

5.3.1. Molecular biology

In our previous work we generated the DNAs (TNFR1ΔCD-GFP and TNFR1ΔCD-RFP) used in the engineering of the TNFR1 FRET biosensor (*190*). Briefly, standard cloning techniques were used to fuse cDNAs encoding truncated TNFR1ΔCD (amino acids 1-242) with the N-terminus of the EGFP and TagRFP vectors. Quikchange mutagenesis (Agilent Technologies) was used to introduce the mutations of the key ligand binding residues (Q107A, S108A, QS107/108AA and M80A) and the control mutant (V90A) in the TNFR1ΔCD-GFP and TNFR1ΔCD-RFP plasmids. This was then sequenced for confirmation. All vectors contain the monomeric mutation A206K to the fluorescent proteins in order to prevent constitutive fluorophore clustering, (*204*).

5.3.2. Cell culture and generation of stable cell lines

Human embryonic kidney cells 293 (HEK293, ATCC) were cultured in phenol red-free Dulbecco's Modified Eagle Medium (DMEM, Gibco). These were supplemented with 2 mM L-Glutamine (Invitrogen), heat-inactivated 10% fetal bovine serum (FBS HI, Gibco), 100 U/ml penicillin and 100 μg/ml streptomycin (Gibco). HAP1 wild-type and TNFR1 knockout cells (Horizon) were cultured in Iscove's Modified Dulbecco's Medium (IMDM, Gibco). These were supplemented with 10% FBS (Gibco), 100 U/ml penicillin and 100 μg/ml streptomycin (Gibco). An incubator with 5% CO_2 (Forma Series II Water Jacket CO_2 Incubator, Thermo Scientific) at 37 ºC was used to maintain the cell cultures. CRISPR/Cas technology was used to generate the HAP1 TNFR1 knockout cell line containing a 70 base pair (bp) insertion in a coding exon of TNFRSF1A. To confirm the

knockout in the cells, Sanger sequencing was performed as a quality control. Our previous work describes how the TNFR1ΔCD-FRET pair stable cell line was generated (*190*). It also describes how they have been monitored continuously for over four years while maintaining expression above 95% characterized by flow cytometry (*190*). The TNFR1ΔCD-FRET pair shows high expression in the stable cell line which indicates that they are functional and applicable in high-throughput screening. HEK293 cells were transiently transfected using Lipofectamine 3000 (Invitrogen) with TNFR1ΔCD-GFP and TNFR1ΔCD-RFP DNAs containing the respective mutations (Q107A, S108A, QS107/108AA, M80A and V90A) in order to generate the mutant forms of the TNFR1 FRET biosensor.

5.3.3. High-throughput screening with LOPAC library

The LOPAC library containing 1280 compounds was purchased from ChemBridge Corp. and a FX liquid dispenser was used to format the compounds into 96-well mother plates. An Echo liquid dispenser was used to subsequently format across 4 plates of the 384-well plate at 50 nl (10 µM final concentration per well). Dimethyl sulfoxide (DMSO) was loaded in columns 1, 2, 23 and 24 (negative controls) as well as matching %v/v as in-plate no-compound controls. The assay plates chosen were the 384-well flat, black-bottom polypropylene plates (PN 781209, Greiner Bio-One) because of their low auto-fluorescence and low inter-well cross-talk. Until the plates were used, they were sealed and stored at −20 °C. Over three different days the triplicate screens were performed with a library screened each day. A fresh vial of TNFR1ΔCD-GFP/RFP (TNFR1ΔCD-FRET pair) cells were thawed, plated in a 225 cm^2 flask (Corning) and checked for expression a week prior to screening. The cells were then expanded into six 225 cm^2 flasks for three days. The stable cells expressing the TNFR1 FRET biosensor were harvested to check for expression and response variation in fluorescent intensity

prior to each day of screening. The stable cells were then dispensed into the drug plates (50,000 cells/well) and incubated with the compounds or DMSO as a negative control. Fluorescence lifetime measurements were then performed on the plates. A prototype fluorescence lifetime plate-reader (Fluorescence Innovations, Inc.) was used to record the fluorescence waveforms as described (*190*).

5.3.4. HTS data analysis

Using least-squares minimization global analysis software (Fluorescence Innovations, Inc.), time-resolved fluorescence waveforms obtained from each well were fitted to single-exponential decays. This was done to obtain donor-acceptor lifetime (τ_{DA}) from the TNFR1ΔCD-GFP/RFP (FRET pair) cell line and donor lifetime (τ_D) from a TNFR1ΔCD-GFP donor-only control cell line. Equation 1 was used to calculate FRET efficiency (*E*).

$$E = 1 - \left(\frac{\tau_{DA}}{\tau_D}\right) \qquad Eq.1$$

Using SBH as a positive control and DMSO as a negative control, the Z-factor, a HTS assay quality indicator, was calculated based on Equation 2 (*192*).

$$Z' = 1 - \frac{3(\sigma_p + \sigma_n)}{|\mu_p - \mu_n|} \qquad Eq.2$$

Where σ_p and σ_n are the standard deviations of the observed τ_{DA} values, and μ_p and μ_n are the mean τ_{DA} values of the positive and negative controls, respectively. We utilized the normalized median absolute deviation (1.4826*MAD) and median in place of the standard deviation and mean, respectively (*225*). This was done to make this metric less sensitive to strong outliers (*225*). The Z-factor obtained was 0.55±0.02 using SBH as a positive control, which indicates excellent assay quality.

Based on analysis of the spectral waveforms of each well from the LOPAC screen, fluorescent compounds were determined to be potential false positives due to interference from compound fluorescence by a set of stringent fluorescent compound filters (*226*). After the fluorescent compounds were removed, a histogram of the FRET distribution from all compounds in the screen was plotted. This histogram was fitted to a Gaussian curve to obtain a mean and standard deviation (SD). A compound that changed the FRET efficiency by more than four times the standard deviation (4SD) relative to the mean was defined as a hit.

5.3.5. FRET dose-response assay

The three hit compounds, SB200646 hydrochloride (SBH) (S0568), candesartan cilexetil (CC) (SML0245), palmitoyl-DL-carnitine chloride (PDLCC) (P4509) were purchased from Millipore Sigma. Each drug compound was dissolved in DMSO to make 10 mM stock solution. Each solution was then serially diluted in 96-well mother plates to obtain eight doses at 50X concentrations. Hits were screened at eight different concentrations (0.1 to 200 μM). Using a Mosquito HV liquid handler (TTP Labtech Ltd.), 1 μl of compounds were transferred from the mother plates into assay plates. The same high-throughput screening methods were used on the cell preparation of the wild-type TNFR1 FRET biosensor in the FRET dose-response assays.

5.3.6. Functional assays (IκBα degradation assay and NF-κB activation assay)

IκBα degradation assay with HEK293 cells were performed with Western blots as described (*190*). Densitometry of the Western blots was performed using ImageJ. The data was normalized to the β-actin loading control and the amount of IκBα in the control cells in the absence of ligand. For the NF-κB activation luciferase assay with HEK293, HAP1 wild-type and TNFR1 knockout cells, the cells were transfected with the NF-κB-

luciferase reporter genes (10 μg of firefly luciferase genes and 1 μg of *Renilla* luciferase genes) in a 100 mm plate with Lipofectamine 3000 (Invitrogen). The cells were lifted with TrypLE and resuspended in phenol red-free DMEM (Gibco) the next day. These cells were dispensed into 96-well assay plates (30000 cells/well, total volume 50 μl) and incubated with SBH (0.1 to 200 μM) or DMSO (negative control) in both the presence (0.1 μg/ml) and absence of LTα for 18 hours at 37 °C. Readings for luciferase activities were recorded after 24 hours. Briefly, 50 μl of Dual-Glo Luciferase Reagent (Promega) was added, incubated at room temperature for 15 min, and firefly luminescence was measured using a Cytation 3 Cell Imaging Multi-Mode Reader luminometer (BioTek). Next, 50 μl of Dual-Glo Stop & Glo Reagent (Promega) was added, incubated at room temperature for 15 min, and *Renilla* luminescence was measured using a luminometer. The luciferase activities were normalized based on *Renilla* expression levels. Luciferase activity of cells in the absence of ligand was used to normalize all of the data from the NF-κB activation assays.

5.3.7. Mechanistic assays (co-immunoprecipitation and native gel characterization)

Co-immunoprecipitation between endogenous TNFR1 and ligand LTα in the presence and absence of SBH was carried out as described previously (*190*). Briefly, lysates of HEK293 cells containing endogenous TNFR1 were prepared. Anti-FLAG magnetic beads were also coated with FLAG-tagged LTα. The cell lysates containing TNFR1 and LTα coated magnetic beads were incubated in the presence of DMSO (control) or SBH (activator, 200 μM). After 24 hours, the proteins were eluted from the magnetic beads using glycine pH 2.5 and Western blots were performed using FLAG (2368S, Cell Signaling Technology) and TNFR1 (sc-8436, Santa Cruz Biotechnology)

antibodies. The overexpression and purification of the N-terminal FLAG-tagged LTα and FLAG-tagged TNFR1 PLAD (residues 30-82) were performed as described previously. Under normal conditions, the soluble PLAD protein was shown to exist as dimers (*190*). The recombinant human TNFR1 extracellular domain (ECD) was purchased from Abcam. 4%–15% SDS-PAGE gels (Bio-Rad) were used to assess the purity of proteins under reducing conditions. Coomassie staining was then performed. The BCA assay (Thermo Fisher Scientific) were used to measure protein concentrations. To test the disruption of receptor-receptor, purified soluble TNFR1 PLAD (5 μg) were assessed by Native-PAGE gels (Bio-Rad) in the absence and presence of SBH (200 μM) or zafirlukast (200 μM) under non-reducing conditions. This was followed by Coomassie staining. The extent of disruption of PLAD-PLAD interactions were then observed.

5.3.8. Surface plasmon resonance (SPR) binding assay

A BIAcore S200 was used to perform SPR analysis to determine the binding affinity between TNFR1 ECD and compounds or ligand. Using amine coupling, the recombinant human TNFR1 ECD (Abcam) was immobilized on the CM5 sensor chip (Biacore, GE Healthcare). Briefly, the dextran surface was activated with a 1:1 mixture of 0.4 M 1-ethyl-3-(3-dimethylaminopropyl)carbodiimide hydrochloride and 0.1 M N-hydroxysuccinimide. TNFR1 ECD (20 μg/ml) in 10 mM sodium acetate at pH 5 was flowed past a working surface before preventing the remaining activated carboxymethyl groups with 1 M ethanolamine at pH 8.5 to reach a level of 2500 RU suitable for binding analysis. The reference surface was activated and only ethanolamine was able to react with the surface.

Compound SBH at eight different concentrations (0.1-200 μM) as well as DMSO-only controls were prepared in HEPES-EP containing a total of 2% DMSO for the direct binding assays between the receptor and the small molecules. Ligand at 50 nM was prepared in HEPES-EP in the presence of saturated dose of SBH (200 μM) or DMSO containing a total of 2% DMSO for the competition assays between ligand and small molecules. The samples were injected over both the reference and ECD immobilized surfaces at 10 μl/min for 90 seconds. They were then dissociated in glycine-HCl with a pH of 2.5. Along with blanks from buffer and DMSO-only controls, all the samples were measured on a 96-well microplate (Biacore, GE Healthcare) at 25 °C. Reflectivity response data points were taken from response curves 5 seconds prior to the end of the injection. This was done to determine steady-state binding. All the data was double referenced with blanks using standard procedures with Biacore S200 Evaluation Software v1.0.

5.3.9. TRADD recruitment co-immunoprecipitation assay

HEK293 cells were cultured in 100 mm plates at 5 million cells per plate. Respective SBH (100 μM) and ligand treatments (0.1 μg/mL) were then performed and incubated for 24 hours. The cells were then harvested and lysed. Anti-FLAG magnetic beads were pre-coated with FLAG-tagged LTα for 24 hours. After 24 hours, the LTα bound beads were washed with PBS for three times and further incubated with the supernatant of the cell lysates for another 24 hours for pulled down of TNFR1 and TRADD (which was recruited to the receptor). After incubation, the beads were washed with PBS for three times and the bound proteins were eluted using 30 μL of glycine pH 2.5. The protein samples were then mixed with the 4X loading dye with β-mercaptoethanol reducing agent and Western blots were performed using FLAG

(2368S, Cell Signaling Technology), TNFR1 (sc-8426, Santa Cruz Biotechnology) and TRADD (3684S, Cell Signaling Technology) antibodies. The Western blots were then stained with respective secondary antibodies and images were acquired using the ChemiDoc™ MP Imaging System (BIO-RAD). Images were quantified by ImageJ for densitometry analysis.

5.3.10. Statistical analysis

Data are shown as mean ± standard deviation unless stated otherwise. To determine the statistical significance for all experiments, data analysis was carried out by a two-tailed unpaired *t* test (Student's *t* test) with *P* values determined using GraphPad Software. Values of $P < 0.05$ were classified as statistically significant. *P* values were denoted in figures using asterisks following the GraphPad style (*$P < 0.05$, **$P < 0.01$, ***$P < 0.001$ and ****$P < 0.0001$).

5.4. Results

5.4.1 Discovery of small molecules that probe conformational states of pre-ligand assembled TNFR1 dimer

To identify small molecules that modulate TNFR1 conformational states, we performed high-throughput screening of the library of pharmaceutically active compounds (LOPAC) containing 1280 compounds using our previously established stable cell lines expressing a TNFR1 FRET biosensor (TNFR1ΔCD-FRET pair construct). The TNFR1 FRET biosensor was engineered by fusing a green or red fluorescent protein (GFP or RFP) to the C-terminus of TNFR1 with a truncated cytosolic domain (ΔCD) (TNFR1ΔCD-GFP as donor and TNFR1ΔCD-RFP as acceptor) and was expressed in living HEK293 cells (**Fig. 5.1A**). The FRET biosensor was validated for its capability to detect changes in cytosolic spacing between the pre-ligand receptor

monomers in response to a change in the backbone conformation of the receptor induced by non-competitive small molecule functional effectors (*190, 191*) (**Fig. 5.1A**). The coupling between fluorescent biosensor engineering and a high-throughput fluorescence lifetime plate-reader technology allows for increased precision and sensitivity as well as reliable detection of subtle changes in protein structures or conformational states induced by allosteric small molecule effectors (*163*).

The FRET efficiency for all of the compounds, after removing the fluorescence interfering compounds, was plotted (**Fig. 5.1B**) and the distribution of efficiency was fitted to a Gaussian distribution to obtain a mean and standard deviation (SD) (**Fig. 5.1C**). We also performed a donor-only screen as a control to further remove compounds that affect the fluorophores rather than the receptor. We found three compounds that showed up as hits in both donor-only screen and FRET screen which were removed as false positives (**Supplementary Fig. S5.1A-B**, highlighted in pentagon). We then selected three reproducible hits that decreased the average FRET by more than 4SD greater than the mean of control cells for further investigation (**Fig. 5.1B**, highlighted in red). To confirm their specific interactions with the biosensor as well as to measure the potency and the extent of receptor perturbation by the hit compounds, they were tested for dose-dependent FRET change. All three hit compounds, SB200646 hydrochloride (SBH), candesartan cilexetil (CC) and palmitoyl-DL-carnitine chloride (PDLCC), had a dose-dependent change in FRET efficiency (**Fig. 5.1D**) with half-maximal effects (relative EC_{50}) ranging between 6.6-20 μM, with SBH having the lowest EC_{50}.

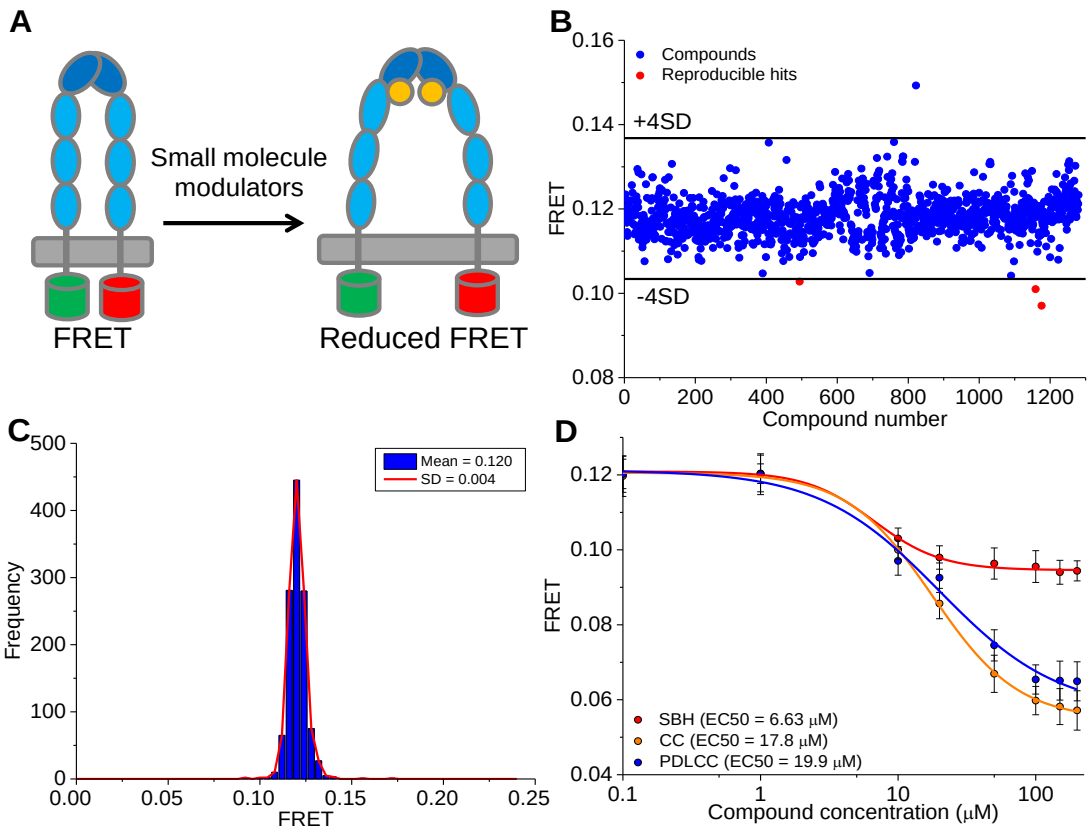

Figure 5. 1. Small molecules probe conformational states of pre-ligand assembled TNFR1 dimer.

(**A**) Schematic of the TNFR1ΔCD-FRET biosensor engineered by fusing the green or red fluorescent proteins (GFP or RFP) to the C-terminus of TNFR1 with truncated cytosolic domain. Ligand-independent association of the fluorophore-tagged receptors through PLAD-PLAD interactions results in fluorescence resonance energy transfer (FRET). The FRET biosensor is capable of detecting changes in the cytosolic spacing between receptor monomers. Small molecules targeting the receptor will induce a FRET change in the biosensor. (**B**) High-throughput screening of library of pharmaceutically active compounds (LOPAC) using the TNFR1 FRET biosensor expressed in HEK293 cells. Potential false positives were removed from the screening plot. Three reproducible hits that decreased FRET below the 4SD applied threshold (black line) were selected for further characterization. Data are representative of three independent

experiments. **(C)** Histogram plot of all compounds from the LOPAC screen after removal of false positives to obtain the average FRET efficiency and the standard deviation (SD) of the screen. (**D**) Secondary FRET analysis of the dose response of the three hit compounds. Data are means ± SD from three independent experiments.

5.4.2. Small molecule activator (SBH) stimulates TNFR1-induced NF-κB signaling pathway

The functional effect of hit compounds was first determined by ligand-induced IκBα degradation using by immunoblotting (**Fig. 5.2A**). The amount of IκBα was degraded to 6-fold of the basal levels in HEK293 cells upon LTα treatment (**Fig. 5.2B**). From all the hit compounds, we found that CC and PDLCC inhibit IκBα degradation (data not shown), which is not the focus of this study. On the other hand, SBH showed a further degradation of IκBα with an EC_{50} of 38 μM, indicating enhanced receptor activation (**Fig. 5.2C**). We then chose SBH for further investigation. We tested SBH in ligand-induced NF-κB activation (**Fig. 5.2D**). SBH further stimulated ligand-induced NF-κB activation in a dose-dependent manner, with a relative EC_{50} value of 5.2 μM (**Fig. 5.2E**). In addition, SBH also activated NF-κB activation in the absence of ligand with a relative EC_{50} values of 6.8 μM (**Fig. 5.2F**). We note that the effective concentrations of SBH in the functional assays are consistent with the FRET results.

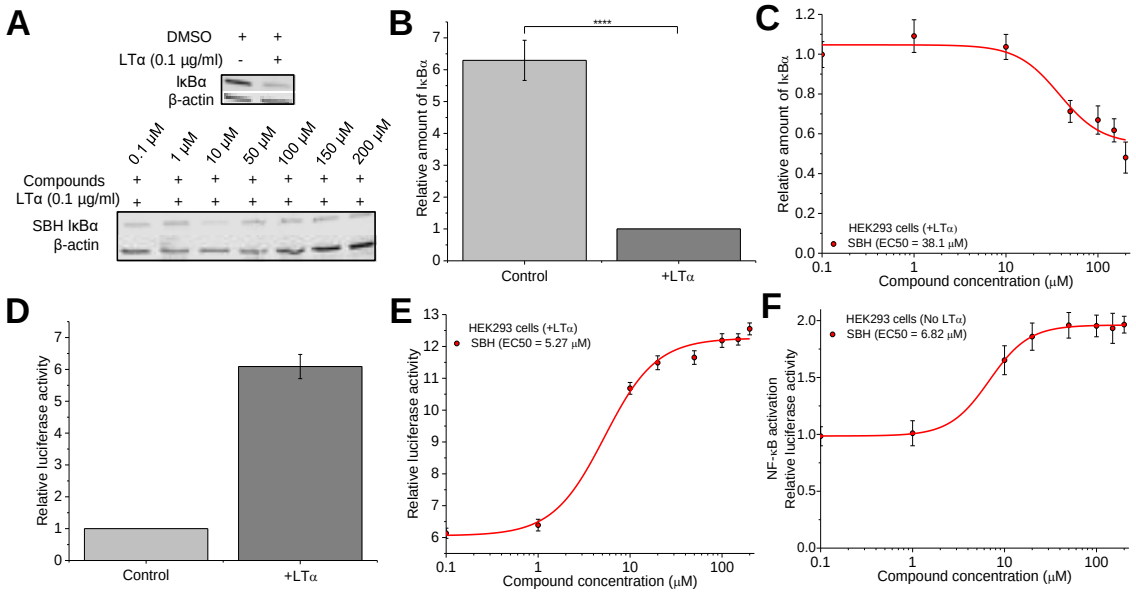

Figure 5. 2. Effect of small molecule activator (SBH) on TNFR1-stimulated NF-κB activation.

(**A** to **C**) Western blot analysis of IκBα abundance in lysates of HEK293 cells treated with LTα and SBH at the indicated doses. Western blots (A) are representative of three independent experiments. Quantified band intensity values (B-C) are means ± SD from all experiments. ****P < 0.0001 versus control by two-tailed unpaired t test. (**D** and **E**) Luciferase assay of NF-κB activation in HEK293 cells transfected with reporter plasmids and treated with (D) LTα and DMSO control or (E) LTα and increasing concentrations of SBH. (**F**) Treatment of SBH to the NF-κB activation luciferase assay in the absence of LTα. Data are means ± SD of three independent experiments. ****P < 0.0001 versus control by two-tailed unpaired t test.

5.4.3. SBH binds TNFR1 and is a receptor-specific activator

To determine if SBH directly binds and acts on TNFR1, we first performed affinity measurements using surface plasmon resonance (SPR). Purified TNFR1 extracellular domain (ECD) was immobilized onto the SPR chip and SBH was flowed through the chip

to allow for binding. SBH showed dose-dependent binding to the TNFR1 ECD with binding affinities (K_d) of 75 μM (**Fig. 5.3A** and **Supplementary Fig. S5.2**).

Next, we used both parental wild-type (WT) and TNFR1 KO HAP1 cell lines (established by CRISPR) to determine whether the receptor is required for the functional effects of the hit compounds or they may be acting through the inhibition of proteins in alternate signaling pathways. In our previous work, we have established that the basal activation of the NF-κB pathway (approximately 20% relative luciferase activity) in the TNFR1 KO HAP1 cells allows them as a first control to ensure that the functional effects we observed in the HEK293 cells were due to direct interactions with TNFR1 and not due to the compounds indirectly acting on other proteins on alternate NF-κB pathways (*191*). We have again showed that the TNFR1 KO HAP1 cells illustrate a basal activation of the NF-κB pathway and were not functionally sensitive to ligand stimulation of TNFR1 (**Fig. 5.3B**). As expected, SBH further stimulated NF-κB activation in both in the presence and absence of the ligand in the WT HAP1 cells to very a similar extent as was observed in the HEK293 cells (EC_{50} values are 8.7–9 μM) (**Fig. 5.3C-D**). On the other hand, SBH increased the basal level of NF-κB activation in the TNFR1 KO cells both in the presence and absence of ligand with EC_{50} values of 124–138 μM which is more than 10-fold of its EC_{50} values in the WT cells (**Figs. 5.3E-F**), making SBH a specific activator of TNFR1 at its effective concentration.

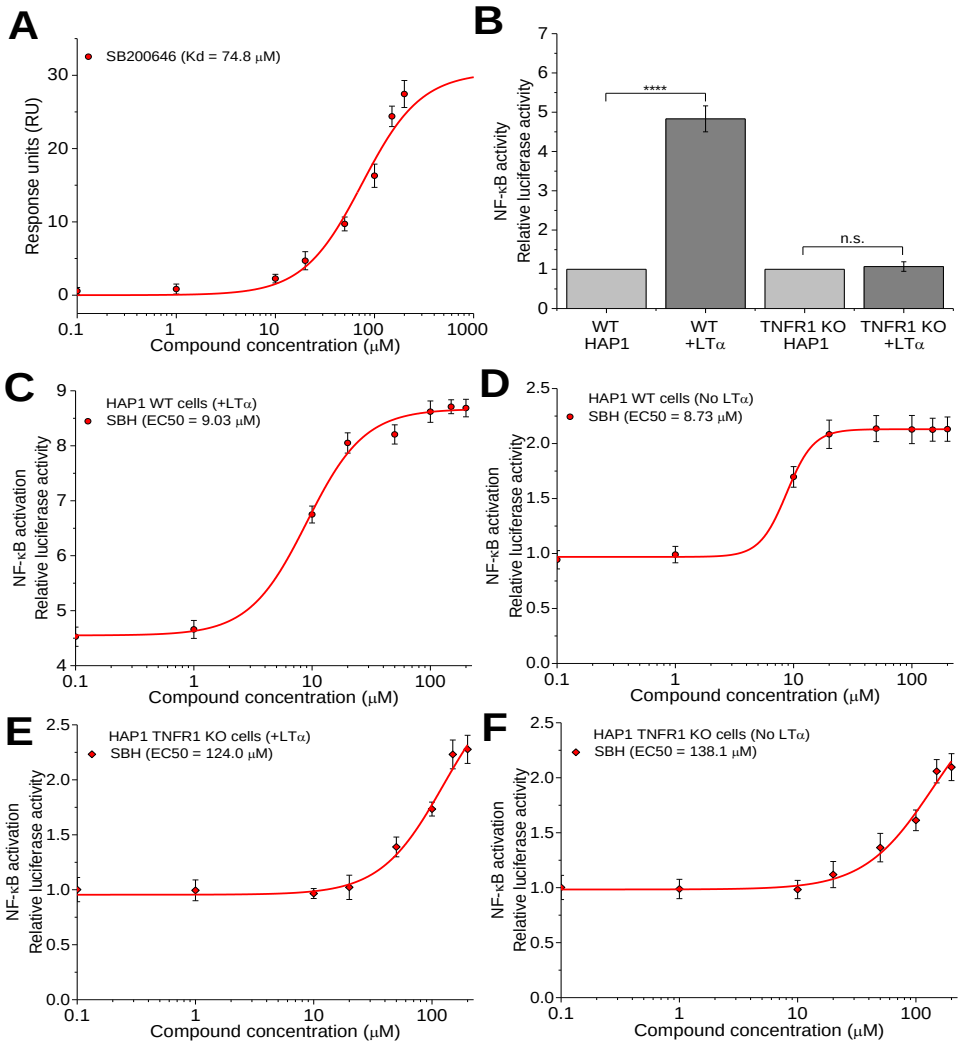

Figure 5. 3. SBH binds TNFR1 and requires the receptor for its functional effect.

(**A**) Direct binding of SBH to the TNFR1 extracellular domain (ECD) was characterized by surface plasmon resonance (SPR). Data are means ± SD from three independent experiments. (**B**) NF-κB activation in WT and TNFR1 KO HAP1 cells with the optimized LTα concentration of 0.1 μg/ml. Data are means ± SD of three independent experiments. ****$P < 0.0001$ versus control by two-tailed unpaired *t* test and n.s. indicates not significant. (**C** and **D**) NF-κB activation in HAP1 WT cells treated with LTα and increasing concentration of (C) SBH as well as (D) SBH in the absence of ligand. (**E** and **F**) NF-κB activation in HAP1 TNFR1 KO cells treated with LTα and

increasing concentration of (E) SBH as well as (F) SBH in the absence of ligand to test the specificity of the compounds to TNFR1. Data are means ± SD of three independent experiments.

5.4.4. SBH perturbs TNFR1 conformational dynamics

After determining the specificity of SBH, we then aimed to delineate the mechanisms of action of SBH to test whether it is perturbing ligand-receptor interactions, disrupting receptor-receptor interactions, or altering conformational states of the receptor. We first monitored the ligand-receptor interactions in the absence and presence of SBH using co-immunoprecipitation (co-IP) and SPR. Co-IP experiments qualitatively confirmed that SBH does not eliminate ligand-receptor interactions (**Fig. 5.4A**). To quantitatively confirm the non-competitive nature of SBH, we performed SPR measurements in the presence of both the ligand and SBH. Both LTα (50 nM) and SBH (200 μM) were passed through the TNFR1 ECD immobilized surface for SPR measurements with individual treatment of ligand-only or compound-only as controls. The response from co-treatment of ligand and SBH was equal to the sum of the individual response from ligand-only or compound-only binding, indicating simultaneous binding of the ligand and the small-molecule activator to the receptor (**Fig. 5.4B**). In addition, we investigated the ability of each compound to disrupt soluble PLAD dimers under native conditions by running native gels of soluble PLAD in the absence and presence of SBH. The result shows that SBH did not disrupt PLAD-PLAD interactions but a previously known inhibitor (zafirlukast) did (**Fig. 5.4C**).

Furthermore, we tested if SBH perturbs TNFR1 receptor conformational dynamics. To do this, we used the previously engineered TNFR1 FRET biosensors with mutations at the ligand binding loop (Q107A, S108A, QS107/108AA, M80A and V90A

(control)) which has been shown to be the conformationally active region of the receptor. We have established that these residues form a critical region in the conformational network within the ECD important in mediating signal propagation from the membrane distal domain to the membrane proximal domain of the receptor and breaking the hydrogen bonds by mutations de-coupled the domains and reduced the ability of the small molecules to cause the conformational change (*191*). We first observed significant FRET reduction in the mutant FRET biosensors upon SBH treatment (**Fig. 5.4D**). Interestingly, there was a significant decrease in the magnitude of the FRET change with treatment of SBH in the mutant biosensors, supporting that the ligand binding loop is mediating signal propagation between the membrane distal and the membrane proximal domains (**Fig. 5.4E**). In addition, the extent of FRET change in V90A (a negative control) FRET biosensor is similar to that of the WT FRET biosensor (**Fig. 5.4E**).

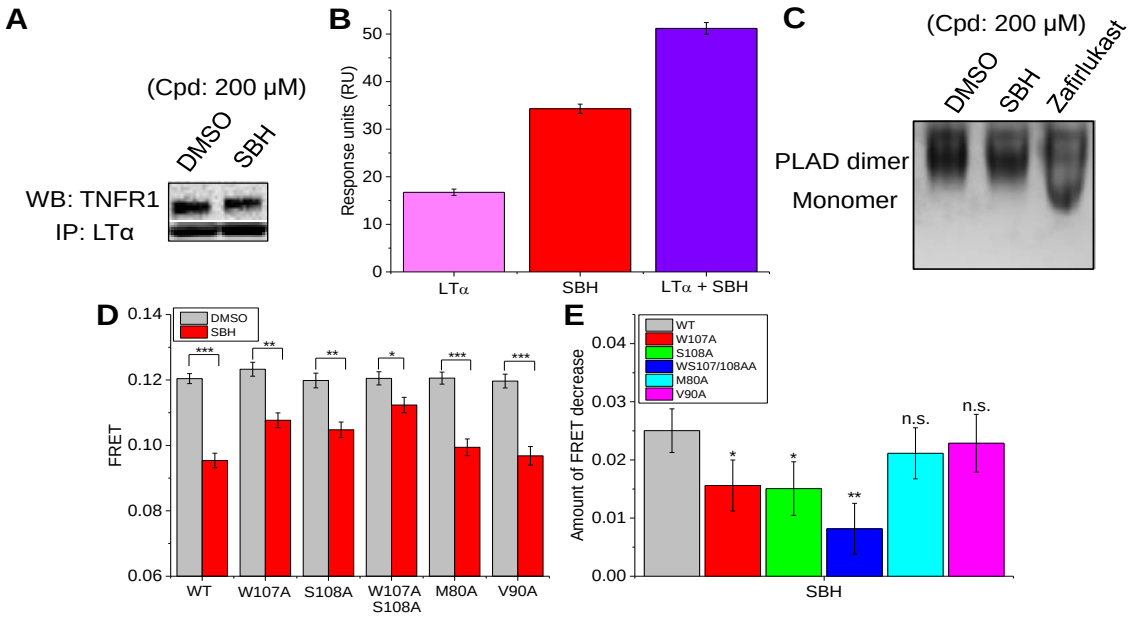

Figure 5. 4. SBH perturbs TNFR1 conformational dynamics.

(**A**) Co-immunoprecipitation between TNFR1 and ligand LTα with treatment of SBH at saturation dose of 200 μM. Equal amount of LTα is shown as pull-down controls. Western blots are representative of three independent experiments. (**B**) Non-competitive binding assay of LTα (50 nM) and SBH (200 μM) to TNFR1 ECD was performed by SPR. Data are means ± SD of three independent experiments. (**C**) Native gel characterization of soluble pre-ligand assembly domain (PLAD) of TNFR1 with treatment of DMSO control, SBH (200 μM) and zafirlukast (200 μM). Gels are representative of three independent experiments. (**D**) SBH (200 μM) reduced FRET significantly in the TNFR1 mutant biosensors (W107A, S108A, WS107/108AA, M80A and V90A (control)). (**E**) Comparison of the amount of FRET decreased between HEK293 cells expressing WT and mutant TNFR1 FRET biosensors (W107A, S108A, WS107/108AA, M80A and V90A) treated with SBH (200 μM) in the absence of ligand. Data are means ± SD of three independent experiments. *P < 0.05, **P < 0.01, ***P < 0.001 and n.s. indicates not significant by two-tailed unpaired *t* test.

5.4.5. Conformational states of TNFR1 as a molecular switch in receptor function

SBH reduced FRET in the TNFR1 biosensor, corresponding to receptor adopting an open conformation, and stimulated NF-κB activation. On the other hand, a previously identified small molecule, DS42, also reduced FRET in the TNFR1 biosensor but inhibited receptor signaling (*191*). This suggests that the two dimensional orientation of the receptor is insufficient in determining its function and the three dimensional orientation of the receptor may be important in its signaling mechanism such as the recruitment of the downstream signaling molecules. To test this, we performed another co-IP experiment to determine the interactions between TNFR1 and the downstream signaling molecule TNFR1 associated death domain (TRADD) with treatment of SBH. The co-IP results indicated that significantly more TRADD was pulled down with treatment of SBH both in the absence or presence of the ligand given the same amount

of TNFR1 in the samples (**Fig. 5.5A-B**). This suggests that receptor conformational states, either two or three dimensional orientation, could affect the recruitment of downstream signaling molecules and correspond to either receptor activation or inhibition, hence behaving like a molecular switch (**Fig. 5.5C**). This new hypothesis would also require higher resolution microscopic or biophysical techniques in studying receptor orientations beyond the two dimensional axis.

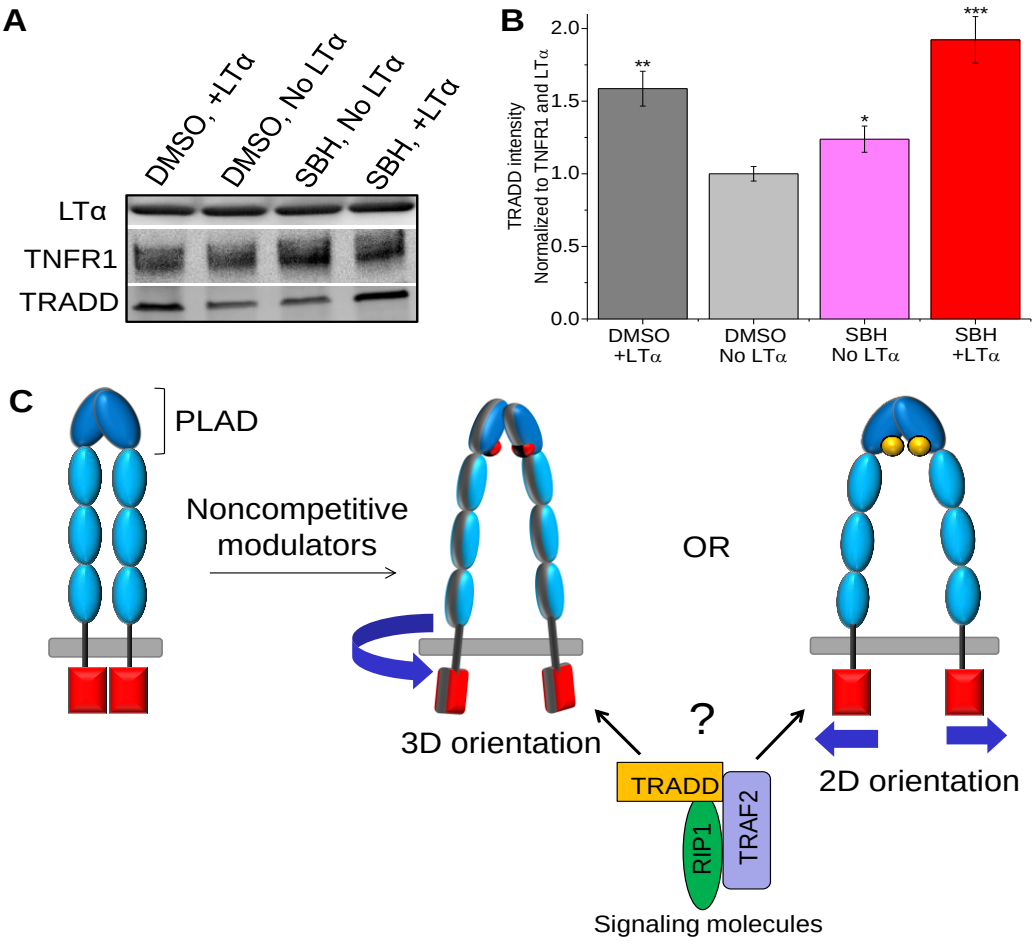

Figure 5. 5. Conformational states of TNFR1 as a molecular switch for receptor function.

(**A**) Co-immunoprecipitation (co-IP) between LTα, TNFR1 and TRADD with and without treatment of SBH (100 μM) and in the absence and presence of the ligand (0.1 μg/mL). Equal amount of

FLAG-tagged LTα coated on the magnetic beads with FLAG antibody is shown as pull-down controls. Western blots are representative of three independent experiments. (**B**) Quantification of the Western blot for co-IP in (A). (**C**) Proposed model of conformational states of TNFR1 as a molecular switch for receptor function. Receptor function can be controlled by altering receptor dynamics with a need to take into account the three dimensional orientation of the receptor for its recruitment of the downstream signaling molecules upon ligand stimulation and the determination of receptor activation or inhibition.

5.5. Discussion

Being a major contributor to the NF-κB activation pathway, TNFR1 activation can significantly lead to increased NF-κB activation for treatment of immune deficiency and neurodegenerative diseases (*259, 260*). To the best of our knowledge, SBH is not only the first small molecule activator of TNFR1, it also acts through a novel mechanism of perturbing receptor conformational states to sensitize the receptor for activation in the absence of ligand or increased activation in addition to ligand stimulation without competing for binding site with the ligand. This receptor-specific mechanism is distinctly different from the existing activators for other TNF receptors that either sensitize receptors to ligand activation or mimic ligand in which the activation efficiency is limited by the need to compete for ligand binding. Some of these examples include small molecules that sensitize FAS receptor to its agonist antibody for killing of cancer cells (*252*), small molecule mimic of Smac that potentiates TRAIL and TNFα mediated deaths in cancer cells (*253*), another small molecule (bioymifi) that can act as a single agent to induce DR5 clustering and aggregation, leading to apoptosis, similar to TRAIL mimics targeting DR5 for cancer therapy (*254*) and compounds that block OX40-OX40L interactions but acting as OX40 agonist/ligand (*255*). Here, we would like to clarify that

SBH works differently from these small molecules in that even though it activates TNFR1 in the absence of ligand, it does not behave as ligand mimic as its effect is not additive to ligand stimulation but instead acts in multiplicity and it does not compete with cognate ligand binding. This suggests that SBH has an amplifying effect in TNFR1 signaling with an estimate of two-fold change regardless of ligand stimulation.

SBH is a known selective inhibitor of 5-HT2C/2B serotonin receptor, though it also inhibits 5-HT2A to some extent (*261*). We note that 5-HT2A serotonin receptor activation has been shown to potently suppresses TNFα induced inflammation in cells and animal models (*262, 263*). This suggests that the effect of SBH in activating TNFR1 may partially due to its inhibition of 5-HT2A receptor, leading to the lifting of the suppression of TNFα effect. However, these effects were restricted to 5-HT2A receptors, as 5-HT2B and 5-HT2C receptor-selective agonists were ineffective in suppressing TNFα-induced inflammation (*264*). In addition, it has been shown that HEK293 cells contain little or no 5-HT2A/2B/2C receptors (*265-268*). Furthermore, we have shown in the current study that TNFR1 is required for the activating effect of SBH. All these suggest that SBH possesses a relatively high specificity to targeting TNFR1.

An obvious benefit of receptor-specific activation by perturbing receptor conformational states is that the effect of activation may be in multiple instead of mere additive. For example, regardless of receptor constitutive signaling in the absence of ligand or ligand stimulation, the receptor activation is estimated increased by two-fold such as the relative luciferase activity changed from 1 to 2 (in the absence of ligand) or 6 to 12 (in the presence of ligand). This indicates that the receptor is adopting an active conformation that sensitizes the receptor to broadly transduce twice the activation signals. In addition, the non-competitive nature of the small molecule allows for

constitutive signaling by the cognate ligand of the receptor in addition to the activation effect of the small molecule, enhancing the overall activation effect. SBH exerts its activation effect by altering the conformational state of the pre-assembled dimer to adopt an open and active conformation. This is consistent with our previous computational study showing that ligand activation of TNFR1 adopts an opening conformation (*62*). This is further supported by other studies on TNF receptors have also shown that opening conformations were adopted and preferred for receptor activation (*180, 219*). From the perspective of understanding the mechanism of TNFR1 activation, this demonstrates that TNFR1 can be both increasingly active when the ligand is bound and the receptor dimer is intact. This suggests that the ensemble of TNFR1 conformational states can be stabilized by small molecules for its activation or inhibition, acting like a molecular switch.

5.6. Supplemental figures

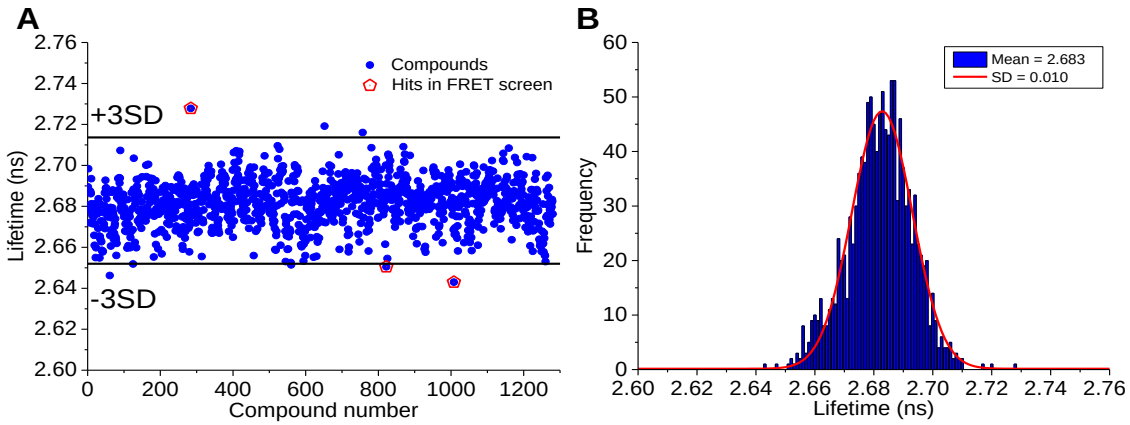

Supplemental Figure 5. 1. Donor-only control screen to remove false positives.

(A) Representative donor-only control screen with LOPAC library using HEK293 cells expressing only TNFR1ΔCD-GFP which do not show FRET signal so the lifetime plot is shown. Applied threshold at a change in lifetime of 3SD is shown by the black lines. Three reproducible hits from

the donor-only screen are the same as that obtained from the FRET screen and they are removed as false positives. **(B)** Histogram plot of all compounds from the LOPAC donor-only screen after removal of fluorescent compounds to obtain the average lifetime and the SD of the screen.

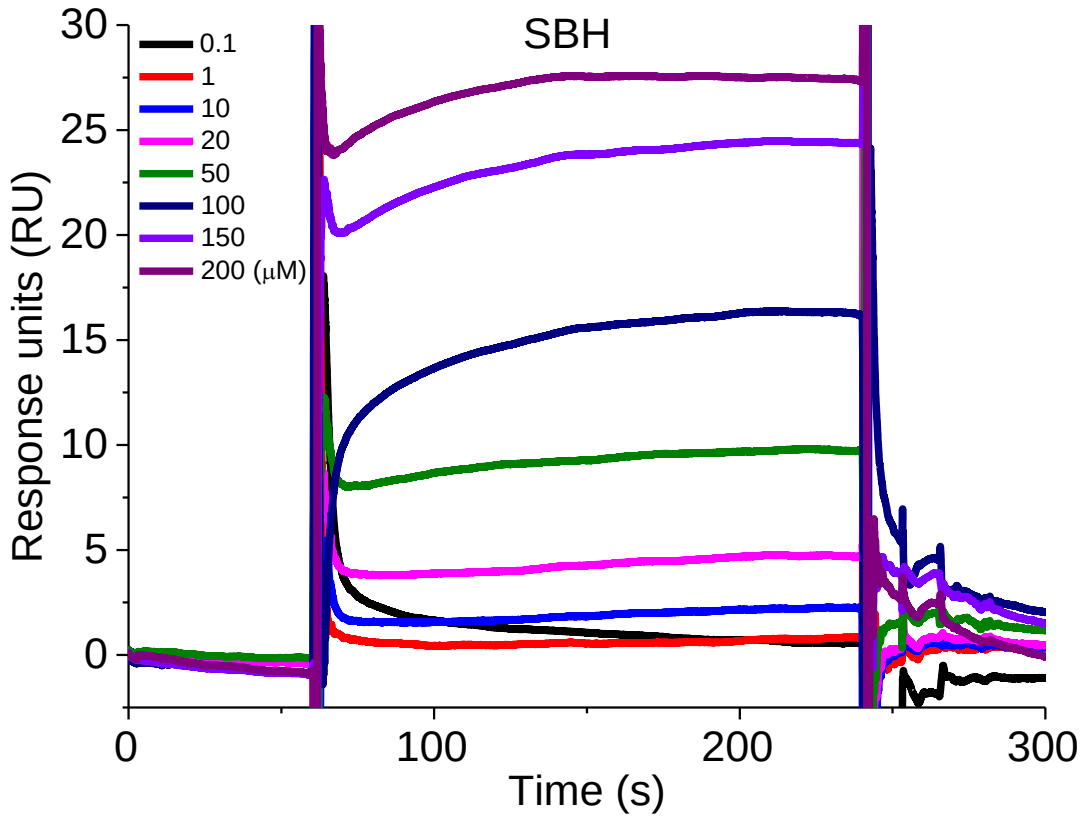

Supplemental Figure 5. 2. The binding of SBH to TNFR1 ECD as characterized by SPR measurements.

SPR raw binding curves for SBH. Bind curves are representative of three independent experiments.

CHAPTER 6: STRUCTURE-ACTIVITY RELATIONSHIP ANALYSIS OF ZAFIRLUKAST FOR POTENT RECEPTOR-SPECIFIC INHIBITION OF TNFR1 SIGNALING

Chih Hung Lo[1], William C. Fiers[2], Breeanne M. Brand[1], Evan Alexander[2], Courtney C. Aldrich[2], and Jonathan N. Sachs[1,*]

Manuscript to be submitted to *Journal of Medicinal Chemistry*

[1]Department of Biomedical Engineering, University of Minnesota, Minneapolis, MN 55455, USA.

[2]Department of Medicinal Chemistry, University of Minnesota, Minneapolis, MN 55455, USA.

Author contributions: C.H.L. designed and conducted all experiments, including chemical synthesis as well as biological, biochemical and binding assays. B.M.B. and W.C.F. contributed to some chemical synthesis. W.C.F., E.A. and C.C.A. provided inputs in analogue design and expertise in medicinal chemistry. C.H.L, C.C.A. and J.N.S. wrote the manuscript.

6.1. Summary

A series of 5-amino-3benzyl-1H-indole was synthesized based on a scaffold of zafirlukast obtained from a FRET-based HTS to discover inhibitors that disrupt TNFR1 receptor-receptor interaction. The SAR shows the sulfonamide moiety of the molecule plays a critical role in the inhibition mechanism and the extent of inhibition while the carbamate domain of the molecule is important for the binding affinity and potency of the molecule. In addition, both the sulfonamide and the carbamate functional groups are

required for compound specificity for TNFR1 as truncation of either or both groups resulted in decrease in specificity. The analogue with 4-(trifluoromethyl)benzene sulfonamide and isopropyl carbamate (**40**) emerged as one of the most promising analogues with an improved inhibition of NF-κB activation (absolute IC_{50}) of the initial hit by more than 60-fold with a half maximum inhibitory concentration at around 800 nM and full inhibition. In addition, compound **40** illustrates similar inhibition mechanism in disruption of receptor-receptor interactions with better potency in the FRET assay as well as high specificity to TNFR1. Future work includes synthesizing additional analogues with variation in the 3-benzylindole core and determining the binding affinity of the compounds using SPR.

6.2. Introduction

Tumor necrosis factor receptor 1 (TNFR1) plays a pivotal role in the signal transduction of the inflammatory pathway (*5*). Binding of cognate ligands, tumor necrosis factor (TNF) or lymphotoxin-alpha (LT-α), to the extracellular domain of TNFR1 leads to IκBα degradation and NF-κB activation (*11*). Upregulation of ligand level has been associated with several inflammatory and autoimmune diseases, including rheumatoid arthritis (RA), multiple sclerosis, inflammatory bowel disease and Crohn's disease (*200*). The prevalence of these autoimmune diseases affected up to 23.5 million in the USA, based on 24 autoimmune diseases with available epidemiologic studies (*17*). However, the American Autoimmune Related Diseases Association predicts, considering all autoimmune diseases, that there are up to 50 million people in the USA affected by an autoimmune disease (*269*). Hence, TNFR1 is a high-value target and therapeutic intervention of the receptor signaling is a billion-dollar industry and of high interest to pharmaceutical companies.

Current treatments involve anti-TNF biologic agents including monoclonal antibodies (infliximab, adalimumab, certolizumab pegol, golimumab) and soluble TNF receptor (etanercept) that function by sequestering ligands and blocking their binding to the receptor (*21, 233-235*). Despite high potency, these therapeutics have several negative consequences as a result of global ligand blockade. These limitations include the development of fatal side effects such as lupus-like symptoms and lymphomas; low rates of disease remission; and the generation of antibodies against biologic anti-TNF (*235, 236*). In addition, compared to small molecules, administration of antibodies result in injection site reactions or infusion reactions and they are expensive and often fail to cross the blood-brain barrier (*21, 237, 238*). In order to overcome these limitations, there is a desperate need to develop new receptor-specific treatments that directly target TNFR1 rather than the ligands.

Most of the current TNFR1 receptor-specific inhibitors are small molecules (*36, 37*) or antibodies (*33, 35, 176, 239*) that competitively block receptor-ligand interactions. Due to the very high affinity for ligand binding to TNFR1 (K_d=0.38 nM) (*38*), the small molecules that work by competitively eliminating ligand binding may not be effective (*177*). In addition, circulating forms of soluble TNFR1 may function as native decoys for the ligand and their TNF neutralizing capacity may be reduced by TNFR1 antagonists that block ligand binding (*39-41*). As such, approaches that do not involve eliminating ligand binding are highly attractive. An approach is to disrupt the pre-assembly of TNFR1 dimers by targeting the pre-ligand assembly domain (PLAD) which is an attractive alternative to blocking ligand binding because the monomer-monomer interaction is weaker than the receptor-ligand affinity (*55, 56*). While it has been suggested that soluble TNFR1 PLAD was able to disrupt TNFR1 receptor-receptor

interaction and inhibit receptor signaling in vitro as well as in a mouse model, the soluble PLAD protein blocked ligand binding, making it inconclusive whether the inhibition mechanism of the small protein was, in fact, disrupting the receptor dimer (*52*).

Recently, we showed for the first time, in a fluorescence resonance energy transfer (FRET) based high-throughput screening study using NIH clinical collection library, that a small molecule lead compound, zafirlukast, is capable of disrupting receptor-receptor interaction and inhibiting ligand-induced NF-κB activation without blocking ligand binding (*190*). However, zafirlukast has relatively weak potency (relative IC_{50} = 26 μM; absolute IC_{50} = 51 μM), low binding affinity to the receptor (86 μM) and only partially inhibits activation (56% inhibition) (*190, 270*). To our knowledge, this was the first and only small-molecule inhibitor that had been demonstrated to inhibit TNFR1 without blocking ligand binding. We were intrigued by the potential of the zafirlukast scaffold (**Fig. 5.1A**) to be repurposed to target TNFR1 based on it being a FDA-approved drug targeting leukotriene receptor with potent anti-inflammatory activity for treatment of asthma, known safety profiles, clearly defined structure–activity relationships and chemical tractability for analogue synthesis (*271-273*). In this study, we describe a systematic and comprehensive SAR analysis of the zafirlukast scaffold that resulted in compounds with improved activity profiles on receptor-specific inhibition of TNFR1 signaling.

6.3. Materials and methods

6.3.1. General procedures (compounds not listed are in progress to be included and some characterizations are currently in process)

General Procedure A for the synthesis of 3-benzylindole (adopted from CHL-I-031)

To a suspension of nitroindole (8.3 g, 51 mmol, 1.7 equiv) in dry dioxane (30 mL) at 25 °C was added zinc bromide (5.3 g, 20 mmol, 0.66 equiv) and *N,N*-diisopropylethylamine (6.58 g, 51 mmol, 1.7 equiv). The mixture was stirred for 20 min, then benzyl bromide (7.9 g, 31 mmol, 1.0 equiv) was added and the reaction was stirred at 25 °C for 40 h. The mixture was concentrated in vacuo and the crude residue was redissolved in CH_2Cl_2 (50 mL) and washed with H_2O (50 mL). The aqueous layer was extracted with CH_2Cl_2 (3 × 50 mL). The combined organic fractions were dried over Na_2SO_4, filtered and concentrated in vacuo. The residue was purified by flash column chromatography (hexanes/EtOAc) on silica gel.

Methyl 3-methoxy-4-(5-nitroindol-3-ylmethyl)benzoate (1) (CHL-I-031).

The title compound was synthesized from 5-nitroindole (8.3 g, 51 mmol) and methyl 4-(bromomethyl)-3-methoxybenzoate (7.9 g, 31 mmol) using the General Procedure **A** to afford a yellow solid (yield: 52%): R_f = 0.19 (80:20 hexanes/EtOAc); ^{1}H NMR (400 MHz, $CDCl_3$) δ 3.90 (s, 3H), 3.95 (s, 3H), 4.15 (s, 2H), 7.11 (s, 1H), 7.16 (d, J = 7.9 Hz, 1H), 7.37 (d, J = 9.0 Hz, 1H), 7.55–7.56 (m, 2H), 8.08-8.11 (m, 1H), 8.40 (s, 1H), 8.59 (s, 1H); ^{13}C NMR (400 MHz, $CDCl_3$) δ information TBD; HRMS (ESI+) calcd for $C_{18}H_{17}N_2O_5$ $[M+H]^+$ 341.1132, found XXX.XXXX (error X.X ppm).

Methyl 4-((5-nitro-1*H*-indol-3-yl)methyl)benzoate (45) (CHL-II-004)

The title compound was synthesized from 5-nitroindole (5.1 g, 0.032 mmol) and methyl 4-(bromomethyl)benzoate (4.6 g, 0.019 mmol) using the General Procedure **A** to afford a yellow solid (yield: 61%): R_f = 0.17 (70:30 hexanes/EtOAc); ^{1}H NMR (400 MHz, CD_3OD) δ 3.87 (s, 2H), 4.23 (s, 2H), 7.28 (s, 1H), 7.41 (d, J = 8.9 Hz, 2H), 7.46 (d, J = 9.3 Hz, 1H), 7.94 (d, J = 7.8 Hz, 2H), 8.02 (d, J = 9.2 Hz, 1H), 8.38 (s, 1H); ^{13}C NMR (400 MHz, CD_3OD) δ information TBD; HRMS (ESI+) calcd for $C_{17}H_{15}N_2O_4$ $[M+H]^+$ 311.1026, found XXX.XXXX (error X.X ppm).

General Procedure B for the methylation of 3-benzylindole (adopted from CHL-I-032)

To a suspension of methyl nitroindolebenzoate (2.75 g, 8.09 mmol, 1.00 equiv) in dry THF (57.3 mL) at 25 °C was added sodium hydride (0.327 g, 8.17 mmol, 1.01 equiv) and iodomethane (2.36 g, 16.7 mmol, 2.06 equiv). The mixture was concentrated in vacuo and the crude residue was redissolved in CH_2Cl_2 (50 mL) and washed with H_2O (50 mL). The aqueous layer was extracted with CH_2Cl_2 (3 × 50 mL). The combined organic fractions were dried over Na_2SO_4, filtered and concentrated in vacuo. The residue was purified by flash column chromatography (hexanes/EtOAc) on silica gel.

Methyl 3-methoxy-4-((1-methyl-5-nitro-1*H*-indol-3-yl)methyl)benzoate (2) (CHL-I-032)

The title compound was synthesized from methyl 3-methoxy-4-(5-nitroindol-3-ylmethyl)benzoate (**1**) (CHL-I-031) (2.75 g, 8.09 mmol) using the General Procedure **B** (yield: 75%): R_f = 0.28 (70:30 hexanes/EtOAc); ^{1}H NMR (400 MHz, $CDCl_3$) δ 3.79 (s, 3H), 3.90 (s, 3H), 3.96 (s, 3H), 4.13 (s, 2H), 6.92 (s, 1H), 7.17 (d, J = 8.1 Hz, 1H), 7.28 (d, J = 9.1 Hz, 1H), 7.54–7.56 (m, 2H), 8.10-8.13 (m, 1H), 8.59 (d, J = 2.2 Hz, 1H); ^{13}C NMR (400 MHz, $CDCl_3$) δ information TBD; HRMS (ESI+) calcd for $C_{19}H_{19}N_2O_5$ $[M+H]^+$ 355.1288, found XXX.XXXX (error X.X ppm).

Methyl 4-((1-methyl-5-nitro-1*H*-indol-3-yl)methyl)benzoate (44) (CHL-II-021)

The title compound was synthesized from methyl 4-((5-nitro-1*H*-indol-3-yl)methyl)benzoate (**45**) (CHL-II-004) (0.780 g, 2.52 mmol) using the General Procedure **B** (Yield: 81%): R_f = 0.19 (70:30 hexanes/EtOAc); ^{1}H NMR (400 MHz, $CDCl_3$) δ 3.78 (s, 3H), 3.88 (s, 3H), 4.14 (s, 2H), 6.90 (s, 1H), 7.27 (d, J = 9.1 Hz, 1H), 7.32 (d, J = 7.9 Hz, 2H), 7.96 (d, J = 7.9 Hz, 2H), 8.06-8.09 (m, 1H), 8.41 (s, 1H); ^{13}C NMR (400 MHz,

$CDCl_3$) δ information TBD; HRMS (ESI+) calcd for $C_{18}H_{17}N_2O_4$ $[M+H]^+$ 325.1183, found XXX.XXXX (error X.X ppm).

General Procedure C for the reduction of nitroindole (adopted from CHL-I-070)

To a suspension of nitroindole (0.44 g, 1.2 mmol, 1.0 equiv) in dry THF (10 mL) at 25 °C was added palladium (0.66 g, 0.62 mmol, 0.50 equiv). The mixture was stirred at 25 °C for 24 h. The mixture was passed through celite to remove the palladium followed by washing with methanol and ethyl acetate to elute the compound. The residue was purified by flash column chromatography (hexanes/EtOAc) on silica gel.

Methyl 4-((5-amino-1-methyl-1*H*-indol-3-yl)methyl)-3-methoxybenzoate (3) (CHL-I-070)

The title compound was synthesized from methyl 3-methoxy-4-((1-methyl-5-nitro-1*H*-indol-3-yl)methyl)benzoate (**2**) (CHL-I-032) (0.44 g, 1.2 mmol) using the General Procedure **C** (yield: 89%): R_f = 0.25 (70:30 hexanes/EtOAc); ^{1}H NMR (400 MHz, $CDCl_3$) δ 3.66-3.67 (m, 3H), 3.93 (s, 3H), 3.96 (s, 3H), 4.07 (s, 2H), 6.68-6.71 (m, 1H), 6.73 (s, 1H), 6.81 (s, 1H), 7.11 (d, J = 8.5 Hz, 1H), 7.18 (d, J = 7.8 Hz, 1H), 7.56–7.58 (m, 1H), 7.60 (s, 1H); ^{13}C NMR (400 MHz, $CDCl_3$) δ 25.2, 32.6, 52.0, 55.5, 104.1, 109.7, 110.7, 110.9, 112.5, 127.0, 127.9, 128.7, 128.9, 129.6, 132.2, 135.7, 139.0, 157.1, 167.2; HRMS (ESI+) calcd for $C_{19}H_{21}N_2O_3$ $[M+H]^+$ 325.1547, found XXX.XXXX (error X.X ppm).

4-((5-amino-1-methyl-1*H*-indol-3-yl)methyl)-*N*-((4-(trifluoromethyl)phenyl)sulfonyl)benzamide (47) (CHL-II-026)

The title compound was synthesized from 4-((1-methyl-5-nitro-1*H*-indol-3-yl)methyl)-*N*-((4-(trifluoromethyl)phenyl)sulfonyl)benzamide (**50**) (CHL-II-024) (0.100 g, 0.193 mmol) using the General Procedure **C** (Yield: TBD): R_f = 0.22 (0:100 hexanes/EtOAc); ^{1}H NMR (400 MHz, $CDCl_3$) δ 3.88 (s, 3H), 3.94 (s, 3H), 4.14 (s, 2H), 7.09 (s, 1H), 7.15 (d, J = 7.9 Hz, 1H), 7.36 (d, J = 9.0 Hz, 1H), 7.52–7.54 (m, 2H), 8.08 (d, J = 8.9 Hz, 1H), 8.38 (s,

1H), 8.57 (s, 1H); ^{13}C NMR (400 MHz, $CDCl_3$) δ information TBD; HRMS (ESI+) calcd for $C_{24}H_{21}F_3N_3O_3S$ $[M+H]^+$ 488.1250, found XXX.XXXX (error X.X ppm).

General Procedure D for addition of carbamate (adopted from CHL-I-071)

To a suspension of aminoindole (0.21 g, 0.64 mmol, 1.0 equiv) in DCM (10 mL) at 25 °C was added chloroformate (0.47 g, 3.2 mmol, 5.0 equiv) and triethylamine (0.32 g, 3.2 mmol, 5.0 equiv). The mixture was stirred at 4 °C for 24 h. The mixture was concentrated in vacuo and the crude residue was redissolved in CH_2Cl_2 (50 mL) and washed with H_2O (50 mL). The aqueous layer was extracted with CH_2Cl_2 (3 × 50 mL). The combined organic fractions were dried over Na_2SO_4, filtered and concentrated in vacuo. The residue was purified by flash column chromatography (hexanes/EtOAc) on silica gel.

Methyl 4-((5-(((cyclopentyloxy)carbonyl)amino)-1-methyl-1*H*-indol-3-yl)methyl)-3-methoxybenzoate (4) (CHL-I-071)

The title compound was synthesized from methyl 4-((5-amino-1-methyl-1*H*-indol-3-yl)methyl)-3-methoxybenzoate (**3**) (CHL-I-070) (0.21 g, 0.64 mmol) and cyclopentylchloroformate (0.47 g, 3.2 mmol) using the General Procedure **D** (yield: 82%): R_f = 0.23 (70:30 hexanes/EtOAc); ^{1}H NMR (400 MHz, $CDCl_3$) δ 1.24-1.53 (m, 8H0, 3.30 (s, 3H), 3.54 (s, 3H), 3.56 (s, 3H), 3.72 (s, 2H), 4.85-4.88 (m, 1H), 6.39 (s, 1H), 6.48 (s, 1H), 6.78-6.85 (m, 3H), 7.17-7.20 (m, 2H); ^{13}C NMR (400 MHz, $CDCl_3$) δ 14.2, 21.0, 23.3, 23.7, 25.2, 32.6, 32.8, 35.5, 52.0, 55.5, 60.4, 73.9, 109.3, 110.8, 112.3, 122.0, 128.0, 128.1, 128.9, 129.6, 130.1, 134.1, 135.5, 157.0, 167.2; HRMS (ESI+) calcd for $C_{25}H_{29}N_2O_5$ $[M+H]^+$ 437.2071, found XXX.XXXX (error X.X ppm).

Cyclopentyl (3-(2-methoxy-4-(((4-(trifluoromethyl)phenyl)sulfonyl)carbamoyl)benzyl)-1-methyl-1*H*-indol-5-yl)carbamate (36) (CHL-II-108)

The title compound was synthesized from 4-((5-amino-1-methyl-1H-indol-3-yl)methyl)-3-methoxy-N-((4-(trifluoromethyl)phenyl)sulfonyl)benzamide (10 mg, 0.019 mmol) and cyclobutyl carbonchloridate (13 mg, 0.097 mmol) using the General Procedure **D** (yield: TBD): R_f = 0.13 (0:100 hexanes/EtOAc); ^{1}H NMR (400 MHz, CD_3OD) δ 2.01-2.34 (m, 6H), 3.70 (s, 2H), 3.89 (s, 1H), 3.99 (s, 1H), 5.34 (s, 1H), 6.84 (s, 1H), 7.03 (s, 1H), 7.15 (s, 1H), 7.20 (s, 1H), 7.43-7.46 (m, 2H), 7.60 (s, 1H), 7.76 (s, 2H), 8.14 (d, *J* = 8.2 Hz, 2H); ^{13}C NMR (400 MHz, CD_3OD) δ information TBD; HRMS (ESI+) calcd for $C_{31}H_{31}F_3N_3O_6S$ $[M+H]^+$ 630.1880, found XXX.XXXX (error X.X ppm).

Tetrahydrofuran-3-yl (3-(2-methoxy-4-(((4-(trifluoromethyl)phenyl)sulfonyl)carbamoyl)benzyl)-1-methyl-1*H*-indol-5-yl)carbamate (43) (CHL-II-019)

The title compound was synthesized from 4-((5-amino-1-methyl-1H-indol-3-yl)methyl)-3-methoxy-N-((4-(trifluoromethyl)phenyl)sulfonyl)benzamide (32 mg, 0.062 mmol) and oxylan-3-yl chloroformate (47 mg, 0.31 mmol) using the General Procedure **D** (yield: TBD): R_f = 0.13 (0:100 hexanes/EtOAc); ^{1}H NMR (400 MHz, CD_3OD) δ 1.96-2.20 (m, 6H), 3.71 (s, 3H), 3.90 (s, 3H), 3.99 (s, 2H), 5.28 (s, 1H), 6.85 (s, 1H), 7.03 (d, *J* = 8.0 Hz, 1H), 7.16 (s, 1H), 7.22 (d, *J* = 8.6 Hz, 1H), 7.43–7.45 (m, 1H), 7.50 (s, 1H), 7.60 (s, 1H), 7.76 (d, *J* = 8.1 Hz, 2H), 8.14 (d, *J* = 8.1 Hz, 2H); ^{13}C NMR (400 MHz, CD_3OD) δ information TBD; HRMS (ESI+) calcd for $C_{30}H_{29}F_3N_3O_7S$ $[M+H]^+$ 632.1673, found XXX.XXXX (error X.X ppm).

Methyl (3-(2-methoxy-4-(((4-(trifluoromethyl)phenyl)sulfonyl)carbamoyl)benzyl)-1-methyl-1*H*-indol-5-yl)carbamate (38) (CHL-II-018)

The title compound was synthesized from 4-((5-amino-1-methyl-1H-indol-3-yl)methyl)-3-methoxy-N-((4-(trifluoromethyl)phenyl)sulfonyl)benzamide (32 mg, 0.062 mmol) and methyl chloroformate (29 mg, 0.31 mmol) using the General Procedure **D** (yield: TBD): R_f = 0.21 (0:100 hexanes/EtOAc); ^{1}H NMR (400 MHz, CD_3OD) δ 3.48-3.71 (m, 6H), 3.90 (s, 3H), 3.99 (s, 2H), 6.84 (s, 1H), 7.04 (d, *J* = 7.9 Hz, 1H), 7.17 (s, 1H), 7.22 (d, *J* = 8.6 Hz, 1H), 7.43 (d, *J* = 7.8 Hz, 1H), 7.48 (s, 1H), 7.58 (s, 1H), 7.76 (d, *J* = 8.1 Hz, 2H), 8.14 (d, *J* = 8.1 Hz, 2H); ^{13}C NMR (400 MHz, CD_3OD) δ information TBD; HRMS (ESI+) calcd for $C_{27}H_{25}F_3N_3O_6S$ $[M+H]^+$ 576.1411, found XXX.XXXX (error X.X ppm).

isopropyl (3-(2-methoxy-4-(((4-(trifluoromethyl)phenyl)sulfonyl)carbamoyl)benzyl)-1-methyl-1*H*-indol-5-yl)carbamate (40) (CHL-I-125)

The title compound was synthesized from 4-((5-amino-1-methyl-1H-indol-3-yl)methyl)-3-methoxy-N-((4-(trifluoromethyl)phenyl)sulfonyl)benzamide (CHL-I-106) (13 mg, 0.025 mmol) and isopropyl chloroformate (16 mg, 0.13 mmol) using the General Procedure **D** (yield: TBD): R_f = 0.07 (50:50 hexanes/EtOAc); ^{1}H NMR (400 MHz, CD_3OD) δ 1.28 (d, *J* = 7.7 Hz, 6H), 3.70 (s, 3H), 3.89 (s, 3H), 3.99 (s, 2H), 6.83 (s, 1H), 7.04 (d, *J* = 8.0 Hz, 1H), 7.15 (s, 1H) 7.21 (d, *J* = 8.2 Hz, 1H), 7.44 (d, *J* = 8.0 Hz, 1H), 7.49 (s, 1H), 7.59 (s, 1H), 7.76 (d, *J* = 8.0 Hz, 1H), 8.13-8.15 (m, 2H) ;^{13}C NMR (400 MHz, CD_3OD) δ information TBD; HRMS (ESI+) calcd for $C_{29}H_{29}F_3N_3O_6S$ $[M+H]^+$ 604.1724, found XXX.XXXX (error X.X ppm).

Cyclohexyl (3-(2-methoxy-4-(((4-(trifluoromethyl)phenyl)sulfonyl)carbamoyl)benzyl)-1-methyl-1*H*-indol-5-yl)carbamate (37) (CHL-II-017)

The title compound was synthesized from 4-((5-amino-1-methyl-1H-indol-3-yl)methyl)-3-methoxy-N-((4-(trifluoromethyl)phenyl)sulfonyl)benzamide (CHL-II-016) (20 mg, 0.040

mmol) and cyclohexyl chloroformate (33 mg, 0.20 mmol) using the General Procedure **D** (yield: TBD): R_f = 0.13 (50:50 hexanes/EtOAc); ^{1}H NMR (400 MHz, CD_3OD) δ 1.78-2.03 (m, 10H), 3.71 (s, 3H), 3.89 (s, 3H), 3.99 (s, 2H), 4.58 (s, 1H), 6.83 (s, 1H), 7.03 (d, *J* = 7.8 Hz, 1H), 7.15 (s, 1H), 7.22 (d, *J* = 8.8 Hz, 1H), 7.44 (d, *J* = 7.9 Hz, 1H), 7.47 (s, 1H), 7.60 (s, 1H), 7.75 (d, *J* = 8.2 Hz, 1H), 8.14 (d, *J* =8.1 Hz, 2H); ^{13}C NMR (400 MHz, CD_3OD) δ information TBD; HRMS (ESI+) calcd for $C_{32}H_{33}F_3N_3O_6S[M+H]^+$ 644.2037, found XXX.XXXX (error X.X ppm).

General Procedure E for saponification of methyl benzoate (adopted from CHL-I-072)

To a suspension of methyl benzoate (0.17 g, 0.39 mmol, 1.0 equiv) in THF (10 mL) and water (5 mL) was added lithium hydroxide (56 mg, 2.3 mmol, 6.0 equiv) and the reaction was stirred at 25 °C for 20 h. The reaction was acidified and kept in cold, and the titled compound precipitated.

4-((5-(((cyclopentyloxy)carbonyl)amino)-1-methyl-1*H*-indol-3-yl)methyl)-3-methoxybenzoic acid (24) (CHL-I-072)

The title compound was synthesized from methyl 4-((5-(((cyclopentyloxy)carbonyl)amino)-1-methyl-1*H*-indol-3-yl)methyl)-3-methoxybenzoate (**4**) (CHL-I-071) (0.17 g, 0.39 mmol, 1.0 equiv) using the General Procedure **E** (yield: 88%): R_f = 0.21 (95:5 DCM/MeOH); ^{1}H NMR (400 MHz, CD_3OD) δ 1.55-1.81 (m, 8H), 3.56 (s, 3H), 3.84 (s, 3H), 3.97 (s, 2H), 5.08 (s, 1H), 6.75 (s, 1H), 7.07-7.13 (m, 3H), 7.45-7.48 (m, 1H), 7.53 (s, 1H), 7.56 (s, 1H); ^{13}C NMR (400 MHz, CD_3OD) δ14.1, 20.1, 24.6, 26.0, 29.8, 30.7, 32.6, 33.7, 55.9, 78.6, 110.1, 110.9, 111.9, 113.4, 116.4, 123.1, 129.2, 130.6, 131.6, 135.6, 137.0, 156.7, 158.4, 170.6; HRMS (ESI+) calcd for $C_{24}H_{27}N_2O_5$ $[M+H]^+$ 423.1914, found XXX.XXXX (error X.X ppm).

4-((1-methyl-5-nitro-1*H*-indol-3-yl)methyl)benzoic acid (47) (CHL-II-022)

The title compound was synthesized from methyl 4-((1-methyl-5-nitro-1*H*-indol-3-yl)methyl)benzoate (**44**) (CHL-II-021) (0.50 g, 1.5 mmol) using the General Procedure **E** (yield: 85%): R_f = 0.23 (95:5 DCM/Methanol); ^{1}H NMR (400 MHz, CD_3OD) δ 3.84 (s, 3H), 4.21 (s, 2H), 7.21 (s, 1H), 7.39 (d, *J* = 8.0 Hz, 2H), 7.48 (d, *J* = 9.1 Hz, 1H), 7.94 (d, *J* = 8.0 Hz, 2H), 8.06–8.09 (m, 1H), 8.41 (d, *J* = 2.3 Hz, 1H); ^{13}C NMR (400 MHz, CD_3OD) δ information TBD; HRMS (ESI+) calcd for $C_{17}H_{15}N_2O_4$ $[M+H]^+$ 311.1026, found XXX.XXXX (error X.X ppm).

General Procedure F for addition of sulfonamide (adopted from CHL-I-073)

To a suspension of benzoic acid (15.0 mg, 0.0355 mmol, 1.00 equiv) in DCM (10 mL) at 25 °C was added sulfonamide (6.38 mg, 0.0373 mmol, 1.05 equiv), DMAP (4.56 mg, 0.0373 mmol, 1.05 equiv) and EDC (7.15 mg, 0.0373 mmol, 1.05 equiv) and the reaction was stirred for 24 h. The mixture was acidified using 1N HCl and the aqueous layer was extracted with CH_2Cl_2 (3 × 50 mL). The combined organic fractions were dried over Na_2SO_4, filtered and concentrated in vacuo. The residue was purified by flash column chromatography (hexanes/EtOAc or DCM/MeOH) on silica gel.

Cyclopentyl (3-(2-methoxy-4-((*m*-tolylsulfonyl)carbamoyl)benzyl)-1-methyl-1*H*-indol-5-yl)carbamate (25) (CHL-I-073)

The title compound was synthesized from 4-((5-(((cyclopentyloxy)carbonyl)amino)-1-methyl-1*H*-indol-3-yl)methyl)-3-methoxybenzoic acid (**24**) (CHL-I-072) (15.0 mg, 0.0355 mmol) and 3-methylbenzene sulfonamide (6.38 mg, 0.0373 mmol) using the General Procedure **F** (yield: TBD): R_f = 0.19 (95:5 DCM/MeOH); ^{1}H NMR (400 MHz, CD_3OD) δ 1.61-1.87 (m, 8H), 2.39 (s, 3H), 3.70 (s, 3H), 3.88 (s, 3H), 4.00 (s, 2H), 5.09-5.12 (m, 1H), 6.85 (s, 1H), 7.06 (d, *J* = 7.7 Hz, 1H), 7.10-7.12 (m, 1H), 7.21 (d, *J* = 8.7 Hz, 1H), 7.36 (d, *J* = 4.6 Hz, 2H), 7.42 (d, *J* = 7.6 Hz, 1H), 7.15 (d, *J* = 7.9 Hz, 1H), 7.36 (d, *J* = 9.0 Hz, 1H), 7.52–7.54 (m, 2H), 7.79-7.18 (m, 1H), 7.84 (s, 1H); ^{13}C NMR (400 MHz,

CD_3OD) δ 14.5, 20.9, 21.3, 23.7, 24.6, 26.0, 30.5, 30.7, 32.7, 33.1, 33.7, 33.8, 55.9, 61.5, 78.6, 110.1, 111.3, 113.7, 122.0, 125.5, 128.7, 129.3, 129.5, 130.4, 134.0, 135.7, 135.9, 139.9, 143.5, 156.8, 158.3; HRMS (ESI+) calcd for $C_{31}H_{34}N_3O_6S$ $[M+H]^+$ 576.2163, found XXX.XXXX (error X.X ppm).

Cyclopentyl (3-(2-methoxy-4-(tosylcarbamoyl)benzyl)-1-methyl-1*H*-indol-5-yl)carbamate (26) (CHL-I-074)

The title compound was synthesized from 4-((5-(((cyclopentyloxy)carbonyl)amino)-1-methyl-1*H*-indol-3-yl)methyl)-3-methoxybenzoic acid (**24**) (CHL-I-072) (15.0 mg, 0.0355 mmol) and 4-methylbenzene sulfonamide (6.38 mg, 0.0373 mmol) using the General Procedure **F** (yield: TBD): R_f = 0.13 (95:5 DCM/MeOH); ^{1}H NMR (400 MHz, CD_3OD) δ 1.61- 1.87 (m, 8H), 2.41 (s, 3H), 3.70 (s, 3H), 3.90 (s, 3H), 4.01 (s, 2H), 5.09-5.12 (m, 1H), 6.87 (s, 1H), 7.09 (d, J = 7.9 Hz, 2H), 7.22 (d, J = 8.7 Hz, 1H), 7.34 (d, J = 8.0 Hz, 3H), 7.44 (s, 1H), 7.51 (s, 1H), 7.92 (d, J = 8.1 Hz, 2H); ^{13}C NMR (400 MHz, CD_3OD) δ 9.2, 14.5, 19.4, 20.9, 21.3, 21.5, 24.6, 28.0, 30.3, 30.8, 32.7, 33.8, 56.0, 61.5, 78.6, 110.1, 111.0, 113.5, 116.4, 121.7, 129.0, 129.3, 129.4, 130.2, 130.6, 131.7, 135.7, 136.5, 145.0, 156.8, 158.5; HRMS (ESI+) calcd for $C_{31}H_{34}N_3O_6S$ $[M+H]^+$ 576.2163, found XXX.XXXX (error X.X ppm).

Cyclopentyl (3-(4-(((4-chlorophenyl)sulfonyl)carbamoyl)-2-methoxybenzyl)-1-methyl-1*H*-indol-5-yl)carbamate (27) (CHL-I-075)

The title compound was synthesized from 4-((5-(((cyclopentyloxy)carbonyl)amino)-1-methyl-1*H*-indol-3-yl)methyl)-3-methoxybenzoic acid (**24**) (CHL-I-072) (15.0 mg, 0.0355 mmol) and 4-chlorobenzene sulfonamide (7.15 mg, 0.0373 mmol) using the General Procedure **F** (yield: TBD): R_f = 0.22 (95:5 DCM/MeOH); ^{1}H NMR (400 MHz, CD_3OD) δ 1.61-1.86 (m, 8H), 3.69 (s, 3H), 3.88 (s, 3H), 4.00 (s, 2H), 5.08-5.11 (m, 1H), 6.86 (s, 1H), 7.07-7.11 (m, 2H), 7.20-7.22 (m, 1H), 7.37 (d, J = 7.8 Hz, 1H), 7.48-7.53 (m, 4H),

7.99-8.00 (m, 2H); ^{13}C NMR (400 MHz, CD_3OD) δ 14.5, 20.9, 24.6, 26.0, 30.8, 31.8, 32.7, 33.8, 55.9, 61.5, 78.6, 110.1, 111.0, 111.3, 113.6, 116.4, 122.0, 129.3, 129.4, 129.8, 130.3, 130.5, 131.6, 135.0, 135.7, 136.2, 139.6, 142.2, 156.8, 158.4; HRMS (ESI+) calcd for $C_{30}H_{31}ClN_3O_6S$ $[M+H]^+$ 596.1617, found XXX.XXXX (error X.X ppm).

Cyclopentyl (3-(4-(((1,3-dimethyl-1*H*-pyrazol-4-yl)sulfonyl)carbamoyl)-2-methoxybenzyl)-1-methyl-1*H*-indol-5-yl)carbamate (33) (CHL-I-076)

The title compound was synthesized from 4-((5-(((cyclopentyloxy)carbonyl)amino)-1-methyl-1*H*-indol-3-yl)methyl)-3-methoxybenzoic acid (**24**) (CHL-I-072) (15.0 mg, 0.0355 mmol) and 1,3,-dimethyl-1H-pyrazole-4sulfonamide (6.54 mg, 0.0373 mmol) using the General Procedure **F** (yield: TBD): R_f = 0.18 (95:5 DCM/MeOH); ^{1}H NMR (400 MHz, CD_3OD) δ 1.62-1.88 (m, 8H), 2.40 (s, 3H), 3.71 (s, 3H), 3.83 (s, 3H), 3.92 (s, 3H), 4.01 (s, 2H), 5.11 (s, 1H), 6.87 (s, 1H), 7.07-7.13 (m, 2H), 7.22 (d, J = 8.6 Hz, 1H), 7.38 (d, J = 7.9 Hz, 1H), 7.51 (s, 2H), 8.03 (s, 1H); ^{13}C NMR (400 MHz, CD_3OD) δ 12.4, 14.5, 20.9, 24.6, 26.0, 32.7, 33.8, 39.2, 56.0, 61.5, 78.6, 110.2, 110.7, 113.3, 116.4, 119.8, 121.4, 129.2, 129.5, 130.8, 132.3, 135.7, 137.3, 137.5, 149.7, 156.8, 158.7, 168.1, 173.0; HRMS (ESI+) calcd for $C_{29}H_{34}N_5O_6S$ $[M+H]^+$ 580.2224, found XXX.XXXX (error X.X ppm).

Cyclopentyl (3-(4-(((4-cyanophenyl)sulfonyl)carbamoyl)-2-methoxybenzyl)-1-methyl-1*H*-indol-5-yl)carbamate (29) (CHL-I-077)

The title compound was synthesized from 4-((5-(((cyclopentyloxy)carbonyl)amino)-1-methyl-1*H*-indol-3-yl)methyl)-3-methoxybenzoic acid (**24**) (CHL-I-072) (15.0 mg, 0.0355 mmol) and 4-cyanobenzene sulfonamide (6.80 mg, 0.0373 mmol) using the General Procedure **F** (yield: TBD): R_f = 0.10 (95:5 DCM/MeOH); ^{1}H NMR (400 MHz, CD_3OD) δ 1.61-1.86 (m, 8H), 3.69 (s, 3H), 3.89 (s, 3H), 4.00 (s, 2H), 5.08-5.11 (m, 1H), 6.87 (s, 1H), 7.10 (d, J = 7.6 Hz, 2H), 7.21 (d, J = 8.7 Hz, 1H), 7.32-7.35 (m, 1H), 7.43 (s, 1H),

7.52 (s, 1H), 7.88-7.90 (m, 2H); ^{13}C NMR (400 MHz, CD_3OD) δ 14.1, 20.2, 24.6, 26.0, 30.7, 32.7, 32.8, 33.8, 33.9, 56.0, 78.6, 110.2, 111.0, 113.4, 116.4, 117.5, 118.5, 121.8, 129.2, 129.4, 129.8, 130.7, 131.7, 133.2, 133.8, 135.7, 137.1, 146.4, 156.8, 158.6, 169.8; HRMS (ESI+) calcd for $C_{31}H_{31}N_4O_6S$ $[M+H]^+$ 587.1959, found XXX.XXXX (error X.X ppm).

Cyclopentyl (3-(2-methoxy-4-(((4-(trifluoromethyl)phenyl)sulfonyl)carbamoyl)benzyl)-1-methyl-1*H*-indol-5-yl)carbamate (28) (CHL-I-078)

The title compound was synthesized from 4-((5-(((cyclopentyloxy)carbonyl)amino)-1-methyl-1*H*-indol-3-yl)methyl)-3-methoxybenzoic acid (**24**) (CHL-I-072) (15.0 mg, 0.0355 mmol) and 4-(trifluoromethyl)benzenesulfonamide (8.40 mg, 0.0373 mmol) using the General Procedure **F** (yield: TBD): R_f = 0.10 (95:5 DCM/MeOH); ^{1}H NMR (400 MHz, CD_3OD) δ 1.61-1.86 (m, 8H), 3.69 (s, 3H), 3.90 (s, 3H), 4.01 (s, 2H), 5.08-5.11 (m, 1H), 6.88 (s, 1H), 7.08-7.12 (m, 2H), 7.21 (d, J = 8.6 Hz, 1H), 7.33 (d, J = 7.9 Hz, 1H), 7.42 (s, 1H), 7.52 (s, 1H), 7.87 (d, J = 8.1 Hz, 2H), 8.23 (d, J = 8.1 Hz, 2H); ^{13}C NMR (400 MHz, CD_3OD) δ 14.5, 20.9, 24.6, 26.0, 32.7, 33.8, 56.0, 61.5, 78.6, 110.1, 111.0, 113.4, 116.4, 121.8, 124.0, 125.8, 126.9, 129.2, 129.4, 129.8, 130.7, 131.7, 133.5, 135.1, 135.3, 135.7, 136.9, 146.2, 156.8, 158.5, 170.0; HRMS (ESI+) calcd for $C_{31}H_{31}F_3N_3O_6S$ $[M+H]^+$ 630.1880, found XXX.XXXX (error X.X ppm).

Cyclopentyl (3-(2-methoxy-4-((morpholinosulfonyl)carbamoyl)benzyl)-1-methyl-1*H*-indol-5-yl)carbamate (34) (CHL-I-079)

The title compound was synthesized from 4-((5-(((cyclopentyloxy)carbonyl)amino)-1-methyl-1*H*-indol-3-yl)methyl)-3-methoxybenzoic acid (**24**) (CHL-I-072) (18.0 mg, 0.0426mmol) and morpholine-4-sulfonamide (7.44 mg, 0.0477 mmol) using the General Procedure **F** (yield: TBD): R_f = 0.13 (50:50 hexanes/EtOAc); ^{1}H NMR (400 MHz, CD_3OD)

δ 1.62-1.88 (m, 8H), 3.35-3.37 (m, 4H), 3.70-3.72 (m, 7H), 3.95 (s, 3H), 4.05 (s, 2H), 6.91 (s, 1H), 7.09-7.15 (m, 2H), 7.23 (d, *J* = 8.8 Hz, 1H), 7.37-7.39 (m, 1H), 7.50-7.54 (m, 2H); ^{13}C NMR (400 MHz, CD_3OD) δ 11.4, 14.5, 19.4, 23.7, 24.6, 25.0, 26.0, 28.1, 30.5, 30.6, 30.8, 31.6, 32.7, 33.1, 33.8, 40.2, 56.0, 67.6, 69.1, 78.6, 110.1, 111.2, 121.8, 129.3, 129.9, 130.5, 132.4, 158.4; HRMS (ESI+) calcd for $C_{28}H_{35}N_4O_7S$ $[M+H]^+$ 571.2221, found XXX.XXXX (error X.X ppm).

Cyclopentyl (3-(2-methoxy-4-((pyridine-4-ylsulfonyl)carbamoyl)benzyl)-1-methyl-1*H*-indol-5-yl)carbamate (32) (CHL-I-080)

The title compound was synthesized from 4-((5-(((cyclopentyloxy)carbonyl)amino)-1-methyl-1*H*-indol-3-yl)methyl)-3-methoxybenzoic acid (**24**) (CHL-I-072) (18.0 mg, 0.0426 mmol) and pyridine-4-sulfonamide (7.08 mg, 0.0477 mmol) using the General Procedure **F** (yield: TBD): R_f = 0.11 (90:10 DCM/MeOH); ^{1}H NMR (400 MHz, CD_3OD) δ 1.62-1.87 (m, 8H), 3.70 (s, 3H), 3.89 (s, 3H), 4.00 (s, 2H), 5.11 (s, 1H), 6.84 (s, 1H), 7.04 (d, *J* = 7.9 Hz, 1H), 7.11-7.13 (m, 1H), 7.22 (d, *J* = 8.7 Hz, 1H), 7.49 (d, *J* = 8.3 Hz, 2H), 7.63 (s, 1H), 7.90-7.92 (m, 2H), 8.67 (d, *J* = 5.1 Hz, 2H); ^{13}C NMR (400 MHz, CD_3OD) δ 24.2, 24.6, 28.0, 30.7, 30.8, 32.7, 33.8, 55.9, 78.6, 101.2, 110.1, 111.2, 111.7, 114.0, 116.4, 122.3, 122.4, 129.3, 130.2, 131.6, 135.0, 135.7, 137.5, 150.7, 154.5, 156.8, 158.2, 175.6, 210.1; HRMS (ESI+) calcd for $C_{29}H_{31}N_4O_6S$ $[M+H]^+$ 563.1959, found XXX.XXXX (error X.X ppm).

Cyclopentyl (3-(2-methoxy-4-(((4-(pentafluoro-λ^6-sulfaneyl)phenyl)sulfonyl)carbamoyl)benzyl)-1-methyl-1*H*-indol-5-yl)carbamate (30) (CHL-I-084)

The title compound was synthesized from 4-((5-(((cyclopentyloxy)carbonyl)amino)-1-methyl-1*H*-indol-3-yl)methyl)-3-methoxybenzoic acid (**24**) (CHL-I-072) (23.4 mg, 0.0554

mmol) and 4-(pentafluoro-sulfanyl)benzenesulfonamide (16.5 mg, 0.0582 mmol) using the General Procedure **F** (yield: TBD): R_f = 0.19 (80:20 hexanes/EtOAc); ^{1}H NMR (400 MHz, CD_3OD) δ 1.61-1.87 (m, 8H), 3.71 (s, 3H), 3.92 (s, 3H), 4.02 (s, 2H), 5.09-5.12 (m, 1H), 6.90 (s, 1H), 7.08-7.14 (m, 2H), 7.22 (d, J = 8.7 Hz, 1H), 7.30-7.33 (m, 1H), 7.40 (s, 1H), 7.51 (s, 1H), 8.05-8.07 (m, 2H), 8.24 (d, J = 8.5 Hz, 2H); ^{13}C NMR (400 MHz, CD_3OD) δ 14.4, 15.4, 24.6, 26.0, 30.8, 32.7, 33.8, 56.0, 78.7, 96.0 ,99.5, 110.1, 111.0, 111.4, 113.4, 116.4, 121.8, 127.7, 129.3, 129.4, 130.0, 130.7, 131.7, 133.4, 135.7, 136.9, 145.9, 156.8, 158.6, 169.9; HRMS (ESI+) calcd for $C_{30}H_{31}F_5N_3O_6S_2$ $[M+H]^+$ 688.1569, found XXX.XXXX (error X.X ppm).

Cyclopentyl (3-(4-(((4-(*tert*-butyl)phenyl)sulfonyl)carbamoyl)-2-methoxybenzyl)-1-methyl-1*H*-indol-5-yl)carbamate (31) (CHL-I-095)

The title compound was synthesized from 4-((5-(((cyclopentyloxy)carbonyl)amino)-1-methyl-1*H*-indol-3-yl)methyl)-3-methoxybenzoic acid (**24**) (CHL-I-072) (15.0 mg, 0.0355 mmol) and tertbutylsulfonamide (7.95 mg, 0.0373 mmol) using the General Procedure **F** (yield: TBD): R_f = 0.16 (80:20 hexanes/EtOAc); ^{1}H NMR (400 MHz, CD_3OD) δ 1.33 (s, 9H), 1.62-1.88 (m, 8H), 3.70 (s, 3H), 3.90 (s, 3H), 3.99 (s, 2H), 5.10-5.11 (m, 1H), 5.33-5.36 (s, 1H), 6.83 (s, 1H), 7.02 (d, J = 7.9 Hz, 1H), 7.15 (s, 1H), 7.21 (d, J = 8.6 Hz, 1H), 7.42-7.45 (m, 1H), 7.48-7.50 (m, 2H), 7.59 (s, 1H), 7.89-7.91 (m, 2H), 7.36 (d, J = 9.0 Hz, 1H), 7.52–7.54 (m, 2H), 8.08 (d, J = 8.9 Hz, 1H), 8.38 (s, 1H), 8.57 (s, 1H); ^{13}C NMR (400 MHz, CD_3OD) δ 14.4, 14.5, 23.7, 24.6, 25.9, 26.9, 28.1, 28.9, 30.3, 30.5, 30.7, 31.6, 32.7, 33.1, 33.8, 35.8, 36.5, 55.9, 62.1, 78.6, 110.0, 111.6, 122.0, 126.1, 128.2, 129.3, 130.1, 130.8, 134.4, 138.1, 142.5, 155.6, 158.1, 170.2; HRMS (ESI+) calcd for $C_{34}H_{40}N_3O_6S$ $[M+H]^+$ 618.2632, found XXX.XXXX (error X.X ppm).

4-((1-methyl-5-nitro-1*H*-indol-3-yl)methyl)-*N*-((4-(trifluoromethyl)phenyl)sulfonyl)benzamide (50) (CHL-II-024)

The title compound was synthesized from 4-((1-methyl-5-nitro-1*H*-indol-3-yl)methyl)benzoic acid (**47**) (CHL-II-022) (0.500 g, 1.62 mmol) and 4-(trifluoromethyl)benzenesulfonamide (0.383 g, 1.70 mmol) using the General Procedure **F** (yield: 40%): R_f = 0.50 (50:50 hexanes/EtOAc); ^{1}H NMR (400 MHz, CD_3OD) δ 3.75-3.78 (m, 3H), 7.13 (d, *J* = 6.5 Hz, 1H), 7.27-7.30 (m, 2H), 7.37-7.42 (m, 1H), 7.76-7.79 (m, 2H), 7.87 (d, *J* = 7.7 Hz, 2H), 7.97–8.02 (m, 1H), 8.17 (d, *J* = 8.2 Hz, 2H), 8.29-8.31 (m, 1H); ^{13}C NMR (400 MHz, CD_3OD) δ information TBD; HRMS (ESI+) calcd for $C_{24}H_{19}F_3N_3O_5S$ $[M+H]^+$ 518.0992, found XXX.XXXX (error X.X ppm).

Ethyl (3-(2-methoxy-4-(((4-(trifluoromethyl)phenyl)sulfonyl)carbamoyl)benzyl)-1-methyl-1*H*-indol-5-yl)carbamate (39) (CHL-I-114)

The title compound was synthesized from 4-((5-((ethoxycarbonyl)amino)-1-methyl-1H-indol-3-yl)methyl)-3-methoxybenzoic acid (CHL-I-037) (12.3 mg, 0.0322 mmol) and 4-(trifluoromethyl)benzene sulfonamide (7.61 mg, 0.0338 mmol) using the General Procedure **F** (yield: TBD): R_f = 0.13 (50:50 hexanes/EtOAc); ^{1}H NMR (400 MHz, CD_3OD) δ 1.30 (s, 5H), 3.70 (s, 3H), 3.89 (s, 2H), 3.99 (s, 2H), 6.84 (s, 1H), 7.03 (d, *J* = 7.8 Hz, 1H), 7.16 (s, 1H), 7.22 (d, *J* = 8.0 Hz, 1H), 7.44 (d, *J* = 8.4 Hz, 1H), 7.49 (s, 1H), 7.59 (s, 1H), 7.76 (d, *J* = 7.8 Hz, 2H), 8.14 (d, *J* = 8.1 Hz, 2H); ^{13}C NMR (400 MHz, CD_3OD) δ information TBD; HRMS (ESI+) calcd for $C_{28}H_{27}F_3N_3O_6S$ $[M+H]^+$ 590.1567, found XXX.XXXX (error X.X ppm).

***Tert*-butyl (3-(2-methoxy-4-(((4-(trifluoromethyl)phenyl)sulfonyl)carbamoyl)benzyl)-1-methyl-1*H*-indol-5-yl)carbamate (41) (CHL-I-115)**

The title compound was synthesized from 4-((5-((tert-butoxycarbonyl)amino)-1-methyl-1H-indol-3-yl)methyl)-3-methoxybenzoic acid (CHL-I-113) (20.4 mg, 0.0497 mmol) and 4-(trifluoromethyl)benzene sulfonamide (11.8 mg, 0.0522 mmol) using the General Procedure **F** (yield: TBD): R_f = 0.23 (50:50 hexanes/EtOAc); ^{1}H NMR (400 MHz, CD_3OD)

δ 1.45-1.53 (m, 9H), 3.70 (s, 3H), 3.90 (s, 3H), 3.99 (s, 2H), 6.8 (s, 1H), 7.03 (d, *J* = 7.8 Hz, 1H), 7.11 (d, *J* = 9.1 Hz, 1H), 7.20 (d, *J* = 8.7 Hz, 1H), 7.43-7.45 (m, 1H), 7.46 (s, 1H), 7.60 (s, 1H), 7.75 (d, *J* = 8.0 Hz, 2H), 8.14 (d, *J* = 8.0 Hz, 2H); ^{13}C NMR (400 MHz, CD_3OD) δ information TBD; HRMS (ESI+) calcd for $C_{30}H_{31}F_3N_3O_6S$ $[M+H]^+$ 618.1880, found XXX.XXXX (error X.X ppm).

2-methoxyethyl (3-(2-methoxy-4-(((4-(trifluoromethyl)phenyl)sulfonyl)carbamoyl)benzyl)-1-methyl-1*H*-indol-5-yl)carbamate (42) (CHL-I-124)

The title compound was synthesized from 3-methoxy-4-((5-(((2-methoxyethoxy)carbonyl)amino)-1-methyl-1H-indol-3-yl)methyl)benzoic acid (CHL-I-119) (12.8 mg, 0.0310 mmol) and 4-(trifluoromethyl)benzene sulfonamide (7.34 mg, 0.0326 mmol) using the General Procedure **F** (yield: TBD): R_f = 0.08 (50:50 hexanes/EtOAc); ^{1}H NMR (400 MHz, CD_3OD) δ 3.38 (s, 3H), 3.63 (s, 2H), 3.7 (s, 3H), 3.89 (s, 3H), 4.00 (s, 2H), 4.22-4.25 (m, 2H), 6.85 (s, 1H), 7.05 (d, *J* = 7.7 Hz, 1H), 7.14-7.16 (m, 1H), 7.22 (d, *J* = 8.4 Hz, 1H), 7.42 (d, *J* = 7.8 Hz, 1H), 7.50 (s, 1H), 7.56 (s, 1H), 7.78 (d, *J* = 8.0 Hz, 2H), 8.16 (d, *J* = 8.0 Hz, 2H); ^{13}C NMR (400 MHz, CD_3OD) δ information TBD; HRMS (ESI+) calcd for $C_{29}H_{29}F_3N_3O_7S$ $[M+H]^+$ 620.1673, found XXX.XXXX (error X.X ppm).

6.3.2. Cell culture

Human embryonic kidney cells 293 (HEK293, ATCC) were cultured in phenol red-free Dulbecco's Modified Eagle Medium (DMEM, Gibco) supplemented with 2 mM L-Glutamine (Invitrogen), heat-inactivated 10% fetal bovine serum (FBS HI, Gibco), 100 U/ml penicillin and 100 μg/ml streptomycin (Gibco). HAP1 wild-type and TNFR1 knockout cells (Horizon) were cultured in Iscove's Modified Dulbecco's Medium (IMDM, Gibco) supplemented with 10% FBS (Gibco), 100 U/ml penicillin and 100 μg/ml

streptomycin (Gibco). Cell cultures were maintained in an incubator with 5% CO_2 (Forma Series II Water Jacket CO_2 Incubator, Thermo Scientific) at 37 ºC. The HAP1 TNFR1 knockout cell line was edited by CRISPR/Cas to contain a 70 base pair (bp) insertion in a coding exon of TNFRSF1A. Sanger sequencing was performed as a quality control to confirm the knockout. The TNFR1ΔCD-FRET pair stable cell line was generated as described in our previous work and have been monitored continuously for over three years with expression maintaining above 95% characterized by flow cytometry (*190*).

6.3.3. NF-κB activation functional assay

Ligand stimulated or TRADD induced NF-κB activation assay with HEK293 cells and HAP1 cells (WT and TNFR1 KO) were carried out as described (*190, 270*). Briefly, the cells were transfected with firefly luciferase reporter genes and *Renilla* luciferase reporter genes for 48 hours. These cells were then dispensed into 96-well assay plates (30000 cells/well, total volume 50 μl) and incubated with drugs or DMSO (negative control) in the presence (0.1 μg/ml) and absence of LTα for 18 hours at 37 °C. Readings for luciferase activities were acquired as described in the dual glo luciferase kit protocol (Promega).

For TRADD-induced NF-κB activation in HEK293 cells, cells (1×10^6) in a 6-well plate were transfected with NF-κB firefly luciferase reporter genes, *Renilla* luciferase reporter genes, TRADD plasmid and control plasmid to give the same total DNA. In the control cells, the TRADD plasmid was replaced with control plasmid. After 3 hours of transfection, cells were harvested and plated (30,000 cells/well, total volume 50 μl) into 96-well white solid bottom assay plates (Greiner Bio-One North America). Drug treatments or DMSO (negative control) was performed 5 hours after cell plating. Luciferase activities were determined 24 hours after treatments as described in the

assay protocol.

6.3.4. Native gel characterization

To test the disruption of receptor-receptor interactions, purified soluble TNFR1 PLAD was assessed by Native-PAGE gels (Bio-Rad) in the absence and presence of hit compounds (200 μM) under non-reducing conditions followed by Coomassie staining. The overexpression and purification of the N-terminal FLAG-tagged TNFR1 PLAD (residues 30-82) were carried out as described previously and the soluble PLAD protein was shown to exist as dimers under native conditions (*190*).

6.3.5. FRET dose-response assay

These synthesized analogues were dissolved in DMSO to make 10 mM stock solution which were then subsequently serially diluted in 96-well mother plates to obtain eight doses at 50X concentrations. Hits were screened at eight different concentrations (0.01 to 100 μM or 0.1 to 200 μM). Compounds (1 μl) were transferred from the mother plates into assay plates using a Mosquito HV liquid handler (TTP Labtech Ltd.). On the day of conducting the assay, the stable cells expressing the TNFR1 FRET biosensor were harvested to check for expression. Stable cells were then dispensed into the drug plates containing the analogues (50,000 cells/well) and incubated with the compounds or DMSO as a negative control followed by fluorescence lifetime measurements. The fluorescence waveforms were acquired by a prototype fluorescence lifetime plate-reader (Fluorescence Innovations, Inc.) as described (*190*).

6.4. Results

6.4.1. Chemistry

The lead structure of zafirlukast can be split into three parts for SAR analysis: the central 3-benzylindole core and an aryl-sulfonamide moiety coupled to the acyl substitution on the benzyl group as well as a cyclopentyl carbamate domain at C-5 of the indole respectively (**Fig. 6.1B**). Based on the previous SAR studies conducted on zafirlukast, majority of the changes in the activity of the molecule primarily lies in the variation of the substituents of the sulfonamide and carbamate region of the molecule (*274-279*). With this, we elected to initially prepare two series of analogues with the replacement of aryl sulfonamide with methyl ester (R_1) or the replacement of the alicyclic carbamate (R_2) with nitro group to establish the importance of each domain in the compound activity in inhibiting TNFR1 signaling.

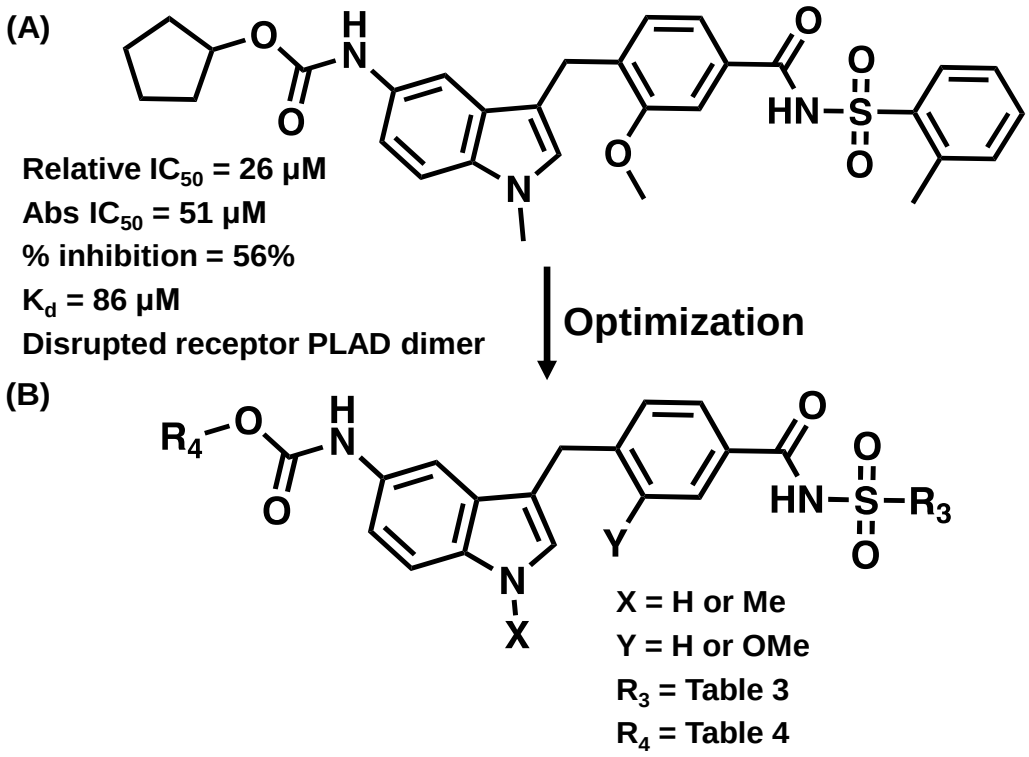

Figure 6. 1. Optimization of zafirlukast, a hit obtained from a FRET-based HTS.

(A) Structure of zafirlukast. (B) Zafirlukast scaffold for synthesis of analogues.

Following the synthesis steps from previous studies on zafirlukast (*274-279*), the indole nitrogen underwent alkylation in the presence of zinc bromide (**1**) followed by methylation to give (**2**). The nitro group was reduced to amine (**3**) and acylated to give the target carbamate compounds without the sulfonamide moiety (**4**-**11**) (R_1 in **Scheme 6.1**). On the other hand, the methyl ester of (**2**) was hydrolyzed to give the corresponding carboxylic acid (**12**) followed by reactions with sulfonamide with various substituents to give the target sulfonamide compounds without the carbamate domain (**13**-**23**) (R_2 in **Scheme 6.2**). In the above two series, we kept the truncated portion of the molecule stable by capping them with methyl ester and nitro group, though we note that

there is liability such as toxicity that associated with the nitro group (*280*). However, we clarify here that our primary goal is to examine if the carbamate domain is required for its inhibition mechanism and not directly for therapeutic purposes. We made analogues of the truncated series to assess preliminarily if the side group has a flat SAR (which may indicate that they are not worth further pursuing in designing subsequent analogues) or if they are indeed contributing to the inhibitory effects.

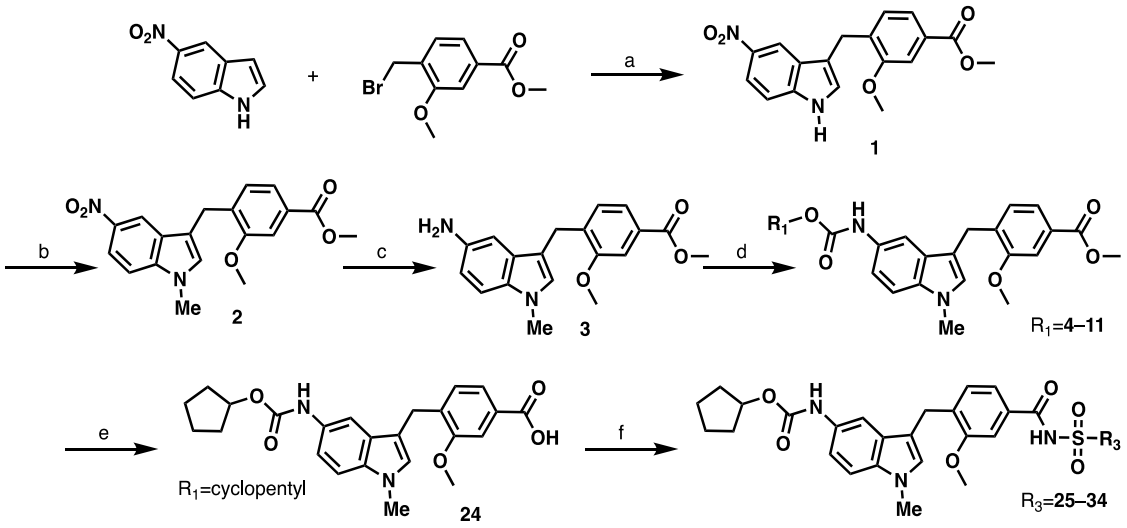

Scheme 6. 1. Variation of R_1 and R_3 groups of the initial zafirlukast structure.

Reagents and conditions: (a) ZnBr2, DIPEA, dioxane, RT, 40 hr, (b) NaH, MeI, THF, RT, 2 hr, (c) Pd/C, H_2, THF, RT, 16 hr, (d) Various chloroformates (R_1), Et_3N, DCM, 4C, 24 hr, (e) LiOH, THF/H_2O, RT, 20 hr, (f) Various sulfonamides (R_3), DMAP, EDC, DCM, RT, 24 hr.

As a result of the reduced percent inhibition and lack of inhibition mechanism of the sulfonamide truncated derivatives (**4-11**), we moved on to explore the importance of this sulfonamide moiety. We maintained the original cyclopentyl carbamate of zafirlukast (**4**) while the methyl benzoate was hydrolyzed to benzoic acid (**24**) and coupled with various sulfonamide substituents to provide the desired analogues (**25-34**) (R_3 in **Scheme 6.1**). We have adopted the strategy to probe the steric involvement of the aryl

sulfonamide by manipulating the position of methyl substituent on the phenyl along with increasing steric bulk as well as the electronegativity of the substituent at the para position. In addition, we tested the carbon tolerance of the compounds by increasing the size of the molecule. Furthermore, we also tested other heterocycles as compared to phenyl with the aim to reduce lipophilicity of the molecule.

On the other hand, carbamate truncated derivatives displayed weakened affinity, leading to our investigation on the significance of the carbamate domain while fixing the most potent 4-(trifluoromethyl)benezene sulfonamide (**28**). Analogue **28** underwent reduction to give amine (**35**) followed by coupling with carbamates with various substituents to afford **36-43** (R_4 in **Scheme 6.2**). We initially varied the size of the alicyclic ring between four to six members. We then built alkyl substituents with increasing branching from methyl to tert-butyl. Finally, we added oxygen to two of the derivatives, again with the goal to reduce the lipophilicity.

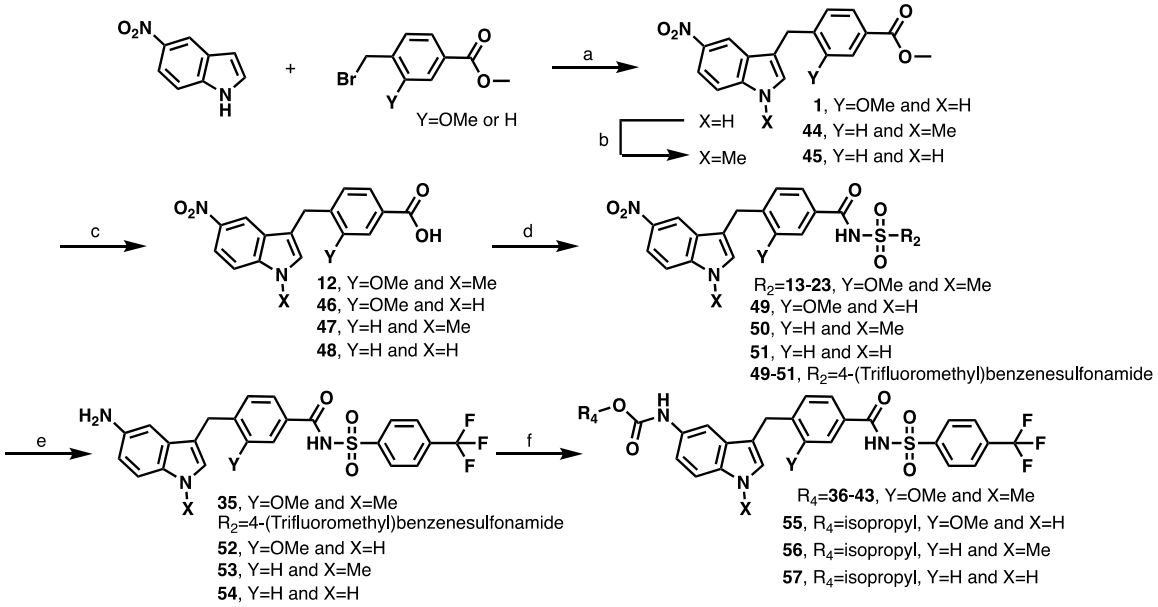

Scheme 6. 2. Variation of the R_2 and R_4 groups of the initial zafirlukast structure.

Reagents and conditions: (a) ZnBr2, DIPEA, dioxane, RT, 40 hr, (b) NaH, MeI, THF, RT, 2 hr, (c) LiOH, THF/H_2O, RT, 20 hr, (d) Various sulfonamides (R_2), DMAP, EDC, DCM, RT, 24 hr, (e) Pd/C, H_2, THF, RT, 16 hr, (f) Various chloroformates (R_4), Et_3N, DCM, 4C, 24 hr.

Currently, we are examining the importance of the substituents on the indole core as well as on the 3-benzyl group. Different intermediates (**44**-**54**) will be prepared with either methyl substituted on the nitrogen or free indole together with either methoxy substituted or free benzyl to couple with the optimized 4-(trifluoromethyl)benezene sulfonamide and the isopropyl carbamate to give the target compounds (**55-57**) (**Scheme 6.2**).

6.4.2. Cellular and biochemical assays to determine the biological activity of analogues

Compounds were evaluated for their potential to inhibit ligand stimulated TNFR1 induced NF-κB activation, both their half maximal effective concentration (IC_{50}) and percent inhibition, in HEK293 cells expressing endogenous TNFR1 which is a validated platform in testing the compounds (*190*). In addition, in order to determine if the compounds are specifically binding the receptor and exerting their functional effects, rather than inhibiting other proteins in the signaling pathways non-specifically, we also used a TNFR1 knockout (KO) HAP1 cell line established by CRISPR, together with the control HAP1 wild-type (WT) cell line (*270*). Furthermore, we tested the effect of compounds in TNFR1-associated death domain (TRADD)-induced NF-κB activation, independent of ligand activation of TNFR1, in HEK293 cells to eliminate non-specific effect in the intracellular signaling directly downstream of TNFR1 (*229, 270*). Once confirming the biological activity of the compounds, we then investigated their mechanism of action in disruption of receptor-receptor interactions by performing native

gels of PLAD with treatments of compounds (**Supplementary Fig. 6.1**) as well as testing their effect on the TNFR1 FRET biosensor (*190, 270*).

Replacement of the aryl sulfonamide in zafirlukast with methyl ester (**4**) significantly decreased percent inhibition and completely abolished the ability of the compounds in disrupting PLAD-PLAD interactions (**Table 6.1**). In addition, all other compounds in this R_1 series, which lack the sulfonamide domain (**5-11**) (**Table 6.1**), also did not show disruption of the dimeric PLAD, directly highlighting the importance of sulfonamide moiety in the inhibition mechanism of the compounds. Keeping the compounds as methyl benzoate, we then varied the carbamate domain to see if we can regain activity. We first switched cyclopentyl to phenyl derivatives (**5-6**) and both the potency and the percent inhibition were weakened. From phenyl, we included a methylene spacer to reduce rigidity by switching the molecule to contain a benzyl carbamate (**7**), which greatly increased the potency and the percent inhibition. However, this molecule did not tolerate larger substituents on the benzyl such as the nitro (**8**) or 9h-fluoren-9-ylmethyl (FMOC) group (**9**) as these molecules had very weak or no activity. Since a large substituent was not favorable, we further reduced the molecule size while keeping the flexibility in alkyl region by synthesizing the ethyl carbamate (**10**) which indeed illustrated the best activity in this series with both improved potency and activity. Finally, we tested a larger alkyl group with a tert-butyl carbamte (**11**) and the activity was reduced, suggesting that a small group is highly favorable at this position. However, we noted that the specificity of the molecule was significantly decreased with the removal of the sulfonamide domain, as shown through the inhibition of the basal NF-κB activation in the HAP1 TNFR1 KO cells, further confirming the importance of the sulfonamide group for TNFR1 specific targeting. Interestingly, the hydrolysis of **4** to benzoic acid (**24**) results in a strong TNFR1 specific activator (**Table 6.1**). This suggests

that the acid element, which contains a negative charge in physiologically condition, rather than the ester, is important for specificity. More importantly, the sulfonamide moiety behaves like a molecular switch in controlling receptor activation (when the molecule does not contain sulfonamide) or inhibition (when it contains a sulfonamide group that results in disruption of receptor-receptor interaction).

Table 6. 1. Alteration of R_1 carbamates on the sulfonamide truncated series.

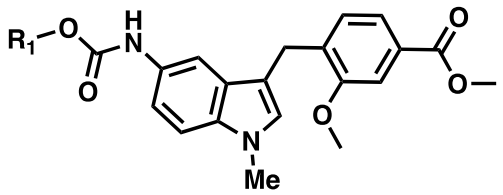

		HEK293 (Ligand induced NF-κB activation)		HAP1 WT (Ligand induced NF-κB activation)		HAP1 TNFR1 KO (Basal NF-κB activation)		HEK293 (TRADD) (TRADD induced NF-κB activation)		Disrupt dimeric PLAD
Cpd	R_1	IC_{50} (μM)	% red	IC_{50} (μM)	% red	IC_{50} (μM)	% red	IC_{50} (μM)	% red	Yes/No
4	Cyclopentyl	14	28	22	20	12	26	-	-	No
5	4-Methylphenyl	145	14	-	-	18	25	-	-	No
6	4-Chlorophenyl	148	47	-	-	125	45	-	-	No
7	Benzyl	8.2	66	-	-	6.8	60	-	-	No
8	4-Nitrobenzyl	127	21	-	-	>200	14	-	-	No
9	9H-Fluoren-9-ylmethyl	>200	0	-	-	>200	25	-	-	No
10	Ethyl	6.5	60	7.9	75	9.3	57	-	-	No
11	Tert-butyl	35	38	-	-	24	44	-	-	No
Compound with benzoic acid		EC_{50} (μM)	% act	EC_{50} (μM)	% act	EC_{50} (μM)	% act	EC_{50} (μM)	% act	Yes/No
24	Cyclopentyl	52	93	56	112	>200	0	-	-	No

The other portion of zafirlukast contains a cyclopentyl carbamate connected at the C-5 of the indole. Replacement of cyclopentyl carbamate with a nitro group (**13**) (**Table 6.2**) resulted in more than four-fold decrease in potency, as shown through the increase in IC_{50} from 25 to 114 μM while the percent inhibition remained similar and the molecule was still able to disrupt the dimeric PLAD. This provides a strong evidence that

the carbamate moiety is highly important in controlling the affinity and potency of the molecule. We followed by testing the effect of varying the sulfonamide domains in this carbamate truncated series (**14-23**) (**Table 6.2**). The compounds were synthesized with the sulfonamide domain containing 1) electron-withdrawing and donating substituents at the ortho, meta, and para positions, 2) varying sizes of substituents (from methyl to naphthyl), 3) different aromatic systems or heterocycles, and 4) N-alkylation of the sulfonamide. Removal of the ortho substituted methyl group or changing it to the meta or para position (**13-16**) resulted in nearly twice increase in the percent inhibition to near full inhibition, while the weak potency remained similar. This suggests that the ortho position may be subject to steric hindrance and hence preventing the inhibition capacity. Changing the para position to from methyl to chloro group (**17**) significantly increased the potency, indicating the need for large electronegative group at this position and the possibility in further improving the potency through changing the para substituent on the phenyl too. However, a larger naphthyl group (**18**) greatly reduced the potency while maintaining relatively high percent inhibition. Deviation from the phenyl group on the sulfonamide (**19-22**) with other heterocycles interestingly resulted in no disruption of PLAD-PLAD interactions and greatly reduced potency and percent inhibition, indicating that the phenyl group or the aromatic ring is highly responsible for the inhibition mechanism and compound activity. Finally, N-alkylation of the sulfonamide (**23**) completely abolished the compound activity, suggesting that the amino group of the sulfonamide is a bioisostere of the carboxylic acid and potentially mimic the negative charge. The compounds in this R_2 series, though illustrating some non-specificity, were in general relatively more specific than the compounds in the R_1 series, potentially due to the presence of the sulfonamide domain.

Table 6. 2. Alteration of R_2 sulfonamides on the carbamate truncated series.

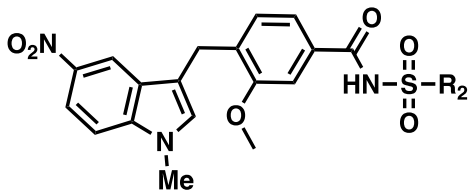

		HEK293 (Ligand induced NF-κB activation)		HAP1 WT (Ligand induced NF-κB activation)		HAP1 TNFR1 KO (Basal NF-κB activation)		HEK293 (TRADD) (TRADD induced NF-κB activation)		Disrupt dimeric PLAD
Cpd	R_2	IC_{50} (μM)	% red	IC_{50} (μM)	% red	Yes/No	% red	IC_{50} (μM)	% red	Yes/No
13	2-Methylphenyl	114	55	115	51	No	58	-	-	Yes
14	3-Methylphenyl	11	91.6	-	-	131	42	-	-	Yes
15	4-Methylphenyl	175	96	-	-	No	0	-	-	Yes
16	Phenyl	12	95	-	-	No	0	-	-	Yes
17	4-Chlorophenyl	86	94	102	90	No	73	-	-	Yes
18	2-Naphthyl	105	87	-	-	No	53	-	-	Yes
19	2-Thiophenyl	124	81	-	-	No	36	-	-	No
20	Methyl	>200	0	-	-	No	55	-	-	No
21	2-Pyridyl	>200	0	-	-	185	30	-	-	No
22	Cyclopropyl	111	41.4	-	-	159	41	-	-	No
23	N,2-dimethylbenzenesulfonamide	176	25	-	-	No	0	-	-	No

From the both truncated series, we observed both the importance of sulfonamide moiety in the inhibition activity and mechanism and the key role of the carbamate domain in determining the affinity of the molecule. Both groups are also important in compound specificity as the removal of either (**Table 6.1 or 6.2**) or both groups (**Supplementary Table 6.1**) greatly reduced the specificity of compound to TNFR1. With this, we synthesized two more series of analogues, first with variation in the sulfonamide group while keeping the cyclopentyl carbamate (R_3, **25-34**) (**Table 6.3**) followed by keeping the optimized sulfonamide side group with the best potency and activity and further changing the carbamate group to improve on the affinity and potency (R_4, **36-43**) (**Table 6.4**). Finally, we sought to combine the knowledge from both series and make further changes to the indole and/or the benzyl group (R_5, **55-57**) (**Table 6.5**) to potentially yield the best molecule.

Table 6. 3. Alteration of R_3 sulfonamides on the initial zafirlukast structure.

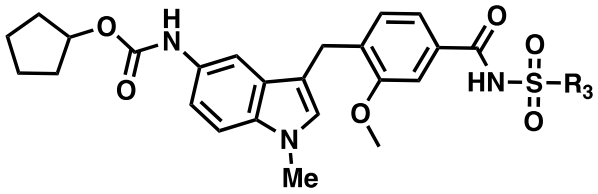

		HEK293 (Ligand induced NF-κB activation)		HAP1 WT (Ligand induced NF-κB activation)		HAP1 TNFR1 KO (Basal NF-κB activation)		HEK293 (TRADD) (TRADD induced NF-κB activation)		Disrupt dimeric PLAD
Cpd	R_3	IC_{50} (μM)	% red	IC_{50} (μM)	% red	Yes/No	% red	IC_{50} (μM)	% red	Yes/No
25	3-Methylphenyl	95	90	-	-	>100	30	>100	0	Yes
26	4-Methylphenyl	30	93	-	-	>50	65	>100	0	Yes
27	4-Chlorophenyl	14	96	-	-	36	54	>100	0	Yes
28	4-Trifluoromethylphenyl	5.2	95	4.9	92	>100	24	>100	38	Yes
29	4-Nitrilephenyl	81	94	-	-	>100	29	>100	0	Yes
30	4-Pentafluorosulfanyl	61	96	-	-	>100	53	>100	13	Yes
31	4-Tertbutylphenyl	120	55	-	-	>50	40	>100	0	Yes
32	4-Pyridyl	135	77	-	-	>50	55	>50	31	No
33	1,3-Dimethyl-1H-pyrazole	149	62	-	-	>100	0	>100	0	No
34	Morpholinyl	155	54	-	-	>100	0	>100	0	No

In the R_3 series of the sulfonamide analogues, we prepared a systematic set of sulfonamide analogues with only a single change from zafirlukast by keeping the cyclopentyl unchanged (**Table 6.3**). As suggested from the R_2 truncated series of compounds, we first changed the methyl substituent from the ortho to the mata position (**25**) which resulted in an expected increase in the percent inhibition (to full inhibition) at the expense of the potency (55 to 95 μM). Interestingly, further changing of the methyl substituent from meta to the para position (**26**) allowed the molecule to regain its potency (95 to 30 μM) while maintaining at full inhibition. As informed by the truncated series that an electronegative substitution such chloro group helps in improving the potency. Indeed, the 4-chlorobenzene group (**27**) further enhanced the potency by two-fold to 14.0 μM. We then further increased the electronegativity of the phenyl substituents by synthesizing a trifluoromethyl group at the para position (**28**) which resulted in another three-fold increase in the potency to 5.2 μM while still maintaining the full inhibition. We then tested the carbon tolerance of the molecule by expanding the size

of the molecule (**29-31**) which interestingly reduced the potency as well as the percent inhibition of the molecule, indicating that an optimized carbon number was achieved in **28**. To confirm the importance the phenyl group or aromatic ring on the sulfonamide domain in disrupting PLAD-PLAD interactions, we synthesized other heterocycles with pyridyl (**32**), pyrazole (**33**) and morpholinyl (**34**) groups attached to the sulfonamide and indeed they did not disrupt the dimeric PLAD and illustrated substantial decreased potency and activity. From this series, we obtained a 4-trifluoromethylphenyl group on the sulfonamide domain (**28**) with a five-fold improvement in the relative IC_{50} (26 to 5.2 μM) and a ten-fold improvement in the absolute IC_{50} (51 to 5.2 μM) with maximum percent inhibition. In addition, the electronegative substituent of trifluoromethyl made the negative charge on the amino group of the sulfonamide more negative charged. In terms of specificity, compound **28** is highly specific to TNFR1 as shown through the HAP1 TNFR1 KO cells. However, it appeared that the increase in potency comes at the expense of some non-specificity in the intracellular signaling pathway, though at high concentration (ten-fold greater than the IC_{50}) in the inhibition of TRADD-induced NF-κB activation. This suggests the need to further optimize the cyclopentyl carbamate portion of **28** to obtain better potency and specificity.

Table 6. 4. Alteration of R_4 carbamates on the initial zafirlukast structure.

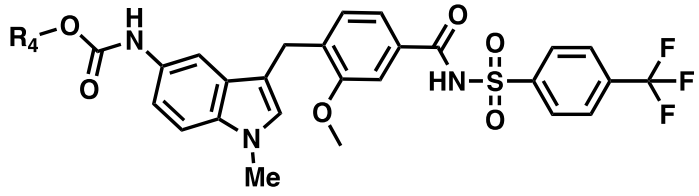

		HEK293 (Ligand induced NF-κB activation)		HAP1 WT (Ligand induced NF-κB activation)		HAP1 TNFR1 KO (Basal NF-κB activation)		HEK293 (TRADD) (TRADD induced NF-κB activation)		Disrupt dimeric PLAD
Cpd	R_4	IC_{50} (μM)	% red	IC_{50} (μM)	% red	IC_{50} (μM)	% red	IC_{50} (μM)	% red	Yes/No
36	Cyclobutyl	41	85	52	82	>100	0	>100	0	Yes
37	Cyclohexyl	36	95	22	88	>100	15	>100	0	Yes

38	Methyl	0.75	54	0.93	60	>100	0	>100	0	No
39	Ethyl	1.6	42	0.96	65	>100	0	>100	0	No
40	Isopropyl	0.86	92	0.72	94	>100	0	>100	0	Yes
41	Tert-butyl	4.5	37	3.4	38	>100	0	>100	0	No
42	Methoxyethyl	3.3	40	3.1	58	>100	0	>100	0	No
43	Tetrahydrofuran-3-yl	4.7	43	4.5	32	>100	0	>100	0	No

In order to further improve the potency and specificity of the molecule, we synthesized analogues with the optimized 4-trifluoromethylphenyl substituent on the sulfonamide moiety with varying carbamate domain (R_4, **36-43**) (**Table 6.4**). We first varied alicyclic substituent from cyclopentyl to cyclobutyl (**36**) or cyclohexyl (**37**). Both **36** and **37** showed a reduction in the potency or IC_{50} of the molecule while maintaining near full inhibition and disrupting dimeric PLAD. As suggested by the R_1 truncated series, an alkyl group may potentially help in improving the potency. We then synthesized four alkyl carbamates with increased branching, consisting of methyl (**38**), ethyl (**39**), isopropyl (**40**) and tert-butyl (**41**) substituents. Strikingly, we observed a significant improvement in the IC_{50} of the molecule from single-digit micromolar to submicromolar potency in **38**-**40**. However, **38** and **39** only exhibited partial inhibition (40-60% inhibition), potentially due to their lack of ability in disrupting PLAD-PLAD interactions. Compound **40** appeared as the best molecule with IC_{50} between the range of 0.72-0.86 μM and exhibited full inhibition with disruption of dimeric PLAD (**Fig. 6.2A**). Further increase in the size of the molecule to tert-butyl carbamate (**41**) reduced the potency back to single-digit micromolar and abolished the ability of the compound to disrupt dimeric PLAD, leading to partial inhibition. We also tested the addition of more polar oxygen atom to the compounds such as the methoxyethyl carbamate (**42**) or the tetrahydrofuran-3-yl carbamate (**43**) to reduce the lipophilicity of the compound but they resulted in weakened potency and percent inhibition respectively. In addition, all the analogues in this R_4 series, including **40**, illustrated very high specificity to TNFR1 as

there is no inhibition in both the basal level of NF-κB activation in the HAP1 TNFR1 KO cells (**Fig. 6.2B**) as well as the TRADD-induced NF-κB activation (**Fig. 6.2C**).

Table 6. 5. Alteration of R_5 3-benzylindole core on the initial zafirlukast structure.

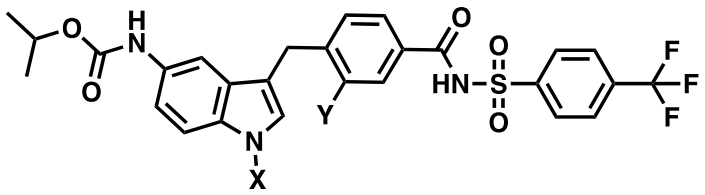

			HEK293 (Ligand induced NF-κB activation)		HAP1 WT (Ligand induced NF-κB activation)		HAP1 TNFR1 KO (Basal NF-κB activation)		HEK293 (TRADD) (TRADD induced NF-κB activation)		Disrupt dimeric PLAD
Cpd	X	Y	IC_{50} (μM)	% red	IC_{50} (μM)	% red	IC_{50} (μM)	% red	IC_{50} (μM)	% red	Yes/No
55	H	OMe	TBD	TBD	TBD	TBD	TBD	TBD	TBD	TBD	TBD
56	Me	H	TBD	TBD	TBD	TBD	TBD	TBD	TBD	TBD	TBD
57	H	H	TBD	TBD	TBD	TBD	TBD	TBD	TBD	TBD	TBD

To further confirm the inhibition mechanism quantitatively, we tested the potency of the analogues in disrupting receptor-receptor interactions by performing the fluorescence resonance energy transfer (FRET) experiments with the previously established TNFR1 FRET biosensor treated with compound **28** and **40** as well as zafirlukast. The FRET results showed that all compounds reduced FRET in the biosensor, confirming the disruption of receptor-receptor interactions. Importantly, both analogues **28** and **40** reduced FRET to a greater extent and with a better potency of 15 and 4.2 μM respectively as compared to 17 μM for zafirlukast (**Fig. 6.2D**). This observation is consistent with the functional effects of the compounds, thus confirming that these analogues are novel receptor-specific inhibitors of TNFR1 with enhanced potency and biological activity.

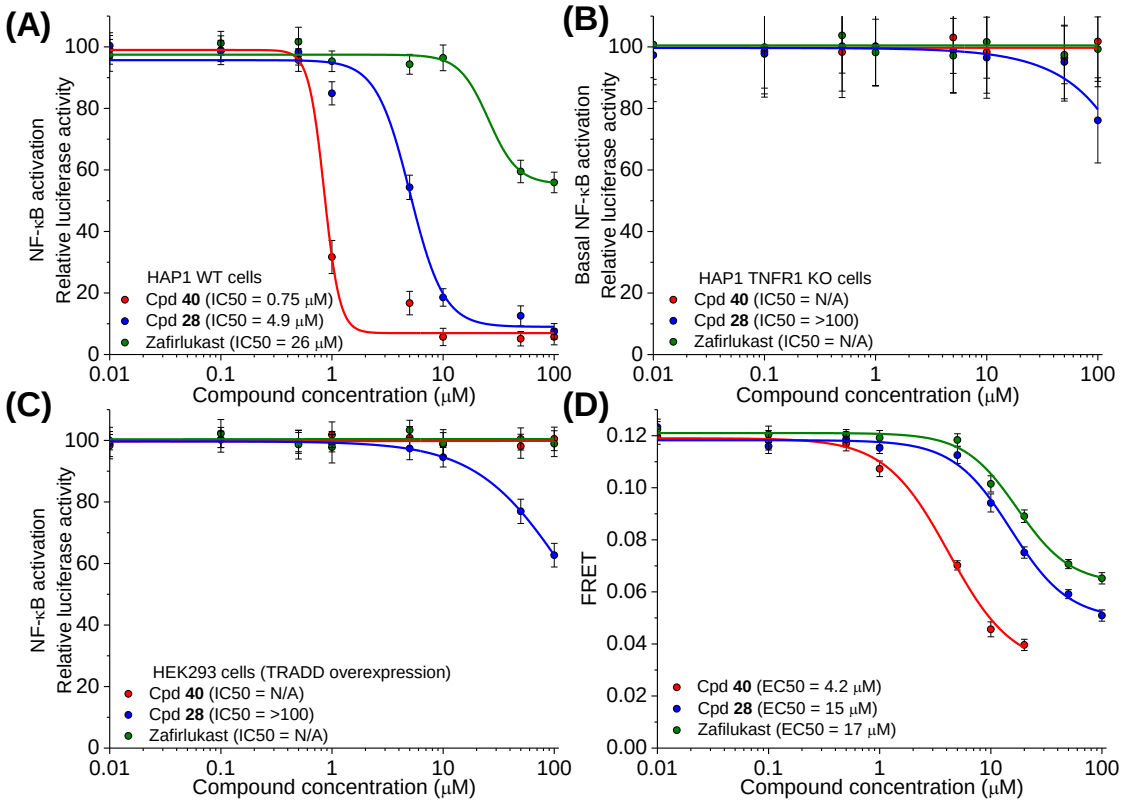

Figure 6. 2. Biological characterization of the best analogues (cpd 40 and 28) and zafirlukast.

Effect of compounds on NF-κB activation in (A) HAP1 WT cells, (B) HAP1 TNFR1 KO cells, (C) HEK293 cells with TRADD overexpression and (D) FRET measurements with TNFR1 FRET biosensors.

6.5. Conclusion

We synthesized a systematic series of 5-amino-3benzyl-1H-indole analogues based on a scaffold of zafirlukast obtained from a FRET-based HTS to discover inhibitors that disrupt TNFR1 receptor-receptor interaction. The SAR demonstrates that the carbamate moiety at C-5 of the indole plays a critical role in the binding affinity and the potency of the molecule. On the other hand, the sulfonamide domain coupled to the benzoic acid is important in the inhibition mechanism and the extent of inhibition. In

addition, both functional groups are required for compound specificity for TNFR1. We obtained an analogue with 4-(trifluoromethyl)benzene sulfonamide and isopropyl carbamate (**40**) that strongly inhibits ligand induced NF-κB activation with more than 60-fold improved potency (absolute IC_{50}) than the initial hit. In addition, compound **40** disrupts receptor-receptor interactions and reduces FRET in the FRET assay with enhanced potency as well as having high specificity to TNFR1. Synthesis of additional analogues with variation in the 3-benzylindole core (as proposed in R_5) may further improve the potency and efficacy of the molecule. We note here that the 4-(trifluoromethyl)benzene sulfonamide and isopropyl carbamate of our current best compound are novel structure (not found in existing literatures that study SAR of zafirlukast), making **40** a novel potent receptor-specific inhibitor of TNFR1 signaling. This new scaffold can increase the compound specificity to TNFR1 and further differentiating inhibitors between TNFR1 and other proteins (e.g. leukotriene receptor).

In addition, there is potential, though outside the scope of this study, to examine those compounds that did not act through disruption of PLAD-PLAD interactions (e.g. **38** and **39**). Some of these compounds that inhibited TNFR1 stimulated NF-κB activation may be allosteric inhibitors and further investigation may be able to understand the interplay between allostery and receptor dimerization. Furthermore, the identification of a receptor-specific activator (**24**) from subtle change in the initial hit suggests the potential in using these analogues as probe to understand TNFR1 activation in general, in addition to finding potent inhibitors. Further efforts will be required to test the pharmacological properties, metabolic stability and effects of the compounds in animal models of inflammation prior to pre-clinical assessment of this class of compounds.

6.6. Supplemental information

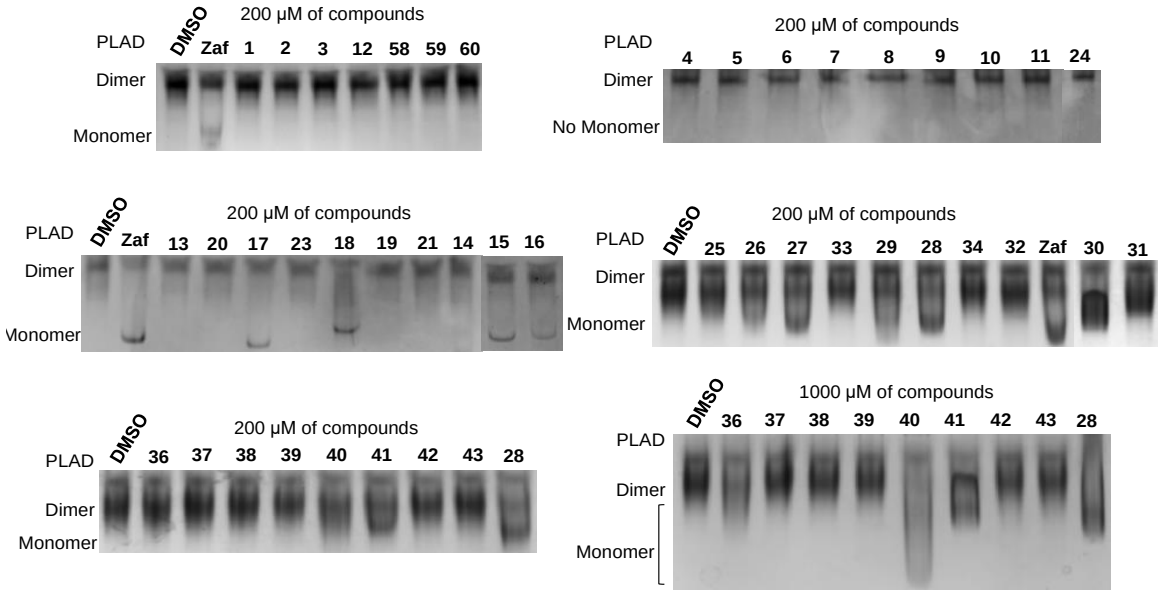

Supplemental Figure 6. 1. Native gel characterization of analogues.

Characterization of the ability of analogues R_1 (4-11 and 24), R_2 (13-23), R_3 (25-34) and R_4 (36-43) as well as R_x and R_y (1-3, 12 and 58-60) in disrupting TNFR1 PLAD-PLAD interactions.

Supplemental Table 6. 1. Alteration of side groups on the 3-benzylindole without the carbamate or sulfonamide domains.

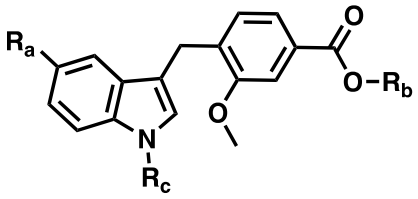

				HEK293 (Ligand induced NF-κB activation)		HAP1 WT (Ligand induced NF-κB activation)		HAP1 TNFR1 KO (Basal NF-κB activation)		HEK293 (TRADD) (TRADD induced NF-κB activation)		Disrupt dimeric PLAD
Cpd	R_a	R_b	R_c	IC_{50} (µM)	% red	IC_{50} (µM)	% red	IC_{50} (µM)	% red	IC_{50} (µM)	% red	Yes/No
2	NO_2	Me	Me	52	59	-	-	39	53	-	-	No
3	NH_2	Me	Me	120	62	-	-	>200	22	-	-	No
12	NO_2	H	Me	>200	33	-	-	>200	0	-	-	No
1	NO_2	Me	H	20	91	-	-	16	78	-	-	No
58	NH_2	Me	H	149	86	-	-	>150	43	-	-	No
59	NO_2	H	H	130	29	-	-	>200	39	-	-	No
60	NH_2	H	H	143	12	-	-	>150	13	-	-	No

CHAPTER 7: TARGETING THE ENSEMBLE OF HETEROGENEOUS TAU OLIGOMERS IN CELLS: A NOVEL SMALL MOLECULE SCREENING PLATFORM FOR TAUOPATHIES.

Adapted with permission from:

Chih Hung Lo[1], Colin Kin-Wye Lim[1], Zhipeng Ding[1], Sanjula P. Wickramasinghe[2], Anthony R. Braun[1], Karen H. Ashe[3,4,5,6], Elizabeth Rhoades[2,7], David D. Thomas[8,9] and Jonathan N. Sachs[1*]. Targeting the ensemble of heterogeneous tau oligomers in cells: A novel small molecule screening platform for tauopathies. *Alzheimer's & Dementias, THE JOURNAL OF THE ALZHEIMER'S ASSOCIATION*, 2019, Accepted, In Press.

[1]Department of Biomedical Engineering, University of Minnesota, Minneapolis, MN 55455

[2]Biochemistry and Molecular Biophysics Graduate Group, University of Pennsylvania, Philadelphia, PA 19104

[3]N. Bud Grossman Center for Memory Research and Care, University of Minnesota, Minneapolis, MN 55455

[4]Institute for Translational Neuroscience, University of Minnesota, Minneapolis, MN 55455

[5]Department of Neurology, University of Minnesota, Minneapolis, MN 55455

[6]Geriatric Research Education and Clinical Center, Veterans Affairs Medical Center, Minneapolis, MN 55417

[7]Department of Chemistry, University of Pennsylvania, Philadelphia, PA 19104

[8]Department of Biochemistry, Molecular Biology and Biophysics, University of Minnesota, Minneapolis, MN 55455

[9]Photonic Pharma LLC, Minneapolis, MN 55410

Author contributions: C.H.L. designed and conducted all the experiments. C.K.W.L. and Z.D. contributed to protein purification and assisted with cell-based assays and biochemical experiments. S.W. and E.R. performed and analyzed the single-molecule FRET experiment. D.D.T. provided expertise on FRET and HTS, and provided comments and edits to the manuscript. A.R.B. and K.H.A. provided comments and edits to the manuscript. C.H.L and J.N.S. wrote the manuscript.

7.1. Summary

Understanding the heterogeneous pathology in Alzheimer's disease (AD) and related tauopathies is one of the most urgent and fundamental challenges facing the discovery of novel disease modifying therapies. Through monitoring ensembles of toxic and non-toxic tau oligomers spontaneously formed in cells, our biosensor technology can identify tool compounds that modulate tau oligomer structure and toxicity, providing much needed insight into the nature and properties of toxic tau oligomers.

Background:

Tauopathies are a group of neurodegenerative disorders characterized by pathological aggregation of the microtubule binding protein tau. Recent studies suggest that tau oligomers are the primary toxic species in tauopathies.

New/Updated Hypothesis:

We hypothesize that tau biosensors capable of monitoring tau oligomer conformation are able to identify tool compounds that modulate the structure and conformation of these tau assemblies, providing key insight into the unique structural fingerprints of toxic tau oligomers. These fingerprints will provide gravely needed

biomarker profiles to improve staging of early tauopathy pathology as well as generate lead compounds for potential new therapeutics. Our time-resolved FRET (TR-FRET) biosensors provide us an exquisitely sensitive technique to monitor minute structural changes in monomer and oligomer conformation. In this proof-of-concept study, we identified a novel tool compound, MK-886, which directly binds tau, perturbs the conformation of toxic tau oligomers, and rescues tau induced cytotoxicity. Furthermore, we show that MK-886 alters the conformation of tau monomer at the proline-rich and microtubule binding regions, stabilizing an on-pathway oligomer.

Major Challenges for the Hypothesis:

Our approach monitors changes in the ensemble of assemblies that are spontaneously formed in cells but does not specifically isolate or enrich unique toxic tau species. However, TR-FRET does not provide high-resolution, atomic scale information, requiring additional experimental techniques to resolve the structural features stabilized by different tool compounds.

Linkage to Other Major Theories:

Our biosensor technology is broadly applicable to other areas of tauopathy therapeutic development. These biosensors can be readily modified for different isoforms of tau, specific post-translational modifications, as well as familial AD associated mutations. We are eager to explore tau interactions with chaperone proteins, monitor cross-reactivity with other intrinsically disordered proteins, and target seeded oligomer pathology.

Objective

This paper emphasizes the need for targeting the heterogeneous ensemble of toxic tau oligomers in Alzheimer's disease (AD) and other tauopathies based on emerging biosensor technology. We report on two novel cellular fluorescence resonance

energy transfer (FRET) biosensors that monitor tau oligomer and monomer conformations and can be used as a high-throughput screening (HTS) platform to identify novel tool compounds that modulate tau oligomer conformations, thereby attenuating their toxicity. With our biosensors and HTS platform we are poised to (1) study the conformational ensemble of tau oligomers; (2) identify novel tool compounds capable of targeting tau species, both monomer and oligomer, to disrupt oligomer formation or stabilize different tau conformations; (3) develop a biophysical fingerprint that delineates toxic and non-toxic oligomers, allowing us to better stage tau pathology, improve biomarker development, and reduce the heterogeneity present in clinical trials; and (4) provide a novel therapeutic pipeline to identify lead compounds that target spontaneously formed, early-stage oligomers, instead of late-stage neurofibrillary tangles (NFTs).

7.2. Introduction

Historical evolution

Tauopathies, including AD, are a group of neurodegenerative disorders characterized by the presence of tau inclusions in affected brain regions (*69*). Despite decades of rigorous and focused research, there are currently no significant disease modifying therapies for AD or related tauopathies (*96*). Furthermore, there is a dearth of compounds that target tau, with only five out of the 105 small molecules currently in clinical trials being tau-focused (*97, 98*). Hence, there is desperate need for technologies that enable the identification of tau-focused disease-modifying therapies (*98-100*).

Tau is an intrinsically disordered protein (IDP) that plays an important role in the regulation of microtubule stability and axonal transport (*68*). Under pathological conditions, tau is hyperphosphorylated and detaches from microtubules, accumulating in

the cytosol (*70*). These pathological conditions have been correlated with upstream mitochondrial dysfunctions in the Krebs cycle and/or the electron transport system, oxidative stress (*71, 72*), as well as defects in neuron morphology and axonal transport (*73*). Unbound tau can misfold, initiating the tau fibrillogenesis cascade with an initial formation of tau oligomers that subsequently nucleate into paired helical filaments (PHFs), and eventually intracellular NFTs (**Fig. 7.1**) (*74*). NFTs have been the primary histopathological hallmark of tauopathies, with their presence in the brain showing significant correlation with the degree of cognitive impairment (*75*). However, recent studies suggest that these large insoluble NFTs are not the principle toxic species, implicating soluble oligomeric tau—intermediate tau assemblies formed prior to PHFs—in the induction of neurodegeneration (*78, 83*). Tau oligomers promote cytotoxicity in vitro and are linked to neurodegeneration and cognitive phenotypes in vivo (*76-82*). They exist as an ensemble of distinct assemblies which include both toxic and non-toxic, on- and off-pathway species along the fibrillogenesis cascade (**Fig. 7.1**) (*87-93*). Critically, no specific toxic tau oligomer species has been isolated or identified to date (*86, 94, 95*).

Rationale

Recent efforts to target toxic tau oligomers have yielded compounds with low micromolar IC_{50} (*137-143*). Of these small molecules, only methylene blue advanced to phase III clinical trials, albeit with unsuccessful results (*144*). One commonality among these molecules is that they were initially identified using in vitro purified protein assays (*137-143*). These systems do not recapitulate the cellular environment, lacking the numerous chaperone proteins that may be required to produce the ensemble of tau oligomers that populate the fibrillogenesis cascade. Additionally, purified protein assays are only capable of identifying hits that directly perturb tau and are wholly naive against indirect mechanism of action (MOA). Furthermore, many of the small molecules

discovered in purified protein assays disrupted both fibrils and tau oligomers, the former having recently been suggested to be potentially inert and neuroprotective (*281*). Therapeutic development for tauopathies has thus begun to shift from targeting large fibrillar aggregates to inhibiting or disrupting the formation of these toxic tau oligomers (*83-86*). The complex heterogeneity of tau oligomers likely requires the cellular environment (e.g. post-translational modifications (PTM) and chaperone proteins) to produce the ensemble of toxic and non-toxic tau assemblies. Hence, a cellular biosensor approach capable of monitoring this ensemble holds promise as a novel HTS platform to discover more effective therapeutics.

Building upon the groundbreaking biosensors developed by the Diamond group (which were engineered to detect pathogenic species in patient biofluids as a biomarker for AD diagnosis) (*282*), we have developed a technology platform that directly monitors spontaneous tau oligomerization in cells, enabling therapeutic targeting of early-stage tau pathology. Our robust assay can be easily modified to accommodate additional tauopathy cell models and new pathological phenotypes as they continue to be elucidated. Through our approach we will develop two unique classes of tool compounds, direct tau binders and indirect tau effectors (modifying tau oligomers through orthogonal pathways). The interplay between direct and indirect MOA and corresponding changes to tau oligomer conformations and toxicity will provide much needed insight into tau pathology.

We engineered two distinct FRET biosensors to monitor tau oligomerization. These biosensors were used for HTS of the NIH Clinical Collection (NCC) library using our state-of-the-art fluorescence lifetime plate reader (FLT-PR) (*283*). Fluorescence lifetime (FLT) detection increases the precision of FRET-based screening by a factor of 30 compared with conventional fluorescence intensity detection (*284*), and provides

exquisite sensitivity to resolve minute structural changes within protein ensembles. This sensitivity allows direct detection of conformational changes within an ensemble of oligomers (e.g. conversion from toxic to non-toxic oligomers), the dissociation of oligomers, or even changes in monomer conformations (*190, 226, 270*). The FRET biosensors express full-length 2N4R wild-type (WT) tau and fluorescent protein fusion constructs in living cells, allowing us to monitor *inter*-molecular or *intra*-molecular tau interactions. Using full-length 2N4R WT tau ensures the targeting of spontaneously formed ensembles of tau oligomers, not fibrils, as the 2N4R isoform of WT tau does not fibrillize without seeding (*285-288*).

After first establishing that the new technology platform specifically monitors tau oligomer formation (using known tau aggregators), we identified a small molecule, MK-886, that directly binds tau and strongly attenuates FRET with an EC_{50} of 1.40 μM in our HTS HEK293 cells (and a FRET EC_{50} of 1.06 μM in SH-SY5Y cells). The compound rescues tau induced cell cytotoxicity with an IC_{50} of 0.523 μM. To elucidate the MOA, we used an advanced single-molecule FRET (smFRET) technique to show that MK-886 perturbs the folding of purified, monomeric tau in the proline-rich and microtubule-binding regions. This effect is recapitulated in our cellular *intra*-molecular FRET biosensor and indicates an unfolding of the two termini of tau.

To further explore MK-886's MOA we employed a heparin induced thioflavin-T (ThT) aggregation assay with purified tau. MK-886 reduces the lag phase of tau fibrillization and is unable to nucleate tau fibrillization without the presence of heparin. It has been shown that overexpression of P301L tau does not induce fibril formation in SH-SY5Y cells (*288*), suggesting that P301L tau induced toxicity is due to toxic oligomer. Because MK-886 rescues tau induced cytotoxicity while not fully ablating tau oligomer associated FRET, we hypothesize that the rescue of P301L tau induced cytotoxicity by

MK-886 is through conversion of toxic tau oligomers into non-toxic oligomers. Whether these new oligomers are on- or off-pathway species is difficult to determine in our cellular system, without the use of inducers. Thus, the rescue of P301L tau induced toxicity could be through an accelerated conversion of toxic tau oligomers into neuroprotective fibrils. Nevertheless, our new technology is well suited to identify novel compounds capable of remodeling tau oligomers and rescuing tau induced cytotoxicity.

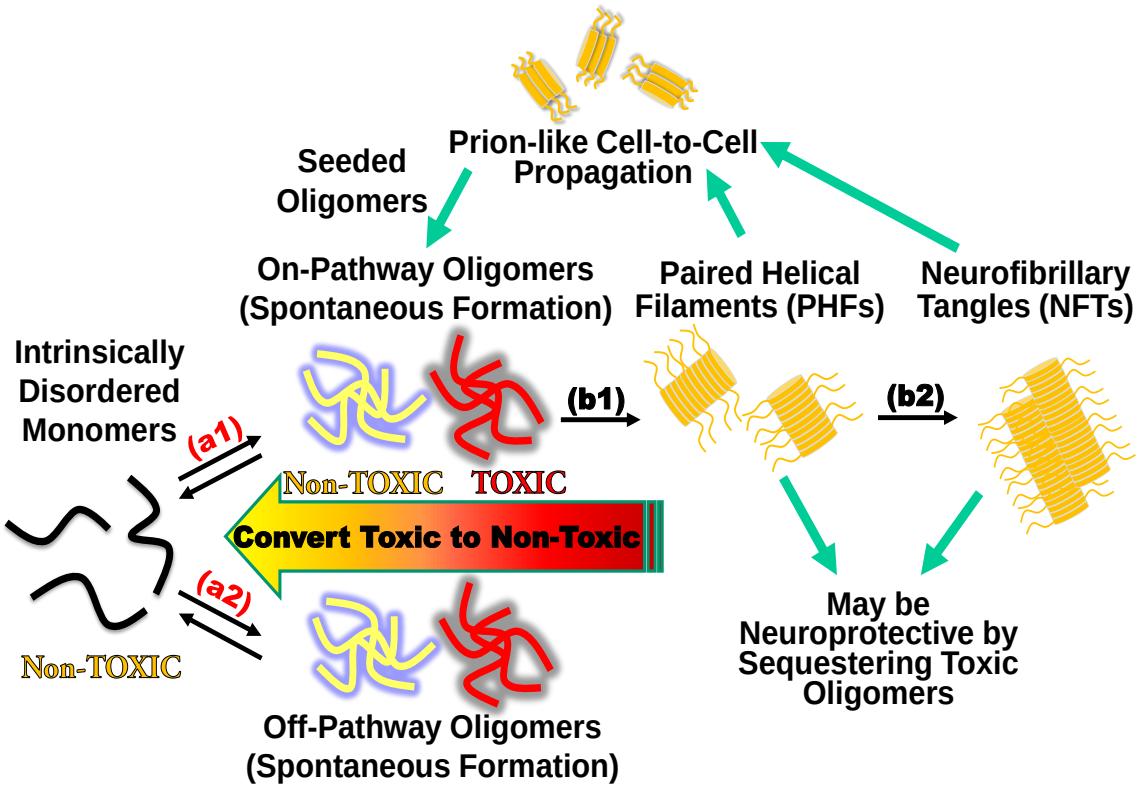

Figure 7. 1. Tau fibrillogenesis cascade for tauopathies and Alzheimer's disease (AD).

The intrinsically disordered tau monomer is capable of misfolding into spontaneously formed oligomers, producing toxic assemblies implicated in AD (arrows a1 and a2). While oligomers are metastable and difficult to monitor with high precision and accuracy, the large assemblies (paired helical filaments (PHFs) and neurofibrillary tangles (NFTs), arrows b1 and b2) form irreversibly with β-sheet structures. The fibrillar species can be excreted via exosomes leading to a prion-like

cell-to-cell propagation of pathology and may induce seeded oligomerization. NFTs may be neuroprotective by sequestering toxic oligomers and disruption of NFTs may induce toxicity from elevated concentrations of toxic oligomers. Our cellular time-resolved fluorescence resonance energy transfer (FRET) biosensors target reversible spontaneous oligomerization (a1 and a2), while also monitoring seeded aggregation and downstream processes such as fibrillization (b1 and b2) with high sensitivity.

New or updated hypothesis

Updated hypothesis: We hypothesize that the spontaneously formed ensemble of tau oligomers includes early-stage toxic tau species and by resolving conformational differences between toxic and non-toxic oligomers, we can target toxic tau assemblies, thereby rescuing tau induced pathology. Small-molecule modulation of tau conformations can be correlated with changes in the FRET signal as well as tau induced cytotoxicity. Lastly, through investigating tau oligomerization in the cellular environment, we include other protein machineries (e.g. chaperone proteins) which may play significant roles in tau pathogenesis.

7.3. Materials and methods

7.3.1. Molecular biology

To generate tau-GFP and tau-RFP, cDNA encoding full-length 2N4R tau (441 amino acids) was fused to the N-terminus of EGFP and TagRFP vectors. The P301L mutation was introduced by QuikChange mutagenesis (Agilent Technologies, Santa Clara, CA) and sequenced for confirmation. The GFP-tau-RFP was generated by fusing the N-terminal of tau to the C-terminus of GFP and the C-terminus of tau to the N-terminus of RFP. All constructs contain the monomeric mutation A206K to prevent constitutive fluorophore clustering (*204*).

7.3.2. Cell culture and generation of stable cell lines

HEK293 and SH-SY5Y cells (ATCC) were cultured in phenol red-free Dulbecco's Modified Eagle Medium (DMEM, Gibco) supplemented with 2 mM L-Glutamine (Invitrogen), heat-inactivated 10% fetal bovine serum (FBS HI, Gibco), 100 U/ml penicillin and 100 μg/ml streptomycin (Gibco). Cell cultures were maintained in an incubator with 5% CO_2 (Forma Series II Water Jacket CO_2 Incubator, Thermo Scientific) at 37 ºC. Both the WT and P301L tau *inter*-molecular FRET biosensor were generated by transiently transfecting HEK293 cells using Lipofectamine 3000 (Invitrogen) with WT or P301L tau-GFP and tau-RFP (1:20 DNA plasmid concentration ratio). The effectiveness of HEK293 cells transfected with FRET constructs as a HTS platform has been demonstrated in our previous work (*190, 226*). P301L tau *inter*-molecular FRET biosensor was also transiently expressed in SH-SY5Y cells using Lipofectamine 3000 (Invitrogen). To generate stable cell lines expressing GFP-tau-RFP or tau-GFP only, HEK293 cells were transiently transfected using Lipofectamine 3000 with GFP-tau-RFP or tau-GFP DNA plasmids. Transiently transfected cells were treated with G418 (Enzo Life Sciences, Farmingdale, NY) to eliminate non-expressing cells. Stable cell lines expressing GFP-tau-RFP or tau-GFP with the largest population of expressing cells were selected by fluorescence microscopy. The GFP-linker-RFP (linker contains 32 amino acids, GFP-32AA-RFP) control stable cell line was generated as described previously (*289*). The control cells expressing only free soluble fluorophores (GFP or RFP only) were generated by transiently transfecting HEK293 cells using Lipofectamine 3000 with plasmids containing GFP or RFP DNAs at the same plasmid concentration as the *inter*-molecular tau FRET biosensor.

7.3.3. Pilot screening with NIH clinical collection (NCC) library

The NIH Clinical Collection (NCC) library, containing 727 compounds, was purchased from Evotec (Hamburg, Germany), formatted into 96-well mother plates using an FX liquid dispenser, and formatted across three 384-well plates at 50 nL (10 μM final concentration/well) using an Echo liquid dispenser. DMSO (matching %v/v) was loaded as in-plate no-compound negative controls to make a total of 960 wells. The 384-well flat, black-bottom polypropylene plates (PN 781209, Greiner Bio-One) were selected as the assay plates for their low autofluorescence and low interwell cross talk. The plates were sealed and stored at −20 °C until use. Two days prior to screening, HEK293 cells were transfected using Lipofectamine 3000 with WT tau-GFP/RFP (WT tau FRET biosensor) in 15 x 100 mm plates (5 x 10^6 cells/plate) and the stable tau-GFP cell line (donor-only control) was expanded in five 225 cm^2 flasks. On each day of screening, the compound plates were equilibrated to room temperature (25 °C). The cells were harvested from the 100 mm plates by incubating with TrypLE (Invitrogen) for 5 min, washed three times in PBS by centrifugation at 300 g and filtered using 70 μm cell strainers (BD Falcon). Cell viability, assessed using a trypan blue assay, was >95%. Cells were diluted to 1 million cells/ml using an automated cell counter (Countess, Invitrogen). Expression of tau-GFP and tau-GFP/RFP (tau FRET biosensor) was confirmed by fluorescence microscopy prior to each screen. After resuspension and dilution in PBS, the biosensor cells were constantly and gently stirred using a magnetic stir bar at room temperature, keeping the cells in suspension and evenly distributed to avoid clumping. During screening, cells (50 μl/well) were dispensed by a Multidrop Combi Reagent Dispenser (Thermo Fisher Scientific) into the 384-well assay plates containing the compounds and allowed to incubate at room temperature for 2 hours before readings were taken by the fluorescence lifetime plate reader (Fluorescence

Innovations, Inc) as described previously (*190, 226*).

7.3.4. HTS and fluorescence lifetime data analysis

As described previously (*190, 226*), time-resolved fluorescence waveforms for each well were fit with single-exponential decays using least-squares minimization global analysis software to give donor-acceptor lifetime (τ_{DA}) and donor-only lifetime (τ_D). FRET efficiency (*E*) was then calculated based on Equation 1.

$$E = 1 - \left(\frac{\tau_{DA}}{\tau_D}\right) \; Eq.1$$

Assay quality was determined with the lead compound (MK-886) as positive control and DMSO as a negative control and calculated based on Equation 2 (*192*),

$$Z' = \; 1 - \frac{3(\sigma_p + \sigma_n)}{|\mu_p - \mu_n|} \; Eq.2$$

where σ_p and σ_n are the standard deviations (SD) of the observed τ_{DA} values, and μ_p and μ_n are the mean τ_{DA} values of the positive and negative controls. To make this metric less sensitive to strong outliers, we utilized the normalized median absolute deviation (1.4826*MAD) and median in place of the standard deviation and mean, respectively (*193*).

Fluorescent compounds were flagged as potential false positives due to interference from compound fluorescence by a set of stringent fluorescent compound filters based on analysis of the spectral waveforms of each well from the NCC screen (*190, 226*). After removal of fluorescent compounds, a histogram of the FRET distribution from all compounds in the screen was plotted and fit to a Gaussian curve to obtain the mean (μ) and standard deviation (σ, SD). A hit was defined as a compound that decreased the FRET efficiency by more than five times the standard deviation (5SD) relative to the mean μ. Five reproducible hits, MK-886 (Cayman Chemical), Benzbromarone (Millipore

Sigma), Bumetanide (Millipore Sigma), Torsemide (Millipore Sigma) and Triclosan (Millipore Sigma) were purchased.

7.3.5. Protein purification

Full-length 2N4R WT tau proteins were purified from *E. coli* using previously published protocols (*290*). Full-length tau was expressed with a cleavable His-tag. After elution from a nickel column, cleavage of the His-tag was achieved by incubation with tobacco etch virus (TEV) protease at room temperature for at least 4 hours, followed by passing through the His-tag column again to separate cleaved and uncleaved protein and remove the TEV. Final purification was performed by size-exclusion chromatography and the purity of the proteins was assessed by 4%–15% SDS-PAGE gels (Bio-Rad) under reducing conditions, followed by Coomassie staining. Fractions of pure proteins from the gels were pooled together and the protein stock concentrations were measured using the BCA assay (Thermo Fisher Scientific). Full-length 2N4R P301L tau protein was purchased (rPeptide).

7.3.6. Surface plasmon resonance (SPR) binding assay

Binding affinity between full-length 2N4R WT or P301L tau and the hit compounds were determined by SPR analysis using BIAcore S200. Recombinant tau proteins were immobilized on the CM5 sensor chip (Biacore, GE Healthcare) via amine coupling. Briefly, the dextran surface was activated with a 1:1 mixture of 0.4 M 1-ethyl-3-(3-dimethylaminopropyl)carbodiimide hydrochloride and 0.1 M N-hydroxysuccinimide. WT or P301L tau proteins (20 μg/ml) in 10 mM sodium acetate at pH 3.5-4.0 were flowed past a working surface before blocking the remaining activated carboxymethyl groups with 1 M ethanolamine at pH 8.5 to achieve a level of 1200 RU suitable for binding analysis. The reference surface was activated and reacted with only

ethanolamine.

For direct binding assays to the tau proteins, hit compounds at eight different concentrations (1 nM to 5 μM), as well as DMSO-only controls, were prepared in HEPES-EP containing a total of 2% DMSO. The samples were injected over both the reference and tau immobilized surfaces at 10 μl/min for 180 seconds and dissociated in glycine-HCl pH 2.5. All the samples, along with blanks from buffer and DMSO-only controls, were measured on a 96-well microplate (Biacore, GE Healthcare) at 25 °C. Reflectivity response data points were extracted from response curves at 5 seconds prior to the end of the injection to determine steady-state binding. All the data were double referenced with blanks using standard procedures with Biacore S200 Evaluation Software v1.0.

7.3.7. FRET dose-response assay

MK-886, which shows direct binding to tau proteins and the strongest change in FRET, was tested in a FRET dose-response assay. The compound was dissolved in DMSO to make a 10 mM stock solution, which was serially diluted in 96-well mother plates. MK-886 was screened at different concentrations (1 nM to 10 μM). Compound (1 μl) was transferred from the mother plates into assay plates using a Mosquito HV liquid handler (TTP Labtech Ltd, UK). Three days prior to conducting the assays, the stable GFP-tau-RFP cells and GFP-32AA-RFP control cells were expanded in two 225 cm^2 flasks (Corning). The preparations for WT or P301L tau-GFP/RFP FRET biosensors and the soluble GFP/RFP controls cells were carried out similar as above.

7.3.8. Cell cytotoxicity assay

Cell cytotoxicity was measured using the CytoTox-Glo (Promega Corporation) luminescence assay kit. SH-SY5Y human neuroblastoma cells were plated at a density

of 1 x 10^6 cells/well in a 6-well plate (Corning) and transfected with unlabeled full-length 2N4R P301L tau or equivalent vector-only control for 24 hours. The transfected cells were then plated at a density of 10000 cells/well in white solid 96-well plate (Corning) with a total volume of 100 μl, followed by treatment with MK-886 at eight different concentrations (1 nM to 2 μM), as well as DMSO-only controls, for another 72 hours. After incubation, 50 μl of CytoTox-Glo Cytotoxicity Assay Reagent was added to all wells followed by mixing by orbital shaking and incubation for 15 minutes at room temperature. The first luminescence reading was measured using a Cytation3 Cell Imaging Multi-Mode Reader luminometer (BioTek). 50 μl of Lysis Reagent with 1% Triton X-100 was then added, followed by incubation at room temperature for 15 min, and luminescence was measured again using the luminometer. Cell cytotoxicity was calculated following the manufacturer protocol. Effect of MK-886 on the suppressors of inhibitors of apoptosis (IAPs) (YM-155 and UC-112) was tested with untransfected SH-SY5Y cells plated in white solid 96-well plate with treatment of YM-155 (1 μM) or UC-112 (1 μM) in the absence or presence of MK-886 (0.5, 1 or 2 μM).

7.3.9. Western blot analysis

To test the expression of tau FRET biosensors, HEK293 cells were plated in a 100 mm plate at a density of 5 x 10^6 cells/plate and transfected with tau-GFP/RFP (tau FRET biosensor) plasmid. To test the clearance and phosphorylation state of tau in the cytotoxicity assay, SH-SY5Y cells were plated in a six-well plate at a density of 1 x 10^6 cells/well and transfected with unlabeled P301L tau plasmid for 24 hours followed by treatment of MK-886 (2 μM) for 72 hours. In both cases, cells were lysed for 30 minutes on ice with radioimmunoprecipitation assay (RIPA) lysis buffer (Pierce RIPA buffer, Thermo Fisher Scientific) containing 1% protease inhibitor (Clontech, Mountain View,

CA) and 1% phosphatase inhibitors (Millipore Sigma), and centrifuged at 15,000 g at 4 °C for 15 min. The total protein concentration of lysates was determined by bicinchoninic acid (BCA) assay (Pierce), and equal amounts of total protein (60 µg) were mixed with 4× Bio-Rad sample buffer and loaded onto 4%–15% Trisglycine sodium dodecyl sulfate–polyacrylamide gel electrophoresis (SDS-PAGE) gels (Bio-Rad, Hercules, CA). Proteins were transferred to polyvinylidene fluoride (PVDF) membrane (Immobilon-FL, EMD Millipore, Billerica, MA) and probed using antibodies against tau (Tau-5, Thermo Fisher Scientific) or antibody specific to Serine 396 of tau (Phospho-Tau S396, Thermo Fisher Scientific) with β-actin (ab8227, Abcam, Cambridge, MA) used as loading control. Blots were quantified on the Odyssey scanner (LI-COR Biosciences, Lincoln, NE).

7.3.10. Protein labelling and single-molecule FRET (smFRET) measurements

For site-specific labeling with maleimide-reactive fluorophores, cysteine residues were introduced using QuikChange Site-Directed Mutagenesis (Stratagene). Naturally occurring cysteines were mutated to serines. Labelling positions were selected to roughly mark the boundaries of the N-terminal domain or the proline-rich and microtubule-binding region of tau. Tau protein was purified as described above and labeled immediately following purification following published protocols (*290*). Briefly, the protein (typically 200 µL of ~100 µM protein) was incubated with 1 mM DTT for 30 minutes at room temperature followed by exchange into labeling buffer (20 mM Tris pH 7.4, 50 mM NaCl, and 6 M guanidine HCl) to remove DTT. The protein was incubated with the donor fluorophore, Alexa Fluor 488 maleimide (Invitrogen), at a protein to dye ratio of 2:1 at room temperature for one hour with stirring. The acceptor dye, Alexa Fluor 594 maleimide (Invitrogen), was added at a 5-fold molar excess and incubated overnight at 4°C with stirring. Excess dye was then removed by buffer-exchanging the labeled

solution into 20 mM Tris (pH 7.4) and 50 mM NaCl buffer using Amicon concentrators (Millipore) and then passed over two coupled HiTrap Desalting Columns (GE Life Sciences).

Single-molecule FRET measurements were carried out using ~30 pM of labelled tau in phosphate buffer (40 mM potassium phosphate, 50 mM KCl, pH 7.4) in 8-chambered Nunc coverslips (ThermoFisher) passivated with poly(ethylene glycol) poly(L-lysine) (PEG-PLL) to reduce protein adsorption to the chambers. Control measurements included DMSO to match the concentration in samples containing MK-886. Measurements were made on a MicroTime 200 time-resolved confocal microscope (Picoquant) in pulsed interleaved excitation FRET (PIE-FRET) mode. Laser power from 485 and 561 nm lasers, operated at 40 MHz pulse rate, was adjusted to ~30 µW before sample illumination. Fluorescence emission was collected through the objective and passed through a 150 µm diameter pinhole. Photons were separated by an HQ585LP dichroic in combination with ET525/50M and HQ600LP filters and detected by avalanche photodiodes. Photon traces were collected in 1 ms time bins for one hour. A cutoff of 25 counts/ms was applied to discriminate between bursts arising from fluorescently labeled protein and background noise. No bursts were identified in photon traces with DMSO only and MK-886 only when this criterion was applied. The FRET efficiency (ETeff) was calculated using SymphoTime 64 software. SmFRET histograms were fit with Gaussian distributions to determine the peak ETeff values. Alignment of instrument and analysis were verified using 10 base pair, 14 base pair and 18 base pair dsDNA standards.

7.3.11. Thioflavin-S (ThS) assay

HEK293 cells were transfected with tau-RFP (at equivalent DNA concentration as used in the tau FRET biosensor) for 48 hours prior to the addition of tau preformed

fibrils (PFF). Tau-GFP was not used as it would interfere with the thioflavin-S (ThS) signal. To make the PFF, 100 µl of purified tau proteins (10 µM) with DTT (5 mM) and heparin (0.4mg/ml) were first incubated for 120 hours at 37°C and shook at 1000 rpm in a thermal shaker (Thermo Fisher Scientific). After incubation, the sample was subjected to ultracentrifugation at 80,000 rpm for 30 minutes. The pellet was collected and sonicated to break up the fibrils into smaller pieces. The concentration of the fibrils was then measured by BCA. The sonicated fibrils were then treated to the transfected cells at a concentration of 40 µg/ml for 24 hours before conducting the ThS assay. Thioflavin-S (ThS, Millipore Sigma, product no. T1892) was dissolved in PBS buffer and was filtered through a 0.2 µm syringe filter to make a stock solution of 2.5 mM. For the ThS assay, cells were fixed with 1 ml of 4% paraformaldehyde in TBS for 15 minutes followed by washing with 1 ml of TBS for 5 minutes twice. After fixing, cells were permeabilized with 1ml of 1% Triton in TBS for 5 minutes, followed by washing with 1ml of TBS for 5 minutes twice. After permeabilization, cells were then treated with 0.002% ThS in TBS and incubate in the dark for 20 minutes. Cells were then washed twice with 50% ethanol for 10 minutes each and finally washed twice with TBS for 5 minutes each. Cells were then imaged with a fluorescence microscope using EVOS-FL cell imaging systems at 20X magnification. Mean fluorescence intensity for each image was quantified using ImageJ and values were normalized to untransfected controls.

7.3.12. Thioflavin-T (ThT) assay

Thioflavin-T (ThT, Sigma, product no. T3516) was dissolved in PBS buffer and was filtered through a 0.2 µm syringe filter to make a stock solution of 2.5 mM. ThT was then diluted to 20 µM prior to addition to the tau proteins. The samples for ThT measurements were prepared by mixing 25 µl of 20 µM tau proteins with 25 µl of 20 µM

of ThT, resulting in final concentrations of 10 µM tau proteins and 10 µM ThT. DTT (5 mM) and heparin (0.4 mg/ml) were then added to the samples; a control sample lacked addition of heparin. Lastly, the samples were treated with MK-886 (0.5 µM or 5 µM) and gossypetin (50 µM) with DMSO added to the no-compound controls. The ThT samples (50 µl each) were transferred to a black 96-well non-binding surface microplate with clear bottom (Corning product no. 3655) and incubated at 37°C with mild shaking (200 rpm) in the Cytation 3 plate reader. The ThT fluorescence was measured by the Cytation 3 plate reader through the bottom of the plate with excitation filter of 440 nm and emission filter of 480 nm. Readings were acquired every 20 minutes for a total of 120 hours.

7.3.13. Statistical analysis

Data are shown as mean ± standard deviation unless stated otherwise. Statistical analysis was performed by a two-tailed unpaired *t* test (Student's *t* test) using GraphPad Software to determine statistical significance for all experiments. Values of $P < 0.05$ were considered statistically significant. GraphPad style in using asterisks to denote *P* values in figures was used (*$P < 0.05$, **$P < 0.01$, ***$P < 0.001$, ****$P < 0.0001$ and n.s. indicates not significant).

7.4. Results

7.4.1. Inter-molecular FRET biosensor directly monitors structural changes in tau oligomers in cells

To develop an in-cell HTS platform that can detect small-molecule modulation of tau oligomerization and/or perturbation of tau conformational states, we engineered two cellular tau FRET biosensors. We used human embryonic kidney 293 cells (HEK293)

expressing full-length 2N4R WT tau fused to green (GFP) or red (RFP) fluorescent proteins (tau-GFP/RFP or "tau FRET biosensor") (**Fig. 7.2A**). Expression and homogeneity of the FRET biosensor were determined by fluorescence microscopy and immunoblotting. Fluorescence microscopy images showed that the tau proteins were evenly distributed in the cytosol of the cells, with no discernable puncta (which would have indicated more progressive aggregation, e.g. fibril formation) or other non-uniformities (**Fig. 7.2B**). Western blot analysis of the tau biosensor cell lysates confirmed the expression of fluorophore-tagged tau (**Supplementary Fig. 7.1A**).

We next tested the functionality of the tau FRET biosensor by measuring FRET efficiency using the FLT-PR (*283*). The value of FRET efficiency reflects the ensemble-averaged *inter*-molecular proximity between tau molecules, which is derived from the distance between the donor and acceptor fluorophore fused to the tau proteins. FRET between tau-GFP (donor) and tau-RFP (acceptor) in live cells showed hyperbolic dependence on acceptor concentration (**Fig. 7.2C**), with a maximum energy transfer efficiency (E) of 0.086±0.002, illustrated through a substantial decrease in the donor FLT in the presence of the acceptor (**Fig. 7.2D**), indicating the formation of tau oligomers in cells. The kinetics of formation of the tau-tau assemblies was also measured by FRET, showing that the WT tau biosensor has an optimal FRET after 48 hours of expression (**Supplementary Fig. 7.1B**). We confirmed that the FRET observed from cells expressing tau biosensor arises from specific tau-tau interactions and not from non-specific interactions between the free fluorophores (**Supplementary Fig. 7.1C-D**). Furthermore, we showed that the FRET biosensor is sensitive to the addition of forskolin, a small molecule known to induce tau hyperphosphorylation and self-association, but not to gossypetin, a small molecule known to inhibit or remodel of tau fibrils (**Supplementary Fig. 7.1E**) (*291*). To confirm that only oligomeric species of tau,

but not fibrils, were present in the tau biosensor cells, we performed a thioflavin-S (ThS) assay in cells expressing tau-RFP at the same concentration of tau-GFP/RFP dual transfected cells (tau-GFP was not used as it will interfere with the ThS signal), with treatment of exogenous tau preformed fibril (PFF) as a positive control. Results from the ThS assay illustrate that only cells treated with PFF have a positive ThS signal (**Fig. 7.2E**) with a significant increase in the ThS intensity (**Supplementary Fig. 7.1F**), confirming that no fibrils (e.g. β-sheet tau assemblies) are present in the biosensor cells, and more importantly that the FRET signal is the result of tau oligomerization.

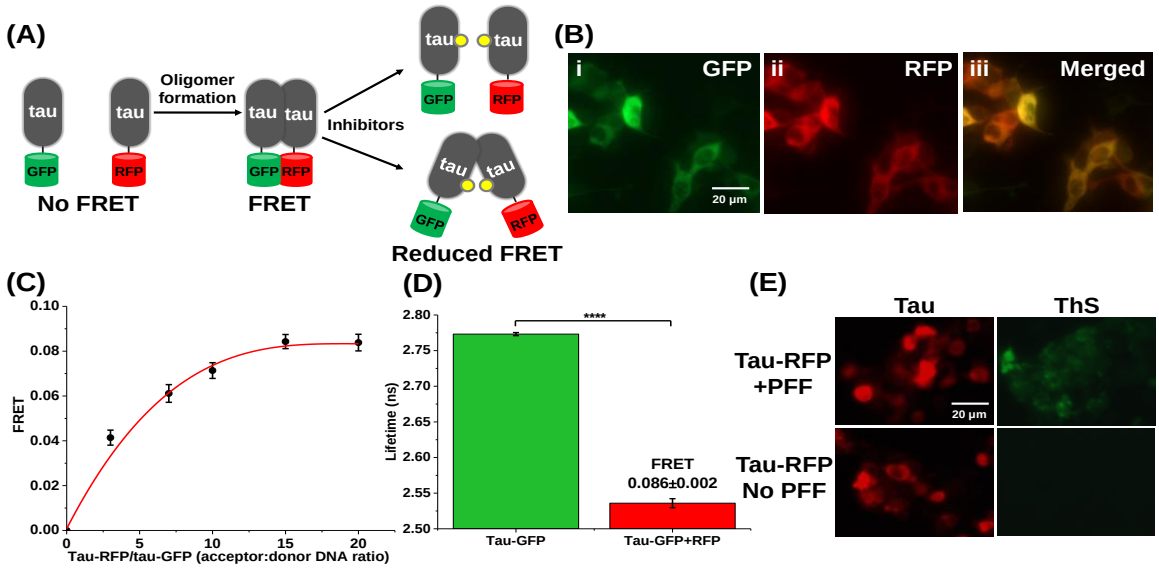

Figure 7. 2. The tau *inter*-molecular FRET biosensor and fluorescence lifetime technology enable direct monitoring of tau oligomerization in cells.

(A) Schematic representation of live-cell based tau *inter*-molecular FRET biosensor. FRET signal is observed when tau oligomers form, which can be modulated by small-molecule inhibitors. Tau oligomer is drawn as a dimer for illustration but it can be any species more than a dimer (≥2-mers). (B) Fluorescence microscopy images of (i) GFP channel, (ii) RFP channel and (iii) merged channel of HEK293 cells expressing tau-GFP/RFP (tau FRET biosensor). (C) Titration of tau-RFP (acceptor) to tau-GFP (donor) illustrates that the FRET efficiency of the biosensor follows a

hyperbolic dependence on acceptor concentration. (D) Fluorescence lifetime measurements of the tau biosensor show efficient FRET, indicating tau self-association. (E) Thioflavin-S (ThS) staining of HEK293 cells expressing tau-RFP (in same total DNA concentration as used in the FRET biosensor) in the presence and absence of the positive control of tau preformed fibrils (PFF). Data are means ± SD of three independent experiments. ****$P < 0.0001$ by two-tailed unpaired *t* test.

7.4.2. Identification of novel small molecules from HTS of the NCC library that perturb the conformational ensembles of tau oligomers

Using our cellular tau FRET biosensor, we performed a HTS of the NCC library (727 bioactive compounds) to identify compounds that perturb the conformational ensembles of tau oligomers. The NCC library is a collection of small molecules that have been previously tested in clinical trials, and have known safety profiles and details on potential MOA.

After an initial quality control check of the tau FRET biosensor on each day of screening (fluorescent waveform signal level and coefficient of variance), the cells were dispensed into drug plates and incubated with the compounds (10 μM) or DMSO control wells for 2 hours. FLT measurements were acquired with the FLT-PR. A single-exponential fit was used to determine the FLT from cells expressing the tau FRET biosensor (τ_{DA}) or expressing a tau-GFP donor-only control (τ_D) to determine FRET efficiency (Eq. 1). As FLT measurements are prone to interference from fluorescent compounds, a stringent fluorescent compound filter was used to flag 30 such compounds as potential false-positives (*190, 226*). FRET efficiency from all compounds that passed the fluorescent compound filter are plotted (**Fig. 7.3A**) and a histogram of the FRET distribution from these compounds was fit to a Gaussian curve to obtain a mean and standard deviation (SD) for the screen (**Supplementary Fig. 7.2A**).

Our initial goal was to discover compounds that alter the conformational ensembles of tau oligomers with the potential of disrupting tau-tau interactions, leading us to focus our search to compounds that reduce FRET (though other compounds that increase FRET could potentially remodel toxic oligomers and be of interest in future studies). Five reproducible hits from the library were shown to decrease FRET by more than 5SD below the mean of all wells (**Fig. 7.3A,** highlighted in red) while not appearing as hits in the donor-only control screen (**Supplementary Fig. 7.2B-C**).

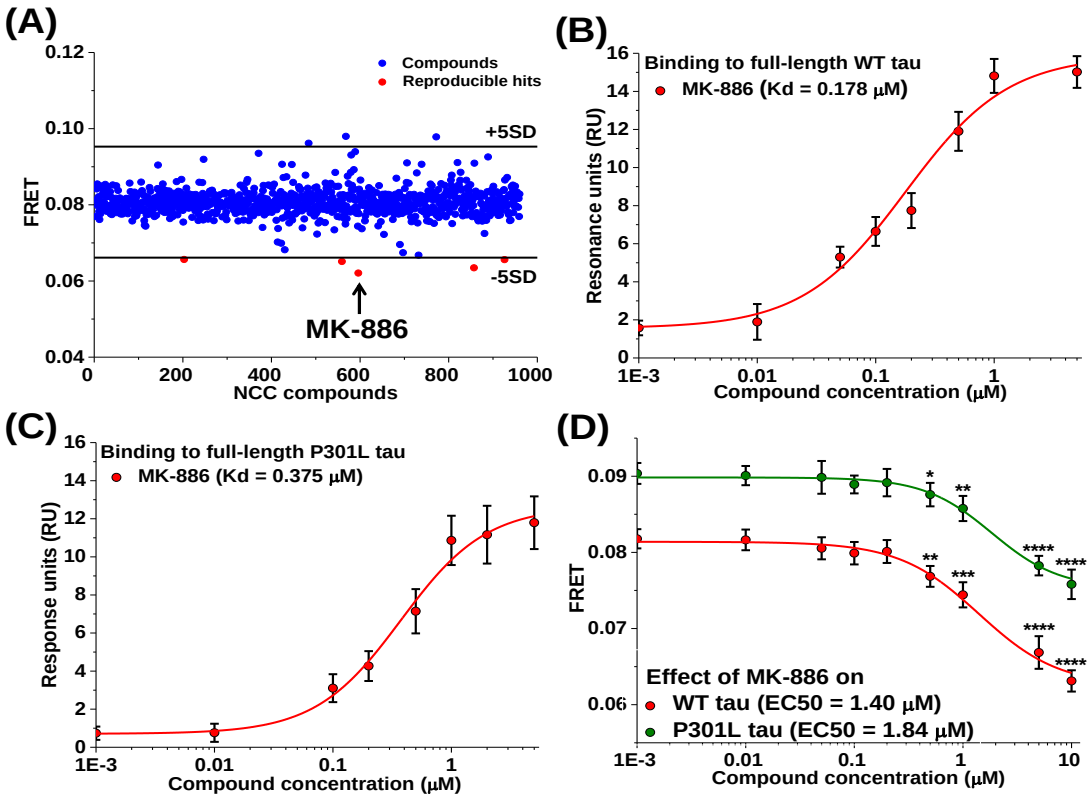

Figure 7. 3. Identification of MK-886 as a small molecule that directly perturbs conformational ensemble of tau oligomers.

(A) Representative pilot screening with NCC library containing 727 compounds. A FRET efficiency cutoff threshold was applied at a change in FRET efficiency of 5SD (*black lines*). Five

reproducible hits decreased FRET by more than 5SD below the mean of all cells (red) and MK-886 induced the largest FRET change (arrow). Surface plasmon resonance (SPR) binding curve for MK-886 to purified recombinant full-length 2N4R (B) wild-type (WT) and (C) P301L tau proteins. (D) FRET analysis of the dose response of MK-886 in both WT and P301L tau *inter*-molecular biosensors indicates EC_{50} values of 1.40 and 1.84 μM respectively. Data are means ± SD of three independent experiments. **P* < 0.05, ***P* < 0.01, ****P* < 0.001 and *****P* < 0.0001 by two-tailed unpaired *t* test.

7.4.3. Binding of hit compounds to purified tau proteins

We next used surface plasmon resonance (SPR) to determine if these five hit compounds bind tau, delineating a potential direct or indirect MOA with tau. Of the five hits that reduced FRET with our tau biosensor, MK-886 was the only hit to demonstrate dose-dependent binding to purified WT tau protein with K_d = 0.178 μM (**Fig. 7.3B** and **Supplementary Fig. 7.2D**). MK-886 also showed binding to purified P301L tau protein, a more aggregation prone mutant of tau (*292*), with K_d = 0.375 μM (**Fig. 7.3C** and **Supplementary Fig. 7.2E**). Interestingly, MK-886 also had the strongest change in FRET (**Fig. 7.3A,** highlighted in arrow). The other four hit compounds did not show direct binding to immobilized tau protein (**Supplementary Fig. 7.2F**) and therefore most likely attenuate tau FRET through an indirect MOA. All subsequent analysis in this study is focused on MK-866. The indirect MOA compounds, although outside the scope of this study, are potentially useful and are briefly discussed below.

7.4.4. FRET dose-response of MK-886 with cellular tau inter-molecular FRET biosensors

The relative effective concentration (EC_{50}) of MK-886 was determined by in-cell FRET measurements using the WT tau biosensor. The compound decreased FRET

efficiency in a dose-dependent manner with an EC_{50} value of 1.40 μM (**Fig. 7.3D**). We also performed a FRET dose response using P301L tau FRET biosensor. The FRET efficiency of this biosensor was found to be higher than that of WT tau biosensor (**Supplementary Fig. 7.3A**) which is consistent with the known tendency of P301L tau to be hyperphosphorylated and hence more oligomeric (*292*). Similar to WT, we observed a dose-dependent decrease in the FRET efficiency of the P301L tau biosensor with MK-886 with an EC_{50} value of 1.84 μM (**Fig. 7.3D**), confirming that the hit compound also remodels tau oligomers in a disease-relevant model. Interestingly, we observed that MK-886 lowered the FRET level of P301L biosensor to the basal FRET level of WT tau biosensor. This may suggest that MK-886 disrupts the toxic oligomers of P301L tau and converts them to less toxic conformations that are similar to the conformations adopted by the WT tau. In addition, we confirmed that the small molecule was acting specifically on tau and was not acting on the cytosolic fluorophores (**Supplementary Fig. 7.3B-D**). Assay quality (Z') was determined using MK-886 (Eq. 2). The Z' value of 0.72±0.02 indicates excellent assay quality, validating MK-886 as a positive control tool-compound for targeting tau oligomers.

We also expressed the P301L tau FRET biosensor in the SH-SY5Y neuronal cell model, and similar FRET was observed as in the HEK293 cells (**Supplementary Fig. 7.4A**). This FRET again reflects the formation of oligomers, as it is known that β-sheet fibrils do not spontaneously form in SH-SY5Y overexpressing P301L tau unless aggregation inducers are used (*288*). MK-886 reduced FRET from P301L tau biosensor in the SH-SY5Y cells with an EC50 of 1.06 μM (**Supplementary Fig. 7.4B**). Importantly, as will now be shown, if toxicity is observed when P301L tau is overexpressed in SH-SY5Y cells, and the toxicity is rescued by MK-886, it will further support the conclusion

that the small molecule converts toxic tau oligomers into a non-toxic conformational state.

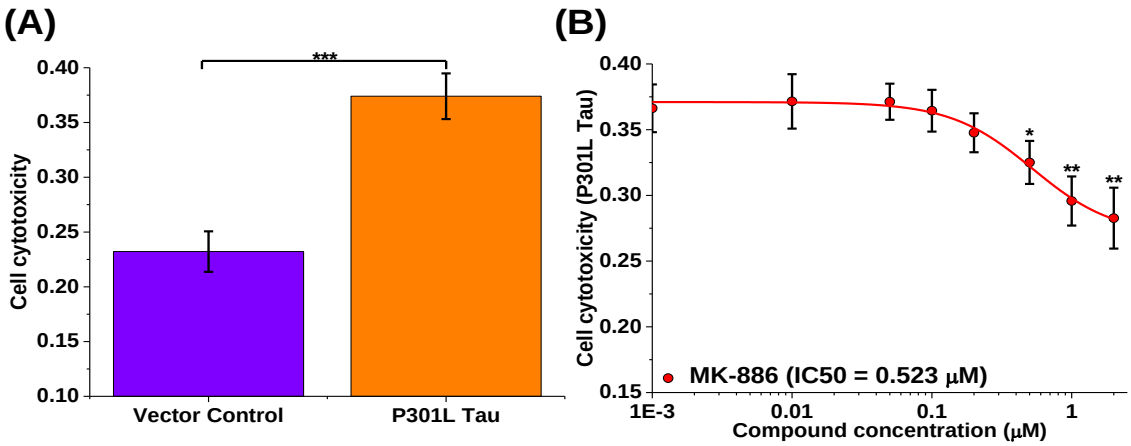

Figure 7. 4. Rescue of tau induced cell cytotoxicity in SH-SY5Y human neuroblastoma cells by MK-886.

(A) SH-SY5Y cells were transfected with vector control and P301L tau. Significant cell death is observed in cells transfected with P301L tau as compared to the vector control. (B) MK-886 rescued P301L tau induced cytotoxicity in SH-SY5Y cells with an IC_{50} of 0.523 μM. Data are means ± SD of three independent experiments. *P < 0.05, **P < 0.01, and ***P < 0.001 by two-tailed unpaired t test.

7.4.5. MK-886 reduces tau induced cell cytotoxicity in SH-SY5Y cells with nanomolar potency

We next tested the effect of MK-886 on P301L tau induced cytotoxicity in the SH-SY5Y neuroblastoma cell model of tauopathy (*81, 137, 293, 294*). Overexpression of P301L tau showed significantly greater cell death (37%) when compared to the vector-only control (23%) after 96 hours of expression (**Fig. 7.4A** and **Supplementary Fig. 7.5A**). Treatment with MK-886 (1 nM to 2 μM) to cells overexpressing P301L tau showed significant rescue of P301L tau induced cytotoxicity in a dose-dependent manner, with

an IC_{50} of 0.523 μM (**Fig. 7.4B**), the same order of magnitude as MK-886's binding affinity for recombinant P301L tau protein. The two-fold difference in IC_{50} of MK-886 in the cell cytotoxicity assay (0.523 μM) and the EC_{50} from the FRET assay (1.06 μM) may be due to the different treatment conditions as well as the expression of unlabeled *vs*. fluorophore-tagged P301L tau in each assay respectively.

We note that MK-886—which was blindly identified in our HTS—has been shown to play a role in modulating AD-related amyloid and tau pathology through inhibition of 5-lipoxygenase (5-LOX)-activating protein (FLAP) (*295*), potentially altering the clearance and phosphorylation state of tau (*296, 297*). Our observations suggest that MK-886 rescues tau induced cytotoxicity through direct binding to tau protein and not by modulating FLAP, a previously undescribed mechanism of action. SH-SY5Y cells do not express 5-LOX or FLAP and therefore are a particularly well suited model to evaluate alternative MOA for MK-886 rescue of tau induced cytotoxicity (*298*). We also confirmed that there were no changes in the relative levels of expressed tau (**Supplementary Fig. 7.5B**) or the phosphorylation state (**Supplementary Fig. 7.5C**) due to MK-886 treatment in the SH-SY5Y cell model, although it remains possible that MK-886 may be altering other PTMs such as acetylation or oxidation.

In addition, it has been shown that expression of P301L tau may also result in cell death through down-regulating the expression of survivin, inhibitor of apoptosis proteins (IAPs) or X-linked inhibitor of apoptosis proteins (XIAPs) (*293*). Thus, we needed to rule out the possibility that MK-886 rescues P301L tau induced cell cytotoxicity by modulating the expression of these genes, rather than by directly altering tau conformations. To do so, we used two small molecules (YM-155 and UC-112) that are potent suppressors of the expression of survivin, IAPs and XIAPs, thus mimicking the effect of P301L tau on this pathway. This allowed us to test whether MK-886 can

rescue cell cytotoxicity in the absence of P301L tau, simply by upregulating these survival genes (*299*). Our results showed that MK-886 did not rescue the cell cytotoxicity induced by YM-155 (1 μM) or UC-112 (1 μM) (**Supplementary Fig. 7.6A-B**). Thus, these important control experiments strongly suggest that MK-886 rescues P301L tau induced cell cytotoxicity by directly perturbing the conformations of the toxic tau oligomers to form a non-toxic conformation.

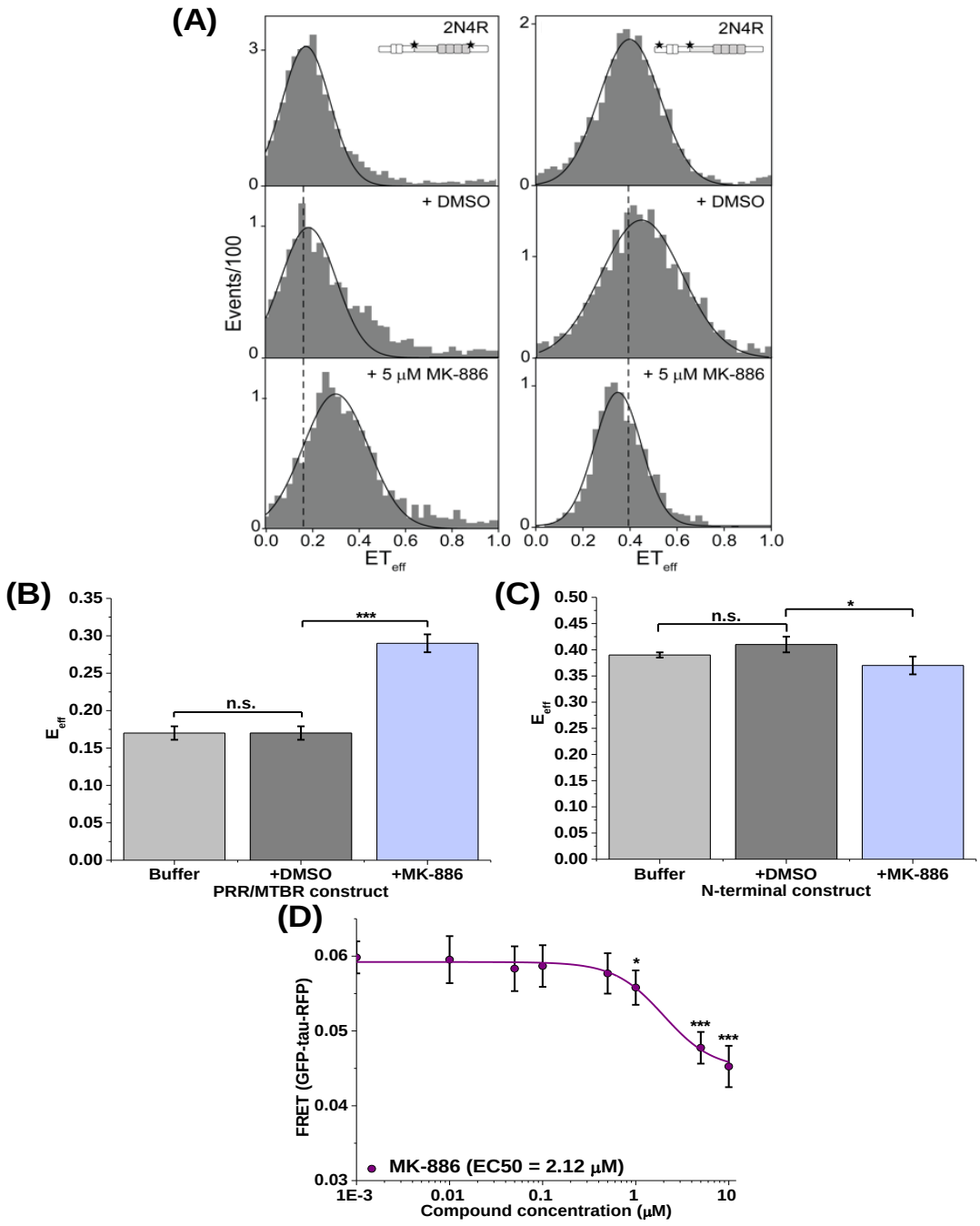

Figure 7. 5. MK-886 binds and perturbs tau monomer conformation.

(A) Single-molecule FRET (smFRET) measurements in the absence and presence of MK-886 with WT 2N4R tau double labeled at the proline-rich region/microtubule binding region (PRR/MTBR, *left*) or at the N-terminal domain (*right*). Tau schematic represents the labelling position for each construct. The black line is drawn from the peak of the histogram in buffer for

comparison with DMSO and MK-886 samples. Representative histograms are shown. (B) Quantification of the smFRET measurements indicates that the PRR/MTBR becomes substantially more compact (increase in FRET) upon binding MK-886 (5 μM) (A, *bottom left*) when compared to tau in buffer (A, *top left*) or DMSO (A, *middle left*) while the N-terminal domain (C) shows only minor differences in the presence of MK-886 (5 μM) (A, *right*). (D) FRET analysis of the dose response of MK-886 in the cellular tau *intra*-molecular biosensor indicates an EC_{50} value of 2.12 μM, similar to that of oligomer modulation, suggesting that the change in conformational states of oligomers is due in part to conformational changes of tau monomer. Data are means ± SD of three independent experiments. *$P < 0.05$, ***$P < 0.001$ and n.s. indicates not significant by two-tailed unpaired *t* test.

7.4.6. MK-886 specifically perturbs the PRR/MTBR of tau monomer and induces conformational changes of the cellular tau intra-molecular biosensor

To further investigate the MOA of MK-886, we used single-molecule FRET (smFRET) to examine the effect of MK-886 on monomeric tau. Using two different doubly fluorescent-labeled tau constructs (labeled at the proline rich region/microtubule binding region (PRR/MTBR) or at the N-terminal domain) (*290*), we monitored the conformation of two distinct regions of tau (**Fig. 7.5A**). The smFRET shows that MK-886 causes a substantial increase in FRET for the PRR/MTBR targeted construct (**Fig. 7.5B**) but only a minor decrease in FRET for the N-terminal domain construct (**Fig. 7.5C**). This suggests that MK-886 specifically binds and induces a conformational change in tau monomer at the PRR/MTBR region, resulting in a subsequent loss of interactions between the N-terminal domain and the PRR/MTBR. To determine whether MK-886 also perturbs the monomer conformation of tau in cells, we tested the compound with a cellular tau *intra*-molecular FRET biosensor (GFP-tau-RFP). The *intra*-molecular FRET biosensor has a basal 6% FRET signal (**Supplementary Fig. 7.7**), illustrating the *intra*-

molecular interactions arising from the paper-clip monomeric structure in which the N- and C-terminus of tau are folded to close proximity (*300*). Treatment with MK-886 reduced *intra*-molecular FRET with an EC_{50} of 2.12 μM, similar to that of oligomer modulation, suggesting that the change in conformational states of oligomers is due in part to perturbation of the tau monomer (**Fig. 7.5D**).

It has been suggested that the folding over of tau's two termini to form the classic "paper-clip" structure is due to electrostatic interactions that arise from the opposite net charges of the N-terminal and MTBR domains (*300*). While this global folding is specific, it has been shown to be a rather weak interaction (*300*). We speculate that the binding of MK-886 to the PRR/MTBR of tau may shield these interactions and lead to an opening of the two termini, resulting in the observed decrease in FRET of the *intra*-molecular FRET biosensor. From our previous observations with smFRET on tau constructs, this type of conformational change is often accompanied by the PRR/MTBR becoming substantially more compact (increase in FRET) in recombinant protein systems (*290*).

7.4.7. MK-886 stabilizes tau conformations that promote the formation of β-sheet-positive fibrils in the presence of aggregation inducer

We have shown that MK-886 directly binds to immobilized tau, modulates tau oligomer and monomer conformation (both in cells and purified proteins), and rescues tau induced cytotoxicity. To further explore MK-886's MOA and identify whether MK-886 targets on- or off-pathway oligomers, we performed a heparin induced thioflavin-T (ThT) aggregation assay in the absence and presence of MK-886. MK-886 shortens the lag phase of tau β-sheet fibril formation in a dose-dependent manner (**Fig. 7.6A**), suggesting that it induces or stabilizes on-pathway, early-stage species in the amyloidogenic cascade. We confirmed that MK-886 did not have a direct effect on ThT fluorescence

(**Supplementary Fig. 7.8A**) and did not act to nucleate for fibril formation (**Supplementary Fig. 7.8B**). In addition, we tested if MK-886 disrupts tau preformed fibrils (PFF). Comparison of MK-886 to gossypetin (a known remodeler of tau fibrils) illustrates that MK-886 did not reduce the ThT signal from tau PFF, whereas gossypetin showed a significant decrease, indicating the disruption of β-sheet fibril structure (**Fig. 7.6B**). These results, in combination with the changes in FRET and reduction of tau induced cytotoxicity, suggest that MK-886 alters the conformational ensemble of tau oligomers favoring a subset of non-toxic, on-pathway oligomers that promote tau fibrillization.

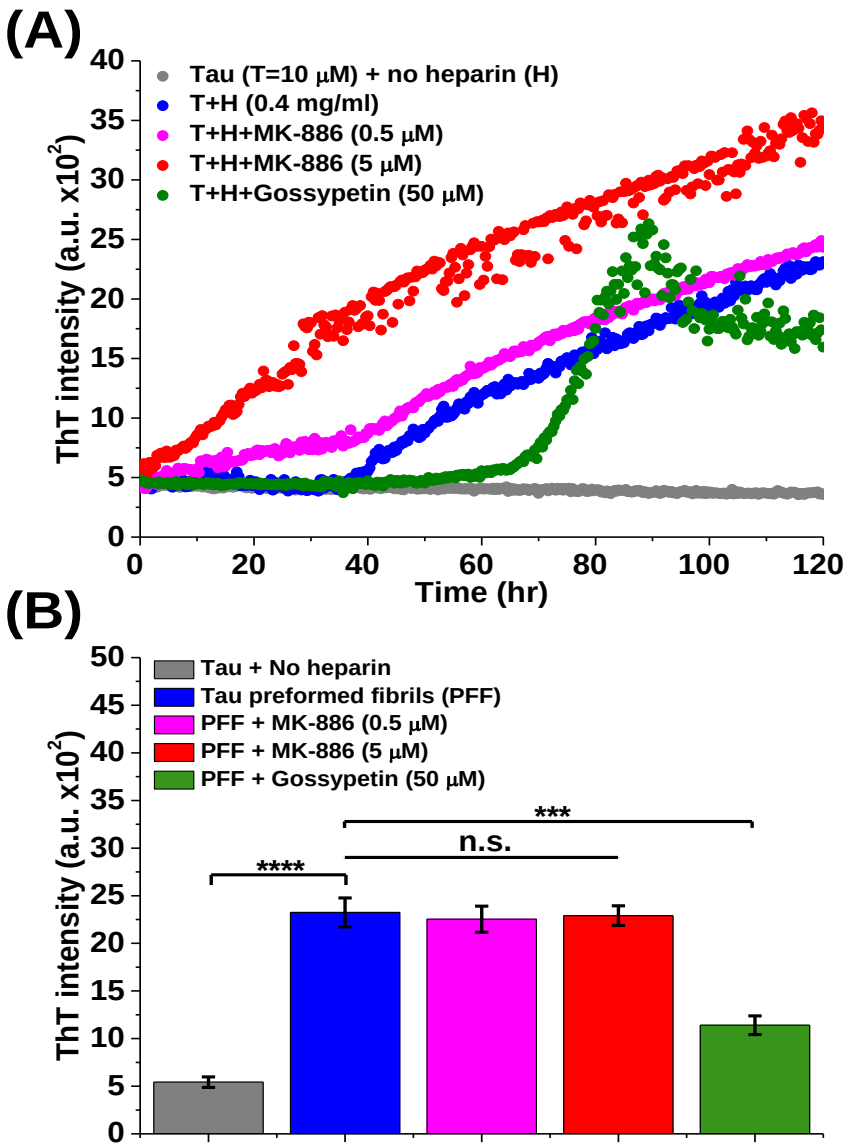

Figure 7. 6. MK-886 alters the ensemble of conformational states of tau oligomers by stabilizing a fibrillization promoting conformation.

(A) Effect of MK-886 on the tau fibrillization cascade as characterizaed by thioflavin-T (ThT) assay with purified WT tau proteins. Fibrillization was induced by heparin (0.4 mg/ml) in the presence of DMSO control, MK-886 (0.5 and 5μM) and gossypetin (50 μM, a known small-molecule inhibitor or remodeler of tau fibrils as positive control). (B) Effect of MK-886 on tau

preformed fibrils (PFF) with gossypetin as a positive control. All samples were treated with DTT (5 mM). Data are means ± SD of three independent experiments. ***$P < 0.001$, ****$P < 0.0001$ and n.s. indicates not significant by two-tailed unpaired *t* test.

7.5. Discussion

The identity of a specific, toxic tau oligomeric species remains elusive. Indeed, it is unlikely that a single, unique toxic conformation exists. It is far more likely that an ensemble of toxic oligomers (differing in size, conformation, and even molecular constituency) populates the fibrillogenesis cascade (*87-93*). This heterogeneity in tau oligomer targets highlights the need for an ultra-sensitive screening platform capable of monitoring structural changes within the ensemble of tau assemblies. Our FRET-based platform for monitoring full-length tau oligomerization in cells is a new technology that is capable of doing this, as well as elucidating novel compounds which alter conformation and oligomerization, thereby providing a new pipeline of therapeutic discovery for tauopathies.

With this technology in hand, we and others are in a position to explore multiple important issues. First, screens will now be done of larger libraries and of libraries built specifically for targeting the central nervous system (CNS) (i.e. favorable blood-brain barrier permeability). These screens will dramatically increase the statistical sampling of small-molecule induced changes in time-resolved FRET (TR-FRET) signatures. With a larger sample, the high information content of TR-FRET can, when complemented with other structural tools (discussed below), be used to cluster compounds into distinct classes based on their myriad of structural effects on the targets (*226*). To more adequately generalize the patho-physiological relevance of these clustered structural motifs, we will move to inducible cell lines (*282*), as well as alternate cell lines including eventually patient-derived induced pluripotent stem cells (iPSC) neurons (*301*) and

iPSC-derived spheroids (*302, 303*). Additional extensions of this technology for small molecule discovery should include using different cellular models of tau pathology including, among others, modification of the oligomerization trigger through the addition of tau seeds (fibrils, oligomers, or monomer), upregulation of specific kinases or chaperone proteins (e.g. GSK3β or HSP70), and treatment with environmental toxins (*83*). This will allow us to examine multiple proposed mechanisms of induced tauopathies, providing key insight into differences between on- and off-pathway oligomerization (*304*). Each of these steps will be critical to building a more complete and useful correlation between structural heterogeneity and toxicity.

Additionally, as we have shown that full-length tau can be engineered as a cell-based, FRET-biosensor of oligomerization (here using the 2N4R isoform), we should now explore potential nuances in how oligomerization depends on tau isoform. Not only will we be able to explore the propensity of different isoforms to oligomerize, but should also test the likelihood that different isoforms co-mingle in heterogenous oligomers. It will be of great interest to ascertain whether lead compounds are isoform specific or can target multiple distinct isoforms. Broadly speaking, information on isoform-specific oligomerization could be useful in designing more effective, patient-stratified design of clinical trials (*305*). The Diamond group pioneered the tau cellular biomarker field with their tau repeat domain (tau-RD) FRET biosensor cells (*282*). Use of full-length tau thus expands on the existing technology and should facilitate additional stratification of potential biomarkers present in AD versus other tauopathies. Following Diamond, experiments that compare the sensitivity and relative reactivity of each biosensor to different tauopathy associated biofluids will provide new insight into heterogeneity in tau assemblies inherent in these distinct diseases.

Ultimately, determining and validating the specific MOA by which lead compounds act—be they through direct binding to tau monomers/oligomers or indirectly by altering cellular processes that lead to alterations in oligomers—will require comprehensive approaches to link biophysical experiments with cell biological observables. One set of immediately accessible questions is how the compounds' impact on monomer folding and/or oligomerization relates to tau localization in cells, most obviously on microtubule binding. Here, future work will further probe post-translational modifications (including hyperphosphorylation, which we started here using forskolin) and acetylation, specifically testing how compounds alter the relationship between microtubule unbinding and tau folding/aggregation. As another example, tau has recently been shown to mislocalize to dendritic spines, disrupting synaptic transmission in primary neurons (*306*). Whether these or numerous other mechanisms related to mislocalization can explain the cytoprotective effects of lead compounds will require additional experiments. For example, nano-imaging modalities like fluorescence-lifetime imaging microscopy (FLIM) and time-correlated single photon counting (TCSPC) can provide the necessary spatial resolution to correlate subcellular localization (e.g. microtubules, cytosol, mitochondria, etc.) and distinct tau conformations (*307*).

Major challenges for the hypothesis

The technology described here is based on the hypothesis that tau biosensors expressed in cells can be used to accomplish two complementary, but distinct goals: 1) they can be used to find small molecules that modulate tau toxicity; and 2) they can provide a direct, albeit low-resolution reporting of the structures and conformations of a heterogeneous ensemble of toxic and non-toxic states. For the first part of this hypothesis, namely modulation of toxicity, we have demonstrated the power of our approach with MK-886. The second part is more of a challenge. This broader and

longer-term hypothesis is built on the idea that biophysical tools, such as TR-FRET, can provide key insight into the unique structural fingerprints of heterogeneous toxic tau oligomers, and that this detail can be exploited in drug discovery. This is a far more nuanced and difficult bar for the field to meet, but is nonetheless a goal that should and, we believe, can be tackled. Why is this difficult? On the one hand, unlike fibrils, oligomers are highly heterogeneous (number of monomers per aggregate, local or transient structural motifs/folds, molecular constituency, etc...), making it improbable that high-resolution structural biology tools are or ever will be applicable to their study (they simply lack well-defined secondary or tertiary structural elements). On the other hand, the field currently relies only on low-resolution techniques that provide little to no structural information (e.g. antibody recognition, protease protection, detergent resistance). Finding a middle ground requires a set of structural techniques that can adequately and accurately interrogate oligomers, but more crucially can stratify structural fingerprints at a quantitatively useful and reproducible resolution. Absent high-resolution structures, we should nonetheless be able to ask: what are the critical amino acids that dictate oligomer-prone monomer folds and what are the deleterious *inter*-monomeric amino acid motifs that dictate toxicity? As an example of how this can begin to happen, we complemented our TR-FRET with smFRET, and were able to isolate the region of tau impacted by MK-886 binding. But this is just a start, as far more detailed information should be obtainable using a set of creative and state-of-the-art experimental and computational approaches to interrogate these structures (*308-310*).

In theory, TR-FRET waveforms contain high-content information that can resolve relative species populations and protein-protein distance distributions (*311*). Unfortunately, TR-FRET alone does not provide atomic structural resolution to uniquely identify specific species. The process of extracting this structural data from TR-FRET

requires model fitting. The challenge is that the model must be constrained by information we do not yet have, including constraints on the stoichiometry of the tau oligomer. This highlights a current limitation in analyzing tau-tau TR-FRET as there are no well-defined structural states and the exact toxic species, including the number of interacting tau monomers, is unknown. To begin to make progress in this regard will require additional biophysical tools. These will include, among others, analytical ultracentrifugation (AUC) and analytical gel filtration for oligomer size. Despite the promise of these techniques for grouping oligomeric species into meaningful clusters, doing so in cells will be the greatest challenge moving forward. Higher resolution structural information for stratifying oligomeric species can be obtained in purified, in vitro assemblies using other spectroscopic techniques such as nuclear magnetic resonance (NMR) and electron paramagnetic resonance (EPR). However, because tau oligomers in cells likely consist of other molecular constituents and are folded with the help of chaperones, there is a real danger in relying too heavily on the folding of these assemblies outside of the native cellular environment. There have been recent advances that allow for the use of high-resolution techniques, such as NMR, in cells (*312-314*). These and other advances in biophysical tools will be of critical importance in the coming years.

Linkage to other major theories

Tauopathies have a vast heterogeneity in their clinical presentations (e.g. AD, fronto-temporal dementia and movement disorders, amongst others) (*315*) which is one of the major challenges that plagues current clinical trials (*316*). This heterogeneity may be explained in part by strong histopathologic differences and differential laminar and regional brain distributions. For therapeutic intervention, an equally important potential

source of this heterogeneity is molecular variations such as isoform composition and post-translational modifications (*315, 317*). Hence, there is a need for robust tools and/or biomarkers to stage and delineate (particularly, at the molecular level) the numerous different tauopathies.

Although our biosensors and HTS technology are focused on the oligomer hypothesis of tauopathy, they are directly translatable into other areas of tauopathy research and therapeutic discovery. The presence of misfolded tau and the formation of the tau oligomers can be attributed to upstream dysfunctions in neurophysiology and axonal transport. For example, mitochondrial dysfunction and oxidative stress are believed to be a prominent early event in the pathogenesis of AD, contributing to tau phosphorylation and the formation of neurofibrillary tangles (*318*). In particular, deterioration of mitochondrial functions such as impairments in the activity of Krebs cycle enzymes and electron transport machineries (e.g. cytochrome c oxidase (COX)) have been correlated with severity in the clinical state of tauopathies and AD (*71, 72*). Importantly, impaired COX activity can potentiate the generation of mitochondrial-derived reactive oxidative species (ROS), suggesting that defective mitochondrial bioenergetics and oxidative stress are coupled in a vicious cycle (*72*). It has also been shown in that in familial AD, tau and amyloid-beta (Aβ) can augment the pathological deterioration of mitochondrial function (*319*). In addition, there is compelling evidence that tau can play a role in controlling motor protein–driven vesicle transport along microtubules (*320*). Furthermore, there is an age-dependent decline in axonal transport rates which correlates with increases in hyperphosphorylated tau (*73*). Our FRET biosensors can be used to study these effects. For example, we can use the *intra*-molecular biosensor to study the global tau folding when it is bound to microtubules versus when it is detached from microtubules. Our *inter*-molecular biosensor can also be

used to monitor the kinetics and the extent of free soluble tau that are detached from microtubules and start to form oligomers, providing important fundamental information in understanding early stage events underlying tau pathology.

Misfolded or oligomerized tau can be a symptom, as much as a cause, of an underlying pathology. Despite our focus on disrupting oligomers, using the cellular tau biosensors to modulate upstream effectors of tau dysfunction may actually hold the most promise. The TR-FRET screen in cells does not discriminate between compounds that act directly on tau folding/oligomerization and those that operate indirectly by binding to other upstream targets. Coupling secondary biophysical assays to the screen allows us to elucidate direct versus indirect MOA. Compounds that act through an indirect MOA—e.g. those that rescue dysfunctional autophagy or mitochondrial functions, endoplasmic reticulum or oxidative stress—can provide insight into specific pathways that are disrupted in tauopathy, giving rise to novel therapeutic targets and strategies. Upon inspection, this appears likely the case for several of the compounds we identified in our screen but whose MOA we have not yet elucidated. Two of these compounds (bumetanide and torsemide) are both loop diuretics which inhibit the sodium-potassium-chloride cotransporter (NKCC1) in vascular smooth muscle and have been shown to reduce the risk of AD dementia in both adults with normal cognition or with mild cognitive impairments (*321*). The other two hits (benzbromarone and triclosan) have been shown to attenuate oxidative stress (*322*) and induce autophagy (*323*) (respectively), both known cellular dysfunctions in AD.

Our biosensors should be useful in a variety of other contexts being pursued aggressively in the field. One example is the prion-like propagation of tau pathology (*282*). We plan to use the technology in an HTS campaign targeting the uptake and propagation of toxic tau species. We have already begun to see the power of the

technology in this way, observing increased FRET due to uptake of WT and truncated tau protein by our biosensor (data not shown). A second example builds on mounting evidence of cross-reactivity and comorbidity amongst misfolded proteins in numerous neurodegenerative diseases. These players include other IDPs, Aβ and α-synuclein (*324*). Our biosensors can directly probe these types of interactions via co-expression of these constructs into the tau biosensor cells, and/or treating the tau biosensor with Aβ or α-synuclein fibrils/oligomers and monitoring FRET, cytotoxicity, and uptake. Different donor and acceptor labelled proteins (e.g. tau-GFP/Aβ-RFP etc.) can also be developed and utilized to study potential direct protein-protein interactions. Our strategy, combining cellular fluorescent biosensor and TR-FRET measurement in a HTS platform, is broadly applicable to other drug discovery efforts targeting IDPs involved in numerous neurodegenerative diseases.

7.6. Supplemental figures

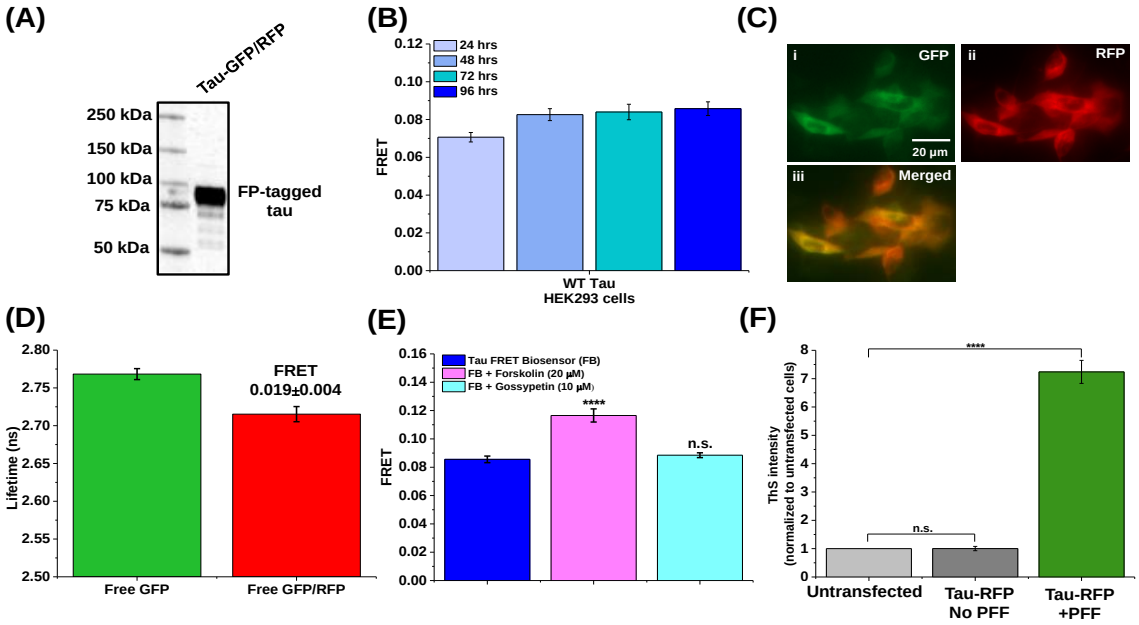

Supplemental Figure 7. 1. Characterization of tau inter-molecular FRET biosensor and soluble free GFP/RFP expressed in HEK293 cells.

(A) Expression of tau-GFP and tau-RFP expressed in HEK293 cells stained with Tau-5 antibody. (B) Kinetic of the FRET measurements for WT tau FRET biosensor expressed in HEK293 cells. (C) Fluorescent microscopy images of soluble free GFP/RFP-only (fluorophore-only control) expressed in HEK293 cells at the same donor-to-acceptor ratio as the FRET biosensor. (D) Fluorescence lifetime measurement of the GFP/RFP-only control indicates the basal FRET from free soluble fluorophore. (E) Confirmation of the functionality of the tau FRET biosensor with addition of forskolin (a known small molecule that induces tau hyperphosphorylation and self-association) and gossypetin (a known inhibitor or remodeler of fibril formation). (F) Quantification of in-cell thioflavin-S (ThS) staining with tau preformed fibril (PFF) used as a positive control. Data are means ± SD of three independent experiments. ****P < 0.0001 and n.s. indicates not significant by two-tailed unpaired *t* test.

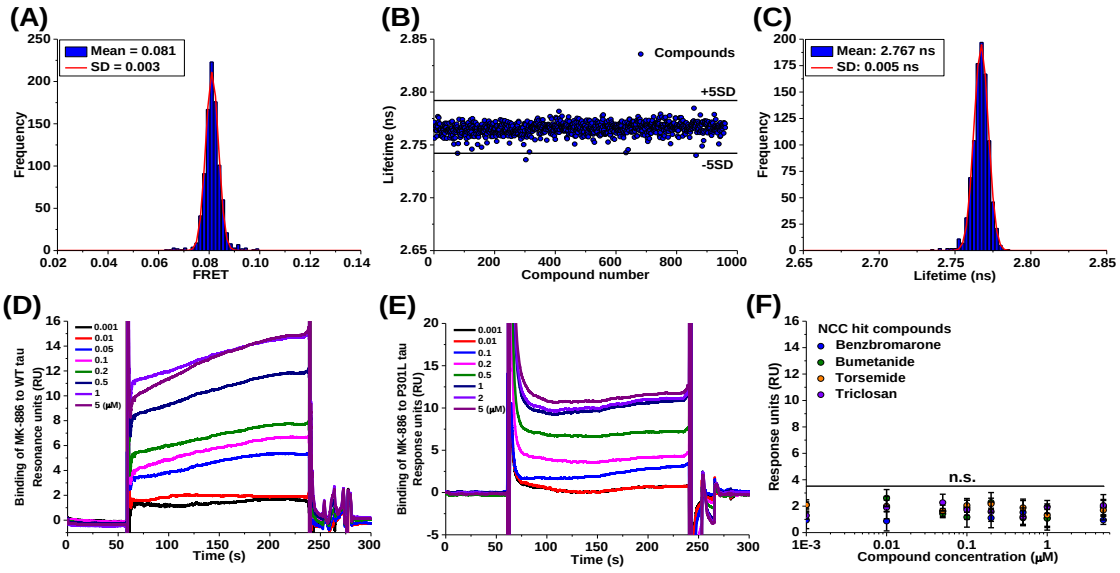

Supplemental Figure 7. 2. Donor-only control screen and surface plasmon resonance (SPR) characterization of hit compounds in binding to purified tau protein.

(A) Histogram plot of all compounds from the NCC screen with the tau *inter*-molecular FRET biosensors after removal of fluorescent compounds to obtain the average FRET efficiency and

the standard deviation (SD) of the screen. (B) Representative donor-only control screen with NCC library using cells expressing only tau-GFP which do not show FRET signal so the lifetime plot is shown. Applied threshold at a change in lifetime of 5SD is shown by the black lines. There is no reproducible hit from the donor-screen indicating that the hits observed are due to random occurrence. In addition, the hit compounds obtained from the FRET screen do not appear as hits in any of the donor-only control screens. (C) Histogram plot of all compounds from the NCC donor-only screen after removal of fluorescent compounds to obtain the average lifetime and the SD of the screen. SPR raw binding curves for MK-886 on (D) purified WT tau protein and (E) purified P301L tau protein. (F) SPR characterization of other four hit compounds show no direct binding or interaction between the compounds and the tau protein. Data are means ± SD of three independent experiments and n.s. indicates not significant by two-tailed unpaired *t* test.

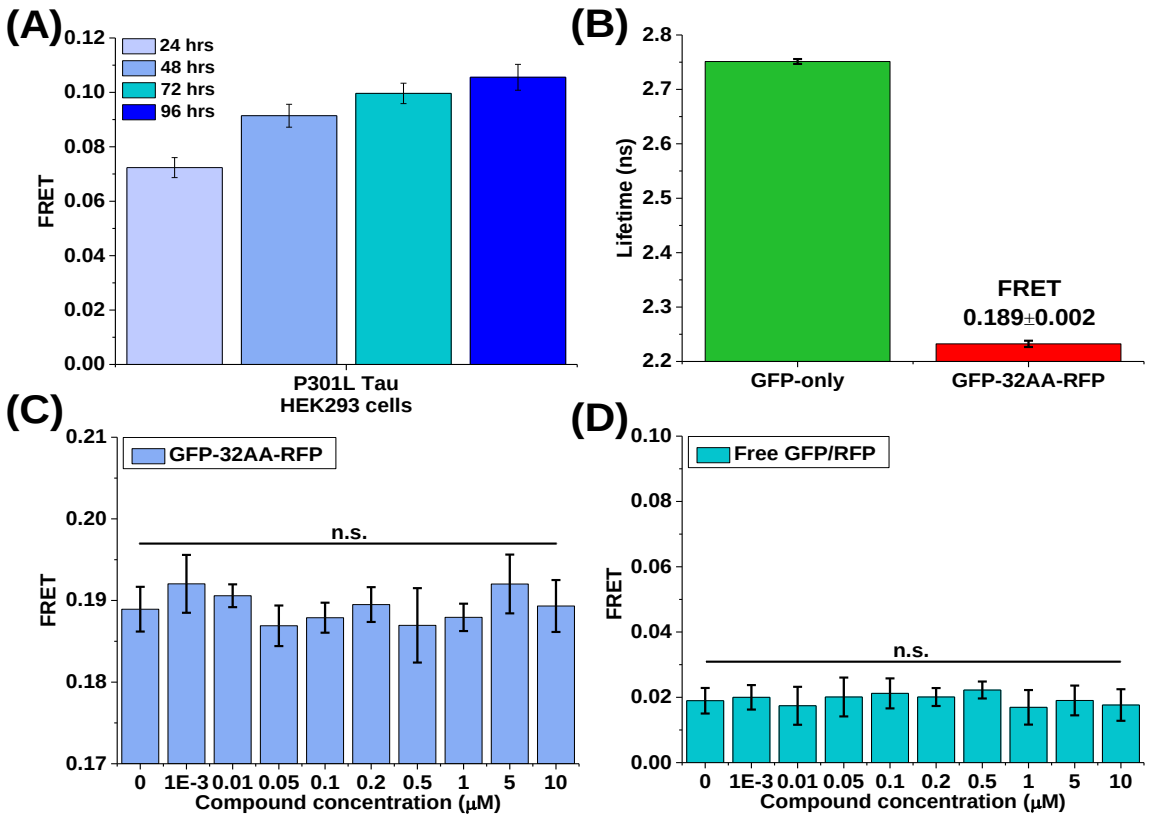

Supplemental Figure 7. 3. Characterization of P301L tau FRET biosensor and the effect of MK-886 on control FRET biosensors.

(A) Kinetic of the FRET measurements for P301L tau FRET biosensor expressed in HEK293 cells. (B) Characterization of the GFP-32AA-RFP (fluorophores-only FRET control) expressing cells indicates FRET. The control FRET biosensor was used to test compound interference with GFP or RFP fluorophores, eliminating non-specific compounds that cause a FRET change in the screen. (C) MK-886 does not cause any significant FRET change in the GFP-32AA-RFP expressing control cells. (D) MK-886 does not cause any significant FRET change in the soluble free GFP/RFP-only expressing control cells. Data are means ± SD of three independent experiments and n.s. indicates not significant by two-tailed unpaired *t* test.

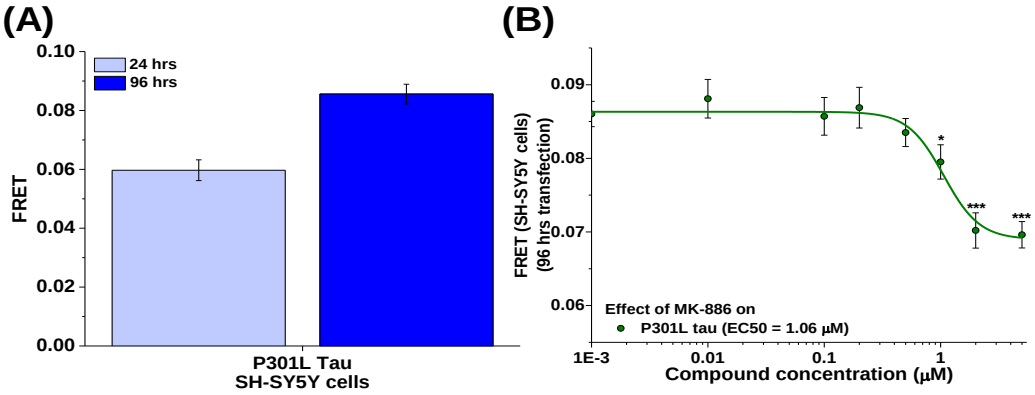

Supplemental Figure 7. 4. Effect of MK-886 on P301L tau FRET biosensor expressed in SH-SY5Y cells.

(A) Kinetic of the FRET measurements for P301L tau FRET biosensor expressed in SH-SY5Y cells. (B) FRET analysis of the dose response of MK-886 in the P301L tau FRET biosensors expressed in SH-SY5Y cells (for 96 hrs) indicates an EC_{50} value of 1.06 μM. Data are means ± SD of three independent experiments. **P* < 0.05 and ****P* < 0.001 by two-tailed unpaired *t* test.

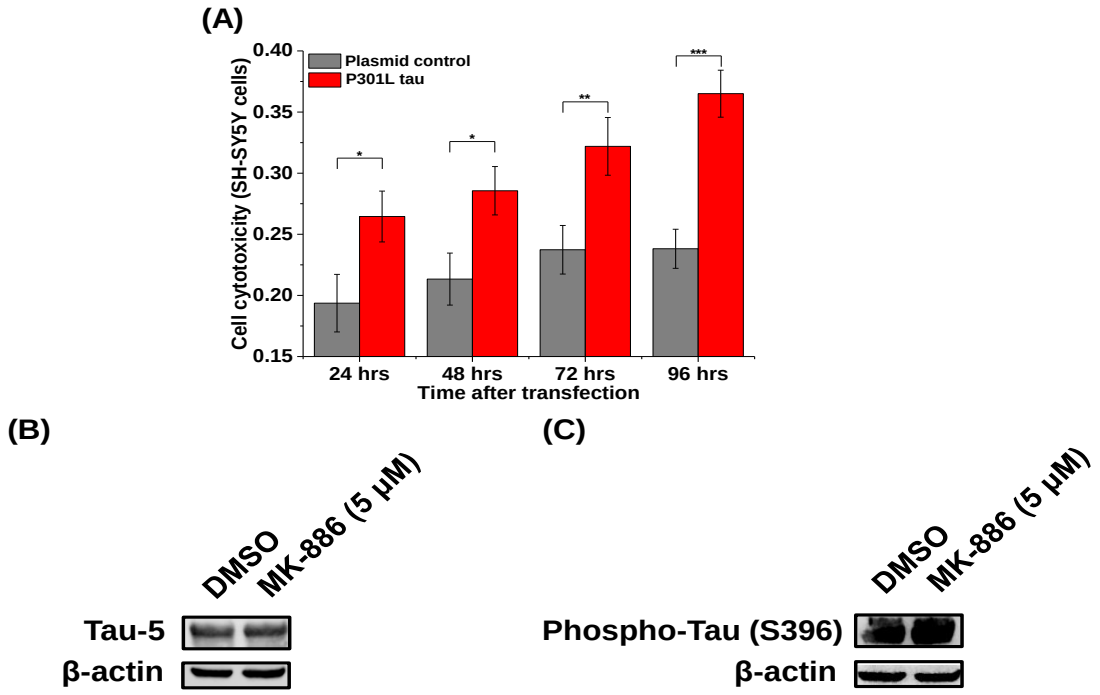

Supplemental Figure 7. 5. Characterization and controls for P301L tau induced cell cytotoxicity assay in SH-SY5Y cells.

(A) Kinetic of the P301L tau induced cell cytotoxicity in SH-SY5Y cells. (B) Effect of MK-886 on the total amount of tau expressed is shown by the Tau-5 antibody staining. (C) Effect of MK-886 on the phosphorylation state Serine 396 of P301L tau expressed in SH-SY5Y cells is shown by the Phospho-Tau S396 antibody. β-actin was used as loading control. Both controls indicate that the rescue of cell death by MK-886 is not due to an indirect mechanism. Data are means ± SD of three independent experiments. *P < 0.05, **P < 0.01 and ***P < 0.001 by two-tailed unpaired t test.

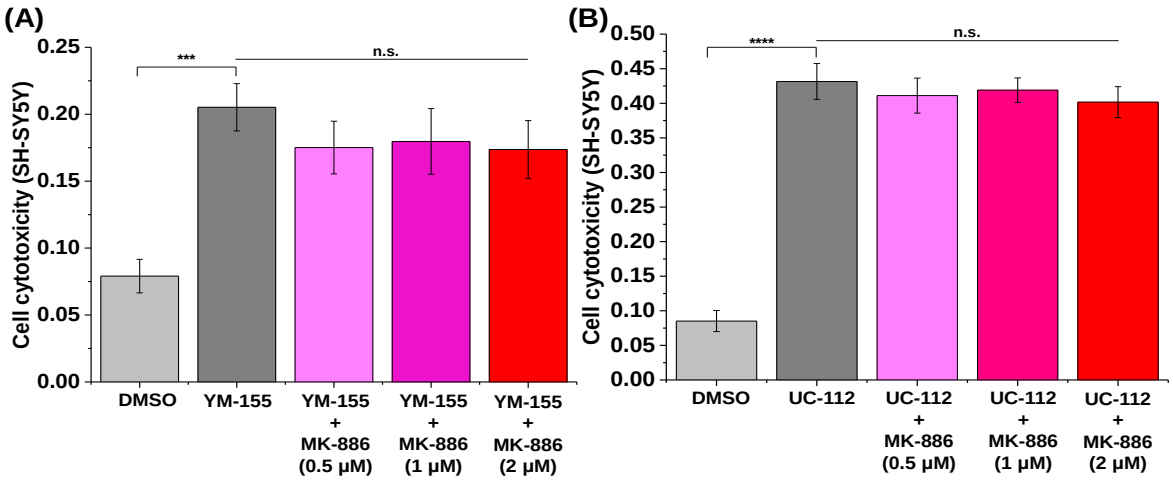

Supplemental Figure 7. 6. Effect of MK-886 on cell cytotoxicity induced by suppressors of survivin, inhibitor of apoptosis proteins (IAPs) or X-linked inhibitor of apoptosis proteins (XIAP).

Both (A) YM-155 and (B) UC-112 induced cell cytotoxicity in SH-SY5Y cells and MK-886 does not rescue any cell death caused by these compounds. Data are means ± SD of three independent experiments. ****P* < 0.001 and *****P* < 0.0001 by two-tailed unpaired *t* test.

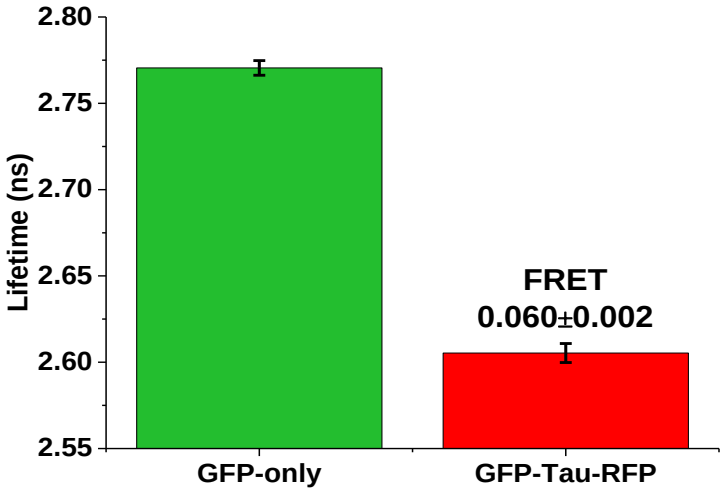

Supplemental Figure 7. 7. Lifetime measurements of the basal FRET of the cellular tau *intra*-molecular biosensor.

The cellular tau *intra*-molecular FRET biosensor shows an efficient basal FRET, illustrating *intra*-molecular interactions arising from the paper-clip monomeric structure where the N and C terminus of tau fold in on each other, bringing the GFP and RFP into close proximity. Data are means ± SD of three independent experiments.

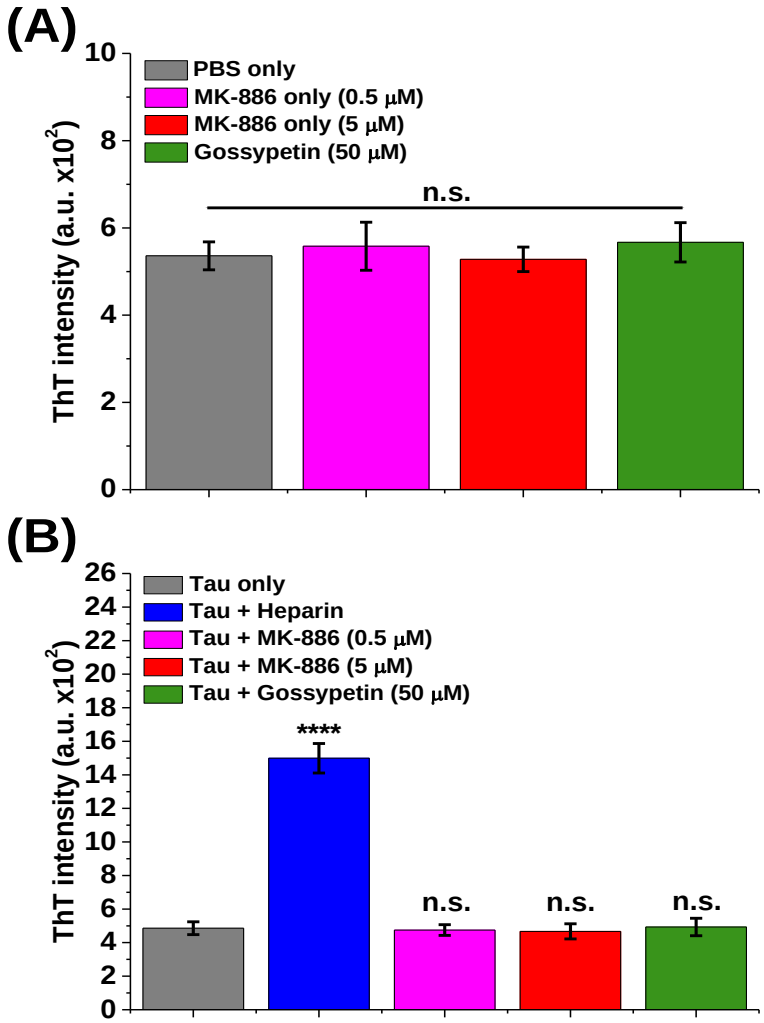

Supplemental Figure 7. 8. Controls for thioflavin-T (ThT) assay with purified WT tau proteins.

(A) MK-886 and gossypetin do not interfere with ThT fluorescence after 72 hours of incubation. (B) MK-886 does not act as a nucleation center for fibril formation after 72 hours of incubation. Only the positive control of heparin shows a significant ThT positive signal. Data are means ± SD

of three independent experiments. ****$P < 0.0001$ and n.s. indicates not significant by two-tailed unpaired *t* test.

CHAPTER 8: SMALL-MOLECULE PERTURBATION OF HUNTINGTIN CONFORMATIONS TO DISRUPT TOXIC AGGREGATE FORMATION IN CELLS

Chih Hung Lo[1], Nitin K. Pandey[2], Colin Kin-Wye Lim[1], Zhipeng Ding[1], Meixin Tao[2], David D. Thomas[3-4], Ralf Langen[2] and Jonathan N. Sachs[1*]

Manuscript to be submitted to *ACS Chemical Neuroscience*

[1]Department of Biomedical Engineering, University of Minnesota, Minneapolis, MN 55455

[2]Zilka Neurogenetic Institute, Keck School of Medicine of USC, Los Angeles, CA 90033

[3]Department of Biochemistry, Molecular Biology and Biophysics, University of Minnesota, Minneapolis, MN 55455

[4]Photonic Pharma LLC, Minneapolis, MN 55410

Author contributions: C.H.L. designed and conducted the experiments. C.K.W.L. and Z.D. contributed to FRET assays and provided assistance to cell-based assays. N.K.P., M.T. and R.L. performed molecular biology, protein purification and the EPR experiments. N.K.P. and R.L. also provided comments and edits to the manuscript. D.D.T. provided expertise on HTS and FRET assays. C.H.L and J.N.S. wrote the manuscript.

8.1. Summary

Huntington's disease (HD) is the most common inherited neurodegenerative disorder and one of the nine polyglutamine (polyQ) diseases characterized by the pathological aggregation of the misfolded huntingtin protein with abnormally long polyQ expansion due to genetic mutation. Recent studies suggest that HD is a conformational disease and perturbing huntingtin protein conformations may be more effective in

targeting the toxic aggregates. To exploit this new therapeutic window, we engineered three FRET based biosensors that monitor the conformations of huntingtin (HTT) exon 1 with different polyQ lengths (Q16, Q39 and Q72) in living cells. These FRET biosensors, together with a high-precision fluorescence lifetime detection platform, enable high-throughput screening of small molecules that target HTT conformations. We found seven small molecules that perturbed HTT conformations and reduced HTT-induced neuronal cell cytotoxicity with submicromolar potency. In addition, these compounds altered FRET in HTT biosensors of shorter polyQ lengths, suggesting that they were acting through perturbing the protein conformations rather than directly binding to the β-sheet aggregates. Using SPR and an advanced EPR technique, we confirmed that the compounds directly bind to both monomeric HTT proteins as well as HTT fibrils and disrupt the protein aggregation. This strategy in targeting the HTT conformations can be applicable to other proteins involved in polyQ diseases.

8.2. Introduction

Huntington's disease (HD) is an inherited neurodegenerative disorder caused by expansion of a CAG repeat in the exon 1 of huntingtin (HTT) gene, which translates into an abnormal polyglutamine (polyQ) in HTT protein (*102, 103*). Despite the past few decades of rigorous and focused research, there are currently no cures or significant disease modifying therapies currently available for Huntington disease (HD) (*103*). Even though clinical trials of potential compounds acting through indirect mechanism (not directly targeting HTT) are imminent, there is currently no ongoing clinical trial of small molecules acting through direct disruption of HTT aggregation, which is still an important area for targeting (*134-136*). In addition, two pivotal trials of potential disease-modifying

agents, coenzyme Q10 and creatine, recently met untimely ends (*136*). Hence, there is a need to discover treatments focusing on targeting HTT aggregation (*325*).

HTT is an intrinsically disordered proteins that regulates fast axonal trafficking, vesicle transport (including transport of brain-derived neurotrophic factor (BDNF)) and synaptic transmission (*105*). It also plays an important role in neurons in the brain and is essential for normal development before birth (*106*). HD is one of the nine neuropathologies caused by an abnormal expansion of CAG repeats, encoding a polyQ stretch in various proteins (*107*). In HD, the expansion occurs at the exon 1 of the IT15 gene of HTT protein. The wild type (WT) protein contains 35 glutamine repeats or less (≤Q35, no pathology) while in the mutant forms the expanded glutamines are more than 35 repeats (Q36-39, late onset; ≥Q40, observed pathology) (*108*). Importantly, the length of the polyQ stretch and the age of disease onset are inversely correlated, with longer stretches resulting in earlier onset and increased severity of the disease (*108-110*). In addition, it has been shown that N-terminal HTT with polyQ tracts in the pathological range (>Q35), but not with polyQ tracts in the normal range (≤Q35), form high molecular weight protein aggregates with a β-sheet fibril morphology(*111*). Mutant HTT protein disrupts many normal physiological processes and leads to unbalanced homeostasis of apoptotic molecules, deficits in autophagy, axonal transport impairment, transcriptional dysregulation, reduced cellular BDNF support, mitochondrial abnormalities, and glutamate excitotoxicity (*116*).

While aggregate formation is the hallmark of HD (*111, 118*), its significance in regard to toxicity remains controversial. It has been suggested that large contained aggregates may form in neurons as a protective response. These prominent inclusion bodies (IBs) have been shown to decrease mutant HTT levels elsewhere in the neuron, prolonging cell survival (*119*). Recently, strong evidence for the toxicity of monomeric

and small oligomeric species of mutant HTT that have adopted specific conformational states has also emerged (*120-130*), but the great majority of cellular studies report on IBs alone and the true toxic species is still unknown (*121, 131-133*).

The molecular details of protein misfolding and aggregation in neurodegenerative disorders may hold the key to therapeutic intervention (*326*). Previous drug discovery effort targeting HTT aggregation has been focusing on direct disruption of the high molecular weight species formed by HTT protein with >Q35 without taking into account HTT conformations (*327*). Recent evidences on small molecules or antibodies modulation of HTT conformations and hence aggregation have suggested a shift in paradigm to target HTT conformations for disruption of aggregates in drug discovery (*152, 328-337*). Specifically, it has been shown in vitro that monomeric HTTex1 proteins adopt similar structural features for both WT and mutant HTT proteins (*335*). In addition, anti-polyQ antibodies have been shown to be able to recognize a common polyQ region in both WT and mutant HTT proteins regardless of the polyQ lengths (*336, 337*). Furthermore, polyQ dependent structuring and rigidification of HTT proteins could be mimicked in HTT with shorter polyQ by a decrease in temperature (*332*). These suggest that besides targeting mutant HTT proteins with pathological polyQ lengths, it may be important to take into account HTT proteins with various polyQ lengths, including WT polyQ lengths, to have a more effective therapeutic targeting strategy. One commonality of the studies above are that they have mostly been done in vitro using purified proteins which do not recapitulate the cellular environment, lacking the numerous chaperone proteins that may be required to produce the ensemble of HTT monomers, oligomers or aggregates. Additionally, purified protein assays are only capable of identifying hits that directly perturb HTT and are wholly naive against indirect mechanism of action.

Here, we shift the HTT aggregation process into the cellular environment, where the ensemble of HTT conformations should more closely recapitulate the distribution of different monomeric, oligomeric or aggregated assemblies. To monitor HTT conformations and discover small molecules that disrupt toxic HTT aggregates, we engineered three distinct fluorescence resonance energy transfer (FRET) biosensors of HTT exon 1 (HTTex1) with different polyQ lengths (Q16, Q39 and Q72) to monitor HTT conformational changes and aggregation. We note that HTT cellular FRET biosensors (Q72 and Q79) have been previously developed and used to measure the extent of HTT aggregation. In this study, we have included both HTTex1 Q16 and Q39 biosensors to study how the conformations of HTTex1 with different polyQ lengths can be perturbed and targeted in different structural states. We used these biosensors in conjunction with a state-of-the-art fluorescence lifetime plate reader (FLT-PR) as a high-throughput screening (HTS) platform for drug discovery (*283*). Fluorescence lifetime detection increases the precision of FRET-based screening by a factor of 30 compared with conventional fluorescence intensity detection (*284*), and provides exquisite sensitivity to resolve minute structural changes within protein ensembles. This sensitivity allows direct detection of conformation changes within an ensemble of oligomers (e.g. conversion from toxic to non-toxic oligomer conformation), the dissociation of oligomers or aggregates, or changes in the ensemble of monomer conformations (*190, 199, 226, 270*). In addition, expression of these biosensors in cells has the added advantage of identifying compounds that act both directly (by binding HTT) and indirectly (through orthogonal biochemical pathways) to modify toxic aggregates.

In this study, we show for the first time that small molecules can target both WT and mutant HTTex1 with different polyQ lengths (Q16, Q39 and Q72) in cells to disrupt toxic HTT aggregate formation and rescue HTT induced cell death. After first

characterizing the expression and FRET signals of the biosensors with different structural states, we performed HTS of the library of pharmacologically active compounds (LOPAC) and identified seven small molecules that directly binds HTT and strongly attenuates FRET with EC_{50} values at a range of 0.040-5 μM. All compounds rescue HTTex1-Q72 induced cell cytotoxicity with the most potent compound having an IC_{50} of 0.25 μM. To elucidate the mechanism of action, we tested the effects of compounds in the all HTTex1 FRET biosensors of different polyQ lengths to see if they perturb the biosensors differently. In addition, we also tested the binding affinity of the compounds to both monomers and β-sheet fibrils using SPR and we observed that some compounds preferentially bound to purified monomeric HTTex1 proteins while some bound preferentially to β-sheet fibrils. Furthermore, we used an advanced electron paramagnetic resonance (EPR) technique to show that all compounds, except one, disrupted HTT aggregation in both unseeded and seeded fibrillization. All these data imply that the compounds are perturbing a common region of the HTTex1 proteins but with different binding affinity to the monomeric or β-sheet conformations of HTTex1, leading to structural changes and disruption of aggregates, hence defining a new therapeutic approach to targeting toxic HTT aggregates.

8.3. Materials and methods

8.3.1. Molecular biology

To generate HTTex1-polyQ-GFP and HTTex1-polyQ-RFP with polyQ of Q16, Q39 and Q72, cDNA encoding the conserved region of the human HTT protein N-terminus (17 amino acids before polyQ and 50 amino acids after polyQ) with different polyQ lengths fused to the N-terminus of EGFP and TagRFP vectors. The unlabeled

HTTex1-Q72 was generated without the fusion fluorescent proteins. All constructs contain the monomeric mutation A206K to prevent constitutive fluorophore clustering (*204*).

8.3.2. Cell culture and generation of cellular FRET biosensors

HEK293 and N2a cells (ATCC) were cultured in phenol red-free Dulbecco's Modified Eagle Medium (DMEM, Gibco) supplemented with 2 mM L-Glutamine (Invitrogen), heat-inactivated 10% fetal bovine serum (FBS HI, Gibco), 100 U/ml penicillin and 100 μg/ml streptomycin (Gibco). Cell cultures were maintained in an incubator with 5% CO_2 (Forma Series II Water Jacket CO_2 Incubator, Thermo Scientific) at 37 ºC. The intermolecular HTTex1 FRET biosensors were generated by transiently transfecting HEK293 cells using Lipofectamine 3000 (Invitrogen) with HTTex1-polyQ-GFP and HTTex1-polyQ-RFP (polyQ = Q16, Q39 or Q72; 1:20 DNA plasmid concentration ratio). The effectiveness of HEK293 cells transfected with FRET constructs as a HTS platform has been demonstrated in our previous work (*190, 226*). The HTTex1-Q72 FRET biosensor expressed in N2a cells was generated by transiently transfecting N2a cells using Lipofectamine 3000 (Invitrogen) with HTTex1-Q72-GFP and HTTex1-Q72-RFP (1:20 DNA plasmid concentration ratio).

8.3.3. Pilot screening with LOPAC library

The library of pharmaceutically active compounds (LOPAC), containing 1280 compounds, was purchased from Evotec (Hamburg, Germany), formatted into 96-well mother plates using an FX liquid dispenser, and formatted across three 384-well plates at 50 nL (10 μM final concentration/well) using an Echo liquid dispenser. DMSO (matching %v/v) was loaded as in-plate no-compound negative controls. The 384-well flat, black-bottom polypropylene plates (PN 781209, Greiner Bio-One) were selected as the assay plates for their low autofluorescence and low interwell cross talk. The plates

were sealed and stored at −20 °C until use. Two days prior to screening, HEK293 cells were transfected using Lipofectamine 3000 with HTTex1-polyQ-GFP/RFP (HTTex1-polyQ FRET biosensor) in 15 x 100 mm plates (5 x 10^6 cells/plate). On each day of screening, the compound plates were equilibrated to room temperature (25 °C). The cells were harvested from the 100 mm plates by incubating with TrypLE (Invitrogen) for 5 min, washed three times in PBS by centrifugation at 300 g and filtered using 70 µm cell strainers (BD Falcon). Cell viability, assessed using a trypan blue assay, was >95%. Cells were diluted to 1 million cells/ml using an automated cell counter (Countess, Invitrogen). Expression of HTTex1-polyQ-GFP/RFP (HTTex1-polyQ FRET biosensor) was confirmed by fluorescence microscopy prior to each screen. After resuspension and dilution in PBS, the biosensor cells were constantly and gently stirred using a magnetic stir bar at room temperature, keeping the cells in suspension and evenly distributed to avoid clumping. During screening, cells (50 µl/well) were dispensed by a Multidrop Combi Reagent Dispenser (Thermo Fisher Scientific) into the 384-well assay plates containing the compounds and allowed to incubate at room temperature for 2 hours before readings were taken by the fluorescence lifetime plate reader (FLT-PR, Fluorescence Innovations, Inc) as described previously (*190, 226*).

8.3.4. HTS data analysis

As described previously (*190, 226*), time-resolved fluorescence waveforms for each well were fit with single-exponential decays using least-squares minimization global analysis software to give donor-acceptor lifetime (τ_{DA}) and donor-only lifetime (τ_D). FRET efficiency (*E*) was then calculated based on Equation 1.

$$E = 1 - \left(\frac{\tau_{DA}}{\tau_D}\right) \quad Eq.1$$

Assay quality was determined with the lead compound (niclosamide) as positive control and DMSO as a negative control and calculated based on Equation 2 (*192*),

$$Z' = 1 - \frac{3(\sigma_p + \sigma_n)}{|\mu_p - \mu_n|} \; Eq. 2$$

where σ_p and σ_n are the standard deviations (SD) of the observed τ_{DA} values, and μ_p and μ_n are the mean τ_{DA} values of the positive and negative controls. To make this metric less sensitive to strong outliers, we utilized the normalized median absolute deviation (1.4826*MAD) and median in place of the standard deviation and mean, respectively (*193*).

Fluorescent compounds were flagged as potential false positives due to interference from compound fluorescence by a set of stringent fluorescent compound filters based on analysis of the spectral waveforms of each well from the NCC screen (*190, 226*). After removal of fluorescent compounds, a histogram of the FRET distribution from all compounds in the screen was plotted and fit to a Gaussian curve to obtain the mean (μ) and standard deviation (σ, SD). A hit was defined as a compound that decreased the FRET efficiency by more than five times the standard deviation (5σ or 5SD) relative to the mean μ. Seven reproducible hits from all screens, niclosamide, 10058-F4, AMG9810, TNP, rottlerin, TBB and dihydroergotamine mesylate (DMS) were purchased (Millipore Sigma).

8.3.5. FRET dose-response assay

The reproducible hit compounds from all screens were dissolved in DMSO to make a 10 mM stock solution, which was serially diluted in 96-well mother plates. The hit compounds were screened at nine different concentrations (1 nM to 10 μM). Compound (1 μl) was transferred from the mother plates into assay plates using a Mosquito HV liquid handler (TTP Labtech Ltd, UK). The preparations for HTTex1-polyQ-GFP/RFP

FRET biosensors (polyQ = Q16, Q39 or Q72) and FRET measurements were carried out similar as above.

8.3.6. Cell cytotoxicity assay

Cell cytotoxicity was measured using the CytoTox-Glo (Promega Corporation) luminescence assay kit. N2a mouse neuroblastoma cells were plated at a density of 5 x 10^6 cells/plate in 100 mm plate (Corning) and transfected with unlabeled HTTex1-Q72 or equivalent vector-only control for 24 hours. The transfected cells were then plated at a density of 5000 cells/well in white solid 96-well plate (Corning) with a total volume of 100 μl, followed by treatment with hit compounds at a dose dependent manner of seven different concentrations (1 nM to 1 μM) or single dose at 0.2 μM, as well as DMSO-only controls, for another 72 hours. After incubation, 50 μl of CytoTox-Glo Cytotoxicity Assay Reagent was added to all wells followed by mixing by orbital shaking and incubation for 15 minutes at room temperature. The first luminescence reading was measured using a Cytation3 Cell Imaging Multi-Mode Reader luminometer (BioTek). 50 μl of Lysis Reagent was then added, followed by incubation at room temperature for 15 min, and luminescence was measured again using the luminometer. Cell cytotoxicity was calculated following the manufacturer protocol.

8.3.7. Thioflavin-S (ThS) assay

HEK293 cells were transfected with HTTex1-polyQ-RFP (polyQ = Q16, Q39 or Q72 at equivalent DNA concentration as used in the HTTex1 FRET biosensor) for 48 hours. HTTex1-polyQ-GFP was not used, as it would interfere with the ThS signal. Thioflavin-S (ThS, Millipore Sigma, product no. T1892) was dissolved in PBS buffer and was filtered through a 0.2 μm syringe filter to make a stock solution of 2.5 mM. For the ThS assay, cells were fixed with 1 ml of 4% paraformaldehyde in TBS for 15 minutes

followed by washing with 1 ml of TBS for 5 minutes twice. After fixing, cells were permeabilized with 1ml of 1% Triton in TBS for 5 minutes, followed by washing with 1ml of TBS for 5 minutes twice. After permeabilization, cells were then treated with 0.002% ThS in TBS and incubate in the dark for 20 minutes. Cells were then washed twice with 50% ethanol for 10 minutes each and finally washed twice with TBS for 5 minutes each. Cells were then imaged with a fluorescence microscope using EVOS-FL cell imaging systems at 20X magnification. Mean fluorescence intensity for each image was quantified using ImageJ and values were normalized to untransfected controls.

8.3.8. Expression, purification of Httex1-Q46 monomer and fibril preparation

The thioredoxin (Trx) fused HTTex1-Q46 protein was expressed and purified as described previously (Pandey et al., JBC, 2018; Isas et al., Biochemistry, 2015). Briefly the cultures of pET32a-Httex1 (Q46) transformed BL21 cells were grown at 37 °C for 4h hour and were further inoculated in a 50-fold access of LB Media and allowed to grow to A_{600nm}=0.7-0.8 at 37 °C. The expression was induced overnight using 1 mM isopropyl1-thio-β-D-galactopyranoside (IPTG) at 18 °C. The successive protein purification was achieved using Nickel affinity chromatography followed by ion exchange chromatography. The biotinylation/spin labeling was achieved by reacting the protein harboring desired cysteine mutation with maleimide-PEG11-biotin (Thermo Fisher) / MTSL spin label (Toronto Research Chemicals) post Ni affinity step and excess spin label was removed using ion exchange chromatography.

Fibrils were prepared by overnight incubation of HTTex1-Q46 fusion protein at 25µM concentration (with desired percentage of biotin label) with EKMax (Invitrogen) to remove fusion tag (Trx) at 4 °C, in the presence of 1% molar ratio of (Q46) seeds. The fibrils were harvested by using bench top centrifuge (Eppendorf) at 15000 rpm. The quality of fibrils was confirmed using JEOL JEM-1400 transmission electron microscope.

8.3.9. Surface plasmon resonance (SPR) binding assay

Binding affinity between HTTex1-Q46 monomer or β-sheet fibril and the hit compounds was determined by SPR analysis using BIAcore S200. Recombinant HTTex1-Q46 monomer or β-sheet fibril was immobilized on the CM5 sensor chip (Biacore, GE Healthcare) via amine coupling. Briefly, the dextran surface was activated with a 1:1 mixture of 0.4 M 1-ethyl-3-(3-dimethylaminopropyl)carbodiimide hydrochloride and 0.1 M N-hydroxysuccinimide. HTTex1-Q46 proteins (20 μg/ml) in 10 mM sodium acetate at pH 5.0 was flowed past a working surface before blocking the remaining activated carboxymethyl groups with 1 M ethanolamine at pH 8.5 to achieve a level of 1200 RU suitable for binding analysis. The reference surface was activated and reacted with only ethanolamine.

For direct binding assays to the HTTex1-Q46 protein, hit compounds at eight different concentrations (0.1 μM to 200 μM), as well as DMSO-only controls, were prepared in HEPES-EP containing a total of 2% DMSO. The samples were injected over both the reference and HTTex1-Q46 monomer or β-sheet fibril immobilized surfaces at 10 μl/min for 180 seconds and dissociated in glycine-HCl pH 2.5. All the samples, along with blanks from buffer and DMSO-only controls, were measured on a 96-well microplate (Biacore, GE Healthcare) at 25 °C. Reflectivity response data points were extracted from response curves at 5 seconds prior to the end of the injection to determine steady-state binding. All the data were double referenced with blanks using standard procedures with Biacore S200 Evaluation Software v1.0.

8.3.10. Continuous Wave (CW)-electron paramagnetic resonance (EPR) measurements

The R1 spin labeled HTTex1-Q46 at 35 position (reporter for structural changes in polyQ site) was prepared by following the previously established protocol ((Pandey et al., JBC, 2018). Briefly the fusion tag (Trx) was removed using EKMax (Invitrogen) and the clean seed-free 35R1 derivative of HTTex1-Q46 was purified using reversed phase chromatography (Phenomenex, C4 column). The lyophilized powder was treated with 0.5% TFA (v/v) in methanol to disaggregate any pre-existing oligomers and the organic was removed under the gentle stream of N_2 gas. The resultant film was reconstituted in the 20 mM phosphate, 150 mM NaCl pH 7.4 buffer (with desired percentage of DMSO) in the absence and presence of compounds.

The resulting samples were loaded into boro glass tubing and the EPR spectra were acquired using a X-band Bruker EMX spectrometer attached with a Bruker ER4119HS resonator. The scan width and the incident power for all the measurements were fixed to 100 Gauss and 12.7 milliwatts, respectively.

The percentage of inhibition was estimated by comparing the change in EPR signal amplitude of R1 spin labeled HTTex1-Q46 in the presence of small molecules to that of protein alone at the desired time point during the HTTex1-Q46 misfolding kinetic study.

8.3.11. Statistical analysis

Data are shown as mean ± standard deviation unless stated otherwise. Statistical analysis was performed by a two-tailed unpaired *t* test (Student's *t* test) using GraphPad Software to determine statistical significance for all experiments. Values of $P < 0.05$ were considered statistically significant. GraphPad style in using asterisks to denote *P* values

in figures was used (*P < 0.05, **P < 0.01, ***P < 0.001, ****P < 0.0001 and n.s. indicates not significant).

8.4. Results

8.4.1. Intermolecular FRET biosensor directly monitors conformational changes in huntingtin (HTT) oligomers and aggregates in cells

To develop a cell-based HTS platform that can detect small-molecule perturbation of HTT conformational states or disruption of HTT aggregates, we engineered three HTT FRET biosensors expressed in living cells (**Fig. 7.1A**). We used HEK293 cells expressing HTTex1 with different polyglutamine (polyQ) lengths of Q16, Q39 or Q72 fused to green (GFP) or red fluorescent proteins (RFP) (HTTex1-(polyQ)-GFP/RFP or HTTex1-(polyQ) FRET biosensors). The three different polyQ lengths were used as HTTex1-Q16, which is typically the non-mutant form of the protein, is known to form mostly monomers or oligomers and not the β-sheet aggregates(*338, 339*). On the other hand, HTTex1-Q39 and -Q72 are known to form β-sheet aggregates with increasing propensity of aggregation with longer polyQ length(*339*). While three different polyQ lengths were used in this study, we want to be clear that our primary goal was to focus on discovering small molecules that target the diseased states caused by HTTex1 aggregation of polyQ length >Q35, with main focus on the HTTex1-Q72 FRET biosensor. Expression and homogeneity of the FRET biosensor were determined by fluorescence microscopy. Fluorescence microscopy images showed that the HTTex1-Q16 proteins were evenly distributed in the cytosol of the cells, with no discernable puncta or other non-uniformities while more distinct puncta was formed in both HTTex1-Q39 and -Q72 which indicated more progressive aggregation and β-sheet aggregate formation (**Fig. 8.1B** and **Supplementary Fig. 8.1A**).

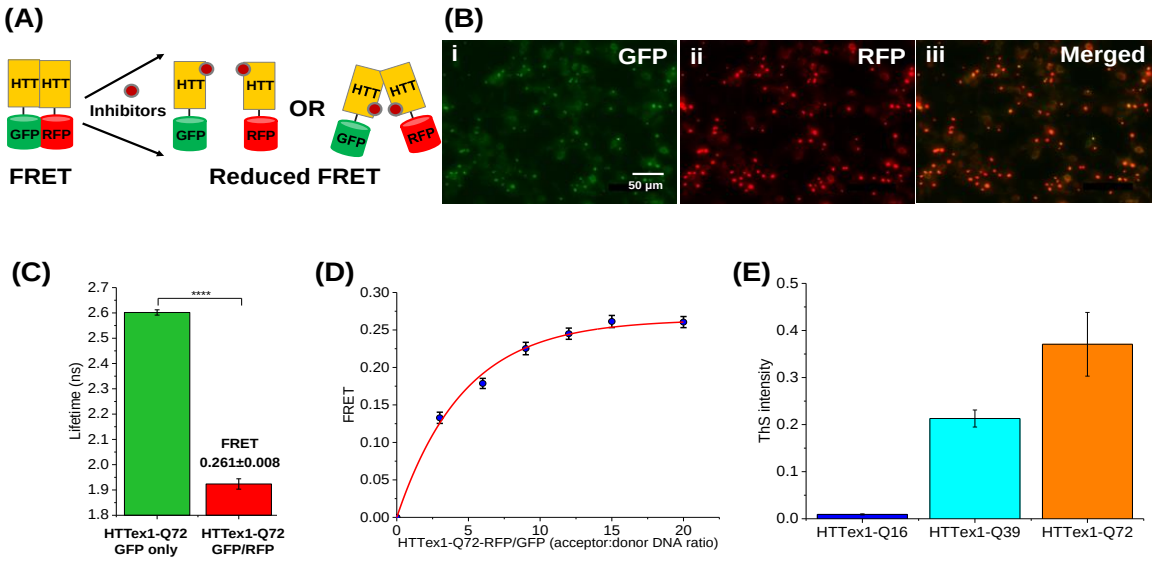

Figure 8. 1. The huntingtin (HTT) intermolecular FRET biosensor and fluorescence lifetime technology enables direct monitoring of HTT aggregation in cells.

(A) Schematic representation of live-cell based HTT intermolecular FRET biosensor. FRET signal is observed when HTT aggregates form, which is modulated by small-molecule inhibitors. HTT aggregate is drawn as a dimer for illustration but it can be more than a dimer (≥2-mers). (B) Fluorescence microscopy images of HEK293 cells expressing HTTex1-Q72-GFP/RFP (HTTex1-Q72 FRET biosensor). (i) GFP channel, (ii) RFP channel, (iii) merged channel showing the presence of both HTTex1-Q72-GFP and HTTex1-Q72-RFP colocalized in the cells. (C) Fluorescence lifetime measurements of the HTTex1-Q72 biosensor show efficient FRET, indicating HTTex1-Q72 aggregation. (D) Titration of HTTex1-Q72-RFP (acceptor) to HTTex1-Q72-GFP (donor) illustrates that the FRET efficiency of the biosensor follows a hyperbolic dependence on acceptor concentration. (E) Quantification of thioflavin-S (ThS) staining of HEK293 cells expressing HTTex1-RFP of various polyglutamine length (Q16, Q39 and Q72) in same total DNA concentration as used in the FRET biosensor (Supplementary Fig. 2). Data are means ± SD of three independent experiments. ****$P < 0.0001$ by two-tailed unpaired *t* test.

We next tested the functionality of the HTTex1 biosensors by measuring FRET efficiency using the fluorescence lifetime plate reader (FLT-PR)(*283*). The FRET efficiency reflects the average of the ensemble intermolecular proximity between HTTex1 molecules, which is derived from the distance between the donor and acceptor fluorophore fused to the proteins. Lifetime measurements between HTTex1-GFP (donor) and HTTex1-RFP (acceptor) for all Q16, Q39 and Q72 in live cells showed a substantial decrease in the donor fluorescence lifetime in the presence of the acceptor, indicating efficient FRET which increased with longer polyQ length and recapitulating the increased propensity of aggregation (**Fig. 8.1C** and **Supplementary Fig. 8.1B**). In addition, FRET observed illustrated a hyperbolic dependence on acceptor concentration with a maximum energy transfer efficiency (E) of 0.261±0.008 (**Fig. 8.1D**) in HTTex1-Q72 FRET biosensor. Furthermore, our previous study showed that a negative control of expression of free soluble GFP and RFP in cells at the same DNA concentrations as the HTTex1 FRET biosensor showed a very low FRET efficiency of 0.019±0.004 between free soluble GFP and RFP(*199*). This indicated that FRET observed from cells expressing HTTex1 FRET biosensor arises from specific HTTex1 self interactions and not from nonspecific interactions between the free fluorophores.

To further confirm the species of HTTex1 (oligomers or β-sheet aggregates) present in the HTTex1 biosensor cells, we performed a thioflavin-S (ThS) assay in cells expressing HTTex1-RFP at the same concentration of HTTex1-GFP/RFP dual transfected cells (HTTex1-GFP was not used as it will interfere with the ThS signal which is green in fluorescence). Results from the ThS assay illustrate that the cells expressing HTTex1-Q16 did not show a ThS signal, similar to that of the untransfected cells, while cells expressing HTTex1-Q39 and -Q72 illustrated increasing ThS positive ThS signal (**Fig. 8.1E** and **Supplementary Fig. 8.2**). This confirms that the observed FRET from

HTTex1-Q16 FRET biosensor is mainly the result of oligomers formation and the observed FRET from HTTex1-Q39 and -Q72 are from β-sheet aggregates formation. The combination of these cellular FRET biosensors and time-resolved FRET detection provides a powerful platform that is sensitive to identify novel compounds that modulate the ensemble of conformationally distinct HTTex1 species (monomers, oligomers or β-sheet aggregates).

8.4.2. Identification of novel small molecules from HTS of the LOPAC library that perturb the conformational ensembles of HTTex1 oligomers and aggregates

Using our cellular HTTex1 FRET biosensors, we performed a HTS of the library of the pharmaceutically active compounds (LOPAC: 1280 bioactive compounds) to identify compounds that perturb the conformational ensembles of HTTex1 oligomers or disrupt the β-sheet fibril aggregates. After an initial quality control check of the cells expressing the HTTex1 FRET biosensors (Q16, Q39, Q72) on each day of screening (fluorescent waveform signal level and coefficient of variance), the cells were dispensed into drug plates and incubated with the compounds (10 μM) or DMSO control wells for 2 hours. Lifetime measurements were acquired with the FLT-PR. A single-exponential fit was used to determine the lifetime from cells expressing the HTTex1 FRET biosensors (τ_{DA}) or expressing a HTTex1-GFP donor-only control (τ_D) to determine FRET efficiency (Eq. 1). As fluorescence lifetime measurements are prone to interference from fluorescent compounds, a stringent fluorescent compound filter was used to flag fluorescent compounds as potential false-positives in all screens due to interference from compound fluorescence (*190, 226*). FRET efficiency from all compounds that passed the fluorescent compound filter are plotted and a histogram of the FRET

distribution from these compounds was fit to a Gaussian curve to obtain a mean and standard deviation (SD) for all the three screens (**Supplementary Fig. 8.3A-F**).

Our initial goal was to discover compounds that both directly disrupt HTTex1 aggregates or alter the conformational ensembles of HTTex1 oligomers with the potential of disrupting HTTex1 aggregation, leading us to focus our search to compounds that reduce FRET (though other compounds that increase FRET could potentially remodel toxic oligomers and be of interest in future studies). Seven reproducible hits from the library were obtained from the separate screens with the three different FRET biosensors that decreased FRET by more than 3SD below the mean of all wells and illustrated dose-dependent FRET reduction in all biosensors (**Fig. 8.2A**).

(A)

Hits that illustrate dose-dependent FRET reduction			
Q72–Hits	Q39–Hits	Q16–Hits	Cpd name
1171	1171	1171	Niclosamide
-	331	331	10058-F4
796	796	796	AMG 9810
495	-	-	TNP
-	-	744	Rottlerin
1090	1090	1090	TBB
-	273	273	DMS

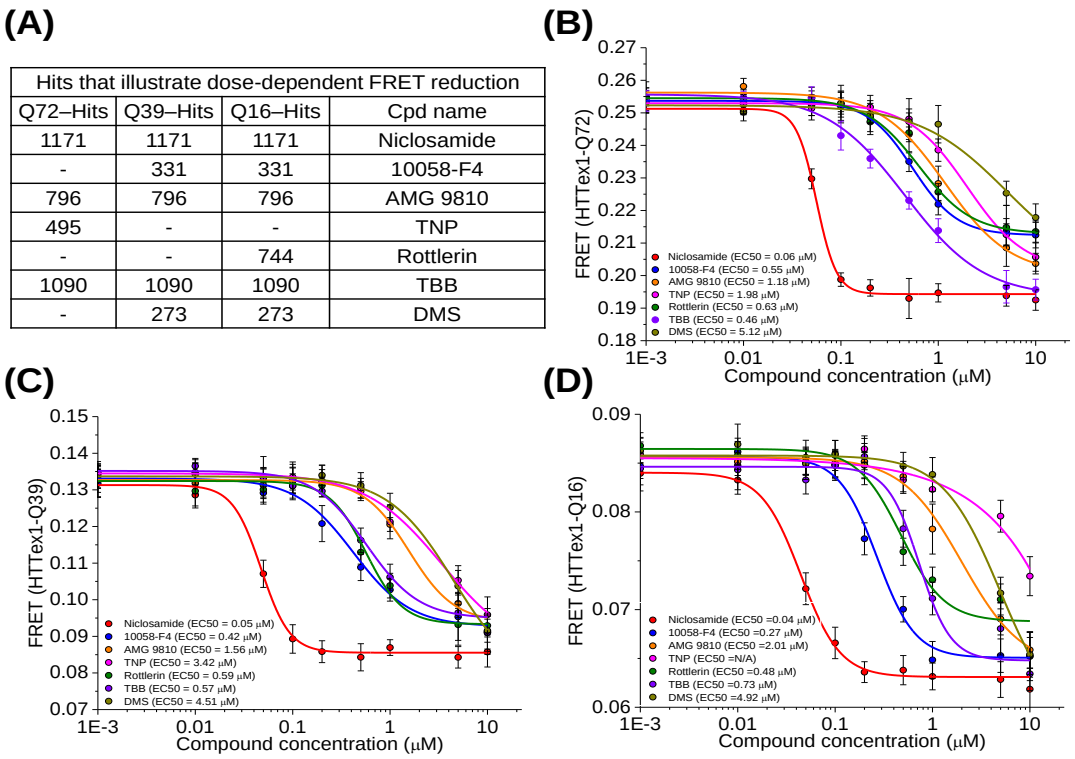

Figure 8. 2. Small-molecule inhibitors of HTTex1 aggregation obtained from high-throughput screening (HTS) of LOPAC library using HTTex1 FRET biosensors (Q16, Q39 and Q72).

(A) Hit compounds obtained from all screens using FRET biosenors with different polyQ lengths (Q16, Q39 and Q72). (B-D) FRET dose-response assays with hit compounds which produced a dose-dependent FRET reduction in (B) HTTex1-Q72, (C) HTTex1-Q39 and (D) HTTex1-Q16 FRET biosensors. Data are means ± SD of three independent experiments.

8.4.3. FRET dose-response of hit compounds with HTTex1 FRET biosensors

Since the hits compounds were selected from different FRET biosensors, we wanted to test their effects in all three biosensors. The relative effective concentration (EC_{50}) of the hit compounds was determined by in-cell FRET measurements using the HTTex1 FRET biosensors with Q16, Q39 and Q72. Surprisingly, all compounds decreased FRET efficiency in all biosensors in a dose-dependent manner (**Fig. 8.2B-D**), with EC_{50} range from of 0.040 to 5 μM. Since the compounds reduced FRET in all biosensors, this suggests that the hit compounds may be targeting common structures or regions that have high homology in all polyQ lengths (*335, 340*).

Assay quality (*Z´*) was determined using niclosamide the best hit compound (Eq. 2). The *Z´* values for different FRET biosensors were 0.71±0.03 (HTTex1-Q72), 0.66±0.02 (HTTex1-Q39), 0.52±0.02 (HTTex1-Q16) which indicate excellent assay quality, validating niclosamide as a positive control tool-compound for targeting HTTex1 oligomers and aggregates.

8.4.4. Hit compounds rescue HTTex1-Q72 induced cell cytotoxicity in N2a cells with nanomolar potency

We next tested the effect of hit compounds on HTT induced cytotoxicity in the N2a cell model which was known to cause cell death(*341*). Overexpression of unlabeled HTTex1-Q72 showed significantly greater cell death when compared to the vector control (**Fig. 7.3A**). Five compounds rescued cell death in a dose-dependent manner

with IC_{50} values ranging from 0.2-0.5 μM (**Fig. 8.3B**) while other two compounds exhibited toxicity at concentration above 0.2 μM. We then tested all compounds at a single dose of 0.2 μM for comparison of their relative potency. All compounds, except TNP and DMS, rescued of HTTex1-Q72 induced cytotoxicity at 0.2 μM (**Fig. 8.3C**). We note that our best compound, niclosamide, again has one of the largest rescue of cell cytotoxicity at 0.2 μM of concentration, comparable to 10058-F4 and rottlerin. To confirm that the rescue of cytotoxicity arises from disruption of HTTex1-Q72 aggregates, we then moved on to test the effects of all the compounds in the HTTex1-Q72 FRET biosensors expressed in N2a cells (**Supplementary Fig. 8.4A**). Treatment of all the hit compounds at their maximum effective doses illustrated significant FRET reduction of the HTTex1-Q72 biosensor (**Supplementary Fig. 8.4B**), supporting that the observed rescue of cytotoxicity was from the disruption of HTTex1-Q72 aggregates. The IC_{50} values of hit compounds in the cell cytotoxicity assay were at similar magnitude as the EC_{50} observed from the FRET assays. The slight differences are likely due to the different treatment conditions as well as labeled vs unlabeled HTTex1-Q72 proteins expressed in cells

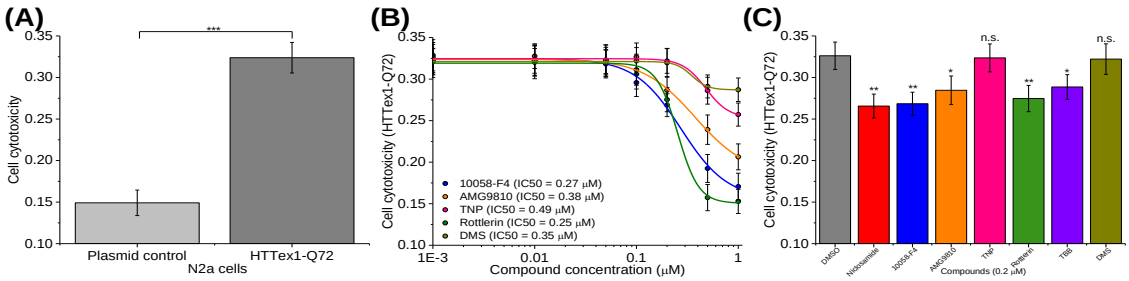

Figure 8. 3. Inhibition of HTTex1-Q72 induced cell cytotoxicity in N2a cells by hit compounds.

(A) N2a cells were transfected with vector control and unlabeled HTTex1-Q72. Significant cell death is observed in cells transfected with HTTex1-Q72 as compared to the vector control. (B) Hit

compounds (10058-F4, AMG9810, TNP, rottlerin and DMS) rescued HTTex1-Q72 induced cytotoxicity in N2a cells in a dose-dependent manner with submicromolar potency. (C) Comparison of the functional effects of all the hit compounds at 0.2 μM. Data are means ± SD of three independent experiments. *P < 0.05, **P < 0.01, and ***P < 0.001 by two-tailed unpaired t test.

8.4.5. Binding of hit compounds to purified HTTex1-Q46 monomers or fibrils

To determine if these seven hit compounds directly act on HTTex1 or modulate HTTex1 FRET by acting through an indirect pathway, we measured the binding affinity for each of the seven hit compounds to purified recombinant HTTex1-Q46 proteins as monomers or fibrils using surface plasmon resonance (SPR). SPR measurements were carried out by immobilizing purified HTTex1-Q46 monomers or fibrils onto the SPR chip followed by compounds flowing through the chip to allow for binding. All the seven hits demonstrated dose-dependent binding to purified HTTex1-Q46 monomers (**Fig. 8.4A** and **Supplementary Fig. 8.5A-G**) and fibrils (**Fig. 8.5B** and **Supplementary Fig. 8.6A-G**). Interestingly, five of the seven compounds illustrated significantly different binding affinity to monomers or fibrils, indicating their preferential binding to a particular species. In particular, this is consistent with how the hits were selected from the screens. Hits that showed better binding affinity to monomers were primarily discovered by HTTex1-Q16 and -Q39 FRET biosensors while hits that illustrated better binding affinity to fibrils were discovered by HTTex1-Q72 FRET biosensors. Even though all compounds showed a common outcome of dose-dependent FRET decrease in the biosensors, it is important to note that they may be perturbing the biosensors through interacting with different species (monomers, oligomers or fibrils).

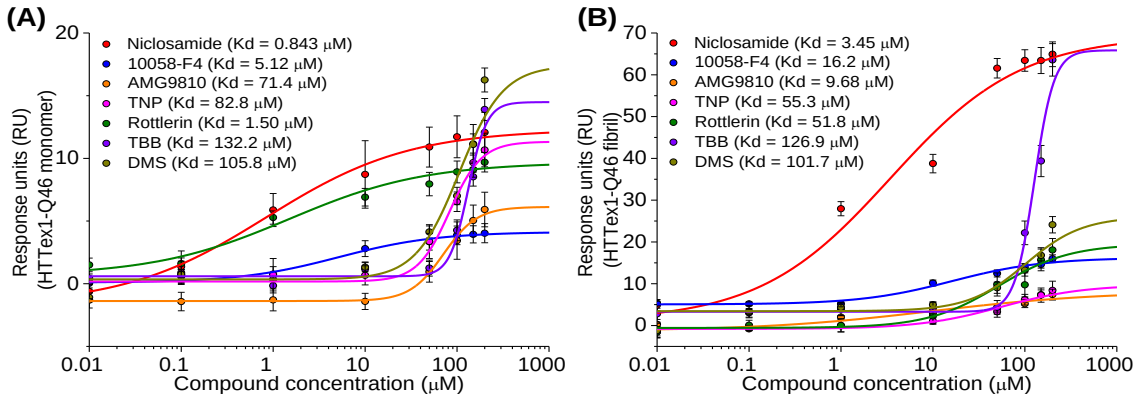

Figure 8. 4. Binding of hit compounds to purified HTTex1-Q46 monomer or fibril.

Surface plasmon resonance (SPR) characterization of binding of hit compounds to (A) HTTex1-Q46 monomer or (B) HTTex1-Q46 fibril. Data are means ± SD of three independent experiments.

8.4.6. The small-molecule inhibitors disrupt both unseeded and seeded aggregation of HTTex1-Q46 protein through EPR

To further investigate if the hit compounds inhibited HTT aggregation, we used electron paramagnetic resonance (EPR) to examine the effect of hit compounds on both unseeded and seeded aggregation of HTTex1-Q46 protein. Using HTTex1-Q46 spin labeled at position 35, we monitored the misfolding of HTTex1-Q46 in the absence and presence of hit compounds and in both unseeded (**Supplementary Fig. 8.7A-B**) and seeded conditions (**Supplementary Fig. 8.7C-D**). The EPR results showed that the addition of hit compounds (20 μM), except TBB, led to inhibition of HTTex1-Q46 misfolding or aggregation in both unseeded (**Fig. 8.5A**) and seeded (**Fig. 8.5B**) conditions. Since the binding affinity of TBB was shown by SPR to be ~130 μM, it is consistent that we did not observe disruption of HTT aggregation at 20 μM of the compound. These results, in combination with the changes in FRET and reduction of HTTex1-Q72 induced cytotoxicity, suggest that the hit compounds alter the

conformational ensemble of HTT monomers, oligomers or aggregates, hence leading to the inhibition of HTT aggregation.

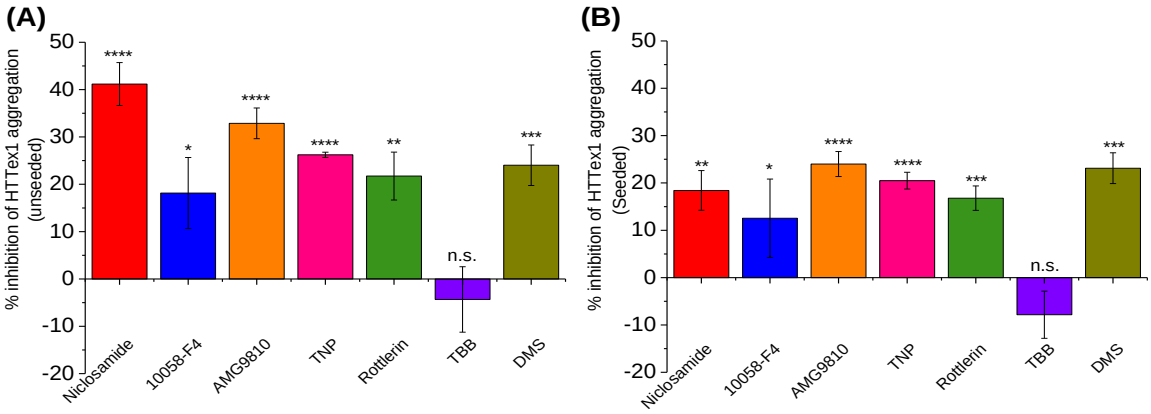

Figure 8. 5. Disruption of HTTex1-Q46 aggregation by hit compounds.

Electron paramagnetic resonance (EPR) characterization of disruption of HTex1-Q46 aggregation of hit compounds in (A) unseeded and (B) seeded conditions. HTTex1-Q46 was spin labeled at position 35 and the aggregation assays, both unseeded and seeded, were tested in the absence (DMSO-only controls) and presence of hit compounds (20 μM) for 20 hours. Data shown are quantification from the EPR raw curves using the relative change in the central line amplitude when treated with hit compounds as compared to the DMSO-only controls. Data are means ± SD of three independent experiments. *$P < 0.05$, **$P < 0.01$, ***$P < 0.001$ and ****$P < 0.0001$ by two-tailed unpaired *t* test.

8.5. Discussion

There are three major classes of screening campaigns targeting HTT including targeted phenotype of aggregation, enhanced clearance and inhibition of cell death (*145*). These include recent efforts in preclinical targeting of HTT through indirect targeting mechanisms (*146*) including antisense oligonucleotides (*148*), antibodies fragments (*147*) and small molecules (*149*). In terms of direct targeting of the aggregation, several recent efforts have screened and discovered small molecules that

target toxic HTT aggregates that yielded efficacious, cytoprotective compounds. These small molecules include methylene blue (MB) (inhibition of protein aggregation by targeting monomer, oligomer and aggregates tested at 1-100 μM; inhibition of cell cytotoxicity tested at 100 nM) (*150*), C2-8 (inhibition of protein aggregation IC_{50}=25 μM; inhibition of cell cytotoxicity tested with IC_{50}=50 nM) (*151*), epigallocatechin gallate (EGCG) inhibition of protein aggregation (perturb oligomer conformation with IC_{50}=~1 μM; inhibition of toxicity tested in yeast model of HD (at 500 μM) and HD transgenic flies (at 0.1–100 μM)) (*152, 153*), leflunomide and teriflunomide (inhibition of HTT-Q72-Luc protein aggregation reporter assay with IC_{50}=1–3 μM; inhibition of HTT protein aggregation tested at 100 μM) (*154*), PGL-135 and PGL-137 (inhibition of HTT aggregation with IC_{50}=40 μM (PGL-135) and IC_{50}=100 μM (PGL-137); reduction of inclusion bodies in cells tested at 25 μM (PGL-135) and 50 μM (PGL-137)) (*155*), congo red (inhibition of HTT aggregation with IC_{50}=0.3 μM)(*129, 156*), thioflavin-S (inhibition of HTT aggregation with IC_{50}=20 μM) (*156*), and xyloketal derivatives (inhibition of HTT aggregation tested in *Caenorhabditis elegans* model of HD at 100 μM) (*157*). However, none of these compounds has successfully advanced to become an effective therapeutic.

One commonality among these molecules is that they were initially identified through direct measurements of HTT aggregation and disaggregation, without monitoring and providing information on the conformational changes or dynamics of the protein. Although small molecules that inhibit or disrupt HTT aggregation have been studied for decades, the targeting of HTT conformations has only recently been proposed, with the majority of efforts being focused on repurposing some of the previously identified small molecules such as MB (*150*), EGCG (*152*) and congo red

(*129*). In addition, with the exception of a few studies, most of them were performed using *in vitro* purified protein assays, which do not reliably represent the cellular environment as these assays lack numerous chaperone proteins that may contribute to the formation of oligomers and aggregates. Inherently, these purified protein assays are only capable of identifying hits that directly perturb HTT protein and are wholly naive against indirect mechanisms of action, affecting other pathologically relevant cellular processes. Hence, a cellular approach that monitors HTT aggregation holds promise as a novel HTS platform to discover more effective therapeutics.

The most potent small-molecule hit compound from the HTS and the FRET assays (EC_{50} = 0.04-0.06 μM) was niclosamide which also showed the strongest binding affinity for recombinant HTTex1-Q46 (K_d = 0.843 μM for monomer and K_d = 3.45 μM for fibril) and the largest effect in inhibition of HTTex1-Q46 aggregation as well as a strong rescue in HTTex1-Q72 induced cytotoxicity at 0.2 μM, comparable to other known HTT aggregation inhibitors. Two other most potent inhibitors in the cytotoxicity assay were rottlerin (IC_{50} = 0.25 μM) and 10058-F4 (IC_{50} = 0.27 μM), which were also relatively potent in the FRET assays (EC_{50} of rottlerin = 0.48-0.63 μM; EC_{50} of 10058-F4 = 0.27-0.55 μM) and were the top binders (K_d of rottlerin = 1.50 μM; K_d of 10058-F4 = 5.12 μM) to HTTex1-Q46 monomer next to niclosamide. This difference in the half maximal effective concentration could be due to different cell types used as well as the presence of the fluorophores in FRET assay that may result in less aggregation as compared to unlabeled HTTex1, hence smaller drug concentration may be sufficient to perturb the conformations. On the other hand, the difference between the cellular assays and the SPR binding assay could be due to the amount of proteins present for compound interactions, though the trend, in terms of potency, remains similar.

Niclosamide, together with rottlerin, were known to be effective mTOR inhibitors that lead to enhanced autophagy (*342, 343*). Since mTOR was present in HEK293 cells, we cannot eliminate that these compounds were also acting through inhibiting mTOR, resulting in the clearance of HTT proteins and hence leading to the rescue of HTT induced cytotoxicity. However, rottlerin has been shown to be inhibitor of huntingtin and prion aggregation (*344, 345*). On the other hand, 10058-F4 and AMG 9810 are known c-Myc inhibitor and TRPV1 receptor antagonist respectively (*346, 347*). Interestingly, we found that HEK293 cells do not express these proteins and hence suggesting that the FRET change was specific to perturbation of HTTex1 conformations (*348*). Other compounds, TNP, TBB and DMS, were known inositol hexakisphosphate kinases inhibitor, casein kinase 2 inhibitor and serotonin receptor agonists respectively which were known to play a role in HD (*349-351*) so we also could not eliminate their effects on acting through these mechanisms. In addition, compounds like TBB, though showing binding to HTT proteins at high concentration through SPR, did not disrupt HTT aggregation through EPR, suggesting that it could be acting through the indirect mechanism of inhibiting CK2 which was shown to potentially rescuing cytotoxicity in HD(*350*). Furthermore, all of the compounds did not completely abolish the FRET signals in the intermolecular FRET biosensors, suggesting that HTT-HTT interactions were not completely disrupted but may have undergone a conformational change from an oligomer or aggregated species with closer proximity between the fluorophores to one with a more open conformation.

Interestingly, our observations in that all small molecules caused perturbation of HTT cellular FRET biosensors with different polyQ lengths (Q16, Q39 and Q72) support the previous postulated model suggesting that both normal and expanded polyQ tracts (polyQ lengths below and above the pathological threshold) in the preaggregation state

share similar structures (*335-337, 352, 353*), rather than a specific toxic structure(*354*). This suggests that HTT proteins with polyQ lengths below and above the pathological threshold may adopt similar oligomeric conformations with the longer polyQ lengths having higher tendency to form β-sheet aggregates. In addition, in the β-sheet aggregates, these proteins may still uphold some of the common conformations originated from oligomers that could be targeted by the small molecules. This might also be inferred that there might be a prefibrillar structure that is capable of forming the toxic oligomers present in polyQ lengths less than the pathological threshold but they do not have the propensity or high enough local concentration to form the actual toxic aggregates. This suggests that the small molecules could potentially stabilize these pre-toxic structures to prevent them from further aggregating into the toxic species. On the other hand, it is possible that these small molecules target another common feature rather than the polyQ tracts of the HTT proteins which made it possible that the molecules affect all polyQ lengths.

The identity of a specific, toxic HTT aggregate remains elusive. Indeed, it is unlikely that a single, unique toxic conformation exists. It is far more likely that an ensemble of toxic oligomers and aggregates (differing in size, conformation and even molecular constituency) populate the amylogenic cascade(*333*). This heterogeneity in potential HTT aggregate targets highlights the need for an ultra-sensitive screening platform capable of monitoring structural changes within the ensemble of HTT assemblies. Our FRET-based platform for monitoring HTT aggregation in cells is a new technology that is capable of elucidating novel compounds which alter conformation and aggregation states of HTT proteins, thereby providing a new pipeline of therapeutic discovery for HD. This strategy, combining fluorescent biosensor and time-resolved FRET measurement in a HTS platform, should be generally applicable to other drug

discovery efforts targeting intrinsically disordered proteins involved in numerous polyglutamine diseases.

8.6. Supplemental figures

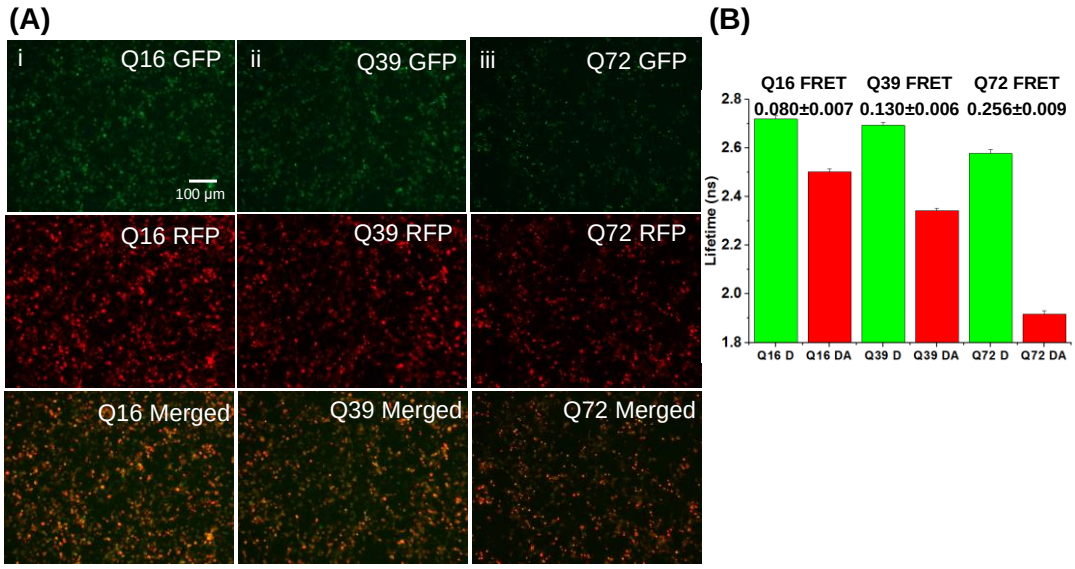

Supplemental Figure 8. 1. Characterization of huntingtin exon 1 (HTTex1) intermolecular FRET biosensors.

(A) Fluorescent microscopy images of GFP and RFP-tagged HTTex1 of various polyglutamine length, (i) Q16, (ii) Q39 and (iii) Q72, expressed in HEK293 cells. (B) Fluorescence lifetime measurements of the three different biosensors. Data are means ± SD of three independent experiments.

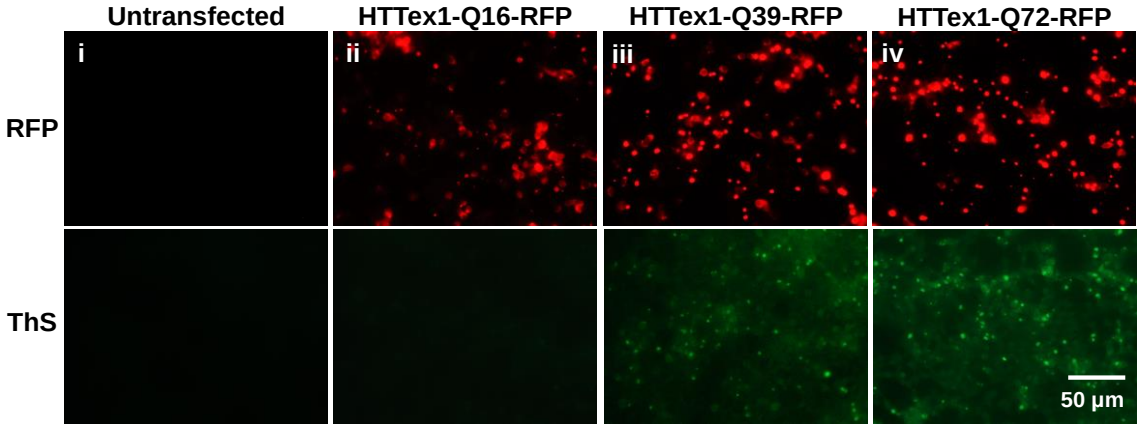

Supplemental Figure 8. 2. Thioflavin-S (ThS) staining of HEK293 cells expressing HTTex1-RFP of various polyglutamine lengths.

Fluorescence images of ThS staining of HEK293 cells being (i) untransfected or transfected with (ii) HTTex1-Q16-RFP, (iii) HTTex1-Q39-RFP and (iv) HTTex1-Q72-RFP. The amount of HTTex1-RFP plasmids transfected for ThS assay is equal to the amount of HTTex1-GFP and HTTex1-RFP plasmids used in the FRET biosensors. HTTex1-GFP is not used because it will interfere with the ThS signal which is green in fluorescence. Images are representative of three independent experiments.

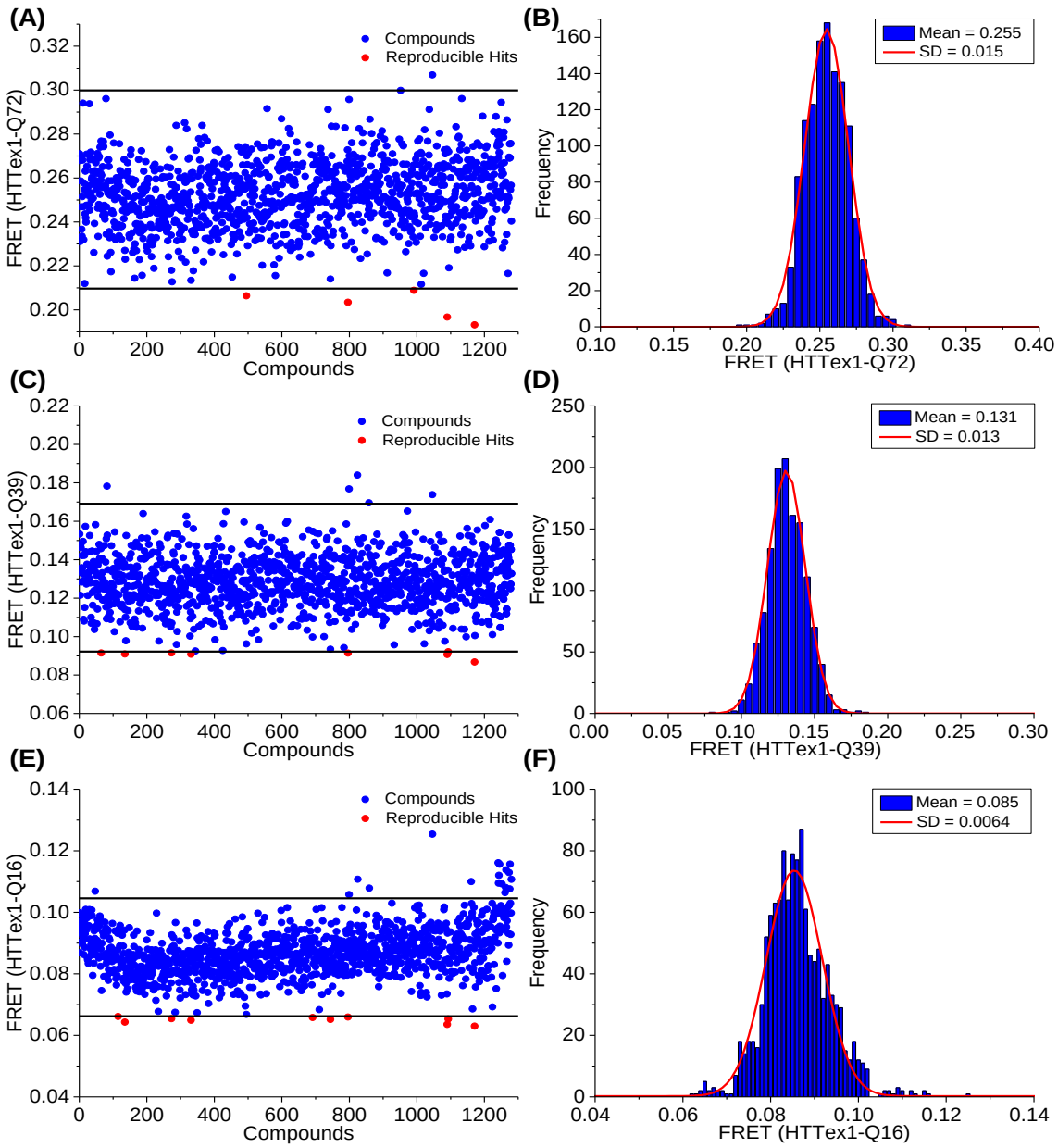

Supplemental Figure 8. 3. High-throughput screening (HTS) of LOPAC library using HTTex1 FRET biosensors and hits identification.

Representative pilot screening plots and Gaussian fits of the LOPAC library containing 1280 compounds screened using (A-B) HTTex1-Q72, (C-D) HTTex1-Q39 and (E-F) HTTex1-Q72 FRET biosensors. A FRET efficiency cutoff threshold was applied at a change in FRET efficiency of 3SD (*black lines*). Reproducible hits that decreased FRET by more than 3SD below the mean

of all cells were highlighted in red. Gaussian fits were performed by plotting histograms of all compounds from the LOPAC screens with the HTTex1 FRET biosensors after removal of fluorescent compounds to obtain the average FRET efficiency and the standard deviation (SD) of the screens. Screening plots are representative of three independent experiments.

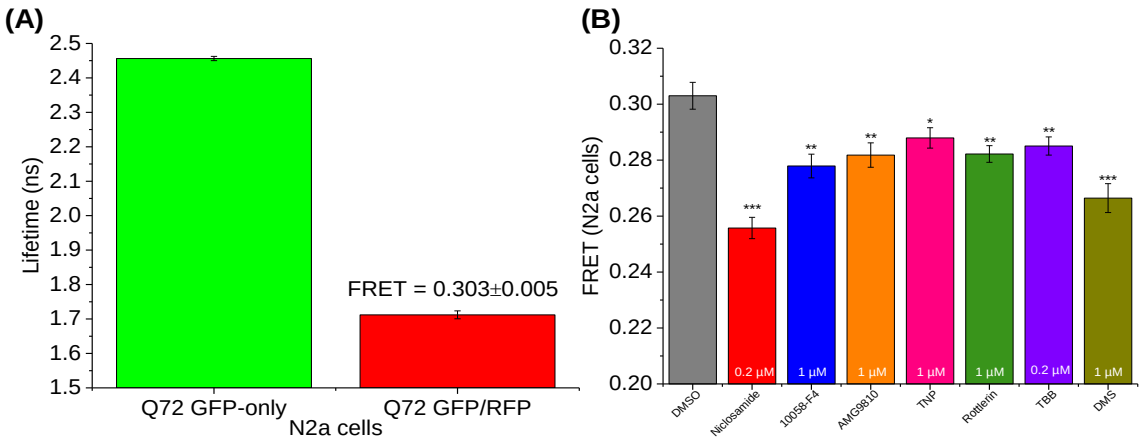

Supplemental Figure 8. 4. Hit compounds reduced FRET in the HTTex1-Q72 biosensor in N2a cells.

(A) Fluorescence lifetime measurements of the HTTex1-Q72 FRET biosensor in N2a cells. (B) Hit compounds reduced FRET in the HTTex1-Q72 biosensor expressed in N2a cells. Data are means ± SD of three independent experiments. *P < 0.05, **P < 0.01, and ***P < 0.001 by two-tailed unpaired t test.

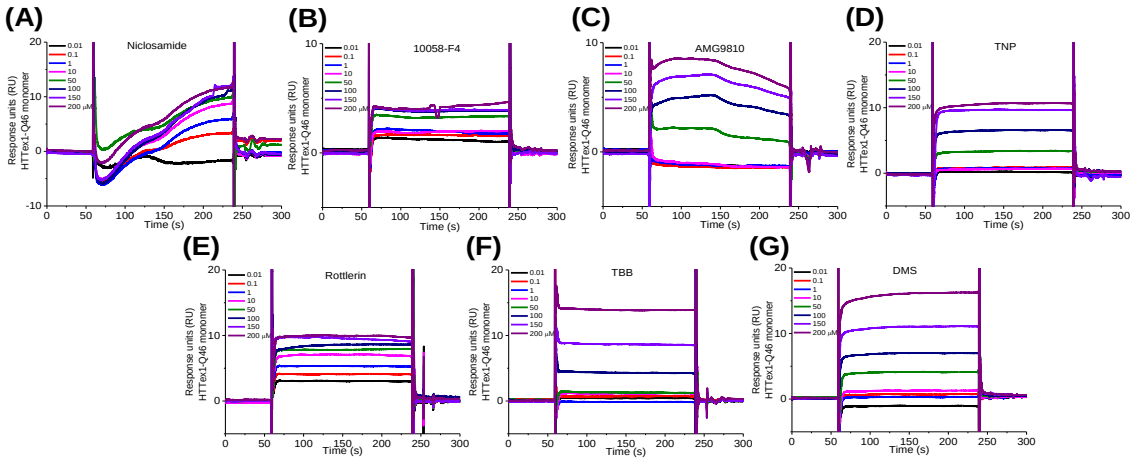

Supplemental Figure 8. 5. Binding of the hit compounds to HTTex1-Q46 monomer as characterized by SPR measurements.

SPR raw binding curves for (A) niclosamide, (B) 10058-F4, (C) AMG9810, (D) TNP, (E) rottlerin, (F) TBB, and (G) DMS. Bind curves are representative of three independent experiments.

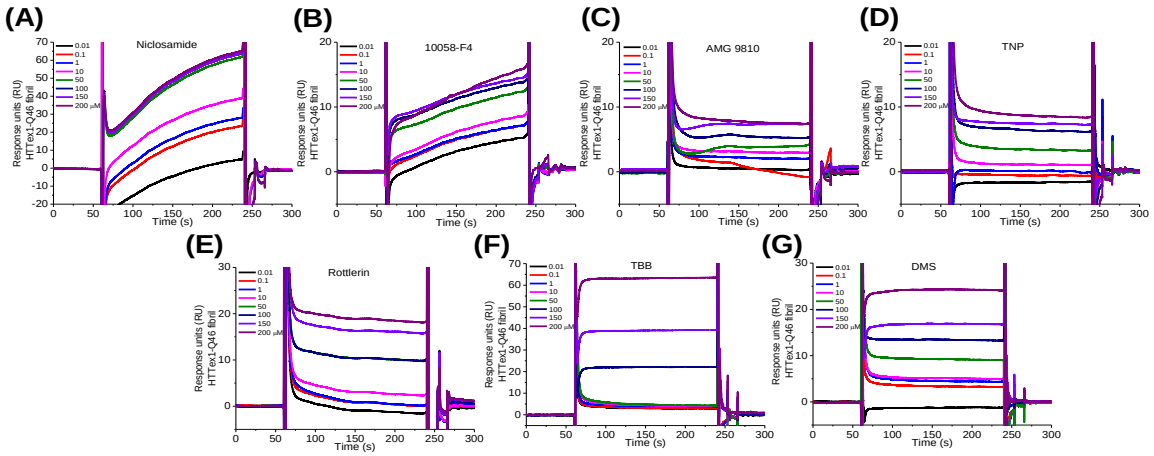

Supplemental Figure 8. 6. Binding of the hit compounds to HTTex1-Q46 fibril as characterized by SPR measurements.

SPR raw binding curves for (A) niclosamide, (B) 10058-F4, (C) AMG9810, (D) TNP, (E) rottlerin, (F) TBB, and (G) DMS. Bind curves are representative of three independent experiments.

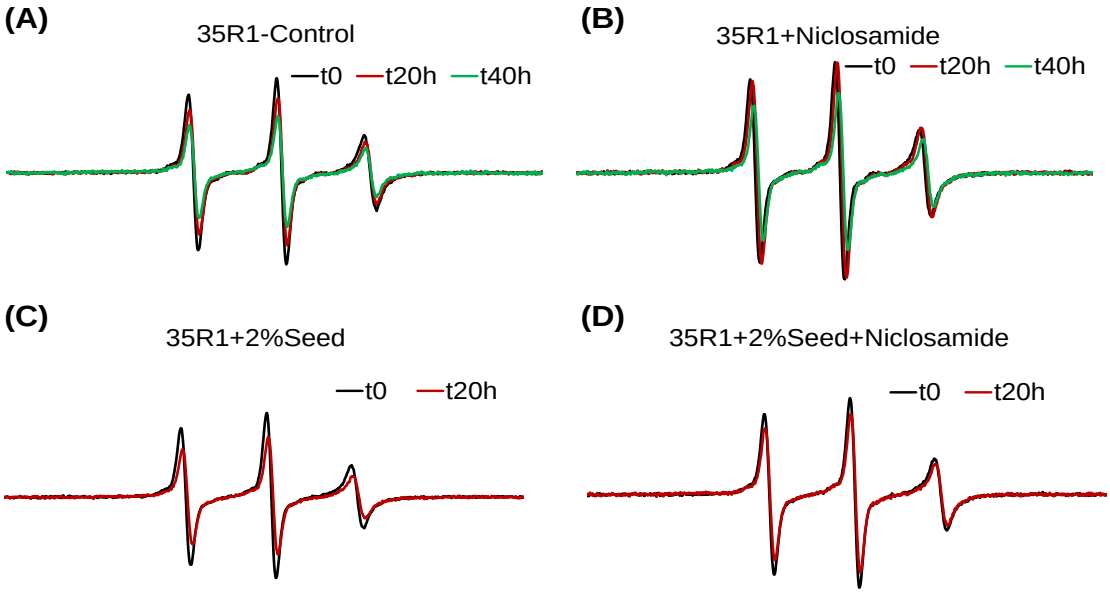

Supplemental Figure 8. 7. Disruption of HTTex1-Q46 aggregation by hit compounds as characterized by Continuous wave (CW)-electron paramagnetic resonance (EPR) measurements.

(A-B) EPR characterization of disruption of HTTex1-Q46 aggregation by in the absence of seed (unseeded) and treated with (A) DMSO only as control or (B) hit compounds (20 μM). Disruption of HTTex1-Q46 aggregation by hit compounds with 2% seed and treated with (C) DMSO only as control or (D) hit compounds (20 μM). EPR raw curves were shown with treatment of niclosamide as a representative compound. HTTex1-Q46 was spin labeled at position 35 and the hit compounds were treated for 20 and/or 40 hours. Aggregation or misfolding causes line broadening and a concomitant reduction in amplitude. EPR raw curves are representative of three independent experiments.

CHAPTER 9: CONCLUDING REMARKS AND FUTURE DIRECTIONS

This thesis research adopts a small molecule drug discovery approach through HTS with FRET biosensors to probe for conformational states of TNFR1 and conformational ensembles of tau oligomers or HTT aggregates. Specifically, we made use of a fluorescence lifetime detection method, which offers high-throughput and high-precision measurements, in conjunction with fluorescent biosensor engineering to create novel screening platforms for targeting TNFR1 and IDPs.

We first performed extensive literature reviews to identify the gaps in the targeting mechanisms of TNFR1 and IDPs. It is clear from the existing studies that targeting receptor-receptor interactions and the conformational dynamics of TNFR1 as well as targeting the heterogeneity of ensembles of tau oligomers or HTT aggregates appear to present the most novel and effective approaches in mediating autoimmune diseases (e.g. rheumatoid arthritis) and neurodegenerative diseases (e.g. AD and HD). To test these hypotheses, engineered TNFR1, tau and HTT FRET biosensors and launched a series of HTS campaigns screening multiple libraries to discover small molecules that potentially work through these novel mechanisms.

First, I discovered a small molecule, zafirlukast, which disrupts the TNFR1 receptor-receptor interactions without disrupting ligand binding. I then discovered two small molecules, DS42 and SB200646 hydrochloride, that alter the conformational states of TNFR1 leading to receptor inhibition and activation respectively. These findings revolutionized the field in that TNFR1 conformational states, which can be altered by small molecule perturbation of the long-range structural couplings, between TNFR1

membrane distal and proximal domains, mediated through the ligand-binding domain, are acting as molecular switch in determining receptor functions. In addition, we conducted preliminary SAR on DS42 and in depth SAR analysis of zafirlukast through medicinal chemistry and showed that their potency and specificity were greatly improved with the newly synthesized analogues that represent promising candidates for therapeutic developments.

Following the TNFR1 work, I extended the investigations on small molecule targeting of PPTs to IDPs including tau and huntingtin proteins, which are implicated in AD and HD. In these works, we found that the conformational ensembles of tau oligomers or HTT aggregates can be perturbed by small molecules. In addition, we discovered small molecule inhibitors that disrupt the oligomerization or aggregation of these proteins and rescue cell cytotoxicity with nanomolar potency.

Future directions

For the TNFR1 studies, immediate future work includes applying similar screening strategies to other TNF receptors such as Death Receptor 5 (currently ongoing) or neurotrophin receptor, which are important targets for cancer and neurodegenerative diseases. In addition, current small molecules that target TNFR1 should be further optimized by medicinal chemistry to obtain more potent molecules, followed by testing the compound pharmacokinetics and pharmacodynamics as well as their functional effect in animal studies. Furthermore, to confirm the structural observations as determined by FRET, higher resolution structural studies, such as X-ray crystallography, NMR or cryo-EM, should be performed to validate the exact receptor structure perturbation by the small molecule effectors.

In terms of a broader picture of receptor activation in general, following the previous studies by our lab suggesting that TNFR1 dimers are a functional subunit of the receptor complex and receptor conformational changes are crucial to its function, my recent results suggest that direct measurement of the receptor monomer spacing may not be the most accurate measure of the structure-function relationship of TNFR1. Instead, we may have to take into account the three-dimensional orientation of the receptor, in addition to the spacing between monomers, to determine the functional states of the receptor. This includes the consideration of receptor conformation in interacting with the downstream signaling molecules such as TRADD. If this hypothesis holds true, new targeting strategies focusing on monitoring the receptor orientation, as well as its interactions with the downstream signaling molecules, will be important in discovering better therapeutics.

For the tau studies, a straightforward improvement will be to express tau in a stable or inducible cell line as well as in human iPSCs for physiological relevance. This will further improve conditions for screening in a native environment. In addition, we will launch further HTS campaigns using the most optimized tau FRET biosensors to screen CNS-focused libraries such as the CNS-MPO or CNS-Set library to ensure that small molecules have a high probability of crossing the blood-brain barrier. In conjunction with smFRET and other techniques such as AUC, the biosensors can be used to develop a clearer picture of how mutations (e.g. P301L), different tau isoforms and post-translation modifications alter the conformations of oligomers, and what determines toxicity. Ultimately, we will need to test the functional effects of the hit compounds in animal models with tau oligomer induced pathology to see if they rescue the pathology. If the compounds are functional in the animal models, they will be poised to be tested in

clinical trials. As for biomarker development, an immediate next step is to compare our biosensor with the existing tau-RD FRET biosensor developed by the Diamond group, to test their sensitivity in cerebrospinal fluid (CSF) from AD patients. If our biosensor is sensitive to these patient samples, we can further investigate how different groups of patient samples may have different effects on our FRET biosensor. This will act as an initial step in potentially stratifying the patients into different groups to be tested in clinical trials for more effective targeting and drug discovery.

In terms of targeting neurodegenerative diseases in general, different FRET-based targeting strategies can be adopted to test other hypothesis in the field. For example, we will be able to test comorbidity among misfolded proteins such as tau, HTT, Aβ and α-synuclein. In addition, we will also be able to study the seeding, uptake and propagation of IDPs. Furthermore, as our biosensors are expressed in cells, we will be able to investigate the roles of cellular components such as kinases or chaperone proteins in IDP oligomerization or aggregation and their implication in neurodegenerative diseases.

10: REFERENCES

1. D. E. Scott, A. R. Bayly, C. Abell, J. Skidmore, Small molecules, big targets: drug discovery faces the protein–protein interaction challenge. *Nature Reviews Drug Discovery* **15**, 533 (04/11/online, 2016).
2. J. Li, Q. Yin, H. Wu, Structural basis of signal transduction in the TNF receptor superfamily. *Adv Immunol* **119**, 135 (2013).
3. V. N. Uversky, Intrinsic Disorder, Protein-Protein Interactions, and Disease. *Advances in protein chemistry and structural biology* **110**, 85 (2018).
4. R. M. Locksley, N. Killeen, M. J. Lenardo, The TNF and TNF receptor superfamilies: integrating mammalian biology. *Cell* **104**, 487 (Feb 23, 2001).
5. A. Ashkenazi, V. M. Dixit, Death Receptors: Signaling and Modulation. *Science* **281**, 1305 (1998).
6. H. Wajant, K. Pfizenmaier, P. Scheurich, Tumor necrosis factor signaling. *Cell Death Differ* **10**, 45 (//print, 2003).
7. T. V. Berghe, A. Linkermann, S. Jouan-Lanhouet, H. Walczak, P. Vandenabeele, Regulated necrosis: the expanding network of non-apoptotic cell death pathways. *Nat Rev Mol Cell Biol* **15**, 135 (02//print, 2014).
8. M. Croft, W. Duan, H. Choi, S.-Y. Eun, S. Madireddi, A. Mehta, TNF superfamily in inflammatory disease: translating basic insights. *Trends in Immunology* **33**, 144 (3//, 2012).
9. Y. Takei, R. Laskey, Tumor Necrosis Factor α Regulates Responses to Nerve Growth Factor, Promoting Neural Cell Survival but Suppressing Differentiation of Neuroblastoma Cells. *Molecular Biology of the Cell* **19**, 855 (06/29/received, 10/30/revised, 12/07/accepted, 2008).
10. T. D. Gilmore, Introduction to NF-[kappa]B: players, pathways, perspectives. *Oncogene* **25**, 6680 (//print, 2006).
11. H. Wajant, P. Scheurich, TNFR1-induced activation of the classical NF-kappaB pathway. *The FEBS journal* **278**, 862 (2011).
12. M. Apostolaki, M. Armaka, P. Victoratos, G. Kollias, Cellular mechanisms of TNF function in models of inflammation and autoimmunity. *Current directions in autoimmunity* **11**, 1 (2010).
13. M. Wong, D. Ziring, Y. Korin, S. Desai, S. Kim, J. Lin, D. Gjertson, J. Braun, E. Reed, R. R. Singh, TNFα blockade in human diseases: Mechanisms and future directions. *Clinical Immunology* **126**, 121 (2//, 2008).
14. R. E. Kontermann, P. Scheurich, K. Pfizenmaier, Antagonists of TNF action: clinical experience and new developments. *Expert opinion on drug discovery* **4**, 279 (Mar, 2009).
15. D. Tracey, L. Klareskog, E. H. Sasso, J. G. Salfeld, P. P. Tak, Tumor necrosis factor antagonist mechanisms of action: A comprehensive review. *Pharmacology & Therapeutics* **117**, 244 (2//, 2008).
16. G. Cessak, O. Kuzawińska, A. Burda, K. Lis, M. Wojnar, D. Mirowska-Guzel, E. Bałkowiec-Iskra, TNF inhibitors – Mechanisms of action, approved and off-label indications. *Pharmacological Reports* **66**, 836 (10//, 2014).
17. NIH, Progress in Autoimmune Diseases Research, Report to Congress, National Institutes of Health, The Autoimmune Diseases Coordinating Committee, March 2005, forward and pages i, 1, 2, 16, 17, 28, 29, 30, 32, 52., (2005).
18. Autoimmune disease. *Nat Biotech*.

19. L. Xiao, Y. Liu, N. Wang, New paradigms in inflammatory signaling in vascular endothelial cells. *American Journal of Physiology - Heart and Circulatory Physiology* **306**, H317 (2014-02-01 00:00:00, 2014).
20. K. Pfizenmaier, D. E. Szymkowski, Workshop Summary: Introduction to Rational Design of New Means for Therapeutic Modulation of Function of the TNF Family. *Advances in experimental medicine and biology* **691**, 487 (2011).
21. L. M. Sedger, M. F. McDermott, TNF and TNF-receptors: From mediators of cell death and inflammation to therapeutic giants – past, present and future. *Cytokine & Growth Factor Reviews* **25**, 453 (2014).
22. C. Monaco, J. Nanchahal, P. Taylor, M. Feldmann, Anti-TNF therapy: past, present and future. *International immunology* **27**, 55 (Jan, 2015).
23. N. L. Sicotte, R. R. Voskuhl, Onset of multiple sclerosis associated with anti-TNF therapy. *Neurology* **57**, 1885 (2001).
24. S. L. Brown, M. H. Greene, S. K. Gershon, E. T. Edwards, M. M. Braun, Tumor necrosis factor antagonist therapy and lymphoma development: Twenty-six cases reported to the Food and Drug Administration. *Arthritis & Rheumatism* **46**, 3151 (2002).
25. N. Shakoor, M. Michalska, C. A. Harris, J. A. Block, Drug-induced systemic lupus erythematosus associated with etanercept therapy. *The Lancet* **359**, 579 (2002).
26. N. R. Slifman, S. K. Gershon, J.-H. Lee, E. T. Edwards, M. M. Braun, Listeria monocytogenes infection as a complication of treatment with tumor necrosis factor α–neutralizing agents. *Arthritis & Rheumatism* **48**, 319 (2003).
27. M. G. Tansey, D. E. Szymkowski, The TNF superfamily in 2009: new pathways, new indications, and new drugs. *Drug Discovery Today* **14**, 1082 (12//, 2009).
28. F. Van Hauwermeiren, R. E. Vandenbroucke, C. Libert, Treatment of TNF mediated diseases by selective inhibition of soluble TNF or TNFR1. *Cytokine & Growth Factor Reviews* **22**, 311 (10//, 2011).
29. P. M. Steed, M. Tansey, xfa, G, J. Zalevsky, E. A. Zhukovsky, J. R. Desjarlais, D. E. Szymkowski, C. Abbott, D. Carmichael, C. Chan, L. Cherry, P. Cheung, A. J. Chirino, H. H. Chung, S. K. Doberstein, A. Eivazi, A. V. Filikov, S. X. Gao, R. Hubert, xe, S, M. Hwang, L. Hyun, S. Kashi, A. Kim, E. Kim, J. Kung, S. P. Martinez, U. S. Muchhal, D.-H. T. Nguyen, C. O'Brien, D. O'Keefe, K. Singer, O. Vafa, J. Vielmetter, S. C. Yoder, B. I. Dahiyat, Inactivation of TNF Signaling by Rationally Designed Dominant-Negative TNF Variants. *Science* **301**, 1895 (2003).
30. J. Zalevsky, T. Secher, S. A. Ezhevsky, L. Janot, P. M. Steed, C. O'Brien, A. Eivazi, J. Kung, D. H. Nguyen, S. K. Doberstein, F. Erard, B. Ryffel, D. E. Szymkowski, Dominant-negative inhibitors of soluble TNF attenuate experimental arthritis without suppressing innate immunity to infection. *Journal of immunology (Baltimore, Md. : 1950)* **179**, 1872 (Aug 1, 2007).
31. M. M. He, A. S. Smith, J. D. Oslob, W. M. Flanagan, A. C. Braisted, A. Whitty, M. T. Cancilla, J. Wang, A. A. Lugovskoy, J. C. Yoburn, A. D. Fung, G. Farrington, J. K. Eldredge, E. S. Day, L. A. Cruz, T. G. Cachero, S. K. Miller, J. E. Friedman, I. C. Choong, B. C. Cunningham, Small-molecule inhibition of TNF-alpha. *Science* **310**, 1022 (2005).
32. P. P. Sfikakis, G. C. Tsokos, Towards the next generation of anti-TNF drugs. *Clinical immunology (Orlando, Fla.)* **141**, 231 (Dec, 2011).
33. H. Shibata, Y. Yoshioka, A. Ohkawa, Y. Abe, T. Nomura, Y. Mukai, S. Nakagawa, M. Taniai, T. Ohta, T. Mayumi, H. Kamada, S.-i. Tsunoda, Y.

Tsutsumi, The therapeutic effect of TNFR1-selective antagonistic mutant TNF-α in murine hepatitis models. *Cytokine* **44**, 229 (2008).
34. F. E. McCann, D. P. Perocheau, G. Ruspi, K. Blazek, M. L. Davies, M. Feldmann, J. L. E. Dean, A. A. Stoop, R. O. Williams, Selective Tumor Necrosis Factor Receptor I Blockade Is Antiinflammatory and Reveals Immunoregulatory Role of Tumor Necrosis Factor Receptor II in Collagen-Induced Arthritis. *Arthritis & Rheumatology* **66**, 2728 (2014).
35. K. A. Zettlitz, V. Lorenz, K. Landauer, S. Münkel, A. Herrmann, P. Scheurich, K. Pfizenmaier, R. E. Kontermann, ATROSAB, a humanized antagonistic anti-tumor necrosis factor receptor one-specific antibody. *mAbs* **2**, 639 (2010).
36. P. H. Carter, P. A. Scherle, J. K. Muckelbauer, M. E. Voss, R. Q. Liu, L. A. Thompson, A. J. Tebben, K. A. Solomon, Y. C. Lo, Z. Li, P. Strzemienski, G. Yang, N. Falahatpisheh, M. Xu, Z. Wu, N. A. Farrow, K. Ramnarayan, J. Wang, D. Rideout, V. Yalamoori, P. Domaille, D. J. Underwood, J. M. Trzaskos, S. M. Friedman, R. C. Newton, C. P. Decicco, Photochemically enhanced binding of small molecules to the tumor necrosis factor receptor-1 inhibits the binding of TNF-alpha. *Proc Natl Acad Sci U S A* **98**, 11879 (2001).
37. S. Chen, Z. Feng, Y. Wang, S. Ma, Z. Hu, P. Yang, Y. Chai, X. Xie, Discovery of Novel Ligands for TNF-α and TNF Receptor-1 through Structure-Based Virtual Screening and Biological Assay. *Journal of Chemical Information and Modeling* **57**, 1101 (2017).
38. R. Murali, X. Cheng, A. Berezov, X. Du, A. Schon, E. Freire, X. Xu, Y. H. Chen, M. I. Greene, Disabling TNF receptor signaling by induced conformational perturbation of tryptophan-107. *Proc Natl Acad Sci U S A* **102**, 10970 (2005).
39. R. Fischer, R. Kontermann, O. Maier, Targeting sTNF/TNFR1 Signaling as a New Therapeutic Strategy. *Antibodies* **4**, 48 (2015).
40. T. Gohda, M. A. Niewczas, L. H. Ficociello, W. H. Walker, J. Skupien, F. Rosetti, X. Cullere, A. C. Johnson, G. Crabtree, A. M. Smiles, T. N. Mayadas, J. H. Warram, A. S. Krolewski, Circulating TNF Receptors 1 and 2 Predict Stage 3 CKD in Type 1 Diabetes. *Journal of the American Society of Nephrology : JASN* **23**, 516 (2012).
41. M. Deng, P. A. Loughran, L. Zhang, M. J. Scott, T. R. Billiar, Shedding of the tumor necrosis factor (TNF) receptor from the surface of hepatocytes during sepsis limits inflammation through cGMP signaling. *Science Signaling* **8**, ra11 (2015).
42. D. Aderka, H. Engelmann, Y. Maor, C. Brakebusch, D. Wallach, Stabilization of the bioactivity of tumor necrosis factor by its soluble receptors. *The Journal of Experimental Medicine* **175**, 323 (1992).
43. Y. Wolf, A. Shemer, M. Polonsky, M. Gross, A. Mildner, S. Yona, E. David, K.-W. Kim, T. Goldmann, I. Amit, M. Heikenwalder, S. Nedospasov, M. Prinz, N. Friedman, S. Jung, Autonomous TNF is critical for in vivo monocyte survival in steady state and inflammation. *The Journal of Experimental Medicine*, (2017).
44. L. Brambilla, G. Guidotti, F. Martorana, A. Iyer, E. Aronica, C. Valori, D. Rossi, Disruption of the astrocytic TNFR1-GDNF axis accelerates motor neuron degeneration and disease progression in amyotrophic lateral sclerosis. *Human Molecular Genetics* **25**, ddw161 (2016).
45. M. R. Arkin, J. A. Wells, Small-molecule inhibitors of protein-protein interactions: progressing towards the dream. *Nat Rev Drug Discov* **3**, 301 (04//print, 2004).

46. Michelle R. Arkin, Y. Tang, James A. Wells, Small-Molecule Inhibitors of Protein-Protein Interactions: Progressing toward the Reality. *Chemistry & Biology* **21**, 1102 (2014).
47. F. K. Chan, The pre-ligand binding assembly domain: a potential target of inhibition of tumour necrosis factor receptor function. *Annals of the Rheumatic Diseases* **59**, i50 (2000).
48. G.-M. Deng, Tumor Necrosis Factor Receptor Pre-Ligand Assembly Domain is an Important Therapeutic Target in Inflammatory Arthritis. *BioDrugs* **21**, 23 (2012//, 2007).
49. J. H. Naismith, T. Q. Devine, B. J. Brandhuber, S. R. Sprang, Crystallographic evidence for dimerization of unliganded tumor necrosis factor receptor. *J Biol Chem* **270**, 13303 (Jun 02, 1995).
50. J. H. Naismith, T. Q. Devine, T. Kohno, S. R. Sprang, Structures of the extracellular domain of the type I tumor necrosis factor receptor. *Structure (London, England : 1993)* **4**, 1251 (Nov 15, 1996).
51. J. Cao, F. Meng, X. Gao, H. Dong, W. Yao, Expression and purification of a natural N-terminal pre-ligand assembly domain of tumor necrosis factor receptor 1 (TNFR1 PLAD) and preliminary activity determination. *The protein journal* **30**, 281 (Apr, 2011).
52. G.-M. Deng, L. Zheng, F. Ka-Ming Chan, M. Lenardo, Amelioration of inflammatory arthritis by targeting the pre-ligand assembly domain of tumor necrosis factor receptors. *Nat Med* **11**, 1066 (2005).
53. G.-M. Deng, L. Liu, G. C. Tsokos, Targeted TNF receptor 1 preligand assembly domain improves skin lesions in MRL/lpr mice. *Arthritis and rheumatism* **62**, 2424 (2010).
54. Y.-L. Wang, F.-C. Chou, S.-J. Chen, S.-H. Lin, D.-M. Chang, H.-K. Sytwu, Targeting pre-ligand assembly domain of TNFR1 ameliorates autoimmune diseases – An unrevealed role in downregulation of Th17 cells. *Journal of Autoimmunity* **37**, 160 (11//, 2011).
55. H.-W. Lee, S.-H. Lee, H.-W. Lee, Y.-W. Ryu, M.-H. Kwon, Y.-S. Kim, Homomeric and heteromeric interactions of the extracellular domains of death receptors and death decoy receptors. *Biochemical and Biophysical Research Communications* **330**, 1205 (2005).
56. J. Cao, F. Meng, X. Gao, H. Dong, W. Yao, Expression and Purification of a Natural N-Terminal Pre-ligand Assembly Domain of Tumor Necrosis Factor Receptor 1 (TNFR1 PLAD) and Preliminary Activity Determination. *The Protein Journal* **30**, 281 (2011).
57. D. W. Banner, A. D'Arcy, W. Janes, R. Gentz, H.-J. Schoenfeld, C. Broger, H. Loetscher, W. Lesslauer, Crystal structure of the soluble human 55 kd TNF receptor-human TNFβ complex: Implications for TNF receptor activation. *Cell* **73**, 431 (1993).
58. F. K.-M. Chan, H. J. Chun, L. Zheng, R. M. Siegel, K. L. Bui, M. J. Lenardo, A Domain in TNF Receptors That Mediates Ligand-Independent Receptor Assembly and Signaling. *Science* **288**, 2351 (2000).
59. J. H. Naismith, T. Q. Devine, B. J. Brandhuber, S. R. Sprang, Crystallographic Evidence for Dimerization of Unliganded Tumor Necrosis Factor Receptor. *Journal of Biological Chemistry* **270**, 13303 (1995).
60. N. Vunnam, C. H. Lo, B. D. Grant, D. D. Thomas, J. N. Sachs, Soluble Extracellular Domain of Death Receptor 5 Inhibits TRAIL-Induced Apoptosis by

Disrupting Receptor–Receptor Interactions. *Journal of Molecular Biology* **429**, 2943 (2017).
61. F. K.-M. Chan, Three is Better Than One: Pre-Ligand Receptor Assembly in the Regulation of TNF Receptor Signaling. *Cytokine* **37**, 101 (2007).
62. A. K. Lewis, C. C. Valley, J. N. Sachs, TNFR1 signaling is associated with backbone conformational changes of receptor dimers consistent with overactivation in the R92Q TRAPS mutant. *Biochemistry* **51**, 6545 (2012).
63. H. Z. Ozsoy, N. Sivasubramanian, E. D. Wieder, S. Pedersen, D. L. Mann, Oxidative stress promotes ligand-independent and enhanced ligand-dependent tumor necrosis factor receptor signaling. *J Biol Chem* **283**, 23419 (Aug 22, 2008).
64. W. Schneider-Brachert, V. Tchikov, J. Neumeyer, M. Jakob, S. Winoto-Morbach, J. Held-Feindt, M. Heinrich, O. Merkel, M. Ehrenschwender, D. Adam, R. Mentlein, D. Kabelitz, S. Schutze, Compartmentalization of TNF receptor 1 signaling: internalized TNF receptosomes as death signaling vesicles. *Immunity* **21**, 415 (Sep, 2004).
65. A. Krippner-Heidenreich, F. Tübing, S. Bryde, S. Willi, G. Zimmermann, P. Scheurich, Control of Receptor-induced Signaling Complex Formation by the Kinetics of Ligand/Receptor Interaction. *Journal of Biological Chemistry* **277**, 44155 (November 15, 2002, 2002).
66. U. Baul, D. Chakraborty, M. L. Mugnai, J. E. Straub, D. Thirumalai, Sequence Effects on Size, Shape, and Structural Heterogeneity in Intrinsically Disordered Proteins. *The Journal of Physical Chemistry B* **123**, 3462 (2019/04/25, 2019).
67. P. Kulkarni, V. N. Uversky, Intrinsically Disordered Proteins in Chronic Diseases. *Biomolecules* **9**, 147 (2019).
68. J. AVILA, J. J. LUCAS, M. PÉREZ, F. HERNÁNDEZ, Role of Tau Protein in Both Physiological and Pathological Conditions. *Physiological Reviews* **84**, 361 (2004).
69. J. G. Wood, S. S. Mirra, N. J. Pollock, L. I. Binder, Neurofibrillary tangles of Alzheimer disease share antigenic determinants with the axonal microtubule-associated protein tau (tau). *Proceedings of the National Academy of Sciences of the United States of America* **83**, 4040 (1986).
70. G. T. Bramblett, M. Goedert, R. Jakes, S. E. Merrick, J. Q. Trojanowski, V. M. Y. Lee, Abnormal tau phosphorylation at Ser396 in alzheimer's disease recapitulates development and contributes to reduced microtubule binding. *Neuron* **10**, 1089 (1993/06/01/, 1993).
71. P. Bubber, V. Haroutunian, G. Fisch, J. P. Blass, G. E. Gibson, Mitochondrial abnormalities in Alzheimer brain: mechanistic implications. *Ann Neurol* **57**, 695 (May, 2005).
72. R. Sultana, D. A. Butterfield, Oxidative modification of brain proteins in Alzheimer's disease: perspective on future studies based on results of redox proteomics studies. *J Alzheimers Dis* **33 Suppl 1**, S243 (2013).
73. T. Majid, Y. O. Ali, D. V. Venkitaramani, M.-K. Jang, H.-C. Lu, R. G. Pautler, In vivo axonal transport deficits in a mouse model of fronto-temporal dementia. *NeuroImage: Clinical* **4**, 711 (2014/01/01/, 2014).
74. N. Sahara, S. Maeda, A. Takashima, Tau Oligomerization: A Role for Tau Aggregation Intermediates Linked to Neurodegeneration. *Current Alzheimer Research* **5**, 591 (2008).

75. C. Ballatore, V. M. Y. Lee, J. Q. Trojanowski, Tau-mediated neurodegeneration in Alzheimer's disease and related disorders. *Nature Reviews Neuroscience* **8**, 663 (2007).
76. C. W. Wittmann, M. F. Wszolek, J. M. Shulman, P. M. Salvaterra, J. Lewis, M. Hutton, M. B. Feany, Tauopathy in Drosophila: Neurodegeneration Without Neurofibrillary Tangles. *Science* **293**, 711 (2001).
77. K. Santacruz, J. Lewis, T. Spires, J. Paulson, L. Kotilinek, M. Ingelsson, A. Guimaraes, M. DeTure, M. Ramsden, E. McGowan, C. Forster, M. Yue, J. Orne, C. Janus, A. Mariash, M. Kuskowski, B. Hyman, M. Hutton, K. H. Ashe, Tau suppression in a neurodegenerative mouse model improves memory function. *Science* **309**, 476 (2005).
78. S. Maeda, N. Sahara, Y. Saito, S. Murayama, A. Ikai, A. Takashima, Increased levels of granular tau oligomers: An early sign of brain aging and Alzheimer's disease. *Neuroscience Research* **54**, 197 (2006/03/01/, 2006).
79. Z. Berger, H. Roder, A. Hanna, A. Carlson, V. Rangachari, M. Yue, Z. Wszolek, K. Ashe, J. Knight, D. Dickson, C. Andorfer, T. L. Rosenberry, J. Lewis, M. Hutton, C. Janus, Accumulation of Pathological Tau Species and Memory Loss in a Conditional Model of Tauopathy. *The Journal of Neuroscience* **27**, 3650 (2007).
80. C. A. Lasagna-Reeves, D. L. Castillo-Carranza, U. Sengupta, J. Sarmiento, J. Troncoso, G. R. Jackson, R. Kayed, Identification of oligomers at early stages of tau aggregation in Alzheimer's disease. *The FASEB Journal* **26**, 1946 (2012/05/01, 2012).
81. K. Flach, I. Hilbrich, A. Schiffmann, U. Gaertner, M. Krueger, M. Leonhardt, H. Waschipky, L. Wick, T. Arendt, M. Holzer, Tau oligomers impair artificial membrane integrity and cellular viability. *Journal of Biological Chemistry*, (November 5, 2012, 2012).
82. S. M. Ward, D. S. Himmelstein, J. K. Lancia, L. I. Binder, Tau oligomers and tau toxicity in neurodegenerative disease. *Biochemical Society transactions* **40**, 667 (2012).
83. J. E. Gerson, D. L. Castillo-Carranza, R. Kayed, Advances in Therapeutics for Neurodegenerative Tauopathies: Moving toward the Specific Targeting of the Most Toxic Tau Species. *ACS Chemical Neuroscience* **5**, 752 (2014/09/17, 2014).
84. L. Guzmán-Martinez, G. A. Farías, R. B. Maccioni, Tau oligomers as potential targets for Alzheimer's diagnosis and novel drugs. *Frontiers in neurology* **4**, 167 (2013).
85. E. Davidowitz, I. Chatterjee, J. Moe, Targeting tau oligomers for therapeutic development for Alzheimer's disease and tauopathies. *Curr Topics Biotechnol* **4**, 47 (2008).
86. K. J. Kopeikina, B. T. Hyman, T. L. Spires-Jones, Soluble forms of tau are toxic in Alzheimer's disease. *Translational neuroscience* **3**, 223 (2012).
87. A. Nath, M. Sammalkorpi, D. C. DeWitt, A. J. Trexler, S. Elbaum-Garfinkle, C. S. O'Hern, E. Rhoades, The conformational ensembles of α-synuclein and tau: combining single-molecule FRET and simulations. *Biophysical journal* **103**, 1940 (2012).
88. E. Akoury, M. Gajda, M. Pickhardt, J. Biernat, P. Soraya, C. Griesinger, E. Mandelkow, M. Zweckstetter, Inhibition of Tau Filament Formation by Conformational Modulation. *Journal of the American Chemical Society* **135**, 2853 (2013/02/20, 2013).

89. J. E. Gerson, A. Mudher, R. Kayed, Potential mechanisms and implications for the formation of tau oligomeric strains. *Critical Reviews in Biochemistry and Molecular Biology* **51**, 482 (2016/11/01, 2016).
90. C. L. Weaver, M. Espinoza, Y. Kress, P. Davies, Conformational change as one of the earliest alterations of tau in Alzheimer's disease. *Neurobiology of Aging* **21**, 719 (2000/09/01/, 2000).
91. A. M. Sharma, T. L. Thomas, D. R. Woodard, O. M. Kashmer, M. I. Diamond, Tau monomer encodes strains. *eLife* **7**, e37813 (2018).
92. H. Mirbaha, D. Chen, O. A. Morazova, K. M. Ruff, A. M. Sharma, X. Liu, M. Goodarzi, R. V. Pappu, D. W. Colby, H. Mirzaei, L. A. Joachimiak, M. I. Diamond, Inert and seed-competent tau monomers suggest structural origins of aggregation. *eLife* **7**, e36584 (2018/07/10, 2018).
93. R. Y.-C. Huang, R. E. Iacob, S. Sankaranarayanan, L. Yang, M. Ahlijanian, L. Tao, A. A. Tymiak, G. Chen, Probing Conformational Dynamics of Tau Protein by Hydrogen/Deuterium Exchange Mass Spectrometry. *Journal of The American Society for Mass Spectrometry* **29**, 174 (January 01, 2018).
94. J. Götz, D. Xia, G. Leinenga, Y. L. Chew, H. Nicholas, What Renders TAU Toxic. *Frontiers in neurology* **4**, 72 (2013).
95. T. F. Gendron, L. Petrucelli, The role of tau in neurodegeneration. *Molecular Neurodegeneration* **4**, 13 (March 11, 2009).
96. M. E. Orr, A. C. Sullivan, B. Frost, A Brief Overview of Tauopathy: Causes, Consequences, and Therapeutic Strategies. *Trends in Pharmacological Sciences* **38**, 637 (2017).
97. J. Cummings, G. Lee, A. Ritter, K. Zhong, Alzheimer's disease drug development pipeline: 2018. *Alzheimer's & Dementia: Translational Research & Clinical Interventions* **4**, 195 (2018/01/01/, 2018).
98. M. Medina, An Overview on the Clinical Development of Tau-Based Therapeutics. *International Journal of Molecular Sciences* **19**, 1160 (2018).
99. K. R. Brunden, J. Q. Trojanowski, V. M. Y. Lee, Advances in tau-focused drug discovery for Alzheimer's disease and related tauopathies. *Nature reviews. Drug discovery* **8**, 783 (2009).
100. E. Giacobini, G. Gold, Alzheimer disease therapy—moving from amyloid-β to tau. *Nature Reviews Neurology* **9**, 677 (2013).
101. A. Pavlova, C.-Y. Cheng, M. Kinnebrew, J. Lew, F. W. Dahlquist, S. Han, Protein structural and surface water rearrangement constitute major events in the earliest aggregation stages of tau. *Proceedings of the National Academy of Sciences* **113**, E127 (2016).
102. M. E. MacDonald, C. M. Ambrose, M. P. Duyao, R. H. Myers, C. Lin, L. Srinidhi, G. Barnes, S. A. Taylor, M. James, N. Groot, H. MacFarlane, B. Jenkins, M. A. Anderson, N. S. Wexler, J. F. Gusella, G. P. Bates, S. Baxendale, H. Hummerich, S. Kirby, M. North, S. Youngman, R. Mott, G. Zehetner, Z. Sedlacek, A. Poustka, A.-M. Frischauf, H. Lehrach, A. J. Buckler, D. Church, L. Doucette-Stamm, M. C. O'Donovan, L. Riba-Ramirez, M. Shah, V. P. Stanton, S. A. Strobel, K. M. Draths, J. L. Wales, P. Dervan, D. E. Housman, M. Altherr, R. Shiang, L. Thompson, T. Fielder, J. J. Wasmuth, D. Tagle, J. Valdes, L. Elmer, M. Allard, L. Castilla, M. Swaroop, K. Blanchard, F. S. Collins, R. Snell, T. Holloway, K. Gillespie, N. Datson, D. Shaw, P. S. Harper, A novel gene containing a trinucleotide repeat that is expanded and unstable on Huntington's disease chromosomes. *Cell* **72**, 971 (1993/03/26/, 1993).

103. C. A. Ross, E. H. Aylward, E. J. Wild, D. R. Langbehn, J. D. Long, J. H. Warner, R. I. Scahill, B. R. Leavitt, J. C. Stout, J. S. Paulsen, R. Reilmann, P. G. Unschuld, A. Wexler, R. L. Margolis, S. J. Tabrizi, Huntington disease: natural history, biomarkers and prospects for therapeutics. *Nature Reviews Neurology* **10**, 204 (2014).
104. NIH. (2019).
105. E. Cattaneo, C. Zuccato, M. Tartari, Normal huntingtin function: an alternative approach to Huntington's disease. *Nature Reviews Neuroscience* **6**, 919 (2005).
106. J. Schulte, J. T. Littleton, The biological function of the Huntingtin protein and its relevance to Huntington's Disease pathology. *Current trends in neurology* **5**, 65 (2011).
107. A. P. Lieberman, V. G. Shakkottai, R. L. Albin, Polyglutamine Repeats in Neurodegenerative Diseases. *Annual review of pathology* **14**, 1 (Jan 24, 2019).
108. S. Podvin, H. T. Reardon, K. Yin, C. Mosier, V. Hook, Multiple clinical features of Huntington's disease correlate with mutant HTT gene CAG repeat lengths and neurodegeneration. *Journal of Neurology* **266**, 551 (March 01, 2019).
109. J. B. Penney Jr, J.-P. Vonsattel, M. E. Macdonald, J. F. Gusella, R. H. Myers, CAG repeat number governs the development rate of pathology in Huntington's disease. *Annals of Neurology* **41**, 689 (1997).
110. S. Finkbeiner, Huntington's Disease. *Cold Spring Harb Perspect Biol* **3**, a007476.
111. E. Scherzinger, A. Sittler, K. Schweiger, V. Heiser, R. Lurz, R. Hasenbank, G. P. Bates, H. Lehrach, E. E. Wanker, Self-assembly of polyglutamine-containing huntingtin fragments into amyloid-like fibrils: Implications for Huntington's disease pathology. *Proceedings of the National Academy of Sciences* **96**, 4604 (1999).
112. P. H. Reddy, U. P. Shirendeb, Mutant huntingtin, abnormal mitochondrial dynamics, defective axonal transport of mitochondria, and selective synaptic degeneration in Huntington's disease. *Biochimica et biophysica acta* **1822**, 101 (Feb, 2012).
113. M. Giacomello, R. Hudec, R. Lopreiato, Huntington's disease, calcium, and mitochondria. *BioFactors* **37**, 206 (2011).
114. S. Kim, K.-T. Kim, Therapeutic Approaches for Inhibition of Protein Aggregation in Huntington's Disease. *Exp Neurobiol* **23**, 36 (3/, 2014).
115. E. Pecho-Vrieseling, C. Rieker, S. Fuchs, D. Bleckmann, M. S. Esposito, P. Botta, C. Goldstein, M. Bernhard, I. Galimberti, M. Muller, A. Luthi, S. Arber, T. Bouwmeester, H. van der Putten, F. P. Di Giorgio, Transneuronal propagation of mutant huntingtin contributes to non-cell autonomous pathology in neurons. *Nature neuroscience* **17**, 1064 (Aug, 2014).
116. L. Scheuing, C.-T. Chiu, H.-M. Liao, G. R. Linares, D.-M. Chuang, Preclinical and clinical investigations of mood stabilizers for Huntington's disease: what have we learned? *Int J Biol Sci* **10**, 1024 (2014).
117. L. Scheuing, C. T. Chiu, H. M. Liao, G. R. Linares, D. M. Chuang, Preclinical and clinical investigations of mood stabilizers for Huntington's disease: what have we learned? *International journal of biological sciences* **10**, 1024 (2014).
118. S. Imarisio, J. Carmichael, V. Korolchuk, C.-W. Chen, S. Saiki, C. Rose, G. Krishna, Janet E. Davies, E. Ttofi, Benjamin R. Underwood, David C. Rubinsztein, Huntington's disease: from pathology and genetics to potential therapies. *Biochemical Journal* **412**, 191 (2008).

119. A. Rowan, Allies in the fight against neurodegeneration. *Nature Reviews Neuroscience* **5**, 896 (2004).
120. Y. Nagai, T. Inui, H. A. Popiel, N. Fujikake, K. Hasegawa, Y. Urade, Y. Goto, H. Naiki, T. Toda, A toxic monomeric conformer of the polyglutamine protein. *Nature Structural &Amp; Molecular Biology* **14**, 332 (2007).
121. J. Miller, M. Arrasate, E. Brooks, C. P. Libeu, J. Legleiter, D. Hatters, J. Curtis, K. Cheung, P. Krishnan, S. Mitra, K. Widjaja, B. A. Shaby, G. P. Lotz, Y. Newhouse, E. J. Mitchell, A. Osmand, M. Gray, V. Thulasiramin, F. Saudou, M. Segal, X. W. Yang, E. Masliah, L. M. Thompson, P. J. Muchowski, K. H. Weisgraber, S. Finkbeiner, Identifying polyglutamine protein species in situ that best predict neurodegeneration. *Nature Chemical Biology* **7**, 925 (2011).
122. J. L. Wacker, M. H. Zareie, H. Fong, M. Sarikaya, P. J. Muchowski, Hsp70 and Hsp40 attenuate formation of spherical and annular polyglutamine oligomers by partitioning monomer. *Nature Structural &Amp; Molecular Biology* **11**, 1215 (2004).
123. M. A. Poirier, H. Li, J. Macosko, S. Cai, M. Amzel, C. A. Ross, Huntingtin Spheroids and Protofibrils as Precursors in Polyglutamine Fibrilization. *Journal of Biological Chemistry* **277**, 41032 (October 25, 2002, 2002).
124. A. K. Thakur, M. Jayaraman, R. Mishra, M. Thakur, V. M. Chellgren, I.-J. L Byeon, D. H. Anjum, R. Kodali, T. P. Creamer, J. F. Conway, A. M Gronenborn, R. Wetzel, Polyglutamine disruption of the huntingtin exon 1 N terminus triggers a complex aggregation mechanism. *Nature Structural &Amp; Molecular Biology* **16**, 380 (2009).
125. J. Legleiter, E. Mitchell, G. P. Lotz, E. Sapp, C. Ng, M. DiFiglia, L. M. Thompson, P. J. Muchowski, Mutant Huntingtin Fragments Form Oligomers in a Polyglutamine Length-dependent Manner in Vitro and in Vivo. *Journal of Biological Chemistry* **285**, 14777 (May 7, 2010, 2010).
126. K. Sathasivam, A. Lane, J. Legleiter, A. Warley, B. Woodman, S. Finkbeiner, P. Paganetti, P. J. Muchowski, S. Wilson, G. P. Bates, Identical oligomeric and fibrillar structures captured from the brains of R6/2 and knock-in mouse models of Huntington's disease. *Human Molecular Genetics* **19**, 65 (2010).
127. M. A. Olshina, L. M. Angley, Y. M. Ramdzan, J. Tang, M. F. Bailey, A. F. Hill, D. M. Hatters, Tracking Mutant Huntingtin Aggregation Kinetics in Cells Reveals Three Major Populations That Include an Invariant Oligomer Pool. *Journal of Biological Chemistry* **285**, 21807 (July 9, 2010, 2010).
128. J. Fox, T. Connor, M. Stiles, J. Kama, Z. Lu, K. Dorsey, G. Liebermann, E. Sapp, R. Cherny, M. Banks, I. Volitakis, M. DiFiglia, O. Berezovska, A. Bush, S. Hersch, Cysteine oxidation within N-terminal mutant huntingtin promotes oligomerization and delays clearance of soluble protein. *Journal of Biological Chemistry*, (March 30, 2011, 2011).
129. I. Sánchez, C. Mahlke, J. Yuan, Pivotal role of oligomerization in expanded polyglutamine neurodegenerative disorders. *Nature* **421**, 373 (2003).
130. C. A. Ross, Polyglutamine Pathogenesis: Emergence of Unifying Mechanisms for Huntington's Disease and Related Disorders. *Neuron* **35**, 819 (2002/08/29/, 2002).
131. S. J. Sahl, L. E. Weiss, W. C. Duim, J. Frydman, W. E. Moerner, Cellular Inclusion Bodies of Mutant Huntingtin Exon 1 Obscure Small Fibrillar Aggregate Species. *Scientific Reports* **2**, 895 (2012).

132. C. A. Ross, M. A. Poirier, Protein aggregation and neurodegenerative disease. *Nature Medicine* **10**, S10 (2004).
133. J. S. Steffan, L. M. Thompson, Targeting aggregation in the development of therapeutics for the treatment of Huntington's disease and other polyglutamine repeat diseases. *Expert Opinion on Therapeutic Targets* **7**, 201 (2003/04/01, 2003).
134. F. B. Rodrigues, E. J. Wild, Huntington's Disease Clinical Trials Corner: August 2018. *Journal of Huntington's disease* **7**, 279 (2018).
135. A. Kumar, S. Kumar Singh, V. Kumar, D. Kumar, S. Agarwal, M. K. Rana, Huntington's disease: An update of therapeutic strategies. *Gene* **556**, 91 (2015/02/10/, 2015).
136. K. M. Shannon, A. Fraint, Therapeutic advances in Huntington's Disease. *Movement Disorders* **30**, 1539 (2015).
137. F. Lo Cascio, R. Kayed, Azure C Targets and Modulates Toxic Tau Oligomers. *ACS Chemical Neuroscience* **9**, 1317 (2018/06/20, 2018).
138. C. M. Wischik, P. C. Edwards, R. Y. Lai, M. Roth, C. R. Harrington, Selective inhibition of Alzheimer disease-like tau aggregation by phenothiazines. *Proceedings of the National Academy of Sciences of the United States of America* **93**, 11213 (1996).
139. H. J. Wobst, A. Sharma, M. I. Diamond, E. E. Wanker, J. Bieschke, The green tea polyphenol (-)-epigallocatechin gallate prevents the aggregation of tau protein into toxic oligomers at substoichiometric ratios. *FEBS Letters* **589**, 77 (2015).
140. J. S. Rane, P. Bhaumik, D. Panda, Curcumin Inhibits Tau Aggregation and Disintegrates Preformed Tau Filaments in vitro. *Journal of Alzheimer's Disease* **60**, 999 (2017).
141. P. Wang, F. Lo Cascio, J. Gao, R. Kayed, X. Huang, Binding and neurotoxicity mitigation of toxic tau oligomers by synthetic heparin like oligosaccharides. *Chemical Communications* **54**, 10120 (2018).
142. S. Taniguchi, N. Suzuki, M. Masuda, S.-i. Hisanaga, T. Iwatsubo, M. Goedert, M. Hasegawa, Inhibition of Heparin-induced Tau Filament Formation by Phenothiazines, Polyphenols, and Porphyrins. *Journal of Biological Chemistry* **280**, 7614 (March 4, 2005, 2005).
143. D. W. Baggett, A. Nath, The Rational Discovery of a Tau Aggregation Inhibitor. *Biochemistry* **57**, 6099 (2018/10/23, 2018).
144. S. Gauthier, H. H. Feldman, L. S. Schneider, G. K. Wilcock, G. B. Frisoni, J. H. Hardlund, H. J. Moebius, P. Bentham, K. A. Kook, D. J. Wischik, B. O. Schelter, C. S. Davis, R. T. Staff, L. Bracoud, K. Shamsi, J. M. D. Storey, C. R. Harrington, C. M. Wischik, Efficacy and safety of tau-aggregation inhibitor therapy in patients with mild or moderate Alzheimer's disease: a randomised, controlled, double-blind, parallel-arm, phase 3 trial. *Lancet* **388**, 2873 (2016).
145. W. Fecke, M. Gianfriddo, G. Gaviraghi, G. C. Terstappen, F. Heitz, Small molecule drug discovery for Huntington's Disease. *Drug Discovery Today* **14**, 453 (2009/05/01/, 2009).
146. E. J. Wild, S. J. Tabrizi, Targets for future clinical trials in Huntington's disease: What's in the pipeline? *Movement Disorders* **29**, 1434 (2014).
147. W. J. Wolfgang, T. W. Miller, J. M. Webster, J. S. Huston, L. M. Thompson, J. L. Marsh, A. Messer, Suppression of Huntington's disease pathology in Drosophila by human single-chain Fv antibodies. *Proceedings of the*

National Academy of Sciences of the United States of America **102**, 11563 (2005).
148. N. Aronin, M. DiFiglia, Huntingtin-lowering strategies in Huntington's disease: Antisense oligonucleotides, small RNAs, and gene editing. *Movement Disorders* **29**, 1455 (2014).
149. A. H. V. Schapira, C. W. Olanow, J. T. Greenamyre, E. Bezard, Slowing of neurodegeneration in Parkinson's disease and Huntington's disease: future therapeutic perspectives. *The Lancet* **384**, 545 (2014/08/09/, 2014).
150. E. M. Sontag, G. P. Lotz, N. Agrawal, A. Tran, R. Aron, G. Yang, M. Necula, A. Lau, S. Finkbeiner, C. Glabe, J. L. Marsh, P. J. Muchowski, L. M. Thompson, Methylene blue modulates huntingtin aggregation intermediates and is protective in Huntington's disease models. *The Journal of neuroscience : the official journal of the Society for Neuroscience* **32**, 11109 (2012).
151. X. Zhang, D. L. Smith, A. B. Meriin, S. Engemann, D. E. Russel, M. Roark, S. L. Washington, M. M. Maxwell, J. L. Marsh, L. M. Thompson, E. E. Wanker, A. B. Young, D. E. Housman, G. P. Bates, M. Y. Sherman, A. G. Kazantsev, A potent small molecule inhibits polyglutamine aggregation in Huntington's disease neurons and suppresses neurodegeneration in vivo. *Proceedings of the National Academy of Sciences of the United States of America* **102**, 892 (2005).
152. D. E. Ehrnhoefer, P. Markovic, S. Engemann, E. E. Wanker, M. Duennwald, S. Lindquist, J. L. Wacker, J. Legleiter, P. J. Muchowski, J. L. Marsh, M. Roark, L. M. Thompson, Green tea (−)-epigallocatechin-gallate modulates early events in huntingtin misfolding and reduces toxicity in Huntington's disease models. *Human Molecular Genetics* **15**, 2743 (2006).
153. E. M. Sontag, G. P. Lotz, G. Yang, C. J. Sontag, B. J. Cummings, C. G. Glabe, P. J. Muchowski, L. M. Thompson, Detection of Mutant Huntingtin Aggregation Conformers and Modulation of SDS-Soluble Fibrillar Oligomers by Small Molecules. *Journal of Huntington's disease* **1**, 119 (2012).
154. R. A. Fuentealba, J. Marasa, M. I. Diamond, D. Piwnica-Worms, C. C. Weihl, An aggregation sensing reporter identifies leflunomide and teriflunomide as polyglutamine aggregate inhibitors. *Human molecular genetics* **21**, 664 (2012).
155. V. Heiser, S. Engemann, W. Bröcker, I. Dunkel, A. Boeddrich, S. Waelter, E. Nordhoff, R. Lurz, N. Schugardt, S. Rautenberg, C. Herhaus, G. Barnickel, H. Böttcher, H. Lehrach, E. E. Wanker, Identification of benzothiazoles as potential polyglutamine aggregation inhibitors of Huntington's disease by using an automated filter retardation assay. *Proceedings of the National Academy of Sciences of the United States of America* **99 Suppl 4**, 16400 (2002).
156. V. Heiser, E. Scherzinger, A. Boeddrich, E. Nordhoff, R. Lurz, N. Schugardt, H. Lehrach, E. E. Wanker, Inhibition of huntingtin fibrillogenesis by specific antibodies and small molecules: Implications for Huntington's disease therapy. *Proceedings of the National Academy of Sciences* **97**, 6739 (2000).
157. Y. Zeng, W. Guo, G. Xu, Q. Wang, L. Feng, S. Long, F. Liang, Y. Huang, X. Lu, S. Li, J. Zhou, J.-M. Burgunder, J. Pang, Z. Pei, Xyloketal-derived small molecules show protective effect by decreasing mutant Huntingtin protein aggregates in Caenorhabditis elegans model of Huntington's disease. *Drug design, development and therapy* **10**, 1443 (2016).
158. M. B. Robers, R. A. Horton, M. R. Bercher, K. W. Vogel, T. Machleidt, High-throughput cellular assays for regulated posttranslational modifications. *Analytical Biochemistry* **372**, 189 (1/15/, 2008).

159. J. Inglese, D. S. Auld, A. Jadhav, R. L. Johnson, A. Simeonov, A. Yasgar, W. Zheng, C. P. Austin, Quantitative high-throughput screening: A titration-based approach that efficiently identifies biological activities in large chemical libraries. *Proceedings of the National Academy of Sciences of the United States of America* **103**, 11473 (04/12/received, 2006).
160. K. P. Leister, R. Huang, B. L. Goodwin, A. Chen, C. P. Austin, M. Xia, Two High Throughput Screen Assays for Measurement of TNF-α in THP-1 Cells. *Current Chemical Genomics* **5**, 21 (02/28/received, 03/23/revised, 03/26/accepted, 2011).
161. S. C. Miller, R. Huang, S. Sakamuru, S. J. Shukla, M. S. Attene-Ramos, P. Shinn, D. Van Leer, W. Leister, C. P. Austin, M. Xia, Identification of known drugs that act as inhibitors of NF-κB signaling and their mechanism of action. *Biochemical Pharmacology* **79**, 1272 (5/1/, 2010).
162. F. F. Hamdan, Y. Percherancier, B. Breton, M. Bouvier, Monitoring Protein-Protein Interactions in Living Cells by Bioluminescence Resonance Energy Transfer (BRET). *Current Protocols in Neuroscience* **34**, 5.23.1 (2006).
163. S. J. Gruber, R. L. Cornea, J. Li, K. C. Peterson, T. M. Schaaf, G. D. Gillispie, R. Dahl, K. M. Zsebo, S. L. Robia, D. D. Thomas, Discovery of enzyme modulators via high-throughput time-resolved FRET in living cells. *Journal of biomolecular screening* **19**, 215 (2014).
164. V. Hemant, C. L. Donald, R. S. Brent, in *Neurobiology of Huntington?s Disease*. (CRC Press, 2010), pp. 121-145.
165. A. M. Davis, S. J. Teague, G. J. Kleywegt, Application and Limitations of X-ray Crystallographic Data in Structure-Based Ligand and Drug Design. *Angewandte Chemie International Edition* **42**, 2718 (2003).
166. S. J. Y. Macalino, V. Gosu, S. Hong, S. Choi, Role of computer-aided drug design in modern drug discovery. *Archives of Pharmacal Research* **38**, 1686 (September 01, 2015).
167. M. Stahl, H. Mauser, Database clustering with a combination of fingerprint and maximum common substructure methods. *J Chem Inf Model* **45**, 542 (2005).
168. G. W. Bemis, M. A. Murcko, The Properties of Known Drugs. 1. Molecular Frameworks. *Journal of Medicinal Chemistry* **39**, 2887 (1996/01/01, 1996).
169. A. Schuffenhauer, P. Ertl, S. Roggo, S. Wetzel, M. A. Koch, H. Waldmann, The Scaffold Tree − Visualization of the Scaffold Universe by Hierarchical Scaffold Classification. *Journal of Chemical Information and Modeling* **47**, 47 (2007/01/01, 2007).
170. S. R. Langdon, N. Brown, J. Blagg, Scaffold diversity of exemplified medicinal chemistry space. *J Chem Inf Model* **51**, 2174 (2011).
171. G. M. Keseru, G. M. Makara, Hit discovery and hit-to-lead approaches. *Drug Discov Today* **11**, 741 (2006).
172. J.-F. Cheng, M. Chen, D. Wallace, S. Tith, T. Arrhenius, H. Kashiwagi, Y. Ono, A. Ishikawa, H. Sato, T. Kozono, H. Sato, A. M. Nadzan, Discovery and structure–activity relationship of coumarin derivatives as TNF-α inhibitors. *Bioorganic & Medicinal Chemistry Letters* **14**, 2411 (5/17/, 2004).
173. D. Brenner, H. Blaser, T. W. Mak, Regulation of tumour necrosis factor signalling: live or let die. *Nat Rev Immunol* **15**, 362 (2015).
174. F. Wolfe, K. Michaud, Lymphoma in rheumatoid arthritis: the effect of methotrexate and anti-tumor necrosis factor therapy in 18,572 patients. *Arthritis Rheum* **50**, 1740 (Jun, 2004).

175. S. Steeland, C. Libert, R. E. Vandenbroucke, A New Venue of TNF Targeting. *Int J Mol Sci* **19**, 1442 (2018).
176. S. Steeland, L. Puimège, R. E. Vandenbroucke, F. Van Hauwermeiren, J. Haustraete, N. Devoogdt, P. Hulpiau, G. Leroux-Roels, D. Laukens, P. Meuleman, M. De Vos, C. Libert, Generation and Characterization of Small Single Domain Antibodies Inhibiting Human Tumor Necrosis Factor Receptor 1. *The Journal of Biological Chemistry* **290**, 4022 (2015).
177. A. Schon, S. Y. Lam, E. Freire, Thermodynamics-based drug design: strategies for inhibiting protein-protein interactions. *Future Med Chem* **3**, 1129 (2011).
178. A. Schon, N. Madani, A. B. Smith, J. M. Lalonde, E. Freire, Some binding-related drug properties are dependent on thermodynamic signature. *Chem Biol Drug Des* **77**, 161 (2011).
179. J. A. Wells, C. L. McClendon, Reaching for high-hanging fruit in drug discovery at protein–protein interfaces. *Nature* **450**, 1001 (2007).
180. Andrew K. Lewis, Zachary M. James, Jesse E. McCaffrey, Anthony R. Braun, Christine B. Karim, David D. Thomas, Jonathan N. Sachs, Open and Closed Conformations of the Isolated Transmembrane Domain of Death Receptor 5 Support a New Model of Activation. *Biophysical Journal* **106**, L21 (2014).
181. C. C. Valley, A. K. Lewis, D. J. Mudaliar, J. D. Perlmutter, A. R. Braun, C. B. Karim, D. D. Thomas, J. R. Brody, J. N. Sachs, Tumor necrosis factor-related apoptosis-inducing ligand (TRAIL) induces death receptor 5 networks that are highly organized. *J Biol Chem* **287**, 21265 (2012).
182. C. C. Valley, A. K. Lewis, J. N. Sachs, Piecing it together: Unraveling the elusive structure-function relationship in single-pass membrane receptors. *Biochimica et Biophysica Acta (BBA) - Biomembranes* **1859**, 1398 (2017).
183. F. Fricke, S. Malkusch, G. Wangorsch, J. F. Greiner, B. Kaltschmidt, C. Kaltschmidt, D. Widera, T. Dandekar, M. Heilemann, Quantitative single-molecule localization microscopy combined with rule-based modeling reveals ligand-induced TNF-R1 reorganization toward higher-order oligomers. *Histochem Cell Biol* **142**, 91 (2014).
184. Y. Wang, K. Bugge, B. B. Kragelund, K. Lindorff-Larsen, Role of protein dynamics in transmembrane receptor signalling. *Current Opinion in Structural Biology* **48**, 74 (2018).
185. T. M. Schaaf, A. Li, B. D. Grant, K. Peterson, S. Yuen, P. Bawaskar, E. Kleinboehl, J. Li, D. D. Thomas, G. D. Gillispie, Red-Shifted FRET Biosensors for High-Throughput Fluorescence Lifetime Screening. *Biosensors (Basel)* **8**, 99 (2018).
186. K. J. Petersen, K. C. Peterson, J. M. Muretta, S. E. Higgins, G. D. Gillispie, D. D. Thomas, Fluorescence lifetime plate reader: Resolution and precision meet high-throughput. *Review of Scientific Instruments* **85**, 113101 (2014).
187. J. M. Muretta, A. Kyrychenko, A. S. Ladokhin, D. J. Kast, G. D. Gillispie, D. D. Thomas, High-performance time-resolved fluorescence by direct waveform recording. *Rev Sci Instrum* **81**, 103101 (2010).
188. T. M. Schaaf, K. C. Peterson, B. D. Grant, P. Bawaskar, S. Yuen, J. Li, J. M. Muretta, G. D. Gillispie, D. D. Thomas, High-Throughput Spectral and Lifetime-Based FRET Screening in Living Cells to Identify Small-Molecule Effectors of SERCA. *SLAS DISCOVERY: Advancing Life Sciences R&D* **22**, 262 (2017/03/01, 2016).

189. T. M. Schaaf, K. C. Peterson, B. D. Grant, D. D. Thomas, G. D. Gillispie, Spectral Unmixing Plate Reader: High-Throughput, High-Precision FRET Assays in Living Cells. *SLAS Discov* **22**, 250 (Mar, 2017).
190. C. H. Lo, N. Vunnam, A. K. Lewis, T.-L. Chiu, B. E. Brummel, T. M. Schaaf, B. D. Grant, P. Bawaskar, D. D. Thomas, J. N. Sachs, An Innovative High-Throughput Screening Approach for Discovery of Small Molecules That Inhibit TNF Receptors. *SLAS DISCOVERY: Advancing Life Sciences R&D* **22**, 950 (2017).
191. C. H. Lo, T. M. Schaaf, B. D. Grant, C. K.-W. Lim, P. Bawaskar, C. C. Aldrich, D. D. Thomas, J. N. Sachs, Noncompetitive inhibitors of TNFR1 probe conformational activation states. *Science Signaling* **12**, eaav5637 (2019).
192. J. H. Zhang, T. D. Chung, K. R. Oldenburg, A Simple Statistical Parameter for Use in Evaluation and Validation of High Throughput Screening Assays. *Journal of biomolecular screening* **4**, 67 (1999).
193. A. Birmingham, L. M. Selfors, T. Forster, D. Wrobel, C. J. Kennedy, E. Shanks, J. Santoyo-Lopez, D. J. Dunican, A. Long, D. Kelleher, Q. Smith, R. L. Beijersbergen, P. Ghazal, C. E. Shamu, Statistical methods for analysis of high-throughput RNA interference screens. *Nature methods* **6**, 569 (2009).
194. R. McAllister, C. Schofield, G. Pettman, C. Mannix, in *Animal Cell Technology: Products from Cells, Cells as Products: Proceedings of the 16th ESACT Meeting April 25–29, 1999, Lugano, Switzerland,* A. Bernard, B. Griffiths, W. Noé, F. Wurm, Eds. (Springer Netherlands, Dordrecht, 2002), pp. 367-369.
195. J. M. Muretta, A. Kyrychenko, A. S. Ladokhin, D. J. Kast, G. D. Gillispie, D. D. Thomas, High-performance time-resolved fluorescence by direct waveform recording. *The Review of scientific instruments* **81**, 103101 (Oct, 2010).
196. R. L. Cornea, S. J. Gruber, E. L. Lockamy, J. M. Muretta, D. Jin, J. Chen, R. Dahl, T. Bartfai, K. M. Zsebo, G. D. Gillispie, D. D. Thomas, High-throughput FRET assay yields allosteric SERCA activators. *J Biomol Screen* **18**, 97 (Jan, 2013).
197. R. T. Rebbeck, M. M. Essawy, F. R. Nitu, B. D. Grant, G. D. Gillispie, D. D. Thomas, D. M. Bers, R. L. Cornea, High-Throughput Screens to Discover Small-Molecule Modulators of Ryanodine Receptor Calcium Release Channels. *SLAS DISCOVERY: Advancing Life Sciences R&D* **22**, 176 (2017/02/01, 2016).
198. D. R. Stroik, S. L. Yuen, K. A. Janicek, T. M. Schaaf, J. Li, D. K. Ceholski, R. J. Hajjar, R. L. Cornea, D. D. Thomas, Targeting protein-protein interactions for therapeutic discovery via FRET-based high-throughput screening in living cells. *Scientific reports* **8**, 12560 (2018).
199. C. H. Lo, C. K.-W. Lim, Z. Ding, S. Wickramasinghe, A. R. Braun, E. Rhoades, D. D. Thomas, J. N. Sachs, A novel small molecule screening platform for disrupting toxic tau oligomers in cells. *bioRxiv*, 510412 (2019).
200. D. Brenner, H. Blaser, T. W. Mak, Regulation of tumour necrosis factor signalling: live or let die. *Nat Rev Immunol* **15**, 362 (06//print, 2015).
201. F. Fricke, S. Malkusch, G. Wangorsch, J. F. Greiner, B. Kaltschmidt, C. Kaltschmidt, D. Widera, T. Dandekar, M. Heilemann, Quantitative single-molecule localization microscopy combined with rule-based modeling reveals ligand-induced TNF-R1 reorganization toward higher-order oligomers. *Histochemistry and Cell Biology* **142**, 91 (2014).
202. F. K. Chan, H. J. Chun, L. Zheng, R. M. Siegel, K. L. Bui, M. J. Lenardo, A domain in TNF receptors that mediates ligand-independent receptor assembly and signaling. *Science* **288**, 2351 (Jun 30, 2000).

203. S. Siebert, C. A. Fielding, B. D. Williams, P. Brennan, Mutation of the extracellular domain of tumour necrosis factor receptor 1 causes reduced NF-kappaB activation due to decreased surface expression. *FEBS letters* **579**, 5193 (Sep 26, 2005).
204. D. A. Zacharias, J. D. Violin, A. C. Newton, R. Y. Tsien, Partitioning of lipid-modified monomeric GFPs into membrane microdomains of live cells. *Science* **296**, 913 (2002).
205. C. R. Corbeil, C. I. Williams, P. Labute, Variability in docking success rates due to dataset preparation. *Journal of computer-aided molecular design* **26**, 775 (Jun, 2012).
206. P. Labute, The generalized Born/volume integral implicit solvent model: estimation of the free energy of hydration using London dispersion instead of atomic surface area. *Journal of computational chemistry* **29**, 1693 (Jul 30, 2008).
207. J. C. Adkins, R. N. Brogden, Zafirlukast. A review of its pharmacology and therapeutic potential in the management of asthma. *Drugs* **55**, 121 (Jan, 1998).
208. S. P. Conway, C. Etherington, D. G. Peckham, A. Whitehead, A pilot study of zafirlukast as an anti-inflammatory agent in the treatment of adults with cystic fibrosis. *Journal of Cystic Fibrosis* **2**, 25.
209. P. Greally, M. J. Hussein, A. J. Cook, A. P. Sampson, P. J. Piper, J. F. Price, Sputum tumour necrosis factor-alpha and leukotriene concentrations in cystic fibrosis. *Archives of disease in childhood* **68**, 389 (Mar, 1993).
210. S. E. Bagenstose, L. Levin, J. A. Bernstein, The addition of zafirlukast to cetirizine improves the treatment of chronic urticaria in patients with positive autologous serum skin test results. *The Journal of allergy and clinical immunology* **113**, 134 (Jan, 2004).
211. A. Smith, J. Oertle, D. Prato, Cancer and Infectious Causes. *Open Journal of Medical Microbiology* **4**, 161 (2014).
212. C. Braconi, T. Patel, Cholangiocarcinoma: new insights into disease pathogenesis and biology. *Infectious disease clinics of North America* **24**, 871 (Dec, 2010).
213. J. C. Epinat, T. D. Gilmore, Diverse agents act at multiple levels to inhibit the Rel/NF-kappaB signal transduction pathway. *Oncogene* **18**, 6896 (Nov 22, 1999).
214. A. Schön, S. Y. Lam, E. Freire, Thermodynamics-based drug design: strategies for inhibiting protein–protein interactions. *Future medicinal chemistry* **3**, 1129 (2011).
215. J. A. Wells, C. L. McClendon, Reaching for high-hanging fruit in drug discovery at protein-protein interfaces. *Nature* **450**, 1001 (12/13/print, 2007).
216. A. Schön, N. Madani, A. B. Smith, J. M. Lalonde, E. Freire, Some Binding-Related Drug Properties are Dependent on Thermodynamic Signature. *Chemical biology & drug design* **77**, 161 (02/02, 2011).
217. M. Vilar, I. Charalampopoulos, R. S. Kenchappa, A. Simi, E. Karaca, A. Reversi, S. Choi, M. Bothwell, I. Mingarro, W. J. Friedman, G. Schiavo, P. I. Bastiaens, P. J. Verveer, B. D. Carter, C. F. Ibanez, Activation of the p75 neurotrophin receptor through conformational rearrangement of disulphide-linked receptor dimers. *Neuron* **62**, 72 (Apr 16, 2009).
218. M. Vilar, I. Charalampopoulos, R. S. Kenchappa, A. Reversi, J. M. Klos-Applequist, E. Karaca, A. Simi, C. Spuch, S. Choi, W. J. Friedman, J. Ericson, G. Schiavo, B. D. Carter, C. F. Ibáñez, Ligand-independent signaling by disulfide-

crosslinked dimers of the p75 neurotrophin receptor. *Journal of Cell Science* **122**, 3351 (2009).
219. N. Vunnam, C. K. Campbell-Bezat, A. K. Lewis, J. N. Sachs, Death Receptor 5 Activation Is Energetically Coupled to Opening of the Transmembrane Domain Dimer. *Biophysical Journal* **113**, 381 (2017).
220. A. K. Lewis, C. C. Valley, S. L. Peery, B. Brummel, A. R. Braun, C. B. Karim, J. N. Sachs, Death Receptor 5 Networks Require Membrane Cholesterol for Proper Structure and Function. *Journal of Molecular Biology* **428**, 4843 (2016).
221. C. R. Reis, A. H. G. van Assen, W. J. Quax, R. H. Cool, Unraveling the binding mechanism of trivalent tumor necrosis factor ligands and their receptors. *Mol Cell Proteomics* **10**, M110.002808 (2011).
222. Y. Mukai, T. Nakamura, M. Yoshikawa, Y. Yoshioka, S.-i. Tsunoda, S. Nakagawa, Y. Yamagata, Y. Tsutsumi, Solution of the Structure of the TNF-TNFR2 Complex. *Science Signaling* **3**, ra83 (2010).
223. É. S. Vanamee, D. L. Faustman, Structural principles of tumor necrosis factor superfamily signaling. *Science Signaling* **11**, (2018).
224. F. K.-M. Chan, R. M. Siegel, D. Zacharias, R. Swofford, K. L. Holmes, R. Y. Tsien, M. J. Lenardo, Fluorescence resonance energy transfer analysis of cell surface receptor interactions and signaling using spectral variants of the green fluorescent protein. *Cytometry* **44**, 361 (2001).
225. A. Birmingham, L. M. Selfors, T. Forster, D. Wrobel, C. J. Kennedy, E. Shanks, J. Santoyo-Lopez, D. J. Dunican, A. Long, D. Kelleher, Q. Smith, R. L. Beijersbergen, P. Ghazal, C. E. Shamu, Statistical methods for analysis of high-throughput RNA interference screens. *Nature methods* **6**, 569 (Aug, 2009).
226. T. M. Schaaf, K. C. Peterson, B. D. Grant, P. Bawaskar, S. Yuen, J. Li, J. M. Muretta, G. D. Gillispie, D. D. Thomas, High-Throughput Spectral and Lifetime-Based FRET Screening in Living Cells to Identify Small-Molecule Effectors of SERCA. *SLAS DISCOVERY: Advancing Life Sciences R&D* **22**, 262 (2017).
227. A. Mamińska, A. Bartosik, M. Banach-Orłowska, I. Pilecka, K. Jastrzębski, D. Zdżalik-Bielecka, I. Castanon, M. Poulain, C. Neyen, L. Wolińska-Nizioł, A. Toruń, E. Szymańska, A. Kowalczyk, K. Piwocka, A. Simonsen, H. Stenmark, M. Fürthauer, M. González-Gaitán, M. Miaczynska, ESCRT proteins restrict constitutive NF-κB signaling by trafficking cytokine receptors. *Science Signaling* **9**, ra8 (2016).
228. Y. Jiang, J. D. Woronicz, W. Liu, D. V. Goeddel, Prevention of Constitutive TNF Receptor 1 Signaling by Silencer of Death Domains. *Science* **283**, 543 (1999).
229. H. Hsu, J. Xiong, D. V. Goeddel, The TNF receptor 1-associated protein TRADD signals cell death and NF-κB activation. *Cell* **81**, 495 (1995/05/19/, 1995).
230. E. S. Day, S. M. Cote, A. Whitty, Binding Efficiency of Protein–Protein Complexes. *Biochemistry* **51**, 9124 (2012).
231. W. Takasaki, Y. Kajino, K. Kajino, R. Murali, M. I. Greene, Structure-based design and characterization of exocyclic peptidomimetics that inhibit TNF alpha binding to its receptor. *Nat Biotechnol* **15**, 1266 (1997).
232. C. C. Valley, A. Cembran, J. D. Perlmutter, A. K. Lewis, N. P. Labello, J. Gao, J. N. Sachs, The methionine-aromatic motif plays a unique role in stabilizing protein structure. *J Biol Chem* **287**, 34979 (2012).
233. P. Li, Y. Zheng, X. Chen, Drugs for Autoimmune Inflammatory Diseases: From Small Molecule Compounds to Anti-TNF Biologics. *Frontiers in Pharmacology* **8**, (2017).

234. K. Lis, O. Kuzawińska, E. Bałkowiec-Iskra, Tumor necrosis factor inhibitors – state of knowledge. *Archives of Medical Science : AMS* **10**, 1175 (2014).
235. G. D. Kalliolias, L. B. Ivashkiv, TNF biology, pathogenic mechanisms and emerging therapeutic strategies. *Nature reviews. Rheumatology* **12**, 49 (2016).
236. F. Marc, M. R. N., Perspectives From Masters in Rheumatology and Autoimmunity: Can We Get Closer to a Cure for Rheumatoid Arthritis? *Arthritis & Rheumatology* **67**, 2283 (2015).
237. V. F. Schabert, C. Watson, G. J. Joseph, P. Iversen, C. Burudpakdee, D. J. Harrison, Costs of Tumor Necrosis Factor Blockers Per Treated Patient Using Real-World Drug Data in a Managed Care Population. *Journal of Managed Care Pharmacy* **19**, 621 (2013).
238. E. Kaltsonoudis, P. V. Voulgari, S. Konitsiotis, A. A. Drosos, Demyelination and other neurological adverse events after anti-TNF therapy. *Autoimmunity Reviews* **13**, 54 (2014).
239. R. E. Kontermann, S. Munkel, J. Neumeyer, D. Muller, M. Branschadel, P. Scheurich, K. Pfizenmaier, A humanized tumor necrosis factor receptor 1 (TNFR1)-specific antagonistic antibody for selective inhibition of tumor necrosis factor (TNF) action. *Journal of immunotherapy (Hagerstown, Md. : 1997)* **31**, 225 (2008).
240. D. Wootten, A. Christopoulos, P. M. Sexton, Emerging paradigms in GPCR allostery: implications for drug discovery. *Nature Reviews Drug Discovery* **12**, 630 (2013).
241. D. J. MacEwan, TNF ligands and receptors--a matter of life and death. *British journal of pharmacology* **135**, 855 (2002).
242. J. K. Chan, W. C. Greene, NF-kappaB/Rel: agonist and antagonist roles in HIV-1 latency. *Current opinion in HIV and AIDS* **6**, 12 (Jan, 2011).
243. L. A. O'Neill, C. Kaltschmidt, NF-kappa B: a crucial transcription factor for glial and neuronal cell function. *Trends in neurosciences* **20**, 252 (Jun, 1997).
244. S. M. Cardoso, C. R. Oliveira, Inhibition of NF-kB renders cells more vulnerable to apoptosis induced by amyloid beta peptides. *Free radical research* **37**, 967 (Sep, 2003).
245. P. Muriel, NF-kappaB in liver diseases: a target for drug therapy. *Journal of applied toxicology : JAT* **29**, 91 (Mar, 2009).
246. M. S. Manuvakhova, G. G. Johnson, M. C. White, S. Ananthan, M. Sosa, C. Maddox, S. McKellip, L. Rasmussen, K. Wennerberg, J. V. Hobrath, E. L. White, J. A. Maddry, M. Grimaldi, Identification of novel small molecule activators of nuclear factor-kappaB with neuroprotective action via high-throughput screening. *Journal of neuroscience research* **89**, 58 (Jan, 2011).
247. H. Kasperczyk, K. La Ferla-Bruhl, M. A. Westhoff, L. Behrend, R. M. Zwacka, K. M. Debatin, S. Fulda, Betulinic acid as new activator of NF-kappaB: molecular mechanisms and implications for cancer therapy. *Oncogene* **24**, 6945 (Oct 20, 2005).
248. J. K. Chan, D. Bhattacharyya, K. G. Lassen, D. Ruelas, W. C. Greene, Calcium/Calcineurin Synergizes with Prostratin to Promote NF-κB Dependent Activation of Latent HIV. *PLOS ONE* **8**, e77749 (2013).
249. N. S. Holden, P. E. Squires, M. Kaur, R. Bland, C. E. Jones, R. Newton, Phorbol ester-stimulated NF-kappaB-dependent transcription: roles for isoforms of novel protein kinase C. *Cell Signal* **20**, 1338 (Jul, 2008).

250. V. Busuttil, V. Bottero, C. Frelin, V. Imbert, J. E. Ricci, P. Auberger, J. F. Peyron, Blocking NF-kappaB activation in Jurkat leukemic T cells converts the survival agent and tumor promoter PMA into an apoptotic effector. *Oncogene* **21**, 3213 (May 9, 2002).
251. L. Grandison, G. P. Nolan, D. W. Pfaff, Activation of the transcription factor NF-KB in GH3 pituitary cells. *Molecular and cellular endocrinology* **106**, 9 (Dec, 1994).
252. A. D. Schimmer, M. P. Thomas, R. Hurren, M. Gronda, M. Pellecchia, G. R. Pond, M. Konopleva, D. Gurfinkel, I. A. Mawji, E. Brown, J. C. Reed, Identification of small molecules that sensitize resistant tumor cells to tumor necrosis factor-family death receptors. *Cancer research* **66**, 2367 (Feb 15, 2006).
253. L. Li, R. M. Thomas, H. Suzuki, J. K. De Brabander, X. Wang, P. G. Harran, A Small Molecule Smac Mimic Potentiates TRAIL- and TNFα-Mediated Cell Death. *Science* **305**, 1471 (2004).
254. G. Wang, X. Wang, H. Yu, S. Wei, N. Williams, D. L. Holmes, R. Halfmann, J. Naidoo, L. Wang, L. Li, S. Chen, P. Harran, X. Lei, X. Wang, Small-molecule activation of the TRAIL receptor DR5 in human cancer cells. *Nat Chem Biol* **9**, 84 (Feb, 2013).
255. Y. Song, E. Margolles-Clark, A. Bayer, P. Buchwald, Small-molecule modulators of the OX40-OX40 ligand co-stimulatory protein-protein interaction. *British journal of pharmacology* **171**, 4955 (Nov, 2014).
256. M. I. Gómez, M. O. Seaghdha, A. S. Prince, Staphylococcus aureus protein A activates TACE through EGFR-dependent signaling. *The EMBO journal* **26**, 701 (2007).
257. U. S. Sajjan, M. B. Hershenson, J. F. Forstner, J. J. LiPuma, Burkholderia cenocepacia ET12 strain activates TNFR1 signalling in cystic fibrosis airway epithelial cells. *Cellular Microbiology* **10**, 188 (2008/01/01, 2008).
258. E. Ma, X. Wang, Y. Li, X. Sun, W. Tai, T. Li, T. Guo, Induction of apoptosis by furanodiene in HL60 leukemia cells through activation of TNFR1 signaling pathway. *Cancer letters* **271**, 158 (Nov 18, 2008).
259. M. S. Hayden, S. Ghosh, Regulation of NF-κB by TNF family cytokines. *Semin Immunol* **26**, 253 (2014).
260. L. Andera, Signaling activated by the death receptors of the TNFR family. *Biomedical papers of the Medical Faculty of the University Palacky, Olomouc, Czechoslovakia* **153**, 173 (Sep, 2009).
261. E. Dremencov, J. H. A. Folgering, S. Hogg, L. Tecott, T. I. F. H. Cremers, in *5-HT2C Receptors in the Pathophysiology of CNS Disease,* G. Di Giovanni, E. Esposito, V. Di Matteo, Eds. (Humana Press, Totowa, NJ, 2011), pp. 249-260.
262. F. Nau, Jr., B. Yu, D. Martin, C. D. Nichols, Serotonin 5-HT2A receptor activation blocks TNF-α mediated inflammation in vivo. *PloS one* **8**, e75426 (2013).
263. B. Yu, J. Becnel, M. Zerfaoui, R. Rohatgi, A. H. Boulares, C. D. Nichols, Serotonin 5-Hydroxytryptamine_{2A} Receptor Activation Suppresses Tumor Necrosis Factor-α-Induced Inflammation with Extraordinary Potency. *Journal of Pharmacology and Experimental Therapeutics* **327**, 316 (2008).
264. M. Pelletier, R. M. Siegel, Wishing away inflammation? New links between serotonin and TNF signaling. *Mol Interv* **9**, 299 (2009).
265. C. S. Knauer, J. E. Campbell, C. L. Chio, L. W. Fitzgerald, Pharmacological characterization of mitogen-activated protein kinase activation by recombinant

human 5-HT2C, 5-HT2A, and 5-HT2B receptors. *Naunyn-Schmiedeberg's Archives of Pharmacology* **379**, 461 (2009/05/01, 2009).
266. K. Herrick-Davis, E. Grinde, T. J. Harrigan, J. E. Mazurkiewicz, Inhibition of Serotonin 5-Hydroxytryptamine2C Receptor Function through Heterodimerization: RECEPTOR DIMERS BIND TWO MOLECULES OF LIGAND AND ONE G-PROTEIN. *Journal of Biological Chemistry* **280**, 40144 (December 2, 2005, 2005).
267. P. Bonaventure, D. Nepomuceno, K. Miller, J. Chen, C. Kuei, F. Kamme, D.-T. Tran, T. W. Lovenberg, C. Liu, Molecular and pharmacological characterization of serotonin 5-HT2A and 5-HT2B receptor subtypes in dog. *European Journal of Pharmacology* **513**, 181 (2005/04/25/, 2005).
268. K. Herrick-Davis, E. Grinde, J. E. Mazurkiewicz, Biochemical and biophysical characterization of serotonin 5-HT2C receptor homodimers on the plasma membrane of living cells. *Biochemistry* **43**, 13963 (Nov 9, 2004).
269. AARDA. (2019).
270. C. H. Lo, T. M. Schaaf, B. D. Grant, C. K.-W. Lim, P. Bawaskar, C. C. Aldrich, D. D. Thomas, J. N. Sachs, Non-competitive inhibition of TNF Receptor 1 through long-range perturbation of conformational states by small molecules. *Science Signaling, Under Revision*, (2019).
271. M. E. Zwaagstra, S. H. H. F. Schoenmakers, P. H. J. Nederkoorn, E. Gelens, H. Timmerman, M.-Q. Zhang, Development of a Three-Dimensional CysLT1 (LTD4) Antagonist Model with an Incorporated Amino Acid Residue from the Receptor. *Journal of Medicinal Chemistry* **41**, 1439 (1998/04/01, 1998).
272. P. R. Bernstein, Chemistry and structure--activity relationships of leukotriene receptor antagonists. *American journal of respiratory and critical care medicine* **157**, S220 (Jun, 1998).
273. M. F. Brown, A. Marfat, G. Antognoli, R. J. Chambers, J. B. Cheng, D. B. Damon, T. E. Liston, M. A. McGlynn, S. P. O'Sullivan, B. S. Owens, J. S. Pillar, J. T. Shirley, J. W. Watson, N-carbamoyl analogs of zafirlukast: Potent receptor antagonists of leukotriene D4. *Bioorganic & Medicinal Chemistry Letters* **8**, 2451 (1998/09/22/, 1998).
274. G. Goverdhan, A. R. Reddy, N. R. Reddy, K. Srinivas, V. Himabindu, G. M. Reddy, Synthesis and characterization of new analogs of zafirlukast. *Organic Communications* **5**, 27 (2012).
275. A. A. Martinez, B. A. Espinosa, R. N. Adamek, B. A. Thomas, J. Chau, E. Gonzalez, N. Keppetipola, N. T. Salzameda, Breathing new life into West Nile virus therapeutics; discovery and study of zafirlukast as an NS2B-NS3 protease inhibitor. *European journal of medicinal chemistry* **157**, 1202 (Sep 5, 2018).
276. J. C. McKew, F. Lovering, J. D. Clark, J. Bemis, Y. Xiang, M. Shen, W. Zhang, J. C. Alvarez, D. Joseph-McCarthy, Structure–activity relationships of indole cytosolic phospholipase A2α inhibitors: substrate mimetics. *Bioorganic & Medicinal Chemistry Letters* **13**, 4501 (2003/12/15/, 2003).
277. D. Rajasekhar, D. Srinivasulu, C. Sridhar, G. V. N. Kumar, P. Ramesh, Synthesis, Spectral Characterization and Antioxidant Activity of Novel Zafirlukast Sulfonyl Derivatives. *Journal of the Chinese Chemical Society* **63**, 267 (2016).
278. S. Schierle, C. Flauaus, P. Heitel, S. Willems, J. Schmidt, A. Kaiser, L. Weizel, T. Goebel, A. S. Kahnt, G. Geisslinger, D. Steinhilber, M. Wurglics, G. E. Rovati, A. Schmidtko, E. Proschak, D. Merk, Boosting Anti-Inflammatory Potency of

Zafirlukast by Designed Polypharmacology. *Journal of Medicinal Chemistry* **61**, 5758 (2018/07/12, 2018).
279. N. Thamban Chandrika, M. Y. Fosso, Y. Alimova, A. May, O. A. Gonzalez, S. Garneau-Tsodikova, Novel zafirlukast derivatives exhibit selective antibacterial activity against Porphyromonas gingivalis. *MedChemComm* **10**, 926 (2019).
280. P. Kovacic, R. Somanathan, Nitroaromatic compounds: Environmental toxicity, carcinogenicity, mutagenicity, therapy and mechanism. *Journal of applied toxicology : JAT* **34**, 810 (Aug, 2014).
281. C. M. Cowan, A. Mudher, Are tau aggregates toxic or protective in tauopathies? *Frontiers in neurology* **4**, 114 (2013).
282. N. Kfoury, B. B. Holmes, H. Jiang, D. M. Holtzman, M. I. Diamond, Trans-cellular propagation of Tau aggregation by fibrillar species. *J Biol Chem* **287**, 19440 (2012).
283. K. J. Petersen, K. C. Peterson, J. M. Muretta, S. E. Higgins, G. D. Gillispie, D. D. Thomas, Fluorescence lifetime plate reader: Resolution and precision meet high-throughput. *The Review of Scientific Instruments* **85**, 113101 (2014).
284. S. J. Gruber, R. L. Cornea, J. Li, K. C. Peterson, T. M. Schaaf, G. D. Gillispie, R. Dahl, K. M. Zsebo, S. L. Robia, D. D. Thomas, Discovery of enzyme modulators via high-throughput time-resolved FRET in living cells. *Journal of Biomolecular Screening* **19**, 215 (2014).
285. J. Kuret, E. E. Congdon, G. Li, H. Yin, X. Yu, Q. Zhong, Evaluating triggers and enhancers of tau fibrillization. *Microscopy Research and Technique* **67**, 141 (2005).
286. L.-w. Ko, M. Deture, N. Sahara, R. Chihab, S.-H. Yen, *Cellular Models for Tau Filament Assembly*. (2003), vol. 19, pp. 311-6.
287. C. N. Chirita, E. E. Congdon, H. Yin, J. Kuret, Triggers of Full-Length Tau Aggregation: A Role for Partially Folded Intermediates. *Biochemistry* **44**, 5862 (2005/04/01, 2005).
288. A. Ferrari, F. Hoerndli, T. Baechi, R. M. Nitsch, J. Götz, β-Amyloid Induces Paired Helical Filament-like Tau Filaments in Tissue Culture. *Journal of Biological Chemistry* **278**, 40162 (October 10, 2003, 2003).
289. T. Schaaf, A. Li, B. Grant, K. Peterson, S. Yuen, P. Bawaskar, E. Kleinboehl, J. Li, D. Thomas, G. Gillispie, Red-Shifted FRET Biosensors for High-Throughput Fluorescence Lifetime Screening. *Biosensors* **8**, 99 (2018).
290. S. Elbaum-Garfinkle, E. Rhoades, Identification of an aggregation-prone structure of tau. *Journal of the American Chemical Society* **134**, 16607 (2012).
291. H. Tak, M. M. Haque, M. J. Kim, J. H. Lee, J. H. Baik, Y. Kim, D. J. Kim, R. Grailhe, Y. K. Kim, Bimolecular fluorescence complementation; lighting-up tau-tau interaction in living cells. *PLoS One* **8**, (2013).
292. N. Sahara, J. Lewis, M. DeTure, E. McGowan, D. W. Dickson, M. Hutton, S.-H. Yen, Assembly of tau in transgenic animals expressing P301L tau: alteration of phosphorylation and solubility. *Journal of neurochemistry* **83**, 1498 (2002).
293. Z. Zhao, L. Ho, J. Suh, W. Qin, H. Pyo, P. Pompl, H. Ksiezak-Reding, G. M. Pasinetti, A role of P301L tau mutant in anti-apoptotic gene expression, cell cycle and apoptosis. *Molecular and Cellular Neuroscience* **24**, 367 (2003/10/01/, 2003).
294. K. L. Schulz, A. Eckert, V. Rhein, S. Mai, W. Haase, A. S. Reichert, M. Jendrach, W. E. Müller, K. Leuner, A New Link to Mitochondrial Impairment in Tauopathies. *Molecular Neurobiology* **46**, 205 (August 01, 2012).

295. J. A. Mancini, P. Prasit, M. G. Coppolino, P. Charleson, S. Leger, J. F. Evans, J. W. Gillard, P. J. Vickers, 5-Lipoxygenase-activating protein is the target of a novel hybrid of two classes of leukotriene biosynthesis inhibitors. *Molecular Pharmacology* **41**, 267 (1992).
296. J. Chu, J.-G. Li, C. Ceballos-Diaz, T. Golde, D. Praticò, The influence of 5-lipoxygenase on Alzheimer's disease-related tau pathology: in vivo and in vitro evidence. *Biological psychiatry* **74**, 321 (2013).
297. E. Valera, R. Dargusch, P. A. Maher, D. Schubert, Modulation of 5-lipoxygenase in proteotoxicity and Alzheimer's disease. *The Journal of neuroscience : the official journal of the Society for Neuroscience* **33**, 10512 (2013).
298. A. Klegeris, P. L. McGeer, Toxicity of human monocytic THP-1 cells and microglia toward SH-SY5Y neuroblastoma cells is reduced by inhibitors of 5-lipoxygenase and its activating protein FLAP. *Journal of Leukocyte Biology* **73**, 369 (2003).
299. M. Xiao, W. Li, Recent Advances on Small-Molecule Survivin Inhibitors. *Curr Med Chem* **22**, 1136 (2015).
300. S. Jeganathan, M. von Bergen, H. Brutlach, H. J. Steinhoff, E. Mandelkow, Global hairpin folding of tau in solution. *Biochemistry* **45**, 2283 (2006).
301. A. Verheyen, A. Diels, J. Dijkmans, T. Oyelami, G. Meneghello, L. Mertens, S. Versweyveld, M. Borgers, A. Buist, P. Peeters, M. Cik, Using Human iPSC-Derived Neurons to Model TAU Aggregation. *PLOS ONE* **10**, e0146127 (2016).
302. H.-K. Lee, C. Velazquez Sanchez, M. Chen, P. J. Morin, J. M. Wells, E. B. Hanlon, W. Xia, Three Dimensional Human Neuro-Spheroid Model of Alzheimer's Disease Based on Differentiated Induced Pluripotent Stem Cells. *PloS one* **11**, e0163072 (2016).
303. W. K. Raja, A. E. Mungenast, Y.-T. Lin, T. Ko, F. Abdurrob, J. Seo, L.-H. Tsai, Self-Organizing 3D Human Neural Tissue Derived from Induced Pluripotent Stem Cells Recapitulate Alzheimer's Disease Phenotypes. *PloS one* **11**, e0161969 (2016).
304. M. Kjaergaard, A. J. Dear, F. Kundel, S. Qamar, G. Meisl, T. P. J. Knowles, D. Klenerman, Oligomer Diversity during the Aggregation of the Repeat Region of Tau. *ACS chemical neuroscience* **9**, 3060 (2018).
305. S. Dujardin, S. Bégard, R. Caillierez, C. Lachaud, S. Carrier, S. Lieger, J. A. Gonzalez, V. Deramecourt, N. Déglon, C.-A. Maurage, M. P. Frosch, B. T. Hyman, M. Colin, L. Buée, Different tau species lead to heterogeneous tau pathology propagation and misfolding. *Acta Neuropathologica Communications* **6**, 132 (November 29, 2018).
306. X. Zhao, L. A. Kotilinek, B. Smith, C. Hlynialuk, K. Zahs, M. Ramsden, J. Cleary, K. H. Ashe, Caspase-2 cleavage of tau reversibly impairs memory. *Nature Medicine* **22**, 1268 (Nov, 2016).
307. W. Chen, L. J. Young, M. Lu, A. Zaccone, F. Ströhl, N. Yu, G. S. Kaminski Schierle, C. F. Kaminski, Fluorescence Self-Quenching from Reporter Dyes Informs on the Structural Properties of Amyloid Clusters Formed in Vitro and in Cells. *Nano Letters* **17**, 143 (2017/01/11, 2017).
308. T. D. Romo, A. K. Lewis, A. R. Braun, A. Grossfield, J. N. Sachs, Minimal Nucleation State of alpha-Synuclein Is Stabilized by Dynamic Threonine-Water Networks. *ACS Chem Neurosci* **8**, 1859 (Sep 20, 2017).
309. M. D. Tuttle, G. Comellas, A. J. Nieuwkoop, D. J. Covell, D. A. Berthold, K. D. Kloepper, J. M. Courtney, J. K. Kim, A. M. Barclay, A. Kendall, W. Wan, G.

Stubbs, C. D. Schwieters, V. M. Lee, J. M. George, C. M. Rienstra, Solid-state NMR structure of a pathogenic fibril of full-length human alpha-synuclein. *Nat Struct Mol Biol* **23**, 409 (May, 2016).
310. J. A. Rodriguez, M. I. Ivanova, M. R. Sawaya, D. Cascio, F. E. Reyes, D. Shi, S. Sangwan, E. L. Guenther, L. M. Johnson, M. Zhang, L. Jiang, M. A. Arbing, B. L. Nannenga, J. Hattne, J. Whitelegge, A. S. Brewster, M. Messerschmidt, S. Boutet, N. K. Sauter, T. Gonen, D. S. Eisenberg, Structure of the toxic core of alpha-synuclein from invisible crystals. *Nature* **525**, 486 (Sep 24, 2015).
311. J. M. Muretta;, A. Kyrychenko;, A. S. L. D. J. Kast;, G. D. Gillispie;, D. D. Thomas, High-performance time-resolved fluorescence by direct waveform recording. *Review of Scientific Instruments* **81**, 103101 (2010).
312. S. Zhang, C. Wang, J. Lu, X. Ma, Z. Liu, D. Li, Z. Liu, C. Liu, In-Cell NMR Study of Tau and MARK2 Phosphorylated Tau. *International Journal of Molecular Sciences* **20**, 90 (2018).
313. F. X. Theillet, A. Binolfi, B. Bekei, A. Martorana, H. M. Rose, M. Stuiver, S. Verzini, D. Lorenz, M. van Rossum, D. Goldfarb, P. Selenko, Structural disorder of monomeric alpha-synuclein persists in mammalian cells. *Nature* **530**, 45 (Feb 4, 2016).
314. I. G. Zigoneanu, G. J. Pielak, Interaction of alpha-synuclein and a cell penetrating fusion peptide with higher eukaryotic cell membranes assessed by (1)(9)F NMR. *Mol Pharm* **9**, 1024 (Apr 2, 2012).
315. G. G. Kovacs, Invited review: Neuropathology of tauopathies: principles and practice. *Neuropathology and Applied Neurobiology* **41**, 3 (2015).
316. G. Devi, P. Scheltens, Heterogeneity of Alzheimer's disease: consequence for drug trials? *Alzheimer's Research & Therapy* **10**, 122 (December 19, 2018).
317. B. Ghetti, A. L. Oblak, B. F. Boeve, K. A. Johnson, B. C. Dickerson, M. Goedert, Invited review: Frontotemporal dementia caused by microtubule-associated protein tau gene (MAPT) mutations: a chameleon for neuropathology and neuroimaging. *Neuropathology and Applied Neurobiology* **41**, 24 (2015).
318. S. Mondragon-Rodriguez, G. Perry, X. Zhu, P. I. Moreira, M. C. Acevedo-Aquino, S. Williams, Phosphorylation of tau protein as the link between oxidative stress, mitochondrial dysfunction, and connectivity failure: implications for Alzheimer's disease. *Oxid Med Cell Longev* **2013**, 940603 (2013).
319. V. Rhein, X. Song, A. Wiesner, L. M. Ittner, G. Baysang, F. Meier, L. Ozmen, H. Bluethmann, S. Drose, U. Brandt, E. Savaskan, C. Czech, J. Gotz, A. Eckert, Amyloid-beta and tau synergistically impair the oxidative phosphorylation system in triple transgenic Alzheimer's disease mice. *Proc Natl Acad Sci U S A* **106**, 20057 (Nov 24, 2009).
320. A. Ebneth, R. Godemann, K. Stamer, S. Illenberger, B. Trinczek, E. Mandelkow, Overexpression of tau protein inhibits kinesin-dependent trafficking of vesicles, mitochondria, and endoplasmic reticulum: implications for Alzheimer's disease. *J Cell Biol* **143**, 777 (Nov 2, 1998).
321. S. Yasar, J. Xia, W. Yao, C. D. Furberg, Q.-L. Xue, C. I. Mercado, A. L. Fitzpatrick, L. P. Fried, C. H. Kawas, K. M. Sink, J. D. Williamson, S. T. DeKosky, M. C. Carlson, I. Ginkgo Evaluation of Memory Study, Antihypertensive drugs decrease risk of Alzheimer disease: Ginkgo Evaluation of Memory Study. *Neurology* **81**, 896 (2013).
322. N. Muraya, D. Kadowaki, S. Miyamura, K. Kitamura, K. Uchimura, Y. Narita, Y. Miyamoto, V. T. G. Chuang, K. Taguchi, T. Maruyama, M. Otagiri, S. Hirata,

Benzbromarone Attenuates Oxidative Stress in Angiotensin II- and Salt-Induced Hypertensive Model Rats. *Oxid Med Cell Longev* **2018**, 7635274 (2018).
323. C. Wang, Z. Yu, X. Shi, X. Tang, Y. Wang, X. Wang, Y. An, S. Li, Y. Li, X. Wang, W. Luan, Z. Chen, M. Liu, L. Yu, Triclosan Enhances the Clearing of Pathogenic Intracellular Salmonella or Candida albicans but Disturbs the Intestinal Microbiota through mTOR-Independent Autophagy. *Frontiers in cellular and infection microbiology* **8**, 49 (2018).
324. S. Moussaud, D. R. Jones, E. L. Moussaud-Lamodiere, M. Delenclos, O. A. Ross, P. J. McLean, Alpha-synuclein and tau: teammates in neurodegeneration? *Mol Neurodegener* **9**, 43 (Oct 29, 2014).
325. T. A. Mestre, C. Sampaio, Huntington Disease: Linking Pathogenesis to the Development of Experimental Therapeutics. *Current Neurology and Neuroscience Reports* **17**, 18 (March 06, 2017).
326. A. Busch, S. Engemann, R. Lurz, H. Okazawa, H. Lehrach, E. E. Wanker, Mutant Huntingtin Promotes the Fibrillogenesis of Wild-type Huntingtin: A POTENTIAL MECHANISM FOR LOSS OF HUNTINGTIN FUNCTION IN HUNTINGTON'S DISEASE. *Journal of Biological Chemistry* **278**, 41452 (October 17, 2003, 2003).
327. J. Bard, M. D. Wall, O. Lazari, J. Arjomand, I. Munoz-Sanjuan, Advances in Huntington Disease Drug Discovery: Novel Approaches to Model Disease Phenotypes. *Journal of Biomolecular Screening* **19**, 191 (2014/02/01, 2013).
328. J. Ko, J. M. Isas, A. Sabbaugh, J. H. Yoo, N. K. Pandey, A. Chongtham, M. Ladinsky, W. L. Wu, H. Rohweder, A. Weiss, D. Macdonald, I. Munoz-Sanjuan, R. Langen, P. H. Patterson, A. Khoshnan, Identification of distinct conformations associated with monomers and fibril assemblies of mutant huntingtin. *Hum Mol Genet* **27**, 2330 (Jul 1, 2018).
329. M. Daldin, V. Fodale, C. Cariulo, L. Azzollini, M. Verani, P. Martufi, M. C. Spiezia, S. M. Deguire, M. Cherubini, D. Macdonald, A. Weiss, A. Bresciani, J.-P. G. Vonsattel, L. Petricca, J. L. Marsh, S. Gines, I. Santimone, M. Marano, H. A. Lashuel, F. Squitieri, A. Caricasole, Polyglutamine expansion affects huntingtin conformation in multiple Huntington's disease models. *Scientific Reports* **7**, 5070 (2017/07/11, 2017).
330. R. Mishra, M. Jayaraman, B. P. Roland, E. Landrum, T. Fullam, R. Kodali, A. K. Thakur, I. Arduini, R. Wetzel, Inhibiting the Nucleation of Amyloid Structure in a Huntingtin Fragment by Targeting α-Helix-Rich Oligomeric Intermediates. *Journal of Molecular Biology* **415**, 900 (2012/02/03/, 2012).
331. X. Cui, Q. Liang, Y. Liang, M. Lu, Y. Ding, B. Lu, TR-FRET Assays of Huntingtin Protein Fragments Reveal Temperature and PolyQ Length-Dependent Conformational Changes. *Scientific Reports* **4**, 5601 (07/07/online, 2014).
332. J. M. Bravo-Arredondo, N. C. Kegulian, T. Schmidt, N. K. Pandey, A. J. Situ, T. S. Ulmer, R. Langen, The folding equilibrium of huntingtin exon 1 monomer depends on its polyglutamine tract. *Journal of Biological Chemistry* **293**, 19613 (December 21, 2018, 2018).
333. S. Bonfanti, M. C. Lionetti, M. R. Fumagalli, V. R. Chirasani, G. Tiana, N. V. Dokholyan, S. Zapperi, C. A. M. La Porta, Molecular mechanisms of heterogeneous oligomerization of huntingtin proteins. *Scientific Reports* **9**, 7615 (2019/05/20, 2019).
334. E. A. Newcombe, K. M. Ruff, A. Sethi, A. R. Ormsby, Y. M. Ramdzan, A. Fox, A. W. Purcell, P. R. Gooley, R. V. Pappu, D. M. Hatters, Tadpole-like Conformations of Huntingtin Exon 1 Are Characterized by Conformational Heterogeneity that

Persists regardless of Polyglutamine Length. *Journal of Molecular Biology* **430**, 1442 (2018/05/11/, 2018).
335. J. B. t. Warner, K. M. Ruff, P. S. Tan, E. A. Lemke, R. V. Pappu, H. A. Lashuel, Monomeric Huntingtin Exon 1 Has Similar Overall Structural Features for Wild-Type and Pathological Polyglutamine Lengths. *Journal of the American Chemical Society* **139**, 14456 (2017).
336. G. E. Owens, D. M. New, A. P. West, Jr., P. J. Bjorkman, Anti-PolyQ Antibodies Recognize a Short PolyQ Stretch in Both Normal and Mutant Huntingtin Exon 1. *Journal of molecular biology* **427**, 2507 (2015).
337. F. A. Klein, G. Zeder-Lutz, A. Cousido-Siah, A. Mitschler, A. Katz, P. Eberling, J. L. Mandel, A. Podjarny, Y. Trottier, Linear and extended: a common polyglutamine conformation recognized by the three antibodies MW1, 1C2 and 3B5H10. *Hum Mol Genet* **22**, 4215 (Oct 15, 2013).
338. S. Luo, H. Mizuta, D. C. Rubinsztein, p21-activated kinase 1 promotes soluble mutant huntingtin self-interaction and enhances toxicity. *Human Molecular Genetics* **17**, 895 (2007).
339. P. Lajoie, E. L. Snapp, Formation and toxicity of soluble polyglutamine oligomers in living cells. *PLoS One* **5**, e15245 (Dec 28, 2010).
340. A. Davranche, H. Aviolat, G. Zeder-Lutz, D. Busso, D. Altschuh, Y. Trottier, F. A. C. Klein, Huntingtin affinity for partners is not changed by polyglutamine length: aggregation itself triggers aberrant interactions. *Human Molecular Genetics* **20**, 2795 (2011).
341. C. Ye, Y. Zhang, W. Wang, J. Wang, H. Li, Inhibition of neurite outgrowth and promotion of cell death by cytoplasmic soluble mutant huntingtin stably transfected in mouse neuroblastoma cells. *Neuroscience Letters* **442**, 63 (2008/09/05/, 2008).
342. M. Renna, M. Jimenez-Sanchez, S. Sarkar, D. C. Rubinsztein, Chemical Inducers of Autophagy That Enhance the Clearance of Mutant Proteins in Neurodegenerative Diseases. *Journal of Biological Chemistry* **285**, 11061 (April 9, 2010, 2010).
343. A. D. Balgi, B. D. Fonseca, E. Donohue, T. C. F. Tsang, P. Lajoie, C. G. Proud, I. R. Nabi, M. Roberge, Screen for Chemical Modulators of Autophagy Reveals Novel Therapeutic Inhibitors of mTORC1 Signaling. *PLOS ONE* **4**, e7124 (2009).
344. J. Schulte, K. J. Sepp, C. Wu, P. Hong, J. T. Littleton, High-Content Chemical and RNAi Screens for Suppressors of Neurotoxicity in a Huntington's Disease Model. *PLOS ONE* **6**, e23841 (2011).
345. B. Y. Feng, B. H. Toyama, H. Wille, D. W. Colby, S. R. Collins, B. C. H. May, S. B. Prusiner, J. Weissman, B. K. Shoichet, Small-molecule aggregates inhibit amyloid polymerization. *Nature Chemical Biology* **4**, 197 (01/27/online, 2008).
346. G. T. Heller, F. A. Aprile, M. Vendruscolo, Methods of probing the interactions between small molecules and disordered proteins. *Cellular and Molecular Life Sciences* **74**, 3225 (September 01, 2017).
347. E. Hakimizadeh, A. Shamsizadeh, A. Roohbakhsh, M. K. Arababadi, M. R. Hajizadeh, M. Shariati, M. R. Rahmani, M. Allahtavakoli, Inhibition of transient receptor potential vanilloid-1 confers neuroprotection, reduces tumor necrosis factor-alpha, and increases IL-10 in a rat stroke model. *Fundamental & Clinical Pharmacology* **31**, 420 (2017).

348. E. Nishihara, T. Y. Hiyama, M. Noda, Osmosensitivity of transient receptor potential vanilloid 1 is synergistically enhanced by distinct activating stimuli such as temperature and protons. *PLoS One* **6**, e22246 (2011).
349. E. Nagata, A. Saiardi, H. Tsukamoto, Y. Okada, Y. Itoh, T. Satoh, J. Itoh, R. L. Margolis, S. Takizawa, A. Sawa, S. Takagi, Inositol hexakisphosphate kinases induce cell death in Huntington disease. *The Journal of biological chemistry* **286**, 26680 (Jul 29, 2011).
350. R. S. Atwal, C. R. Desmond, N. Caron, T. Maiuri, J. Xia, S. Sipione, R. Truant, Kinase inhibitors modulate huntingtin cell localization and toxicity. *Nat Chem Biol* **7**, 453 (May 29, 2011).
351. M. Pytliak, V. Vargova, V. Mechirova, M. Felsoci, Serotonin receptors - from molecular biology to clinical applications. *Physiological research* **60**, 15 (2011).
352. X. Cui, Q. Liang, Y. Liang, M. Lu, Y. Ding, B. Lu, TR-FRET assays of Huntingtin protein fragments reveal temperature and polyQ length-dependent conformational changes. *Scientific reports* **4**, 5601 (2014).
353. M. J. Bennett, K. E. Huey-Tubman, A. B. Herr, A. P. West, Jr., S. A. Ross, P. J. Bjorkman, A linear lattice model for polyglutamine in CAG-expansion diseases. *Proc Natl Acad Sci U S A* **99**, 11634 (Sep 3, 2002).
354. C. Peters-Libeu, J. Miller, E. Rutenber, Y. Newhouse, P. Krishnan, K. Cheung, D. Hatters, E. Brooks, K. Widjaja, T. Tran, S. Mitra, M. Arrasate, L. A. Mosquera, D. Taylor, K. H. Weisgraber, S. Finkbeiner, Disease-associated polyglutamine stretches in monomeric huntingtin adopt a compact structure. *J Mol Biol* **421**, 587 (Aug 24, 2012).
355. K. F. Chan, M. R. Siegel, J. M. Lenardo, Signaling by the TNF receptor superfamily and T cell homeostasis. *Immunity* **13**, 419 (Oct, 2000).
356. K. V. Prasad, B. S. Prabhakar, Apoptosis and Autoimmune Disorders. *Autoimmunity* **36**, 323 (2003/09/01, 2003).
357. S. C. Cazanave, J. L. Mott, S. F. Bronk, N. W. Werneburg, C. D. Fingas, X. W. Meng, N. Finnberg, W. S. El-Deiry, S. H. Kaufmann, G. J. Gores, Death Receptor 5 Signaling Promotes Hepatocyte Lipoapoptosis. *Journal of Biological Chemistry* **286**, 39336 (November 11, 2011, 2011).
358. S. Affo, M. Dominguez, J. J. Lozano, P. Sancho-Bru, D. Rodrigo-Torres, O. Morales-Ibanez, M. Moreno, C. Millan, A. Loaeza-del-Castillo, J. Altamirano, J. C. Garcia-Pagan, V. Arroyo, P. Gines, J. Caballeria, R. F. Schwabe, R. Bataller, Transcriptome analysis identifies TNF superfamily receptors as potential therapeutic targets in alcoholic hepatitis. *Gut* **62**, 452 (Mar, 2013).
359. H. Matsuno, K. Yudoh, R. Katayama, F. Nakazawa, M. Uzuki, T. Sawai, T. Yonezawa, Y. Saeki, G. S. Panayi, C. Pitzalis, T. Kimura, The role of TNF-alpha in the pathogenesis of inflammation and joint destruction in rheumatoid arthritis (RA): a study using a human RA/SCID mouse chimera. *Rheumatology (Oxford, England)* **41**, 329 (Mar, 2002).
360. R. Alzani, A. Corti, L. Grazioli, E. Cozzi, P. Ghezzi, F. Marcucci, Suramin induces deoligomerization of human tumor necrosis factor alpha. *J Biol Chem* **268**, 12526 (Jun 15, 1993).
361. J. J. Gomez-Reino, L. Carmona, V. R. Valverde, E. M. Mola, M. D. Montero, Treatment of rheumatoid arthritis with tumor necrosis factor inhibitors may predispose to significant increase in tuberculosis risk: a multicenter active-surveillance report. *Arthritis Rheum* **48**, 2122 (Aug, 2003).

362. F. Van Hauwermeiren, R. E. Vandenbroucke, C. Libert, Treatment of TNF mediated diseases by selective inhibition of soluble TNF or TNFR1. *Cytokine Growth Factor Rev* **22**, 311 (2011).
363. G. Papoff, P. Hausler, A. Eramo, M. G. Pagano, G. Di Leve, A. Signore, G. Ruberti, Identification and characterization of a ligand-independent oligomerization domain in the extracellular region of the CD95 death receptor. *J Biol Chem* **274**, 38241 (Dec 31, 1999).
364. C. H. Lo, N. Vunnam, A. K. Lewis, T. L. Chiu, B. E. Brummel, T. M. Schaaf, B. D. Grant, P. Bawaskar, D. D. Thomas, J. N. Sachs, An Innovative High-Throughput Screening Approach for Discovery of Small Molecules That Inhibit TNF Receptors. *SLAS Discov*, 2472555217706478 (May 01, 2017).
365. L. Clancy, K. Mruk, K. Archer, M. Woelfel, J. Mongkolsapaya, G. Screaton, M. J. Lenardo, F. K. Chan, Preligand assembly domain-mediated ligand-independent association between TRAIL receptor 4 (TR4) and TR2 regulates TRAIL-induced apoptosis. *Proceedings of the National Academy of Sciences of the United States of America* **102**, 18099 (Dec 13, 2005).
366. H. W. Lee, S. H. Lee, H. W. Lee, Y. W. Ryu, M. H. Kwon, Y. S. Kim, Homomeric and heteromeric interactions of the extracellular domains of death receptors and death decoy receptors. *Biochem Biophys Res Commun* **330**, 1205 (May 20, 2005).
367. S. Neumann, J. Hasenauer, N. Pollak, P. Scheurich, Dominant negative effects of tumor necrosis factor (TNF)-related apoptosis-inducing ligand (TRAIL) receptor 4 on TRAIL receptor 1 signaling by formation of heteromeric complexes. *J Biol Chem* **289**, 16576 (Jun 6, 2014).
368. A. Ashkenazi, V. M. Dixit, Apoptosis control by death and decoy receptors. *Current opinion in cell biology* **11**, 255 (Apr, 1999).
369. P. C. Cheng, B. K. Brown, W. X. Song, S. K. Pierce, Translocation of the B cell antigen receptor into lipid rafts reveals a novel step in signaling. *J Immunol* **166**, 3693 (Mar 15, 2001).
370. S. G. Hymowitz, H. W. Christinger, G. Fuh, M. Ultsch, M. O'Connell, R. F. Kelley, A. Ashkenazi, A. M. de Vos, Triggering cell death: the crystal structure of Apo2L/TRAIL in a complex with death receptor 5. *Mol Cell* **4**, 563 (Oct, 1999).
371. C. King, M. Stoneman, V. Raicu, K. Hristova, Fully quantified spectral imaging reveals in vivo membrane protein interactions. *Integr Biol (Camb)* **8**, 216 (Feb, 2016).
372. J. H. Song, K. Kandasamy, A. S. Kraft, ABT-737 induces expression of the death receptor 5 and sensitizes human cancer cells to TRAIL-induced apoptosis. *J Biol Chem* **283**, 25003 (Sep 05, 2008).
373. S. B. Gibson, R. Oyer, A. C. Spalding, S. M. Anderson, G. L. Johnson, Increased expression of death receptors 4 and 5 synergizes the apoptosis response to combined treatment with etoposide and TRAIL. *Mol Cell Biol* **20**, 205 (Jan, 2000).
374. M. Leverkus, M. Neumann, T. Mengling, C. T. Rauch, E. B. Brocker, P. H. Krammer, H. Walczak, Regulation of tumor necrosis factor-related apoptosis-inducing ligand sensitivity in primary and transformed human keratinocytes. *Cancer research* **60**, 553 (Feb 1, 2000).
375. C. Benedict, D. Zajonc, I. Nemcovicova, S. Verma. (Google Patents, 2017).
376. F. C. Kischkel, D. A. Lawrence, A. Chuntharapai, P. Schow, K. J. Kim, A. Ashkenazi, Apo2L/TRAIL-dependent recruitment of endogenous FADD and caspase-8 to death receptors 4 and 5. *Immunity* **12**, 611 (Jun, 2000).

377. R. M. Siegel, J. K. Frederiksen, D. A. Zacharias, F. K. Chan, M. Johnson, D. Lynch, R. Y. Tsien, M. J. Lenardo, Fas preassociation required for apoptosis signaling and dominant inhibition by pathogenic mutations. *Science* **288**, 2354 (Jun 30, 2000).
378. D. Merino, N. Lalaoui, A. Morizot, P. Schneider, E. Solary, O. Micheau, Differential inhibition of TRAIL-mediated DR5-DISC formation by decoy receptors 1 and 2. *Molecular and cellular biology* **26**, 7046 (Oct, 2006).
379. S.-J. Park, K. Bijangi-Vishehsaraei, A. R. Safa, Selective TRAIL-triggered apoptosis due to overexpression of TRAIL death receptor 5 (DR5) in P-glycoprotein-bearing multidrug resistant CEM/VBL1000 human leukemia cells. *International Journal of Biochemistry and Molecular Biology* **1**, 90 (06/29/received, 07/15/accepted, 2010).
380. S. B. Gibson, R. Oyer, A. C. Spalding, S. M. Anderson, G. L. Johnson, Increased Expression of Death Receptors 4 and 5 Synergizes the Apoptosis Response to Combined Treatment with Etoposide and TRAIL. *Molecular and cellular biology* **20**, 205 (06/04/received, 07/19/rev-request, 09/27/accepted, 2000).

11. APPENDIX A: SOLUBLE EXTRACELLULAR DOMAIN OF DEATH RECEPTOR 5 INHIBITS TRAIL-INDUCED APOPTOSIS BY DISRUPTING RECEPTOR–RECEPTOR INTERACTIONS

Adapted with permission from:

Nagamani Vunnam[1], Chih Hung Lo[1], Benjamin D.Grant[2], David D.Thomas[3,4], Jonathan N.Sachs[1*]

Journal of Molecular Biology, 2017 September 15; 429(19): 2943-2953.

1. Department of Biomedical Engineering, University of Minnesota, Minneapolis, MN 55455, United States
2. Fluorescence Innovations Inc., Minneapolis, MN 55455, United States
3. Department of Biochemistry, Molecular Biology and Biophysics, University of Minnesota, Minneapolis, MN 55455, United States
4. Photonic Pharma LLC, Minneapolis, MN 55410, United States

11.1. Summary

Dysregulation of tumor necrosis factor receptor (TNFR) signaling is a key feature of various inflammatory disorders. Current treatments for TNF-related diseases function either by sequestering ligand or blocking ligand-receptor interactions, which can cause dangerous side effects by inhibiting the receptors that are not involved in the disease condition. Thus, alternate strategies that target receptor-receptor interactions are needed. We hypothesized that the soluble extracellular domain (ECD) of long isoform of Death Receptor 5 (DR5) could block endogenous receptor assembly, mimicking the biological effect of decoy receptors that lack the death domain to trigger apoptosis.

Using live-cell FRET studies, we demonstrated that soluble ECD disrupts endogenous DR5-DR5 interactions. Cell viability assays were used to demonstrate the complete inhibition of TRAIL-induced apoptosis by the ECD, even though TRAIL is still able to bind to the receptor. Importantly, we used mutagenesis to prove that the inhibition of TRAIL-induced apoptosis by the ECD predominantly comes from the disruption of DR5 oligomerization, and not ligand-sequestration. Inhibition of death receptor activation should have important therapeutic applications in diseases such as non-alcoholic fatty liver disease. More generally, this approach should be generalized to enable the inhibition of other TNF receptor signaling mechanisms that are associated in a wide range of clinical conditions.

11.2. Introduction

Members of the tumor necrosis factor receptor (TNFR) and tumor necrosis factor (TNF) superfamilies (TNFRSF/TNFSF) play a vital role in the homeostasis of the immune system (*4, 355*). However, increased expression of TNFR/TNF cytokines can cause severe inflammatory reactions and tissue injury (*12, 356*). For example, overexpression of death receptor 5 (DR5/TNRSF10B), a member of TNFR superfamily, in hepatocytes results in non-alcoholic fatty liver disease (*357, 358*); likewise, accumulation of excess TNF-α in joints results in arthritis (*359*). Current treatments for TNF-related ailments function either by sequestering ligand or blocking ligand-receptor interactions that activate TNFR signaling (*16, 29-31, 33-36, 360*). Unfortunately, these anti-TNF drugs cause significant side effects due to their interference with the host immune system. Furthermore, because members of the TNF family of ligands can bind to several related receptors, sequestration of ligands can cause adverse effects by inhibiting the receptors that are not involved in the disease condition (*24, 361, 362*). As

such, for the improved management of TNFR signaling diseases, there is a pressing need to develop receptor-specific therapies that do not interfere with ligand binding.

Recently, pre-ligand assembly of TNF receptors has been acknowledged as an essential precursor to activation (*49, 202, 203, 363*). Hence, targeting the pre-assembled TNFR structures (e.g. receptor dimers and/or trimers) has been considered a potential therapeutic target (*52, 364*). DR5 is an excellent case study for this approach. This is because, unlike other members of the TNFR superfamily, the death receptors and related decoys receptors—which lack a complete functional cytoplasmic death domain and inhibit signaling—are capable of forming heterophilic complexes in a ligand-independent manner (*181, 365-367*). Originally, decoy receptors were thought to inhibit apoptosis by sequestering ligand from the death receptors (*368*). However, recent studies have suggested that ligand-independent heteromeric complex formation between decoy receptors and death receptors, as opposed to ligand sequestration, may be the primary mechanism of signal inhibition (*365-367*). As a consequence, mimicking the biological action of decoy receptors with soluble proteins or small peptides should, in principle, serve as a receptor-specific approach to inhibition.

Here, we show that it is possible to inhibit TNFR signaling by perturbing native, pre-assembled receptor-receptor complexes. Specifically, we targeted the pre-ligand assembly of DR5 to inhibit the apoptosis induced by TNF-related apoptosis inducing ligand (TRAIL/TNFSF10/Apo2L). DR5 is a pro-apoptotic TNF-receptor with an N-terminal extracellular domain (ECD) made up of three cysteine-rich domains (CRD1-3), a transmembrane domain, and a cytoplasmic death domain, which is crucial for initiation of death signaling upon binding of TRAIL. We aimed to control TRAIL-induced apoptosis by using the isolated, soluble ECD of DR5, which lacks the functional death domain.

Soluble ECD, which contains both the presumed pre-ligand assembly domain (PLAD, CRD1) and ligand-binding domains (CRD2 and CRD3), could form both ECD-DR5 and ECD-TRAIL complexes (**Fig**. **10.1**). We hypothesized that soluble ECD might act as a competitive inhibitor, which we anticipated in our experimental design, by masking the endogenous DR5 interaction site and making it inaccessible for its binding partner. Using a combination of biophysical, biochemical and cell-based techniques, we show that the soluble ECD binds directly to endogenous DR5 and effectively inhibits activation. Importantly, we prove that this mode of inhibitory action of ECD is at the receptor-receptor interface, and thus provide the first direct demonstration that this approach is viable even while ligand is still able to bind (*52*). This strategy may be applicable to all the members of clinically important TNFR superfamily.

11.3. Materials and methods

11.3.1 Cell Cultures and Reagents

HEK293 cells were cultured in phenol red-free DMEM (Gibco) and Jurkat cells were cultured in RPMI 1640 medium (ATCC). All media were supplemented with 2 mM L-Glutamine (Invitrogen), heat-inactivated 10% fetal bovine serum (FBS HI, Gibco), 100 U/mL penicillin and 100 μg/mL streptomycin (HyClone). Cell cultures were maintained in an incubator with 5% CO_2 (Forma Series II Water Jacket CO_2 Incubator, Thermo Scientific) at 37 ºC. Antibodies for Western blots, DR5 antibodies (mAb6313) and fluorescent secondary antibody (NL637) were purchased from R&D systems. DR5 (D4E9) XP, Flag-tag (2044S) and FADD (2782S**)** antibodies were purchased from Cell Signaling Technology. β-actin (ab8227) was purchased from Abcam. His-tagged ECD protein was purchased from Origene.

11.3.2 Molecular Biology

EGFP and TagRFP vectors were a kind gift from David D Thomas. cDNAs encoding DR5ΔCD (1-240) was inserted at the N-terminus of the EGFP and TagRFP vectors using standard cloning techniques. To prevent the dimerization and aggregation of EGFP, we mutated alanine 206 to lysine (A206K). All mutations were introduced by Quikchange mutagenesis and sequenced for confirmation.

11.3.3 Overexpression and Purification of Recombinant proteins

Extracellular domain of DR5 (residues 1–148) was overexpressed using the champion pET SUMO expression system in E.coli and purified according to the manufacturer's instructions. The N-terminal FLAG-tagged TRAIL (residues 114–281) was overexpressed using the pT7-FLAG-1 inducible expression system in E.coli and purified by anti-FLAG-affinity column (M2 anti- FLAG-agarose resin). Purity of the proteins was assessed by 4-15% SDS-PAGE gels (Bio-Rad) under reducing conditions followed by Coomassie staining. Protein concentrations were estimated using BCA assay (*369*).

11.3.4 Spectral Characterization

Secondary structure of ECD was determined by using circular dichroism (CD) spectroscopy. Spectral data were collected using a Jasco J-815 Circular Dichroism (CD) spectropolarimiter. Wavelength scans were recorded at 25 °C at a total protein concentration of 100 μM in 140 mM NaCl and 10 mM HEPES (pH 7.4) using a 0.5 mm path length cuvette. Spectral data were corrected for buffer signal and analyzed with Jasco secondary structure estimator.

11.3.5 Generation of Stable Cell Line

HEK293 cells were transiently transfected (Lipofectamine 3000 (Invitrogen)) with DR5ΔCD-GFP only or both DR5ΔCD-GFP and DR5ΔCD-RFP (1:5 ratio) plasmids. Two days later, cells were plated in limiting dilution into 10 cm tissue culture plates and selected with 500 μg/mL G418 (Enzo Life Sciences).

11.3.6 Fluorescence Lifetime Measurements

HEK293 cells with a stable expression of DR5ΔCD/GFP and DR5ΔCD/GFP/RFP were grown to 80-90% confluence in a 10 cm plate. For lifetime measurements, stable cells were lifted with trypsin, washed three times with PBS and resuspended in ~4 ml of PBS at a concentration of 1 million cells/ml and dispensed (50 μL/well) into a 384-well glass-bottom plate by using multidrop combi reagent dispenser (Thermo Scientific). Donor lifetime in the presence and absence of acceptor with +/- ECD/M99A was measured by using fluorescence lifetime plate reader (Fluorescence Innovations, Inc., Minneapolis, MN). GFP fluorescence was excited with a 473 nm microchip laser and emission was filtered with 488 nm long pass and 517/20 nm band pass filters. Time-resolved fluorescence waveforms for each well were fitted to single-exponential decays using least-squares minimization global analysis software (Fluorescence Innovations, Inc.) to give donor lifetime (τ_D) and donor-acceptor lifetime (τ_{DA}). FRET efficiency (*E*) was then calculated based on the equation 1

$$E = 1 - \left(\frac{\tau_{DA}}{\tau_D}\right) \qquad Eq.1$$

11.3.7 Colocalization

To test the colocalization of soluble-ECDs with DR5, ECD and M99A proteins were labeled with Alexa Fluor 555 (Molecular probes by Life Technologies) according to

the manufacturer's instructions. Next, HEK293 cells with a stable expression of DR5ΔCD/GFP were grown on 35 mm glass bottom MatTek culture dishes (MatTek Corporation) and treated with Alexa-555 labeled soluble ECD proteins and incubated for 2-4 hours at 37 °C. Next, cells were gently washed two times with PBS to remove the unbound soluble proteins and fixed with 2% formaldehyde. Slides were then mounted with ProLong diamond antifade reagent (Molecular probes by Life technology) and images were acquired using an Olympus FluoView FV1000 IX2 Inverted Confocal microscopy equipped with a FluoView FV1000 laser scanning confocal head and 60× (1.42NA) oil immersion objective lenses.

11.3.8 Western Blotting

Cells were pelleted by centrifugation, washed with cold PBS and lysed in RIPA buffer (50mM Tris-HCl pH 7.5, 150 mM NaCl, 0.5% Sodium deoxycholate, 1% NP-40) supplemented with protease inhibitors for 30-60 minutes at 4 °C. Total protein concentration of lysates was determined by BCA assay (*369*) and equal amounts of total protein (~60 µg) were mixed with 4X Biorad sample buffer and boiled for 3-5 minutes, and loaded on 4-15% Tris-glycine SDS-PAGE gels (Bio-rad). Proteins were transferred to a PVDF transfer membrane (EMD Millipore) and probed using antibodies against DR5, FLAG-tag, FADD and β-Actin.

11.3.9 Pull-down Assay

ECD-DR5 complex formation was tested by a pull-down assay with His-tagged ECD. His-tagged ECD protein (0.1 mg/ml) was mixed with Cobalt-conjugated magnetic beads (Clontech Talcon beads) and incubated at 4 °C for 2 hours. The beads were then washed three times with wash buffer (50 mM NaH_2PO_4, 300 mM NaCl, and 5 mM imidazole) to remove the unbound His-tagged ECD protein. Jurkat cell pellet was

washed three times with ice-cold PBS and lysed with native lysis buffer (Abcam) containing complete protease inhibitor cocktail (Clontech). Cells were then sonicated for 30 seconds, incubated for 30 minutes on ice, and centrifuged at 16,000 g at 4 °C for 30 minutes. Supernatant was transferred to tube containing His-tagged ECD protein bound to cobalt-conjugated magnetic beads and rotated at 4 °C for 2-4 hours. Then beads were washed three times with wash buffer. Finally, proteins were eluted with elution buffer (50 mM NaH_2PO_4, 300 mM NaCl, and 250 mM imidazole). Eluted proteins were resolved by 4-20% SDS-PAGE under reducing condition and then immunoblotted with MAB6313 antibody.

11.3.10 Co-immunoprecipitation

Soluble FLAG-tagged proteins were (FLAG-TRAIL) mixed with Anti-FLAG magnetic beads and incubated at 4 °C for 2-4 hours. Then beads were washed three times with wash buffer (150 mM NaCl, 50 mM Tris, 10% Glycerol, pH 7.5) to remove the unbound FLAG-tagged protein. Jurkat cells were washed three times with ice-cold PBS and lysed with IP buffer (20 mM Tris-HCl, 1 mM EDTA, 100 mM NaCl, pH 7.5 and 0.5% NP- 40) containing complete protease inhibitor cocktail (Clontech). Cells were then sonicated for 30 seconds, incubated for 30 minutes on ice, and centrifuged at 16,000 g at 4 °C for 30 minutes. Supernatant was transferred to tube containing FLAG-tagged protein bound anti-FLAG antibody coated magnetic beads (Sigma-Aldrich) and rotated at 4 °C for 4 hours, followed by three washes with IP buffer. Whole-cell lysates and Immunoprecipitate samples were resolved using 4-15% SDS-PAGE gels and subjected to western blotting using anti-DR5 antibody (DR5 (D4E9) XP).

11.3.11 MTT Assay

The effect of ECD on TRAIL-induced apoptosis was determined using MTT

assay. Jurkat cells were seeded in 96-well plates at 15,000 cells/well and incubated for 24 hours at 37 °C, 5% CO_2. Cell were treated with ECD and incubated for 1-2 hours and then treated with TRAIL (0.001-16 µg/ml) and incubated further for 24 hours at 37 °C. Cell proliferation was assessed by MTT assay according to the manufacturer's instructions (Sigma-Aldrich). Experiments were repeated three times, and data represented as the mean of six wells ± SD.

11.3.12 Caspase-Glo 8 Assay

Jurkat cells were seeded in 96-well plates at 15,000 cells/well and incubated for 24 hours at 37 °C. Cell were treated with ECD and incubated for 1-2 hours and then treated with TRAIL (0.5 µg/ml), followed by 24 hours of incubation at 37 °C. An equal volume of Caspase-Glo 8 reagent (Promega) was added to each well, and the luminescence was measured after 30 minutes using a Cytation 3 Cell Imaging Multi-Mode Reader luminometer (BioTek). Experiments were repeated three times, and data represented as the mean of six wells ± SD.

11.3.13 Analysis of TRAIL-induced recruitment of FADD to DR5

Jurkat cells were treated with soluble ECD proteins (200 µg/ml) and incubated for 2-4 hours at 37 °C and then stimulated with TRAIL (1 µg/ml) for 2-4 hours. Post stimulation cells were washed with cold PBS and lysed in RIPA buffer (50mM Tris-HCl pH 7.5, 150 mM NaCl, 0.5% Sodium deoxycholate, 1% NP-40) supplemented with protease inhibitors for 30 minutes at 4 °C and centrifuged at 16000 g for 30 minutes at 4 °C. Supernatants were transferred to tube containing FLAG-tagged protein bound anti-FLAG antibody coated magnetic beads and rotated at 4 °C for 12-16 hours, followed by three washes with IP buffer. Immunoprecipitate samples were resolved using 4-15% SDS-PAGE gels and subjected to western blotting using anti-DR5 (DR5 (D4E9) XP and

FADD antibodies.

11.4. Results

11.4.1. Biochemical characterization of soluble ECD and recombinant FLAG-tagged TRAIL proteins

We postulated that soluble ECD could inhibit TRAIL-induced apoptosis by forming both ECD-DR5 and ECD-TRAIL complexes, which lack the functional death domain complexes (**Fig**. **11.1**).

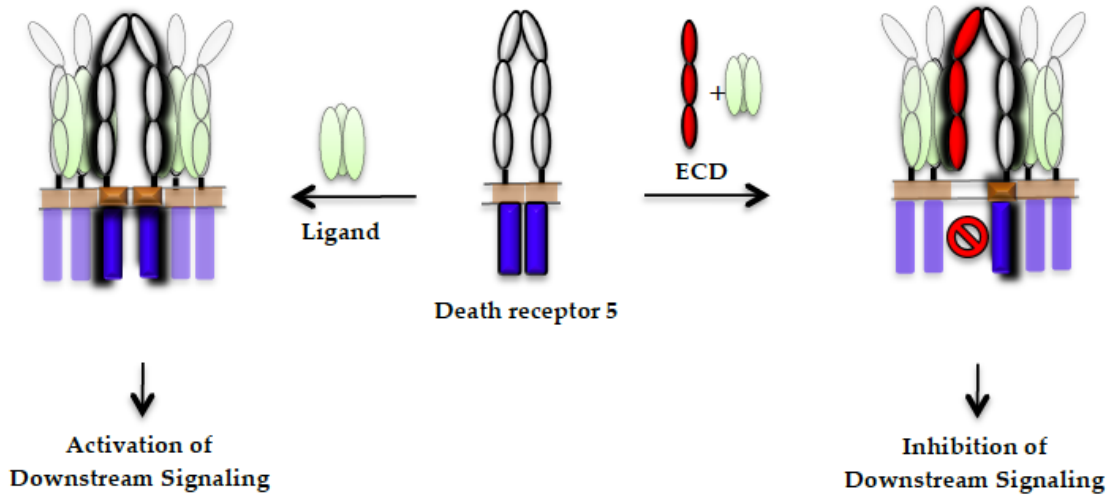

Figure 11. 1. Viable strategy for inhibition of DR5 signaling.

Isolated ECD protein could prevent ligand-induced apoptosis by complexing with DR5 and preventing the formation of the requisite cytosolic death domain dimer.

To test this hypothesis, we produced soluble ECD and FLAG-tagged TRAIL using the champion pET-SUMO and pT7-FLAG-1 expression systems, respectively. Purified proteins were characterized by electrophoresis under denaturing and reducing conditions. ECD appeared as a single band at 17 kDa and Flag-tagged TRAIL at 22 kDa, which are similar to their theoretical molecular weights based on the amino acid

sequences (**Fig. 11.2a**). Soluble ECD was further confirmed by immunoblotting (**Fig. 11.2b**). The secondary structure of soluble ECD was determined by using circular dichroism (CD) spectroscopy. CD spectral data showed a weak shoulder peak at 220 nm and a negative peak at 210 nm (**Fig. 11.2c**), which suggest that the ECD construct is primarily composed of random coil, turns, and a very small percent of ordered structures like β-sheets and α-helix. These results are in agreement with computationally (ExPAsy and STRIDE) predicted secondary structure based on the amino acid sequence of ECD and also with crystal structure of ECD-TRAIL complex (PDB: 1D0G) (*370*). Thus, the spectral data confirm that ECD is folded correctly. We further tested the ligand binding ability of the soluble-ECD by native gel electrophoresis. To confirm the ligand-binding property of soluble-ECD, we analyzed the ECD, TRAIL, and the mixture of ECD/TRAIL by a native-PAGE gel followed by Coomassie blue staining. A new higher molecular weight band was found in the ECD/TRAIL mixture (**Fig. 11.2d**), which suggests that ECD is forming a complex with TRAIL.

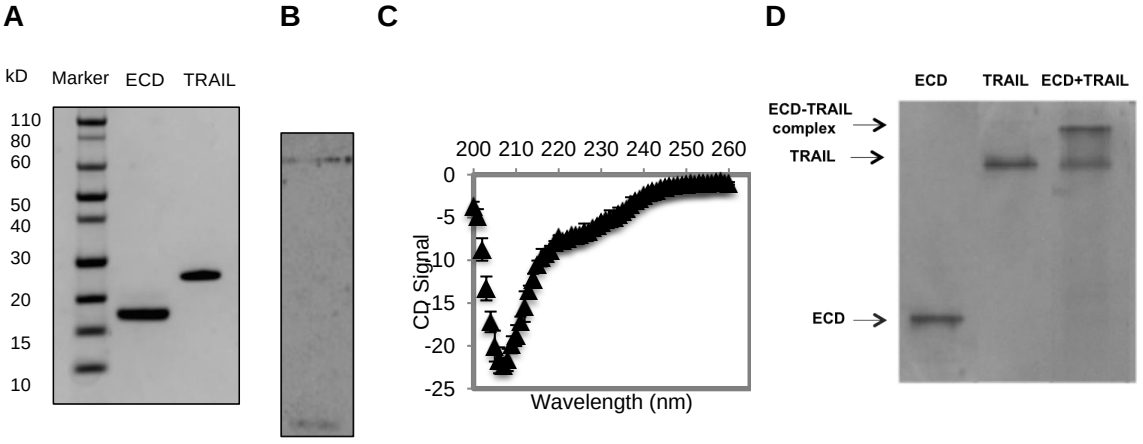

Figure 11. 2. Characterization of recombinant proteins.

(A) Coomassie-stained SDS-PAGE gel of ECD and TRAIL. Equal amounts of ECD and TRAIL proteins were resolved on a 4-15% Tris-glycine gel under reducing conditions. (B) Expression of

ECD was confirmed by western blot using antibody against DR5. (C) CD spectrum of ECD in the Apo-state (10 mM HEPES, 140 mM NaCl, pH 7.4). (D) Coomassie-stained native-PAGE gel of ECD, TRAIL and ECD/TRAIL mixture.

11.4.2. Soluble ECD interacts with DR5 and disrupts the endogenous DR5-DR5 interactions

It has been shown previously that several members of the TNF receptor superfamily exist as ligand-independent, homophilic and heterophilic oligomers. Here, we determined the interaction between endogenous DR5s by measuring live-cell time-resolved fluorescence resonance energy transfer (TR-FRET) with green and red fluorescent-tagged receptors (GFP and RFP). Experiments were carried out in HEK293 cells stably expressing DR5ΔCD fused to GFP and coexpressing DR5ΔCD fused to GFP and RFP just downstream of the transmembrane (TM) domain of the receptors (**Fig. 11.3a**). Measurements showed a substantial decrease in the fluorescence lifetime of the donor in presence of the acceptor compared with the donor only (**Fig. 11.3b**), which confirms efficient energy transfer between the FRET pairs (**Fig**. **11.3c**). These data show that DR5ΔCD receptors are capable of homophilic interactions in the absence of TRAIL (confirming the existence of a pre-assembled oligomeric form) and cytoplasmic death domain. These results are in good agreement with previously published data (*181, 365-367*). Although ligand-independent oligomerization of DR5 has been recognized as an integral component of receptor signaling, the binding affinity of DR5-DR5 interaction in the context of the cell membrane is still an open question. Quantification of DR5-DR5 interactions in the live cell plasma membrane is important for a complete understanding of DR5 signaling function and drug design. Methodologies to quantify membrane protein-protein interactions have been slow to develop. Recently, Kalina et al. developed

a new quantitative fluorescence imaging technique that yields apparent FRET efficiencies and the binding affinities of fluorescently labeled receptors in the plasma membrane (*371*). We will use this method to determine the binding affinity of DR5-DR5 interaction in the context of cell membrane in the near future.

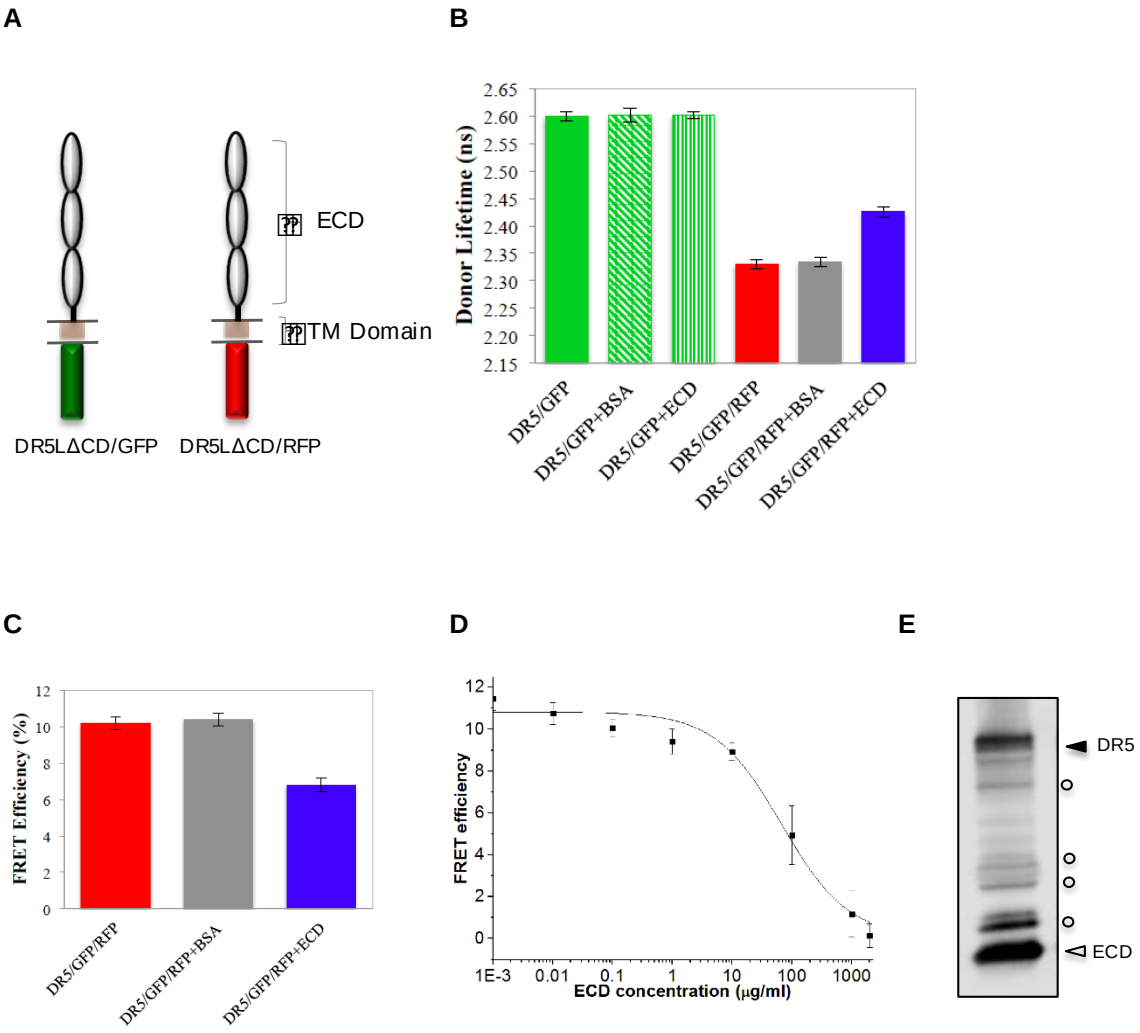

Figure 11. 3. Ligand-independent interaction between soluble ECD and endogenous DR5.

(A) Schematic of GFP or RFP fused DR5ΔCD construct. (B) Lifetime measurements of donor (DR5ΔCD/GFP) - in the presence and absence of acceptor molecule (DR5ΔCD/RFP) with +/- ECD and BSA as a negative control (n=16). (C) FRET efficiency in the presence and absence of

ECD. Results are mean ± SD of triplicate determinations. (D) HEK293 cell lines stably expressing DR5ΔCD/GFP/RFP receptors were treated with indicated amount of soluble ECD. Dose-dependent FRET changes in response to soluble-ECD was determined by TR-FRET assay (n=6). (E) ECD-DR5 complex formation was determined by a pull-down assay with His-tagged ECD. Eluted protein sample was analyzed by electrophoresis, followed by western blotting with antibody against DR5. Open arrowheads, bait; filled arrowhead, prey; open circles, nonspecific signals.

Next, we evaluated the effect of ECD on endogenous DR5 interactions. We speculated that, given sufficient self-affinity of the DR5 PLAD, the ECD should form a ligand-independent complex with DR5 receptors pre-assembled in the plasma membrane. We therefore tested the disruption of endogenous DR5-DR5 interactions by measuring TR-FRET before and after ECD treatment. Strikingly, cells treated with soluble ECD showed significantly lower FRET compared with untreated cells (**Fig**. **11.3c**). These results suggest that ECD is forming heterophilic complex with DR5 and hence increasing the distance between donor-acceptor pairs on pre-assembled receptors. Cells treated with soluble Bovine serum albumin (negative control) caused no significant FRET change compared with untreated cells (**Fig**. **11.3c**), which suggests that the decrease in FRET in the presence of ECD is originating from ECD-DR5 complex formation. Next, we determined the effective concentration of ECD for disruption of membrane bound DR5-DR5 interactions by measuring a soluble ECD concentration-depended FRET efficiency change in HEK293 cells expressing DR5ΔCD/GFP/RFP. Soluble-ECD decreased FRET efficiency in a dose-dependent manner (**Fig. 11.3d**), with half-maximal effective concentration of ~4.6 μM. To further confirm the interaction between ECD and DR5, a pull-down experiment was conducted with His-tagged ECD. Western blot analysis showed both ECD and DR5 bands in the pull-down sample, which

suggests that His-tagged ECD is complexing with endogenous DR5 (**Fig**. **11.3e**). Next, we sought to directly observe the interaction between soluble-ECD and membrane bound DR5 by confocal microscopy. To do so, we labeled the soluble ECD with Alexa fluor 555 and observed its interaction with DR5ΔCD/GFP on the cell surface. Confocal images showed a certain degree of colocalization of fluorescently labeled ECD and DR5ΔCD/GFP on the surface of HEK293 stable cells **(Fig. 11.4)**. However, some stable cells were only stained with Alexa fluor labeled ECD, which might be due to a slight variability in DR5ΔCD-GFP expression. Moreover, fluorescently labeled ECD may also be binding to HEK293 cells, which have very low levels of endogenous DR5 expression (*372, 373*), that are resistant to the G418, but are not expressing DR5ΔCD-GFP. In summary, these results confirm that ECD is interacting with DR5 by disrupting endogenous DR5-DR5 interactions in the plasma membrane.

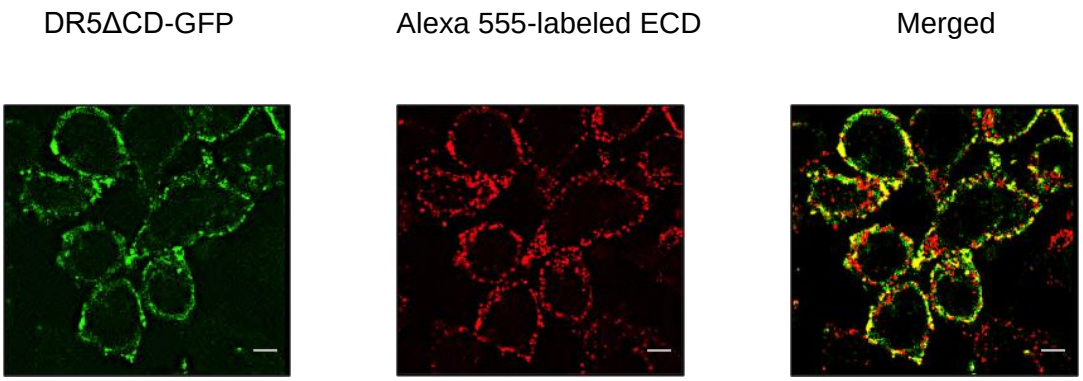

Figure 11. 4. Interaction between soluble-ECD and membrane bound DR5 on the cell surface.

DR5ΔCD-GFP and Alexa Fluor 555-labled ECD co-localized at the surface of HEK293 cells. Scale bars correspond to 50 μm.

11.4.3. ECD is a functional inhibitor of TRAIL-induced apoptosis

To determine whether soluble ECD inhibits TRAIL-induced apoptosis, we treated

Jurkat cells with ECD and compared to untreated cells. Cell proliferation assay (MTT) showed that cells treated with ECD were significantly protected against TRAIL-induced apoptosis compared with untreated cells (**Fig**. **11.5a**) and increased the effective concentration of TRAIL. We further determined the IC_{50} of ECD by measuring TRAIL-induced cell death at different doses of ECD (0.01-200 μg/ml) (**Fig**. **11.5b**). We then specifically tested whether the effect of ECD was on the DR5 apoptotic pathway, which can be determined by monitoring caspase-8 activity (*374*). First we tested the cytotoxicity of ECD by measuring the caspase-8 activity before and after ECD treatment. Cells treated with ECD showed a very low luminescence signal, which indicates that the ECD cannot induce caspase-8 activity and therefore not toxic to cells. Next, we determined the TRAIL-induced caspase-8 activity in the presence and absence of ECD. We observed a significant decrease in caspase-8 activity in ECD-treated cell compared with untreated cells in presence of TRAIL (**Fig**. **11.5c**). Taken together, these results confirm that the soluble ECD is a functional inhibitor of TRAIL-induced apoptosis. Since, ECD contains both PLAD and ligand-binding pockets, the antiapoptotic effect of ECD might be due to disruption of pre-ligand assembly of DR5 receptors and/or sequestration of TRAIL. We therefore investigated the effect of ECD on TRAIL-DR5 interactions by coimmunoprecipitation. Western blot results show that ECD does not block ligand binding: TRAIL and DR5 interact similarly in the presence and absence of ECD (**Fig**. **11.5d**), thus confirming our model **(Fig**. **11.1**). This result also implies that TRAIL is not completely sequestered by any excess ECD that is not bound to cell-surface DR5 receptors.

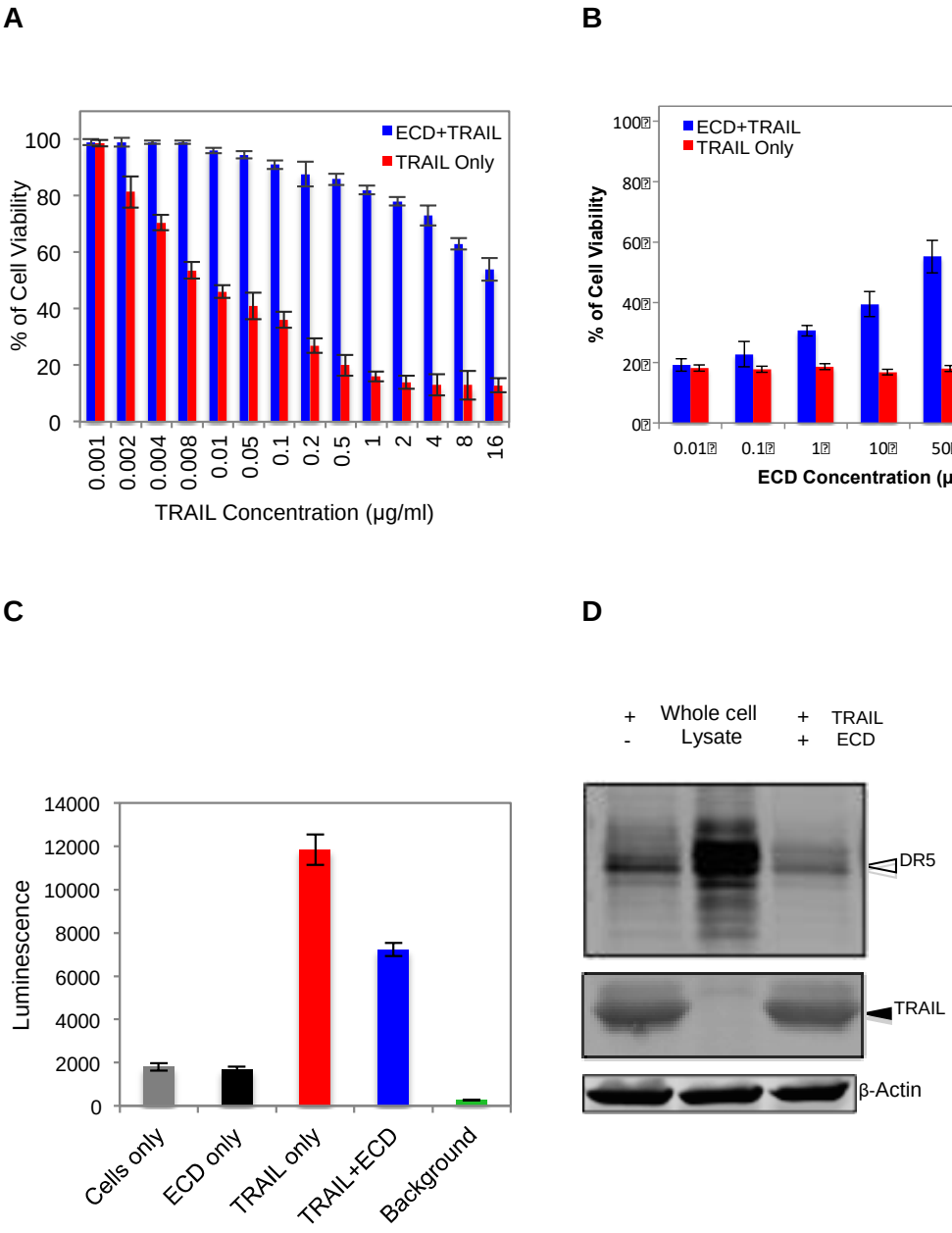

Figure 11. 5. Effect of ECD on TRAIL-induced apoptosis.

(A) Cell viability assay in the presence and absence of ECD. Jurkat cells were plated on a 96-well plate and treated with TRAIL (0.001-16 µg/ml) in the presence (100 µg/ml) and absence of ECD protein. After 24 hours of incubation, the percentage of cell survival was determined by MTT assay. (B) ECD median inhibitory concentration (IC_{50}) was determined by MTT assay. (C) Caspase-8 activity was measured in Jurkat cells treated with TRAIL (0.5 µg/ml), ECD only (50

μg/ml), and TRAIL+ECD. Results are mean ± SD. (D) TRAIL-DR5 complex formation was determined by coimmunoprecipitation with anti-FLAG–conjugated magnetic beads, followed by Western blot analysis.

11.4.4. ECD inhibits ligand-induced apoptosis through ligand-independent association with DR5

To further control against the potential effects of ligand sequestration and prove that the ECD bound to cell-surface DR5 is causing the inhibition, we created a known binding mutation (*181, 365, 375*) in the ligand-binding pocket of ECD (ECD/M99A) and examined its effect on TRAIL-induced apoptosis. Quantification of ligand binding affinity of M99A is critical to prove that the inhibitory effect of soluble ECD is due to the disruption of endogenous DR5-DR5 interactions rather than sequestration of TRAIL. We tested the ligand binding properties of soluble ECD and M99A by a pull-down assay. These results show that ECD/M99A mutation significantly reduced the TRAIL-binding affinity to soluble ECD (**Supplementary Fig. 11.1A** and **B**). Our qualitative pull-down assay results are consistent with that of Benedict et al., who showed that M99A binds TRAIL with much lower affinity (Kd = 202 nM) than WT (Kd = 4 nM) (*375*).

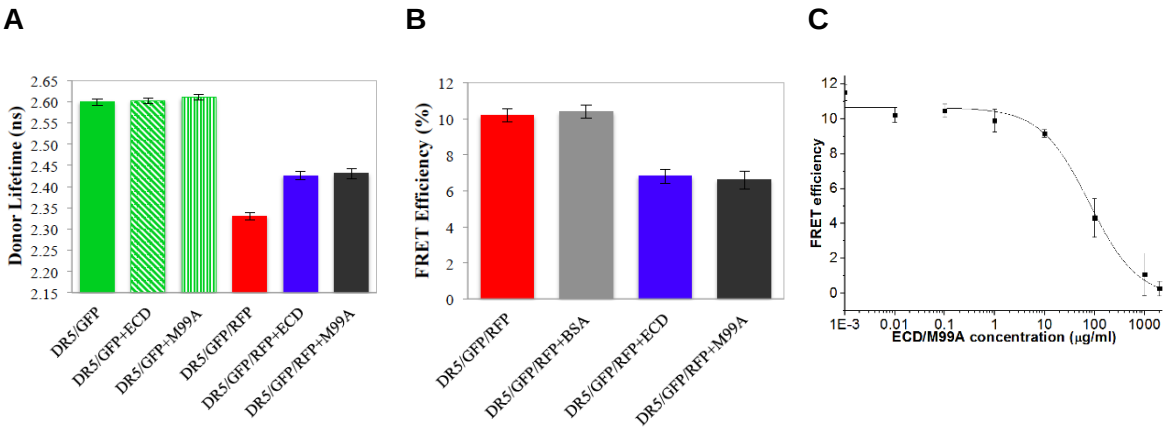

Figure 11. 6. Ligand-independent interaction between soluble M99A and endogenous DR5.

(A) Lifetime measurements of donor (DR5ΔCD /GFP) - in the presence and absence of acceptor molecule (DR5ΔCD /RFP) with +/- ECD and M99A (n=16). (B) FRET efficiency in the presence and absence of ECD/M99A and BSA as a negative control. Results are mean ± SD of triplicate determinations. (C) HEK293 cell lines stably expressing DR5ΔCD/GFP/RFP receptors were treated with indicated amount of soluble ECD/M99A. Dose-dependent FRET changes in response to soluble-ECD/M99A was determined by TR-FRET assay (n=6).

Next, we tested whether the ECD/M99A mutant disrupts the endogenous DR5-DR5 interactions. We evaluated the effect of ECD/M99A mutation on endogenous DR5-DR5 interactions by measuring TR-FRET before and after M99A treatment. Interestingly, cells treated with soluble ECD/M99A showed a longer lifetime compared with untreated cells (**Fig**. **11.6a**), which confirms lower energy transfer between the FRET pair (**Fig**. **11.6b**). These results suggest that ECD/M99A is forming heterophilic complex with DR5 and hence increasing the distance between donor-acceptor pairs on pre-assembled receptors. Subsequently, we determined the effective concentration of M99A for disruption of membrane bound DR5-DR5 interactions by measuring a soluble M99A concentration-dependent FRET efficiency change in HEK293 cells expressing DR5ΔCD/GFP/RFP. Soluble-ECD/M99A decreased FRET efficiency in a dose-dependent manner (**Fig. 11.6c**), with half-maximal effective concentration of ~4.8 μM. In order to directly observe the interaction between soluble-ECD/M99A and DR5, we labeled the soluble ECD/M99A with Alexa fluor 555 and looked at its interaction with DR5ΔCD/GFP on the surface of HEK293 stable cells. Confocal images showed the co-localization of fluorescently labeled ECD/M99A and DR5ΔCD/GFP (**Fig**. **11.7**).

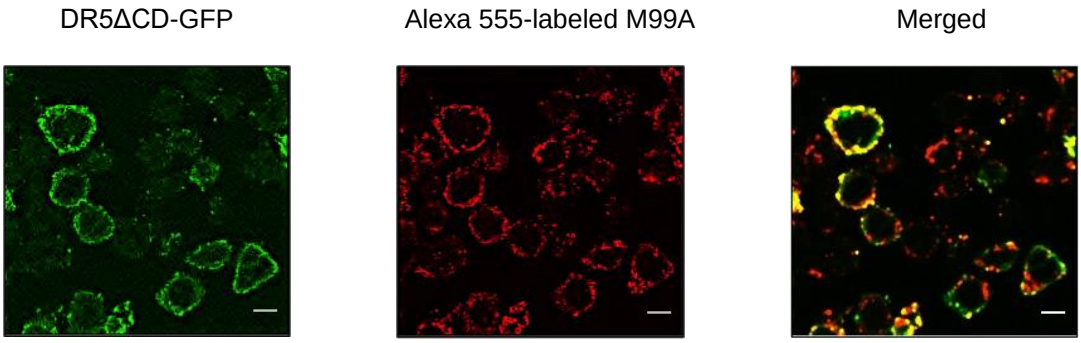

Figure 11. 7. Interaction between soluble-ECD and membrane bound DR5 on the cell surface.

DR5ΔCD-GFP and Alexa Fluor 555-labled ECD/M99A co-localized at the surface of HEK293 cells. Scale bars correspond to 50 μm.

These results confirm that the M99A mutation did not affect the receptor-receptor interaction. We then tested whether the ECD/M99A mutant protects the cells from TRAIL-induced apoptosis. Cells treated with ECD and ECD/M99A functioned similarly, with both proteins significantly protecting the cells against TRAIL-induced apoptosis compared with untreated cells (**Fig**. **11.8a**). Next, we tested the effect of soluble-ECD and M99A on TRAIL-induced recruitment of Fas-associated protein with death domain (FADD) to DR5 by Co-immunoprecipitation assay with anti-FLAG M2 antibody and Flag-tagged TRAIL (**Fig. 11.8b**). It has been previously shown that TRAIL induces recruitment of endogenous FADD to DR5 (*376*). To determine whether soluble ECD and M99A inhibit TRAIL-induced recruitment of FADD to DR5, we treated Jurkat cells with these soluble ECD proteins and compared to untreated cells. Co-immunoprecipitation assay showed that cells treated with ECD and M99A significantly inhibited TRAIL-induced recruitment of FADD to DR5 compared with untreated cells (**Fig**. **11.8b**). These results

suggest that the soluble ECD of DR5, which lacks the functional death domain, might act as a competitive inhibitor by masking the endogenous DR5 interaction site and making it inaccessible to its binding partner, which is important for DISC formation. This observation, thus, further support our hypothesis. Taken together, these data clearly show that inhibition of TRAIL-induced apoptosis by ECD predominantly emanates from the disruption of DR5-DR5 interactions on the cell surface.

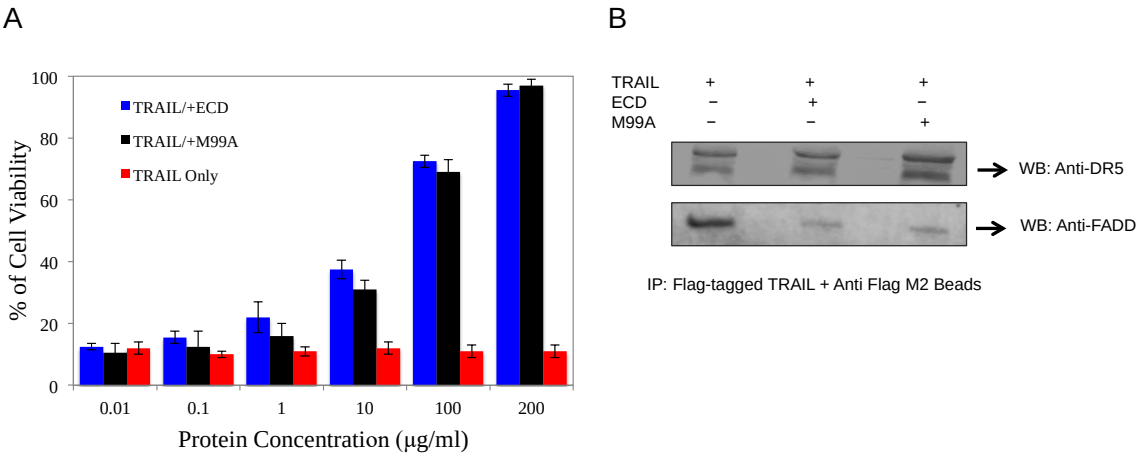

Figure 11. 8. Inhibition of TRAIL-induced apoptosis by ECD predominantly comes from the disruption of DR5 oligomerization on the cell surface.

(A) Jurkat cells treated with TRAIL (0.5µg/ml) in the presence (0.01-200 µg/ml) and absence of ECD proteins. Cell viability was determined by MTT assay. Results are mean ± SD of triplicate determinations. (B) Jurkat cells were treated with soluble ECD and M99A proteins, and then stimulated with Flag-tagged Apo2L/TRAIL-Flag for 2-4 hours and analyzed for FADD recruitment. Lysates were subjected to IP with anti-FLAG–conjugated magnetic beads, followed by western blot analysis.

11.5. Discussion

Several of the most heavily studied and targeted members of the TNFR superfamily (e.g. TNFR1, FAS and DR5) exist as ligand-independent, homophilic

oligomers (*49, 202, 363, 365-367, 377*) on the cell surface. These oligomers are stabilized by the extracellular pre-ligand assembly domain (PLAD), which exists within the amino-terminal side of the cysteine-rich domains (CRDs) of the receptors. Mutations in the PLAD regions of FAS and TNFR1 have been found to participate in pathogenesis of autoimmune lymphoproliferative syndrome and TNFR-associated periodic syndrome, respectively (*202, 203, 377*). As a consequence, competitively blocking pre-ligand assembly via the PLAD has been considered as a potential therapeutic target. Over a decade ago, it was famously proposed that soluble-PLAD could inhibit TNFR1 assembly and prevent TNF-α induced TNFR1 signaling. Using a soluble GST-tagged PLAD protein, the authors showed inhibition of TNF-α induced TNFR1 signaling *in vitro* and subsequent amelioration of arthritis in animal models. Unfortunately, however, the GST-tagged PLAD interfered with ligand binding (*52*).

Therefore, it remained unproven until now that disruption of TNF receptor-receptor interactions by soluble proteins, without inhibiting ligand binding, is a viable therapeutic strategy. We demonstrated here that soluble ECD inhibits TRAIL-induced apoptosis via forming heteromeric complexes with endogenous DR5. Deficiency of death domains in the ECD-DR5 complex significantly reduces the signal transduction pathway that induces apoptosis. Our data clearly show that soluble ECD does not block ligand binding. In fact, our mutational studies (ECD/M99A) ruled out the alternate explanation, sequestration of ligand, for the anti-apoptotic effect of soluble ECD. Thus, we can definitively conclude that the inhibitory effect of ECD predominantly originates from the disruption of DR5-DR5 interactions on the cell surface. We should note here that we attempted to perform this study with just the CRD1 domain of DR5 (in attempt to mirror the TNFR1 mouse study (*52*)). In our case, because we wanted to avoid any chance of interfering with ligand binding, we did not include a GST-tag. Interestingly, we found that

the isolated CRD1 domain was insoluble. Rather than pursuing strategies to increase the solubility of CRD1, we instead decided to work with the entire ECD, which has no solubility issues.

DR5 was an ideal system in which to test this targeting strategy because it is already known that a similar biological mechanism exists (the decoy receptors). In particular, it is known that TRAIL can bind to heterophilic complexes of DR5 and decoy receptors (*378*). DR5 is most well-known as an anti-cancer target, because it is overexpressed in cancer cells (*379, 380*). In that case, TRAIL or antibody agonists have been used to overactivate, not inhibit, the receptor. Progress in this therapeutic effort has been slowed by TRAIL resistance mechanisms. In the context of the current study, there are alternative diseases in which inhibition of DR5 is a sought after strategy. In particular, DR5 signaling plays a major role in progression of nonalcoholic fatty liver disease and nonalcoholic steatohepatitis (NASH). Recent studies have shown that ligand independent DR5 signaling promotes hepatocyte lipoapotosis (*357*), which is a clinical hallmark of NASH. Hence, inhibition of ligand independent assembly of DR5 and signaling may have a therapeutic value in NASH.

In general, soluble peptides that mimic the protein-protein interaction interfaces should bind targets with greater specificity than small molecules. Consequently, peptides should show negligible off-target effects, which might help to overcome the dangerous side effects of conventional anti-TNF therapeutics. Additionally, rapid clearance of soluble peptides prevents the accumulation of harmful metabolites and decreases the risk of toxicity. Thus, it is tempting to suggest that small peptides engineered to mimic the essential binding residues in the PLAD may be even more effective than the full-length ECD or isolated PLAD. To conclude, our therapeutic approach using a soluble protein that targets receptor-receptor interactions shows great promise for ongoing

efforts to develop more effective receptor-specific drugs.

11.6. Supplemental information

A **B**

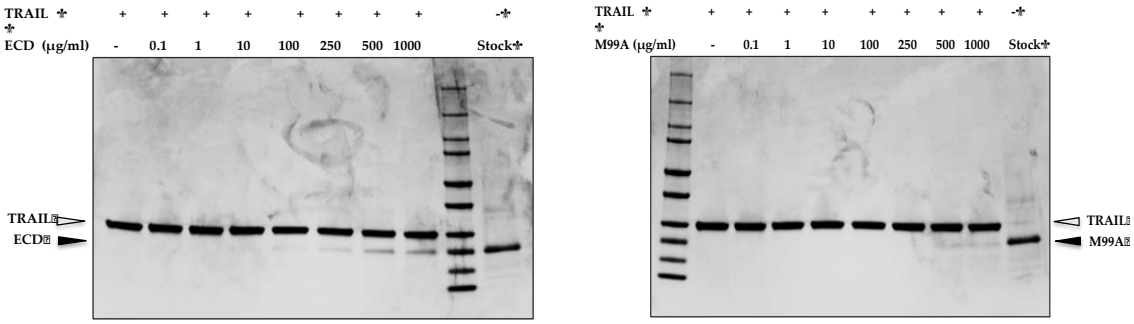

Supplemental Figure 11. 1. Effect of M99A mutation on TRAIL binding affinity.

(A) TRAIL-ECD and TRAIL-ECD/M99A (B) complex formation was determined by pull-down assay with anti FLAG–conjugated magnetic beads. Eluted protein samples were analyzed by 4-20% Tris-glycine SDS-PAGE gels. Open arrowheads, bait (TRAIL); filled arrowhead, prey (ECD); Results are representative of three experiments.

12. APPENDIX B: COMPLETE LIST OF PUBLICATIONS,

PATENTS AND PRESENTATIONS

12.1 Peer Reviewed Publications

- **C. H. Lo**, W. D. Fiers, B. M. Brand, C. C. Aldrich, J. N. Sachs. (2019) Structure-activity relationship analysis of TNF Receptor 1 inhibitors for elucidation of inhibition mechanisms and therapeutic developments. *Manuscript to be submitted to Journal of Medicinal Chemistry*.
- **C. H. Lo**, Evan C. Huber and J. N. Sachs (2019). Conformational states of TNFR1 as a molecular switch in receptor function. *Manuscript to be submitted to Protein Science.*
- **C. H. Lo**, N. K. Pandey, C. K. Lim, Z. Ding, M. Tao, R. Langen, D. D. Thomas, J. N. Sachs. (2019) Discovery of novel small-molecule inhibitors of huntingtin aggregation by FRET-based high-throughput screening. *Manuscript to be submitted to ACS Chemical Neuroscience*.
- **C. H. Lo**, D. D. Thomas and J. N. Sachs (2019). Fluorescence based TNFR1 biosensor for monitoring of receptor structural and conformational dynamics and discovery of small molecule modulators. *Manuscript to be submitted to Methods in Molecular Biology*.
- Braun, A. R., Zahid, H., Johnson, J., Horvath, M., **Lo, C. H.**, Young, M. C., Pomerantz, W., Luk, K., David, D. D., Sachs, J. N. (2019) Potent inhibitors of toxic alpha-synuclein oligomers identified via novel cellular time-resolved FRET biosensor. *Manuscript in preparation*.
- **C. H. Lo**, C. K. Lim, Z. Ding, S. P. Wickramasinghe, A. R. Braun, K. H. Ashe, E. Rhoades, D. D. Thomas and J. N. Sachs. (2019) Targeting the ensemble of heterogeneous tau oligomers in cells: A novel small molecule screening platform for tauopathies. *Alzheimer's and Dementia, Accepted, In Press; published in bioRxiv*.
- **C. H. Lo**, T. M. Schaaf, B. D. Grant, C. K. Lim, P. Bawaskar, C. C. Aldrich, D. D. Thomas and J. N. Sachs (2019). Noncompetitive inhibition of TNF Receptor 1 through long-range perturbation of conformational states by small molecules. *Science Signaling 12(592): eaav5637*.
- N. Vunnam, **C. H. Lo**, B. D. Grant, D. D. Thomas and J. N. Sachs (2017). Soluble extracellular domain of death receptor 5 inhibits TRAIL-induced apoptosis by disrupting receptor-receptor interactions. *Journal of Molecular Biology* 429(19): p.2943-2953.
- **C. H. Lo**, N. Vunnam, A. K. Lewis, T. L. Chiu, B. E. Brummel, T. M. Schaaf, B. D. Grant, P. Bawaskar, D. D. Thomas and J. N. Sachs (2017). An innovative high-throughput screening approach for discovery of small molecules that inhibit TNF Receptors. *SLAS Discovery* 22(8): p.950-961.

12.2. Patents

Jonathan Sachs and **Chih Hung Lo**, 2019, Methods to identify modulators of tau protein oligomerization. U.S. Provisional Application No. 62/806,345. Filed on Feb 15 2019, Patent Pending.

12.3. Oral Presentations

- **C. H. Lo**, N. K. Pandey, C. K. Lim, Z. Ding, M. Tao, D. D. Thomas, R. Langen, J. N. Sachs. Small molecule perturbation of huntingtin conformations to disrupt toxic aggregates in cells, Society for Neuroscience 49th Annual Meeting, Chicago, United States, 2019, Abstract accepted as oral presentation.
- **C. H. Lo**, C. K. Lim, Z. Ding, D. D. Thomas, J. N. Sachs. Perturbation of the ensemble of conformational states of toxic tau oligomers by small molecules, Society for Neuroscience 48th Annual Meeting, San Diego, United States, 2018
- **C. H. Lo**, N. Vunnam, A. K. Lewis, T. L. Chiu, B. E. Brummel, T. M. Schaaf, B. D. Grant, P. Bawaskar, D. D. Thomas, J. N. Sachs, FRET-Based High-Throughput Screening of Small-Molecule Inhibitors of TNF Receptors, 2nd Bioengineering and Translational Medicine Conference, Minneapolis, United States, 2017

12.4 Conference proceedings

- **C. H. Lo**, C. K. Lim, Z. Ding, D. D. Thomas, J. N. Sachs. Discovery of Novel Small-Molecule Inhibitor of Tau Oligomerization by FRET-Based High-Throughput Screening, Institute for Engineering in Medicine Annual Conference, Minneapolis, United States, 2018
- **C. H. Lo**, B. M. Brand, W. D. Fiers, D. D. Thomas, C. C. Aldrich, J. N. Sachs. Structure-Activity Relationship Analysis of TNF Receptor Inhibitors for Elucidation of Inhibition Mechanisms and Therapeutic Developments, 256th ACS National Meeting & Exposition, Boston, United States, 2018
- **C. H. Lo**, C. K. Lim, Z. Ding, T. M. Schaaf, B. D. Grant, D. D. Thomas, J. N. Sachs. Manipulation of Tau Oligomerization and Aggregation Characterized by Time-Resolved FRET, Biophysical Society 62nd Annual Meeting, San Francisco, United States, 2018
- M. C. Young, A. R. Braun, N. Vunnam, **C. H. Lo**, J. N. Sachs. Developing Novel FRET Based Biosensors that Monitor -Synuclein Assembly for Use in High Throughput Screening. Biophysical Society 62nd Annual Meeting, San Francisco, United States, 2018
- **C. H. Lo**, N. Vunnam, A. K. Lewis, T. L. Chiu, B. E. Brummel, T. M. Schaaf, B. D. Grant, P. Bawaskar, D. D. Thomas, J. N. Sachs, An Innovative High-Throughput Screening Approach for Discovery of Small Molecules that Inhibit TNF Receptors, American Society for Biochemistry and Molecular Biology (ASBMB) Annual Meeting, Chicago, United States, 2017
- N. Vunnam, **C. H. Lo**, B. D. Grant, D. D. Thomas, J. N. Sachs, Viable Strategy for Inhibition of Death Receptor 5 Signaling by Disrupting Receptor-Receptor Interactions, American Society for Biochemistry and Molecular Biology (ASBMB) Annual Meeting, Chicago, United States, 2017
- **C. H. Lo**, N. Vunnam, A. K. Lewis, T. L. Chiu, B. E. Brummel, T. M. Schaaf, B. D. Grant, P. Bawaskar, D. D. Thomas, J. N. Sachs, Inhibition of Tumor Necrosis Factor Receptor 1 Signaling by Small Molecules, Biophysical Society 61st Annual Meeting, New Orleans, United States, 2017
- **C. H. Lo**, N. Vunnam, A. K. Lewis, T. M. Schaaf, B. D. Grant, P. Bawaskar, D. D. Thomas, J. N. Sachs, Cell-Based FRET Biosensor for High-Throughput Screening of Small-Molecule Inhibitors of TNFR1, Biomedical Engineering Society (BMES) 2016 Annual Meeting, Minneapolis, United States, 2016
- **C. H. Lo**, A. K. Lewis, T. M. Schaaf, B. D. Grant, N. Vunnam, P. Bawaskar, D. D.

Thomas, J. N. Sachs, Manipulation of the TNF-Receptor Affinity and Oligomerization Characterized by Fluorescence Lifetime Measurements, Biophysical Society 60th Annual Meeting, Los Angeles, United States, 2016